Physiological phenotyping of human frailty

Thesis submitted to the University of Nottingham for the degree of Doctor of Philosophy

March 2024

Joseph Taylor, **MSc**

Supervisory team:

Professor Paul Greenhaff

Professor Susan Francis

Professor John Gladman

Abstract

Frailty is an age-related syndrome characterised by an enhanced vulnerability to adverse health outcomes compared to the non-frail state. However, the physiological phenotype of frailty is poorly understood. This thesis aimed to provide novel insight into the frailty phenotype, thus identifying physiological targets for further research into mechanisms driving frailty progression. A deep physiological phenotyping study was performed in older (aged 65-91 years) non-frail, pre-frail and frail females with no overt disease. Frailty status was defined using the Physical Frailty Phenotype criteria: weakness, slowness, exhaustion, weight loss and low physical activity. Participants were deemed non-frail if no criteria were present, pre-frail if one or two criteria were present, or frail if three or more components were present. Assessments of physical function, neuromuscular characteristics and multi-organ MRI were performed.

In Chapter Three, resting cardiac MRI revealed no differences in structural or functional cardiac parameters between older non-frail, pre-frail and frail females, indicating physiological differences within the cardiovascular system in resting supine volunteers do not differentiate the frail versus non-frail phenotypes.

Chapter Four highlighted lower skeletal muscle volume of the leg and lower isometric strength, functional quality (isometric strength normalised to thigh muscle volume), work output and neuromuscular control of the knee extensors in pre-frail and frail versus non-frail females. For example, dominant leg skeletal muscle volume was lower in pre-frail (1979 ± 177 cm^3/m^2) and frail (1893 ± 169 cm^3/m^2) individuals compared to non-frail females (2162 ± 175 cm^3/m^2; non-frail vs pre-frail: $P = 0.026$; non-frail vs frail: $P = 0.011$). Knee extensor isometric strength was also lower in pre-frail (80 ± 18 Nm) and frail (64 ± 14 Nm) females versus non-frail females (105 ± 23 Nm; non-frail vs pre-

frail: P = 0.011; non-frail vs frail: P = 0.002). No differences in muscle fat fraction or visceral adipose tissue volume were observed.

Chapter Five highlighted lower regional grey and white matter volumes and differences in cortical folding in frail versus non-frail volunteers. For example, lower grey and white matter volumes were evident in the postcentral gyrus (P < 0.001) and frontal pole (P < 0.001) in frail versus non-frail females, which may be related to lower proprioceptive and cognitive performance in frail individuals. In regression analyses, grey and white matter volumes in motor function- and cognition-related brain regions were strongly associated with physical function measures. For example, grey matter volume in the lateral occipital cortex (T = 4.74; P < 0.001) and precentral gyrus (T = 4.49; P < 0.001) exhibited the strongest associations with knee extensor work output. Functional and haemodynamic measures of the brain were no different between groups.

Chapter Six integrated physiological and physical function data from experimental Chapters Three to Five with correlation analyses. Significant correlations were observed between several cardiac, body composition and brain morphometry measures, such as positive correlations between grey matter volume and leg muscle volume (r = >0.35; P < 0.01), suggesting the phenotype of frailty may be underpinned by interactions between multiple organs. Reinforcing the findings from Chapters Four and Five, the strongest associations with physical function were observed in body composition and brain morphometry characteristics. For example, dominant leg fat fraction and white matter hyperintensity volume showed significant negative correlations with knee extensor work output (r < -0.35; P < 0.05 for both comparisons).

The robust multi-organ measurement techniques adopted in this thesis provided novel insight into the physiological phenotype of human frailty. Novel assessments of several

organ parameters were performed, (e.g., cardiac T1 mapping and oxygen utilisation of the brain), thus improving understanding of the multi-organ phenotypic traits of frailty. Integration of physiological and physical function data revealed that the physiological phenotype of frailty is primarily characterised by alterations and interactions within the skeletal muscle and brain. This thesis has identified a research pathway to inform on the design of longitudinal studies to determine the physiological changes underlying frailty progression.

Acknowledgements

Firstly, I would like to sincerely thank my supervisors Professor Paul Greenhaff and Professor Susan Francis for all their support and guidance, without which completion of this PhD would not have been possible. You have both taught me a huge amount and I feel very lucky to have had such amazing mentors. I extend this thank you to Paul for always encouraging my development with opportunities to present at conferences and inviting me to collaborate on the review publication. Also for the many reminders to “believe in your data!”. I would also like to thank Professor John Gladman for the great guidance and efforts to push recruitment.

To my work Mum, Aline Nixon, you played a huge part in the completion of this PhD. Thank you for your never-ending support, can-do attitude and numerous iEMG trouble shooting sessions. You cheered me on during the highs, kept me going through the lows, and taught me a great deal.

A special thank you also goes to Dr Rosemary Nicholas for being my first point of call for all things MRI and MATLAB. You were an invaluable resource and always remained patient despite my many questions.

I would like to thank Dr Ayushman Gupta for help with running the study and many instances of clinical cover (sometimes on your days off!). Also for giving me a front row seat for many muscle biopsies in DYNAMO.

I express my gratitude to the NUH consultants who were instrumental in the recruitment of volunteers for this PhD. In particular, Professor Tahir Masud, who’s fantastic rapport with patients played a huge part in recruitment - when asked their reason for participating, volunteers would always reply: “anything for Prof Masud!”.

Thank you to all the volunteers giving up their time and effort for participation in this study. It was a pleasure getting to know each participant and they shared many pearls of wisdom.

I would like to thank the staff at the Sir Peter Mansfield Imaging Centre for study and analysis support, especially Dr Christopher Bradley for the seamless operating of the MRI scanner during study visits. My thanks also go the fantastic staff at the David Greenfield Human Physiology Unit for support with running the study.

To my girlfriend Caitlin, thank you for putting up with me this past year. Your encouragement and understanding has played a huge part in keeping me going through the hard times. Your Michelin star quality meals were also the highlights of my long days of writing (insert thumbs up emoji here).

To my incredible parents, Mike and Ruth, it is impossible to put into words how grateful I am for everything you have done for me over the years. I'm lucky to have parents as amazing as you, and I would not be where I am today without all of your guidance and support. Thank you for everything.

Impact of COVID-19

This PhD project began in October 2019 and was designed to involve the recruitment of older human volunteers for a physiological and functional phenotyping study. Ethical approval for the study was granted on 2nd October 2020. However, the COVID-19 restrictions on human volunteer research, beginning mid- March 2020, lasted until May 2021, meaning that recruitment of human volunteers for this study could not begin for 8 months following ethical approval. Following authorisation to recommence face-to-face human volunteer research in May 2021, many individuals were reticent to participate in the research due to concerns about COVID-19 transmission. The vulnerable nature of the older and frail volunteers recruited into the study seemed to make potential participants further reticent to participate. Therefore, the impact of COVID-19 made recruitment of volunteers for this study difficult.

Due to the loss of time available for recruitment and execution of the study protocol, requests for a 26-week extension of time and funding were submitted to, and accepted by, the University of Nottingham and Medical Research Council Versus Arthritis Centre for Musculoskeletal Research, respectively.

Abstracts, Conference communications and Publications

During my doctoral study period the data presented in this thesis resulted in the following abstracts, conference communications and publications.

Abstracts

Taylor, J.A., Francis, S.T., Gladman. J.R.F., Piasecki, M., Masud, T., Ollivere, B.J., Greenhaff, P.L. (2022). Investigating the physiological characteristics of frailty using magnetic resonance imaging. In: NIHR Nottingham Biomedical Research Centre (BRC) Musculoskeletal theme: virtual conference proceedings 24th & 25th February 2022. East Midlands Research into Ageing Network (EMRAN) Discussion Paper Series ISSN 2059-3341. Issue 47, April 2022 pp15. DOI: https://doi.org/10.17639/rcn7-2804.

Taylor, J.A., Nixon, A., Gladman J.R. F., Piasecki, M., Masud, T., Weerasuriya, N., Aw, D., Sahota, O., Ollivere, B.J., Francis, S.T., Greenhaff, P.L. (2023). Physical function and brain volumes in older non-frail, pre-frail and frail volunteers. *CIMA/CMAR Joint Meeting - Musculoskeletal ageing research from discovery to improved health.*

Conference communications

(17/11/2022) British Geriatrics Society Symposium

Oral presentation titled “The physiological frailty phenotype”.

(14/07/2022) University of Nottingham PGR Annual Conference

Oral presentation titled “Physiological phenotyping of frailty using magnetic resonance imaging”.

Runner up: Best Oral Presentation (Physiology and Anatomy).

(12/07/2021) University of Nottingham PGR Annual Conference

Poster presentation (online due to COVID-19) titled “Physiological phenotyping of frailty using magnetic resonance imaging (MRI)”.

Winner: Best Poster (Physiology and Anatomy).

Publications

Taylor, J. A., Greenhaff, P. L., Bartlett, D. B., Jackson, T. A., Duggal, N. A., and Lord, J. M. (2023). Multisystem physiological perspective of human frailty and its modulation by physical activity. *Physiological Reviews.* 103 (2), pp. 1137-1191.

Table of contents

List of Abbreviations

AC-PC	Anterior commissure-posterior commissure
ADL	Activities of daily living
ADP	Adenosine diphosphate
ANOVA	Analysis of variance
AOFLOW	Aortic flow
ASL	Arterial spin labelling
ATP	Adenosine triphosphate
BAK-1	BCL2 antagonist/killer 1
Bax	B cell/lymphoma 2 associated x
BDNF	Brain-derived neurotrophic factor
BIA	Bioelectrical impedance analysis
BIANCA	Brain Intensity AbNormality Classification Algorithm
BMI	Body mass index
BSA	Body surface area
CAT12	Computational Anatomy Toolbox 12
CBF	Cerebral blood flow
CI	Cardiac index
$CMRO_2$	Cerebral metabolic rate of oxygen
CO	Cardiac output
COPD	Chronic obstructive pulmonary disease
CSA	Cross-sectional area
CSF	Cerebrospinal fluid
CT	Computed tomography
CV	Coefficient of variation
CVD	Cardiovascular disease
DARTEL	Diffeomorphic Anatomical Registration Through Exponentiated Lie Algebra
DEXA	Dual-energy X-ray absorptiometry
DGHPU	David Greenfield Human Physiology Unit

DHEAS	Dehydroepiandrosterone sulfate
DNA	Deoxyribonucleic acid
DTI	Diffusion tensor imaging
ECG	Electrocardiogram
EDT	Euclidean distance transform
EDV	End diastolic volume
EDVi	End diastolic volume index
EF	Ejection fraction
ELSA	English Longitudinal Study of Ageing
ESV	End systolic volume
ESVi	End systolic volume index
eTE	effective Echo time
FA	Flip angle
FAIR	Flow-alternating inversion recovery
FGFBP1	Fibroblast growth factor binding protein 1
fMRI	functional MRI
FOV	Field of view
FOXM1	Forkhead box M1
FR	Firing rate
FWHM	Full width half maximum
FSL	FMRIB software library
GLM	General linear model
GM	Grey matter
GMV	Grey matter volume
HR	Heart rate
iEMG	Intramuscular electromyography
IGF-1	Insulin-like growth factor 1
IL	Interleukin
IMAT	Intramuscular adipose tissue
J	Joules

LAX	Long axis
LCFA	Long-chain fatty acid
Lrp4	Low density lipoprotein receptor-related protein 4
LV	Left ventricular
LVGFI	Left ventricular global function index
MATLAB	Matrix laboratory
MD	Mean diffusivity
mDIXON	multipoint Dixon
miR	MicroRNA
MRC	Medical Research Council
MRI	Magnetic resonance imaging
mRNA	Messenger ribonucleic acid
MRS	Magnetic resonance spectroscopy
mtDNA	Mitochondria DNA
mTOR	Mammalian target of rapamycin
MOLLI	Modified look-locker inversion
MPRAGE	Magnetisation-prepared rapid acquisition gradient echo
MU	Motor unit
MUP	Motor unit potential
MVC	Maximum voluntary contraction
MYLK4	Myosin light chain kinase 4
NEADL	Nottingham Extended Activities of Daily Living
NHS	National health service
NFKB	Nuclear factor kappaB
NIRS	Near-infrared spectroscopy
Nm	Newton metres
NMJ	Neuromuscular junction
NNMT	Nicotinamide N-methyltransferase
NSA	Number of signal averages
OGTT	Oral glucose tolerance test

PC-MRI	Phase contrast-magnetic resonance imaging
PCr	Phosphocreatine
pH	Potential hydrogen
PHENOFRIM	Physiological phenotyping of frailty using magnetic resonance imaging
PPU	Peripheral pulse monitor
pSTAT	phosphorylated signal transducer and activator of transcription
PUMA	p53-Upregulated modulator of apoptosis
PVE	Partial volume estimate
RASM	Relative appendicular skeletal muscle mass
RCT	Randomised control trial
RNA	Ribonucleic acid
ROI	Region of interest
ROS	Reactive oxygen species
SAX	Short axis
SBM	Surface based morphometry
SD	Standard deviation
SENSE	Sensitivity encoding
SPM	Statistical Parametric Mapping 12
SPMIC	Sir Peter Mansfield Imaging Centre
SSS	Superior sagittal sinus
SV	Stroke volume
T	Tesla
TE	Time to echo
TFAM	Mitochondrial transcription factor A
TGF- β1	Transforming growth factor-β1
TI	Time to inversion
TIV	Total intracranial volume
TNF-a	Tumor necrosis factor-alpha
TR	Repetition time
TRUST	T2-Relaxation-Under-Spin-Tagging

T1	Longitudinal relaxation time
T1FFE	T1 fast field echo
T1*	Longitudinal relaxation time (inclusive of magnetic field inhomogeneities)
T2	Transverse relaxation time
T2-FLAIR	T2-weighted-fluid-attenuated inversion recovery
VBM	Voxel-based morphometry
VCG	Vectorcardiogram
VENC	Velocity encoding
VL	Vastus lateralis
WM	White matter
WMH	White matter hyperintensity
WMV	White matter volume
Y_a	Arterial oxygenation
YKL-40	Chitinase-3-like protein 1
Y_v	Venous oxygenation
2D QFLOW	Two-Dimensional Quantitative Flow
3D	Three dimensional
3T	Three Tesla
11-bHSD1	11β-Hydroxysteroid dehydrogenase type 1

Chapter One: General Introduction

1.1 Introduction

Advances in medicine and public health policy over the last 150 years have contributed to a doubling in life expectancy, which continues to increase globally. In the United Kingdom, predictions indicate that one in four adults will be aged over 65 years by the year 2050, and 20% of boys and 26% of girls born in 2019 are expected to reach their 100th birthday [1]. Despite this increased longevity, the average amount of years spent in poor health is increasing, as healthy life expectancy (the length of time we can expect to live in a healthy, disease-free state) has not kept pace with the extension of life span. In the period from 2009–2011 to 2016–2018, life expectancy in the United Kingdom increased by for males and females by 0.8 years and 0.6 years, respectively. In contrast, healthy life expectancy for males increased by 0.4 years, and for females it actually decreased by 0.2 years in this same period [2]. Due to this discordance between healthy life expectancy and life span extension over decades, older males and females now spend an average of 16.5 years and 19.8 years in ill health, respectively, with multimorbidity and frailty major contributors to poor health in old age.

Frailty is an age-related clinical syndrome characterised by an enhanced vulnerability to adverse health outcomes and death when compared to the non-frail state [3]. In a systematic review of data derived from 62 countries and >1.7 million individuals, O'Caoimh et al., reported a global frailty prevalence of between 12% and 24%, depending on the method of frailty assessment used [4]. The transition from health to frailty is a crucial factor in the loss of independence in old age. As such, the impact on health and social care services of an ageing population has led the United Kingdom government to set a target of adults spending 5 more years in independent living by 2035. Hence, understanding the factors underpinning the progression to frailty and

developing interventions and approaches to mitigate this progression will be fundamental in achieving this target.

The aim of this Chapter was to outline the current definitions and presentations of frailty, followed by the physiological characteristics of frailty from an organ/systems-based perspective to determine if the syndrome harbours a distinct physiological phenotype. Evidence surrounding increased systemic inflammation, greater physical inactivity, and sedentary behaviour, with consequent increased adiposity, was assessed as potential mechanisms of frailty development. A perspective on the major knowledge gaps in the understanding of the physiological characteristics of frailty, and how this thesis will aim to address the gaps, will form the conclusion of the Chapter. All abbreviations used in this Chapter are outlined on pages 13-17.

1.2 Current definitions of frailty

A consensus group has defined frailty as “a medical syndrome with multiple causes and contributors that is characterised by diminished strength, endurance, and reduced physiologic function that increases an individual’s vulnerability for developing increased dependency and/or death” [3]. Importantly, frailty is conceptually different from, but distinctly related to, ageing, comorbidity, and disability [5, 6]. For example, in a cross-sectional study of 740 older community-dwelling individuals, 29.1% of those with frailty had ADL disabilities, and 81.8% had at least one comorbidity [6]. These findings underpin the difficulties in producing an exact frailty definition by portraying that frailty can present alongside, and potentially be a consequence of, disability and comorbidity, but may also occur in the absence of these conditions. The absence of detailed physiological insight relating to the syndrome likely contributes to the current lack of understanding of frailty aetiology and development.

Despite this poor understanding, numerous studies have demonstrated that frailty is strongly associated with an increased risk of negative events, such as falls, hospitalisation, and mortality [7, 8]. Furthermore, some signs and symptoms appear essential for describing the frailty state, the most important of which may be the deterioration of physical function. For example, diminished performance in measures such as skeletal muscle strength, mobility, and ADL, is highly predictive of frailty presence [9]. Conceptually, frailty development involves decreases in functional capacity following a stressor event (e.g., a minor acute illness or fall), with this capacity then remaining impaired relative to baseline following recovery from the stressor [10] (**Figure 1.1**). Progressively decreasing functional capacity instigates a cascade of functional decline resulting in frailty, whereby an individual loses independence and becomes at significantly increased risk of disability, morbidity, and mortality [11, 12].

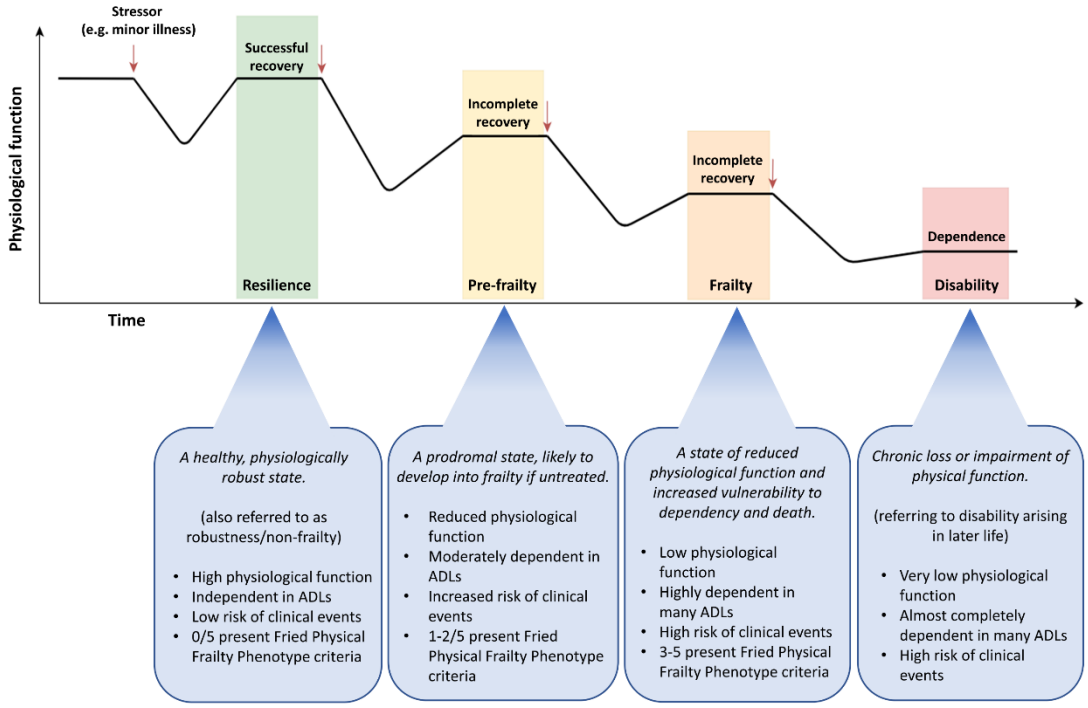

Figure 1.1: *Key stages of frailty development. The cascade of functional decline in older adults from a resilient (non-frail) state through to frailty and disability (in the absence of intervention). Figure adapted from Ref. [10], with permission under the Creative Commons license: https://creativecommons.org/licenses/by/4.0/.*

The heterogeneous nature of frailty (i.e., a syndrome with multiple causes and contributors) has led to the syndrome being likened with other frameworks aiming to capture the heterogeneity of the ageing process, such as the concepts of intrinsic capacity and resilience. The World Health Organization introduced intrinsic capacity, defined as the composite of all the physical and mental capacities that individuals can draw on at any point in their life, as a framework to monitor ageing and functional ability over time [13]. Intrinsic capacity is assessed using a combination of questionnaires, functional tests and clinical presentations, which are grouped into five domains: locomotion, cognition, vitality, psychological capacity and sensory capacity [14], Similarly to frailty, intrinsic capacity is a dynamic construct, as lifestyle factors and

stressor events can negatively impact the trajectory of intrinsic capacity [15] (akin to the progression of frailty following stressors) and the framework can be used to effectively predict negative outcomes (e.g., functional decline and falls) in older adults [16]. Furthermore, intrinsic capacity assessments share similar components to frailty measurement tools, such as handgrip strength and gait speed - criteria outlined in Fried's Physical Frailty Phenotype [17]. Emerging research indicates frailty and intrinsic capacity are interrelated constructs. For example, in a 2-year longitudinal study of older adults, intrinsic capacity impairments were observed in 93.3% of frail adults at baseline, and impairments in the domains of locomotion (odds ratio: 3.6) and vitality (odds ratio: 3.0) were associated with a higher possibility of progression from non-frailty to frailty at follow-up [18]. However, it is important to state that intrinsic capacity and frailty are distinct constructs. Intrinsic capacity aims to measure capacities of the individual longitudinally in a community-based setting as a monitoring tool, whereas frailty determines the accumulation of deficits and responses to stressors (**Figure 1.1**) in a person, and is usually assessed cross-sectionally in a clinical setting. Resilience is another concept similar to frailty, defined by an individual's ability to cope with recover from stressors, which may present better comparisons to frailty than intrinsic capacity, given both frailty and resilience definitions are centred around a disruption of homeostasis. The relationship between resilience and frailty, and how these two constructs can be studied, is discussed later in this Chapter (Section 1.6).

1.3 Frailty assessment

Although typically present, functional decline is not the only clear presentation of a frail individual. Instead, frailty is often defined by multiple measures of functional decline. This has been operationalised by Fried et al., [17] as the concurrent presence of three

or more of the following criteria: low handgrip strength, slow walking speed, exhaustion, low physical activity levels, and unintentional weight loss - termed the Physical Frailty Phenotype [17]. These authors also defined a state of pre-frailty, when one or two criteria are present, which identifies individuals at increased risk of becoming frail [17]. The Physical Frailty Phenotype is the current recommended international standard for frailty identification and assessment, as concluded by a working group of subject-matter experts in the field of frailty [10]. An alternative framework for the identification of frailty has been proposed by Mitnitski et al., [19] which concerns deficit accumulation to determine the presence of frailty by employing a Frailty Index, which is calculated by considering several (usually 40 or more) potential deficits (e.g., age-related symptoms, signs, and diseases). Despite numerous methods of frailty assessment (evidence indicating over 50 [20]), the Physical Frailty Phenotype and Frailty Index are the two most cited frailty assessment tools within the literature [21], with both validated as predictive of clinically important outcomes (e.g., hospitalisation, mortality) [22].

Due to an incomplete understanding of the associated pathophysiology of frailty, the syndrome is currently operationalised by measured outcomes rather than underlying physiological or biological drivers of these outcomes. This lack of pathophysiological insight limits the development of interventions to mitigate and reverse the syndrome's progression, which is particularly important given frailty is dynamic state with potential for reversal [23-25]. Therefore, a clear goal for emerging frailty research has been to elucidate the syndrome's physiological characteristics and improve subsequent treatment options to combat frailty development.

1.4 The physiological phenotype of frailty

The term “phenotype” has been defined as “the observable traits of the organism,” which encompasses various characteristics such as morphology, physiology, and behaviour [26]. The physiological phenotype of a human can be influenced and altered by disease and degenerative syndromes, resulting in measurable differences between healthy and disordered states. The condition of sarcopenia, defined as the loss of skeletal muscle mass, quality, and function with age [27], is one example of a syndrome that can negatively influence the physiological phenotype of a person through various mechanisms of skeletal muscle deterioration, which in turn leads to observable presentations such as functional decline. Elucidating precisely how states of health and disorder differ will aid in identifying biological targets for interventions to combat medical conditions and provide greater understanding of the aetiology and pathophysiology of complex conditions such as frailty. As such, given that people with frailty are at increased risk of adverse events, focus should be applied to the identification of a distinct physiological phenotype differentiating frail from non-frail states. Comprehensively characterising the frailty phenotype would undoubtedly aid in developing strategically targeted interventions against the condition by highlighting typical locations and features of dysregulation.

1.5 The physiological phenotype of frailty – the resting state condition

Characterising the physiological phenotype of frailty in humans is a challenging prospect. Phenotyping in this way requires intuitive methods to encapsulate complex physiological variables in conjunction with investigations into how different organs and physiological processes interact and affect each other. Further, greater mechanistic insight would require well designed longitudinal studies investigating temporal relationships between frailty development and underlying physiological changes. In

the ideal scenario, the most robust characterisation would require integrative modelling of individual component parts to predict the overall collective response, i.e., the physiological phenotype. However, despite an in increase in the research focus on frailty in recent years, this level of insight is far from being achieved. The majority of studies have incorporated assessments of physiological characteristics in individual organs under resting-state conditions, which seems inappropriate considering frailty seems to be best characterised by a decline in functional capacity and adverse response to stressors. Nonetheless, the following sections review six physiological systems that potentially contribute to the physiological phenotype of frailty, namely, skeletal muscle, the neuromuscular junction and motor unit, the brain, cardiovascular systems, adiposity and subsequently, multisystem dysregulation. A summary of the physiological characteristics of the frailty phenotype, based on current findings, is presented in **Figure 1.2**.

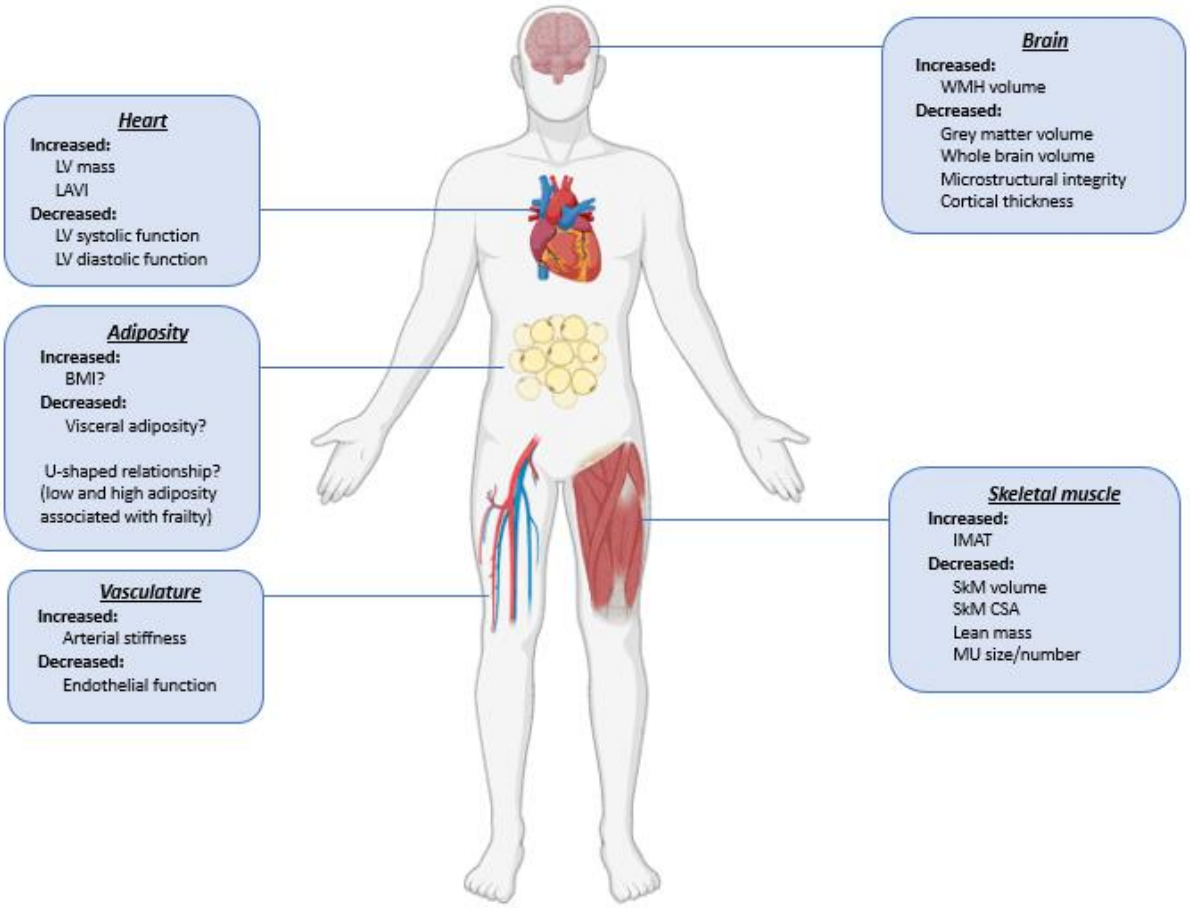

Figure 1.2: *Summary of the physiological characteristics of a frail person (compared to a non-frail person), from an organ/systems-based perspective. BMI, body mass index; CSA, cross-sectional area; IL-10, interleukin 10; IMAT, intramuscular adipose tissue; LAVI, left atrial volume index; LV, left ventricular; MU, motor unit; SkM, skeletal muscle; WMH, white matter hyperintensity. Image created with BioRender.com, with permission.*

1.5.1 Skeletal muscle

Frailty is an age-related syndrome and ageing is accompanied by a loss of skeletal muscle mass [28], which oftens results in sarcopenia [27, 29]. Sarcopenia reduces insulin sensitivity [30] and promotes deconditioning and the associated loss of mitochondrial mass [31]. These observations point to age-related changes in lifestyle factors (e.g., physical inactivity) inducing these muscle-level changes, particularly as prescribed, supervised exercise intervention can at least partly restore muscle mass and function [32] and mitochondrial mass [33], even in frail very old people [34].

Sarcopenia also influences functional deficits associated with frailty, such as a loss of mobility, diminished strength, and a greater risk of bone fractures [35, 36]. Therefore, loss of skeletal muscle mass and quality likely contributes to frailty development. Appropriately, frailty and sarcopenia are linked, but distinct, correlates of musculoskeletal ageing. This is evidenced by overlap, but incomplete concurrence, in frailty and sarcopenia prevalence in older persons. For example, one study of 100 older females reported that sarcopenia and frailty were concurrently present in 19% of participants [37]. Nonetheless, the interrelated nature of frailty and sarcopenia makes it essential to consider skeletal muscle characteristics as contributing factors toward the frailty phenotype (**Figure 1.2**).

1.5.1.1 Whole body lean mass

DEXA is an X-ray scanning modality permitting the quantification of lean tissue mass (a composite of non-fat and non-bone tissue) and fat mass at a regional or whole-body level. Similarly, BIA assesses lean and fat masses based on the notion that lipid-rich adipose tissue is more resistant to the passage of an electrical current compared with tissues rich in water (e.g., muscle tissue). Although DEXA and BIA do not provide direct measures of muscle mass, they are routinely employed in studies of ageing, with lean tissue mass observed to decrease with advancing age [38]. For example, in a longitudinal study of ageing, Koster et al., [39] reported that the loss of leg lean muscle mass occurred at a rate of 0.7–0.8% per years during a 7-year follow-up of individuals in their 70s. Moreover, lean mass reductions with age have been associated with traits of frailty, including lower physical function and quality of life [27, 40] and can be used as a predictor of mortality [41]. Together, these findings justify the use of lean mass as a valid physiological variable and indicate lean tissue estimates derived from BIA and

DEXA modalities may have utility in investigating skeletal muscle characteristics during frailty.

Concerning studies defining frailty with the Physical Frailty Phenotype [17], lower whole body lean mass has been observed in pre-frail and frail individuals compared with non-frail counterparts following DEXA assessments [42]. In a study of 1,839 older Taiwanese adults, frail participants exhibited significantly lower total body and appendicular lean mass compared with pre-frail and non-frail adults [43]. Similarly, BIA assessments in 220 older adults revealed whole body lean mass was significantly lower in frail and pre-frail compared with non-frail older males and females [44]. However, these findings have been contradicted by others reporting no differences in appendicular lean mass across non-frail, pre-frail, and frail groups in a study of 250 older women [45]. Therefore, although several studies point to lower lean mass in frail versus non-frail individuals, this finding is not always reported.

1.5.1.2 Skeletal muscle cross-sectional area

As outlined above, DEXA and BIA do not directly quantify muscle mass, which may contribute to the variance in study outcomes focused on muscle mass. More robust measures of skeletal muscle quantity include muscle volume and CSA, which can be directly quantified with imaging methods such as MRI and CT. The methods are considered the gold standard for muscle volume and CSA measurement, due to their excellent accuracy compared with cadaver analysis ($r = 0.99$) [46] and have been utilised to demonstrate lower muscle volume and CSA in older compared to younger adults [47, 48].

There are few studies utilising MRI and CT to quantify muscle volume in frail individuals, with CSA measures being adopted most often in studies of muscle quantity

in frailty. One study reported 6.4% lower thigh muscle CSA (expressed as the percentage of muscle vs IMAT in the thigh) in frail compared with non-frail males and females when quantified by MRI [49]. Similarly, lower MRI-derived quadriceps muscle CSA has been observed frail haemodialysis patients compared to non-frail counterparts [50]. However, the adoption of different frailty classification criteria hinders comparisons across these studies. Nonetheless, studies using CT to assess muscle CSA have also reported lower skeletal muscle quantity in frailty. In a study of 923 participants, frail individuals exhibited significantly lower muscle calf areas compared to those without frailty [51]. A smaller thigh muscle CSA in frail compared with non-frail nonagenarians has also been reported following CT assessments [52]. It should be noted, however, that lower skeletal muscle CSA has not always been reported in frail versus non-frail individuals. For example, one study assessing calf muscle CSA with MRI observed similar values when comparing non-frail (n = 12) and frail (n = 11) individuals [53]. These discrepancies demonstrate the need for further application of imaging methodologies to definitively identify the skeletal muscle characteristics of frail individuals. In particular, it appears that previous studies adopting CT and MRI have quantified skeletal muscle CSA, which only provides an estimate of muscle area within a specific region and therefore may not be indicative of whole muscle volume. Assessments of whole muscle volume are required in future studies employing imaging techniques to provide insight into the associations between frailty and loss of skeletal muscle volume. This greater validity is fundamental in identifying muscle groups that could then be targeted with future interventions (e.g., exercise training). For example, if regional differences in muscle volume are apparent during frailty, areas more prone to the loss of mass and quality would be key targets for interventions.

1.5.1.3 Skeletal muscle quality

The quantity of skeletal muscle (i.e., CSA or volume) may not be the only important muscle-related physiological parameter within the context of frailty. The quality of skeletal muscle, which can be assessed with metrics such as IMAT, aerobic capacity and functional quality of the muscle, diminishes with ageing and is associated with impaired muscle function and mobility [35]. Therefore, lower muscle quality may be associated with frailty and contribute to the lower functional capacity observed in frail versus non-frail individuals [54]. Findings from a recent multicomponent exercise intervention in older adults highlighted improvements in functional capacity, however these improvements were not mediated by alterations in muscle CSA of the lower extremities [55]. The augmentation of functional capacity evidenced in this study may therefore be attributable to enhanced muscle quality, such as improved aerobic capacity underpinned by increased mitochondrial mass, which would be consistent with the physiological adaptations induced by endurance exercise training intervention in older people [33, 56]. This finding reinforces the notion that muscle quality maybe related to frailty and functional capacity.

In addition to the muscle volume assessments permitted by MRI, this technique also provides a non-invasive and accurate method for measurement of skeletal muscle quality, through the quantification of IMAT. Melville et al., [57] used MR spectroscopy to highlight greater IMAT content in the vastus lateralis and medialis of pre-frail and frail individuals compared with non-frail counterparts. However, the combination of pre-frail and frail participants into a single group for analysis potentially blunted contrast between groups in this study [57]. Greater IMAT in frail adults has also been reported by others using MRI methods. Addison et al., [49] observed significantly greater IMAT in the thigh muscles of frail compared with non-frail males and females. Similar

findings were also observed in a study utilising MRI, in which frail individuals exhibited 30% (expressed as a percentage of total muscle area) greater IMAT CSA of the calf muscles compared with non-frail counterparts [53]. Altogether, the limited number of studies assessing IMAT point to greater lipid infiltration within the skeletal muscle during frailty. The validity of these findings, however, may be impacted by the lack of stratification between sexes prior to analyses [49, 53], which is an important consideration given the reported differences in IMAT between older males and females [58]. It should also be acknowledged that these previous studies quantified IMAT from either a partial cross section within the calves or thighs [49, 53], or from a 2 cm^3 ROI in the mid portion of each quadriceps muscle [57]. Therefore, these assessments may not reflect IMAT content within the whole muscle. Future work should therefore perform assessments of whole muscle IMAT to improve the validity of findings from these previous studies.

The functional quality of the muscle is another measure of skeletal muscle quality, which measures the force producing capacity of the muscle per unit of muscle volume or mass. Functional quality reflects the metabolic quality of the skeletal muscle, as force production is normalised to the amount of muscle, as opposed to strength measurements whereby force output from the whole muscle is quantified, thus is a function of muscle mass. Lower functional quality of the knee extensors has been observed in frail compared to non-frail individuals in a previous study [59], thus pointing to lower metabolic quality of skeletal muscle in frail versus non-frail individuals. However, this study adopted DEXA-derived estimates of lean mass [59], which is not a direct measure of muscle mass, thus further work utilising direct MRI-derived whole muscle volume measurements are required to provide a more robust characterisation of muscle functional quality during frailty.

1.5.1.4 Potential mechanisms of skeletal muscle deterioration in frailty

Several age-related mechanisms potentially contribute to the reported lower skeletal muscle mass, quality, and function in frailty. Sarcopenia is considered to be a core component of frailty [60], with this notion supported by reports of overlap in the presence of sarcopenia and frailty [37]. As such, the deterioration of skeletal muscle mediated by sarcopenia may underpin lower muscle mass and quality in frailty. However, definitive longitudinal data in humans are missing.

1.5.1.4.1 Anabolic resistance

Anabolic resistance is one mechanism proposed to influence the loss of muscle mass with ageing, which relates to the inability of feeding and/or exercise to stimulate muscle protein synthesis or inhibit muscle protein breakdown to the same extent as that seen in young individuals. Seminal research in this area utilised stable isotope tracer infusion methods to investigate protein turnover in healthy young and older men following essential amino acid infusion, thereby avoiding any age-related impact on gut amino acid absorption [61]. The authors reported a blunting of muscle protein synthesis in response to infusion of essential amino acids in older versus young participants. Furthermore, enhanced phosphorylation of anabolic signalling proteins thought to regulate muscle protein translation initiation, such as mTOR, was also lower in the older volunteers in response to essential amino acid infusion, indicating that impaired muscle nutrient sensing, rather than nutrient availability, was driving the lower muscle protein synthetic response [61]. Similarly, other authors have reported a diminished muscle protein synthetic response, synonymous with a blunting of the exercise-induced increase in phosphorylation of anabolic signalling molecules, following acute resistance exercise in older compared with young men [62]. Notably,

in a study that quantified muscle protein synthesis over the course of a 6-week resistance exercise intervention, chronic muscle protein synthesis was reportedly diminished in healthy older compared with young volunteers [63]. Furthermore, this was accompanied by a blunted muscle hypertrophic response to the training intervention in the older volunteers, which appeared to reflect lower ribosomal biogenesis and translational efficiency and lower blood anabolic hormone concentrations [63]. It is currently unknown whether the extent of anabolic resistance is greater in older frail adults compared with non-frail older adults or whether anabolic resistance is a feature of ageing per se and/or occurs secondary to factors that accompany ageing such as decreased physical activity levels. Nevertheless, the consensus is that reduced muscle protein synthesis, as opposed to increased muscle protein breakdown, is the primary driver of anabolic resistance in older people [64].

1.5.1.4.2 Inflammation

Greater IL-6 mRNA and protein content in the vastus lateralis muscle has been observed in nonobese frail individuals compared with non-frail individuals, purportedly due to the release of proinflammatory cytokines from greater amounts of IMAT in the frail individuals [49]. These authors concluded that this intramuscular adipose tissue-inflammatory axis provided a potential link between intramuscular adiposity and decreased muscle mass and mobility function in frailty. However, parallel associations involving muscle TNF-a were not observed. Nevertheless, potential processes underlying inflammation-mediated muscle loss include exacerbation of anabolic resistance by downregulated muscle anabolic signalling. For example, atrophy of rodent skeletal muscle is induced following intramuscular IL-6 infusion at concentrations consistent with chronic inflammation [65]. Further, atrophy was accompanied by a 60% reduction in the phosphorylation of ribosomal S6 kinase, 33%

reduction of pSTAT5, and a two-fold increase in pSTAT3. This effect is likely mediated through reduced IGF-1, as transgenic overexpression of IL-6 in mice results in reduced serum IGF-1 levels, possibly due to increased proteolysis of IGF-1 binding protein 3 or increased IGF-1 clearance [66]. Accordingly, lower serum IGF-1 concentrations have been observed in frail individuals with low RASM compared with frail persons with normal RASM [67], reinforcing the notion that muscle loss may be mediated by inflammation during frailty.

Another potential mechanism underlying age-related muscle loss relates to the increasing levels of circulating TNF-a with advancing age. This pro-inflammatory cytokine induces upregulation of 11-bHSD1 in skeletal muscle, in turn increasing local generation of the catabolic steroid cortisol. Importantly, 11-bHSD1 expression in muscle increases with age in women and is negatively correlated with hand grip strength [68]. Taken together, these findings highlight possible mechanisms by which inflammation may induce muscle mass loss during frailty, by impairing muscle regeneration and anabolic processes. However, it remains unclear whether these muscle-level characteristics are drivers of muscle deterioration in frailty or a consequence of it.

1.5.1.4.3 Physical inactivity

Another likely important driver of muscle atrophy and impaired muscle quality in frailty is physical inactivity. This is evidenced by lower step counts and greater sedentary behaviour in frail adults [69-71], which potentially contributes to increased muscle anabolic resistance [72]. Physical activity levels typically decline with advancing age [73], however cross-sectional studies investigating muscle mass and functional decline with age have rarely controlled for differences in physical activity levels across

age groups. In this context, therefore, data from studies of episodic periods of increased bed rest are informative, and this will likely induce a greater physiological burden than reduced step count [74]. Ten days of bed rest in older individuals has been shown to induce a loss of ~1-kg of lean mass from the lower extremities and a 16% decline in knee extensor strength, with these effects attributed to a 30% reduction in muscle protein synthesis [75]. A metanalysis of human transcriptomic data from studies of disuse or bed rest (~7 days) revealed significant increases in transcripts involved in protein ubiquitination, immune signalling, and apoptosis, in conjunction with downregulation of genes involved in mitochondrial organisation and metabolic function [76], which is consistent with transcriptomics data from studies of frail persons [77]. Other studies further highlight bed rest-induced reductions in skeletal muscle protein synthesis that may underpin muscle atrophy and functional losses [78, 79]. Accordingly, these findings indicate the increased burden of bed rest and illness may explain why hospitalisation can transition an older person from the non-frail to the frail state [8, 80]. Whether bed rest induces increased muscle mass loss and functional decline in an already frail person is currently unknown but warrants consideration.

1.5.2 The neuromuscular junction and motor unit

The size and function of the MU (the motor neuron and all fibres it innervates) have become a recent focus of ageing research, and it has been proposed that muscle fibre atrophy and loss promote age-related sarcopenia [81]. The iEMG technique enables the quantification of human MU characteristics. In brief, the technique involves the insertion of a needle electrode into the muscle of interest (e.g., the vastus lateralis or tibialis anterior) during isometric contractions. The needle electrode samples electrical signals produced from action potentials within the muscle fibres during contraction to quantify the MUP, which reflects the sum of signal produced from action potentials.

The size of an MUP is proportional to the number of fibres contributing to it [82] and therefore, as outlined in **Figure 1.3**, MUP size is indicative of MU size.

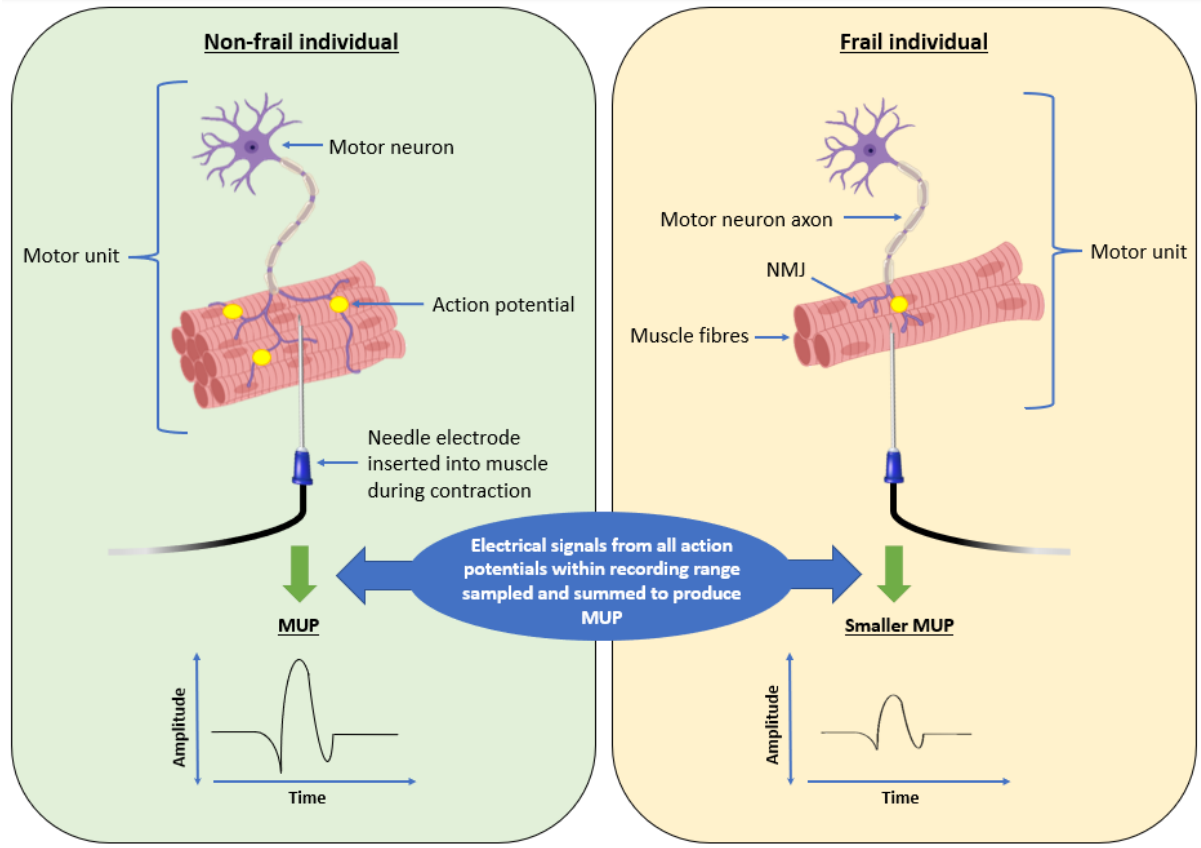

Figure 1.3: *Neuromuscular function in frailty. Schematic overview of the measurement of motor unit potential (MUP) by intramuscular electromyography. Frailty (right panel) is associated with a smaller MUP compared to the non-frail state (left panel), thought to arise from smaller motor units. NMJ, neuromuscular junction.*

Distinct reorganisation of MU fibres is observed with advancing age (for a comprehensive review of ageing effects on the MU and neuromuscular junction (NMJ) see Ref. [83]), which precedes the grouping of muscle fibre types and localised atrophy [84-86]. Reorganisation has been demonstrated by an increase in MU size with age [87, 88], which proposedly results from branching of nearby motor neurons to reinnervate denervated fibres [89, 90]. Morphological changes also occur within the NMJ, with findings from electron and light microscopy techniques highlighting an

expansion of the junction perimeter along fibres and more complex branching of the nerve terminal with the synaptic site [91, 92]. These morphological changes may occur as compensatory mechanisms following a gradual loss of motoneurons during ageing due to denervation. In this way, an age-associated reduction in myelinated neurons has been illustrated in human peripheral nerves [93, 94], suggesting that denervation is promoted by ageing (**Figure 1.3**). In parallel with morphological alterations, age-related neuromuscular deterioration has also been inferred from the lower MU firing rate observed by iEMG in the vastus lateralis of older versus younger men [88], suggesting the function of MUs declines with age. Furthermore, by combining iEMG measures with muscle CSA measurements, this study demonstrated that older males had 50–60% fewer MUs [88].

In contrast to the age-related increase in MUP size [88] smaller MUPs have been reported in sarcopenic versus non-sarcopenic individuals during voluntary muscle contractions [81], suggesting that reinnervation of denervated fibres occurs to expand MU size in the muscle during healthy ageing but not during sarcopenia [81]. Building on these findings, a recent study demonstrated smaller MUP size in the vastus lateralis of frail versus non-frail males during isometric contractions, independent of age and BMI [95]. These results suggest that frailty exacerbates the loss of MU size compared to normal ageing, which may reflect a failure of reinnervation of denervated fibres. This is the only study to assess MU size in frail individuals and the sample adopted was comprised of males only [95]. Considering MU characteristics, such as MU firing rate and firing rate variability, have been shown to be different between males and females [96], further investigation into MU characteristics in frail females is required. Further investigations are also required as smaller MU size has been linked to lower functional performance (e.g., skeletal muscle strength and power) during ageing [97]. Therefore,

the lower MU size in frail versus non-frail males may be related to impaired functional performance during frailty [54]. This notion is reinforced by the findings of greater muscle fibre reinnervation capacity in master athletes compared to pre-frail and frail individuals, with the master athletes also performing better on measures of physical function, such as gait speed and timed up and go test assessments [98].

1.5.2.1 Potential mechanisms for neuromuscular junction and motor unit deterioration during frailty

The mechanisms underlying NMJ and MU deterioration with age are complex and remain poorly understood. DNA damage and modification during ageing are proposed mechanisms of NMJ functional deterioration and motoneuron loss, producing the aged neuromuscular phenotype [99]. Apoptotic cell death of spinal motoneurons occurs following treatment with neurotoxic intermediates of glycation, suggesting that byproducts of glycation may also contribute to motoneuron degeneration [100]. Furthermore, the absence of several molecules involved in NMJ formation and maintenance appears to produce pre- and post-synaptic alterations in aged muscle. Genetic deletion of the molecule agrin (a molecule involved in the formation of synapses between neurons) [101, 102], or its muscle receptor Lrp4 [103, 104], results in degeneration of motor axon terminals and subsequent partial or complete endplate denervation, indicating that effects on these molecules may contribute to NMJ deterioration (**Figure 1.3**).

Within the context of frailty, the relationship between MU characteristics and plasma concentrations of anabolic hormones has been investigated, with one study highlighting that greater free testosterone was associated with greater MU size (regression coefficient: 0.30; $P = 0.009$) in frail individuals, when adjusted for age, BMI

and diabetes [105]. When taken with the earlier reports of lower MU size in frail versus non-frail males [95], this finding suggests that lower androgen availability may contribute to MU degeneration in frailty. Accordingly, a rodent model of spinal cord injury provides mechanistic insight by illustrating that atrophy of motor unit dendrites and muscle fibres was prevented by four weeks of subcutaneous testosterone administration at normal physiological concentrations [106]. Similarly, testosterone administration has been shown to mitigate motor neuron atrophy following castration in male adult rats [107, 108]. Thus, hypogonadism during frailty may contribute to the associated decline in MU size and number.

1.5.3 The brain

Various changes in brain structure and function are associated with ageing. Age-related structural changes include atrophy of global and regional brain volumes, cortical thinning, and an increase in the presence and volume of white matter lesions (also termed WMHs), which have been linked with cognitive decline [109], whereas functional alterations include reductions in cerebral blood flow [110] and oxygenation [111]. Incidence of brain-related diseases such as Alzheimer's and other dementias also increases with age [112]. Frailty is similarly associated with an increased risk of cognitive decline and dementia [113-116], suggesting that alterations in structural and haemodynamic parameters of brain may contribute to the physiological phenotype of frailty. A summary of structural brain changes associated with frailty is presented in **Figure 1.2**. **Figure 1.4** outlines established MRI techniques currently being employed to study brain structure and function and how these measures have been applied to the study of frailty.

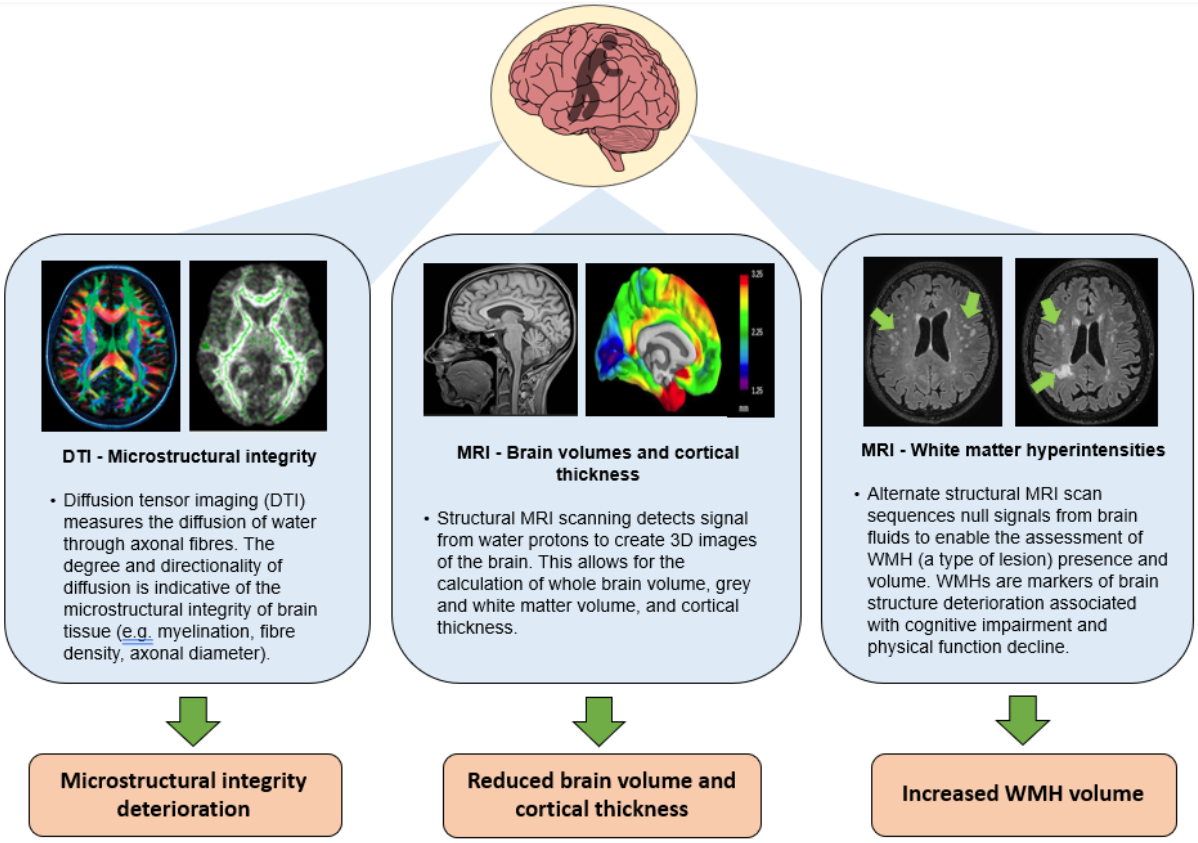

Figure 1.4: *Schematic overview of magnetic resonance imaging (MRI) techniques currently being used to quantify brain architecture in frailty. DTI, diffusion tensor imaging; WMH, white matter hyperintensity.*

1.5.3.1 Global brain volumes

Early studies related to frailty highlighted global cortical atrophy and lower grey matter volume in frail versus non-frail adults [116, 117]. However, a small sample size of frail individuals in one of these studies resulted in the combination of pre-frail and frail participants into a single group, possibly reducing the contrast between this group and non-frail individuals during analysis [116]. Further, the use of different frailty assessments across these studies makes comparisons difficult. More recent studies adopting the Physical Frailty Phenotype assessment [17] have provided better insight. Kant et al., [118] reported lower total brain volume and grey matter volume in frail compared with pre-frail and non-frail older adults. However, no differences were

observed between pre-frail and non-frail states [118]. Adopting a similar MRI scan sequence, another study also observed significantly lower total brain volume in frail versus non-frail subjects [119]. These findings indicate the presence of global grey matter atrophy during frailty (**Figure 1.4**), although given evidence is currently limited to cross-sectional associations, it is unknown whether associations are causative or a consequence of frailty.

Global white matter volume has also been assessed in previous studies, although in contrast to the findings of lower grey matter volume, studies have reported no differences in global white matter volumes between non-frail, pre-frail and frail states [116, 118]. The tissue composition of grey and white matter differs, in that grey matter in mainly comprised of neuronal cell bodies and dendrites involved in processing electrical and chemical signals in the brain, whereas white matter is primarily composed of myelinated axons which are fundamental for the transmission of electrical signals across different brain regions [120]. Therefore, the lower grey matter volumes in frail versus non-frail individuals points to the shrinkage (as opposed to loss) of neuronal cells, given shrinking of neurons drives the loss of grey matter volume in ageing [109, 121], whereas the lack of differences in white matter volume indicates that myelinated axons are not affected during frailty. One consideration of these previous studies the adoption of mixed sex participant samples [116, 118]. As sex-related differences in global brain volumes have been observed previously [122], further study of global brain volumes in samples of frail individuals stratified by sex are required.

1.5.3.2 Regional brain volumes

In addition to assessments of global brain volumes, a small number of studies have investigated relationships between regional grey matter volumes and frailty. In a study of over 40,000 individuals, frailty severity was negatively associated with grey matter volumes in 75 brain regions (Cohen's d = 0.027 – 0.082, P < 0.01), including the thalamus, hippocampus and cerebellum [123]. The large sample size in this study provides strong evidence that frailty is associated with lower regional grey matter volumes. Similarly, lower grey matter volume in several brain regions such as the cerebellum and supplementary motor area has been observed in a collapsed group of pre-frail and frail individuals versus non-frail counterparts in another previous study [116].

Whilst studies have evidenced lower regional grey matter volumes in frail versus non-frail individuals, regional assessments of white matter volumes have not been performed. As outlined in the previous Section (Section 1.5.3.1), investigations of white matter are important to provide information of myelinated axons which enable electrical and chemical signalling within the brain. Furthermore, lower white matter volume in numerous brain regions, such as the hippocampus (t = 3.72, P < 0.001) and precentral gyrus (t = 3.36, P < 0.001), has been associated with older age [124]. Therefore, further studies should determine if regional white matter atrophy is observed during frailty when compared to normal ageing.

1.5.3.3 Associations between regional brain volume and physical function

Some studies investigating regional brain volumes in frailty studies have also determined associations between grey matter volume and functional traits of frailty, such as low handgrip strength and slow walking speed [116, 125]. For example, grey

matter volume in several brain regions, such as the hippocampus, have been negatively associated with handgrip strength (t = 4.0, $P < 0.001$) and walking speed (t = 5.0, $P < 0.001$) in a study of non-frail, pre-frail and frail individuals [125]. Furthermore, grey matter volume of the cerebellum has also been negatively associated with walking speed (t = 4.31, $P < 0.05$) in a sample of non-frail, pre-frail and frail individuals [116]. These findings indicate that alterations in brain structure may be related to functional decline during frailty, particularly as these associations between brain atrophy and functional impairments have been observed in regions of the brain responsible for motor functions, such as the cerebellum. However, regional volume relationships are currently limited to grey matter volumes, leaving associations between other structural indices of the brain, such as white matter volume, and functional capacity in frail individuals to be explored. In a previous 2.5 year longitudinal study of older adults, atrophy of white matter has been associated with greater decline in gait speed (regression coefficient: = 0.25, $P < 0.001$) [126]. This suggests white matter atrophy may be related to functional deterioration in frail individuals, which should be explored in future research.

1.5.3.4 Cortical thickness

The distance between the outer cortical surface and the grey-white matter boundary is termed cortical thickness [127] and is another structural marker of grey matter volume quantified by MRI (**Figure 1.4**). Cortical thinning in several brain regions has been noted during ageing [127-129] and within individuals with Alzheimer's disease [130]. Thus, cortical thickness has been proposed as a valid biomarker of neurodegeneration [131].

Few studies have assessed the relationship between cortical thickness and frailty. A recent cross-sectional analysis study reported lower cortical thickness in pre-frail versus non-frail individuals but no differences between the frail and non-frail groups [132]. Whilst this finding indicates that pre-frailty, but not frailty, is associated with lower cortical thickness compared to healthy ageing, the sample size of frail individuals (n = 12) was markedly lower compared to the number of pre-frail (n = 200) and non-frail (n = 272) individuals recruited, which the authors acknowledged compromised the statistical power of the analyses. This conveys the need for further studies to confirm the relationship between frailty and cortical thickness.

1.5.3.5 Gyrification and sulcus depth

MRI also permits the assessment of cortical folding measures, including gyrification and sulcus depth, with surface-based morphometry. Gyrification refers to the degree of folding of gyri on the cortical surface and sulcus depth is defined as the distance between the cortical surface and the cerebral hull. Cortical surface folding is proposed to occur to increase the cortical surface area within the confines of the skull, thus increasing the number of neurons and neuronal connectivity [133]. As such, gyrification has been strongly correlated with cortical surface area ($r = 0.92$; $P < 0.001$) [134]. There are no previous reports quantifying gyrification and sulcus depth in frail individuals. However, assessment of these parameters is important as previous studies have demonstrated an inverse association between age and gyrification in brain regions such as the pre-frontal cortex ($r = -0.13$; $P = 0.0004$) and negative associations between regional gyrification and cognitive function ($r = -0.13$; $P < 0.0003$) [135]. Similarly, a reduction in sulcus depth of the parieto-occipital brain region has been observed in a 5 year longitudinal study of older adults [136] and lower sulcus depth has been observed in cognitively impaired older individuals versus healthy

controls [137]. Therefore, given the higher prevalence of cognitive impairment in frail versus non-frail individuals [138], frailty may be related to changes in gyrification and sulcus depth.

1.5.3.6 White matter hyperintensities

Lesions within brain white matter, termed WMHs, are common features of the ageing brain, with an increase in WMH volume observed with advanced age [139]. Greater WMH volume has been associated with adverse outcomes linked to frailty, such as cognitive impairment [140], slow gait [141], and lower physical function [142], indicating that these lesions may be associated with frailty.

Recent studies have attempted to clarify the relationship between WMHs and frailty when defined by the Physical Frailty Phenotype [17], with significantly greater WMH volume observed in frail and pre-frail compared with non-frail participants [119, 143]. Further, in the study utilising the UK Biobank data gathered from over 40,000 individuals, greater WMH volume was positively associated with frailty severity (Cohen's d = 0.084, P < 0.0001) [123]. Unfortunately, analysis of WMH volume between pre-frail and frail individuals was lacking in these studies, limiting insight between these two states. The findings of greater WMH volume during frailty has been corroborated in several studies adopting the Frailty Index assessment [19], with larger WMH volume shown to be related to higher Frailty Index scores [144, 145]. In addition to these findings from cross-sectional studies, prospective studies have also indicated that frailty progression is related to greater WMH volume. Ducca et al., [146] reported a 1.46 higher odds of frailty at 6.6 years follow up with each standard deviation of greater of WMH volume at baseline. However, this prospective design leaves speculation as to the actual change in WMH volume at follow up, as this was not

measured. Nonetheless, these findings provide growing evidence that frailty is associated with greater WMH volume. The logical next step is to perform longitudinal assessments to determine if frailty progression is associated with increases in WMH volume over time. WMHs may then be identified as potential targets for interventions aiming to mitigate frailty development.

1.5.3.7 Microstructural integrity

DTI is an MRI modality enabling assessment of the microstructural integrity of white and grey matter tissue by mapping the directionality of water molecule diffusion [147] (**Figure 1.4**). Common measures of diffusion assessed during DTI include fractional anisotropy (the orientation of water diffusion) and mean diffusivity (a measure of how freely water molecules move in brain tissue). Using DTI, lower white matter microstructural integrity has been demonstrated in ageing, shown by greater mean diffusivity (indicating degeneration of the tissue that prevents undirected water diffusion) in older versus young individuals [148, 149]. These findings warrant the investigation of microstructural integrity as a physiological feature of the frailty state.

Greater mean diffusivity in white matter tissue has been reported in frail versus non-frail individuals [150], with similar findings also reported in the grey matter tissue of another cohort of frail and non-frail individuals [119]. Some studies have also demonstrated prospective associations between frailty and microstructural integrity. For example, greater baseline white matter mean diffusivity in the anterior thalamic radiation has been associated with a higher risk of frailty (hazard ratio 2.3; $P = 0.017$) when assessed at a 3 year follow-up [151]. However, this prospective design did not include assessments of white matter microstructural integrity at follow up, which leaves speculation as to the actual change in mean diffusivity over time. Nonetheless, these

findings demonstrate indicate that frailty is accompanied with a loss of organised structure in brain tissue.

1.5.3.8 Cerebral blood flow, perfusion and oxygenation

Despite several investigations of structural characteristics of the brain (i.e., global and regional grey matter volumes and WMH volume) in frail individuals, reports of cerebral haemodynamic and functional parameters, such as CBF and oxygenation, are scarce, particularly those adopting imaging methods such as MRI. Lower CBF [110, 152] and cerebral oxygenation [111] has been demonstrated in older versus young individuals. Furthermore, lower CBF and oxygenation in older versus young individuals has been associated with lower cognitive function (R^2 = 0.46, P = 0.008) [152], and lower cerebral oxygenation has been observed in Alzheimer's Disease patients versus healthy counterparts [153]. As previous work has shown an inverse correlation between frailty severity and cognitive function (r = -0.58; $P < 0.05$) [154] and a higher prevalence of neurodegenerative diseases in frail versus healthy individuals (40.02 % vs 11.27 %; $P < 0.0001$) [155], CBF and cerebral oxygenation may therefore be lower in frail versus non-frail individuals.

CBF velocity has been quantified in a small number of previous studies of frailty using transcranial Doppler ultrasound of the cerebral arteries. One study reported lower CBF velocity of the left and right carotid arteries of frail compared to non-frail participants following ultrasound assessments [156]. However, despite Aguilar-Navarro et al., [156] adopting the Physical Frailty Phenotype criteria to assess frailty in their study, volunteers were classified as non-frail when one or two criteria were met, which, according to the original criteria proposed by Fried et al., [17], would classify these

participant as pre-frail. This shortcoming limits insight into the potential differences in CBF velocity between frail and healthy states.

A similar haemodynamic parameter is cerebral perfusion which refers to oxygen delivery to capillaries within the brain. Cerebral perfusion can be quantified with the ASL MRI sequence, which involves applying magnetism to “label” arterial blood before flowing into the brain, and then subsequently imaging the contrast between labelled blood and brain tissue. One study has assessed global grey matter perfusion with ASL in frail individuals, which evidenced no association between frailty and global grey matter perfusion [143]. Though this lack of differences may have been underpinned by the low sample size of frail participants adopted (n = 13), which the authors acknowledged compromised the statistical power of their analyses [143].

Regarding cerebral oxygenation, one study adopting NIRS assessments has noted no differences in cerebral oxygenation between non-frail, pre-frail and frail states [157]. A consideration of NIRS is the limited sampling range of 2 cm beneath the skull [158], therefore measurements may not be indicative of global cerebral oxygenation. Furthermore, this technique does not permit the assessment of cerebral oxygen utilisation. In contrast, the TRUST MRI technique quantifies global cerebral oxygenation by magnetically labelling venous blood within the sagittal sinus, then tracing labelled blood throughout the brain with subsequent images. The amount of magnetic signal lost (measured in subsequent images) indicates blood oxygenation levels (i.e., more signal lost from oxygenated blood indicates greater oxygenation). TRUST MRI also provides measures of global cerebral oxygen extraction fraction and metabolic rate of oxygen, which are measures of how much oxygen is extracted from the blood and metabolised in brain tissue. Studies of ageing employing TRUST have demonstrated a lower cerebral oxygenation and greater cerebral metabolic rate of

oxygen in older versus young adults [159, 160]. For example, one study reported a 1.4% decrease in cerebral oxygenation per decade of life [159]. However, TRUST MRI has not been performed in studies of frail individuals, which should be addressed in further research to provide insight the relationships between frailty and global cerebral oxygenation.

1.5.3.9 Potential mechanisms of brain deterioration in frailty

The observational nature of current research into physiological changes of the brain during frailty leaves the mechanisms of brain deterioration in frail individuals poorly understood. However, some insight can be gained from studies of older individuals.

Physical inactivity and sedentary behaviour have been proposed as potential mechanisms promoting brain atrophy and greater WMH volume. White matter atrophy has been negatively associated with sedentary behaviour time (regression coefficient: = -0.11; $P = 0.0007$) in a 5-year longitudinal study of older adults [161]. Sedentary time has also been positively correlated with WMH volume ($r = 0.31$; $P < 0.01$) in older individuals [162]. Potential mechanisms underpinning these relationships include lower CBF during sedentary time, which has been evidenced by lower CBF in individuals subjected to prolonged periods of physical inactivity, when compared to conditions of regular physical activity [163]. In this way, stenosis of the cerebral arteries and a reduction in CBF has been shown to induce cortical atrophy in gerbils [164]. Similarly, lower CBF and greater WMH volume has been observed in patients with carotid artery stenosis compared to controls [165], and restoration of cerebral blood flow by carotid artery revascularisation in these patients has resulted in a reduction in WMH volume [166]. Accordingly, frail individuals have been shown to be more physically inactive compared to non-frail counterparts [69, 70], and one study has

reported lower blood velocity in the cerebral arteries of frail versus non-frail older adults [156], which may contribute to brain atrophy and greater WMH volume. However, these indirect associational relationships across different studies require clarification with simultaneous assessments of physical inactivity, CBF and brain structure measurements in frail individuals to improve insight.

Another potential mechanism of brain atrophy is neuroinflammation, which is a common feature of ageing [167, 168] and neurodegenerative disorders such as Alzheimer's disease, Parkinson's disease, and multiple sclerosis [169]. Given frailty is an age-related syndrome associated with neurodegenerative disease [170], it seems reasonable to infer neuroinflammation may be related to deterioration of the brain in frail individuals. However, relationships between neuroinflammation and frailty have not yet been explored. Nevertheless, research combining cerebrospinal fluid sampling and brain MRI indicates that lower cognitive function is associated with greater levels of the neuroinflammatory marker YKL-40 in older adults [171]. Furthermore, a 2-year longitudinal study has reported that cerebrospinal fluid and YKL-40 concentrations are positively correlated with attenuated white matter microstructural integrity and brain atrophy of older individuals [172]. Neuroinflammation may therefore be related to brain atrophy and impairments of white matter microstructural integrity during frailty.

1.5.4 The cardiovascular system

A meta-analysis of 6,000 non-frail, 7,000 prefrail, and 1,500 frail individuals revealed frail (odds ratio = 3.4) and prefrail (odds ratio = 1.5) adults are at greater risk of CVD compared with non-frail counterparts [173], thus providing associative evidence for the role of cardiovascular dysregulation as a phenotypic feature of frailty. However, the specific alterations in cardiovascular structure and function that might contribute to

frailty remain unclear. **Figure 1.2** shows a summary of findings related to cardiac and vascular characteristics present during frailty.

1.5.4.1 Cardiac parameters

The heart undergoes various structural and functional changes during ageing, such as an increase in LV wall thickness, atrial fibrillation, and a decrease in LV ejection fraction [174]. Further, impairments in cardiac structure and function have been associated with physical function deterioration in older adults [175, 176], indicating cardiac dysregulation may contribute to frailty.

Some findings are consistent across studies investigating cardiac parameters in frail versus non-frail individuals. For example, in the Cardiovascular Health Study, frail adults exhibited greater LV mass compared to non-frail participants [177], with several other studies since reporting larger LV mass and left atrial volume index in frail compared with non-frail individuals [178-180]. Despite these common findings, discrepancies are evident for numerous other cardiac parameters during frailty. For example, lower LV ejection fraction has been observed in frail versus non-frail groups in some studies [179, 180] but not others [181, 182]. These differential findings may be underpinned by an older mean age of participants in some studies [179] and the implementation of differing echocardiographic protocols. It would be worthwhile to build on these echocardiography-derived findings by utilising cardiac MRI, which has been shown to be less prone patient- and investigator-related variance [183-185]. Furthermore, cardiac MRI enables the assessment of myocardial scarring and diffuse fibrosis [186], which may underpin the greater LV mass observed in frail individuals. Unfortunately, it appears there are currently no assessments of cardiac parameters

with MRI within the frailty literature, reinforcing the need to apply this modality to improve insight in this area.

A previous study adopting a sample of 211 frail individuals highlighted LV hypertrophy and lower LV systolic and diastolic function in frail compared with non-frail individuals [180]. Interestingly, this study reported greater prevalence of abnormal cardiac measures in the frail even after impairments in the pulmonary, renal, hematologic, and adipose systems had been accounted for in the analysis. Furthermore, cardiac abnormalities, such as LV hypertrophy, showed the greatest association with frailty of all the organ systems studied [180]. This study therefore portrays cardiac dysregulation as a significant contributor to the physiological frailty phenotype, which should be explored further with robust cardiac MRI.

1.5.4.2 Vascular parameters

Physiological changes of the vasculature are also observed with advancing age, such as increased arterial stiffness [187], wall thickness [188], and endothelial dysfunction (e.g., reduced vasodilation and nitric oxide bioavailability) [189, 190]. Vascular dysfunction is also associated with sarcopenia, potentially through decreased muscle microperfusion [191] and greater amounts of sedentary time [192], indicating that pathophysiology within the vasculature may contribute to the phenotype of frailty. However, few studies have assessed parameters of vascular structure and function during frailty. Two large-sample studies, including the Framingham Heart Study, reported greater arterial stiffness in frail versus non-frail individuals, when assessed by carotid-femoral pulse wave velocity [180, 193]. Markers of endothelial dysfunction, such as abnormal ankle-brachial index, pulse wave velocity, and low levels of flow-mediated dilation, have also been associated with frailty [194]. Furthermore, frailty has

been linked to a greater serum concentration of dimethylarginine [195], which is elevated in endothelial dysfunction and is an independent risk factor for major adverse cardiovascular events, and reduced flow-mediated dilation [196, 197]. This small number of studies provide some indications of vascular deterioration during frailty.

1.5.4.3 Potential mechanisms of cardiovascular dysregulation in frailty

1.5.4.3.1 Inflammation

Features of cardiac dysregulation, such as increased LV mass and diastolic dysfunction, are associated with higher serum inflammatory markers in older individuals [198]. Given that these cardiac abnormalities are also evident during frailty [180], enhanced inflammation may promote cardiac deterioration in frail individuals. Inflammatory cytokines have been proposed as regulators of cardiac dysregulation through several mechanisms. For example, overexpression of TNF-a in mouse cardiac tissue leads to proteasome dysfunction and the accumulation of ubiquitinated proteins in the left ventricle [199], which may be a mechanism underlying greater LV mass during frailty [177]. Similarly, chronic TNF-a overexpression restricted to cardiac tissues attenuates the activity of collagenolytic enzymes, leading to reduced LV dilation [200]. These processes may underpin cardiac dysfunction during frailty, mediated by a chronically heightened inflammatory state in the heart.

1.5.4.3.2 Physical inactivity

Physical inactivity may also promote cardiovascular deterioration during frailty [69]. For example, lower LV ejection fraction, which has been observed during frailty [179, 180], is associated with lower physical activity levels in middle-aged adults [201]. The physiological mechanism for this may include a physical inactivity-induced promotion of cardiac atrophy [202], thus attenuating LV function through the loss of myocardial

tissue which in turn reduces heart contractility. This is supported by findings from a limb unloading model, highlighting marked reductions in the synthesis of cardiac proteins and significant cardiac tissue loss in response to the unloading [203]. Enhanced arterial stiffness in frail individuals may also be attributed to lower physical activity levels, given that greater arterial stiffness is observed in older adults with increased amounts of sedentary time [204]. Arterial stiffening may also be influenced by low vascular blood flow during sedentary time, leading to lower endothelial shear stress and impaired endothelial function [205]. As such, low endothelial shear stress is associated with low nitric oxide synthase expression [206] and blocking the synthesis of nitric oxide promotes arterial stiffness in vivo [207].

1.5.5 Adipose tissue

Increased whole body and abdominal fat deposition has been associated with ageing [208-211]. The health implications of enhanced adiposity with age are complex and remain poorly understood. For example, adiposity in overweight and obese older people has been positively associated with mortality in some studies [212, 213] but not others [214]. Obesity has even been associated with better outcomes in various medical conditions [214-216] and a lower risk of clinical events in individuals with frailty [217]. Despite contrasting findings, the links between adiposity and physical function deterioration and disability [218, 219], in conjunction with weight loss being a criterion of the physical frailty phenotype assessment [17], warrant the investigation of adipose tissue within the context of frailty.

Indirect measures of adiposity (e.g., BMI and waist circumference) have been employed within studies of frailty, which have produced conflicting results. A systematic review of six longitudinal studies has revealed a direct association between obesity (BMI ≥ 30 kg/m^2) and frailty incidence [220]. For example, one of the

longitudinal studies included in this review, recruiting 28,181 older women, reported a near fourfold-increased risk of frailty development in obese individuals compared to counterparts with a normal BMI after a 3-year follow-up [221]. This finding has been corroborated in a separate large sample study, observing an increased risk of frailty with each additional year of obesity [222]. Findings from cross-sectional studies have also demonstrated associations between obesity and a greater risk of pre-frailty and frailty in older women [223]. It is unknown if this is a direct causative relationship, although this association remained statistically significant after adjustment for multiple conditions (such as diabetes mellitus and heart failure,) and inflammation status [223].

In contrast to the evidence detailed above, longitudinal studies have demonstrated a greater risk of frailty in individuals with low BMI (<18.5 kg/m^2) compared with those with normal BMI (18.5–24.9 kg/m^2) [221]. The observation of greater frailty risk with low BMI is supported by cross-sectional data highlighting a significantly lower BMI in frail versus non-frail individuals [224]. As such, a U-shaped relationship between frailty and adiposity may be evident, with low and high (as opposed to normal) levels of adipose tissue contributing to greater frailty risk. Of course, insight into the relationship between frailty and adipose tissue is limited by the application of crude and indirect measurements of adiposity (i.e., body mass and waist circumference) in these studies.

Studies using imaging techniques to quantify adiposity in frail individuals are scarce. Idaote et al., [52] used CT scanning to highlight greater pericardial and visceral adipose tissue CSA in the lumbar spine region of non-frail versus frail participants, supporting the longitudinal associations between low BMI and frailty [221]. A reduction in adiposity may therefore underpin the non-intentional weight loss trait of frailty [17]. However, in contrast to Idaote et al., [52] a large-sample study utilising CT scanning reported no differences in lower leg subcutaneous adipose tissue CSA between non-

frail and frail individuals [51]. Direct comparisons of these results to those of Idaote et al., [52] are difficult as adipose tissue CSA was quantified in different regions of the body between studies. Consequently, future studies should employ imaging techniques to directly quantify whole body and regional adiposity to improve understanding of the complex relationship between adipose tissue and frailty

DEXA estimates of fat mass in frail individuals are also inconclusive. One study has reported a greater percentage of body fat (i.e., total fat mass relative to total body mass) in frail versus non-frail participants [42]. However, no significant differences were observed when fat mass was expressed as an absolute quantity (measured in grams) [42]. No differences in DEXA-derived total fat mass between non-frail, pre-frail and frail individuals has also been reported in a large sample study of Taiwanese older adults [43] and a smaller cohort from the Women's Health and Aging Study [45]. Therefore, these conflicting findings reflect a poor understanding of the relationship between adiposity and frailty, reinforcing the requirement for standardised measurement approaches and large-sample longitudinal studies to improve insight.

1.5.5.1 Potential mechanisms of altered adiposity during frailty

Physical inactivity and greater amounts of sedentary behaviour promote an accumulation of fat mass [225, 226]. Considering these behaviours are linked to frailty [69, 227] and low physical activity is a criterion for the Physical Frailty Phenotype [17], physical inactivity may contribute to increased fat mass in frail individuals. Mechanisms underpinning physical inactivity-induced increases in adiposity may involve reduced skeletal muscle insulin sensitivity and consequent accumulation of central and visceral adipose tissue [228, 229]. For example, bed rest models of inactivity have demonstrated reduced insulin sensitivity and dysregulated oxidation of

lipids and glucose alongside enhanced adiposity and IMAT accumulation [230], particularly under conditions of positive energy balance [231, 232]. These findings are supported by evidence of greater hepatic free fatty acid uptake rates in individuals with low physical activity levels [233], whereas habitual endurance training has been associated with lower hepatic free fatty acid uptake [234]. Whilst these findings are not specific to frailty, they present potential mechanisms by which inactivity may contribute to greater adiposity in frail individuals.

Elevated levels of adiposity may contribute to the increased inflammatory state observed in frail individuals [235, 236]. Greater concentrations of circulating IL-6 have been attributed to increased fat mass and obesity [237], with previous work demonstrating that up to 30% of circulating levels of IL-6 may be released from subcutaneous adipose tissue in obese adults [238]. Furthermore, proinflammatory cytokines may also negatively influence other physiological systems, such as muscle mass and function [239]. IMAT is also a proposed site of inflammatory cytokine release. As such, greater IMAT and IL-6 protein content within the vastus lateralis has been observed in frail compared to non-frail individuals [49], which may indicate that greater IMAT content further promotes an inflammatory environment and facilitates atrophy of skeletal muscle in frail individuals. Indeed, obese older men, who presented with heightened systemic inflammation and markedly greater adiposity compared to nonobese age-matched controls, also exhibited a blunted muscle protein synthetic response to increased nutrient delivery [240]. However, these same individuals presented with greater lean tissue mass and had no impairment of muscle strength or knee extensor work output. Muscle mRNA expression analysis in these obese older men illustrated lower levels of transcripts for cytochrome c, peroxisome proliferator-activated receptor-a, peroxisome proliferator-activated receptor-c coactivator 1a, and

TFAM, which are associated with mitochondrial biogenesis or oxidative phosphorylation. Further, greater expression of myostatin, a negative regulator of muscle growth, has been observed in the skeletal muscle of obese versus non-obese individuals [240]. It is unknown whether these observations are representative of frail individuals, but the mRNA pattern in this study was consistent with muscle deconditioning being an underpinning of metabolic dysregulation [240], which is pertinent to frailty.

1.5.6 Multisystem dysregulation

Research into the physiological markers of ageing and frailty, including the majority of studies cited thus far, has traditionally focused on individual biomarkers. However, these investigations into single-mechanism explanations of ageing, such as inflammation and oxidative stress, have produced multifactorial conclusions, in which several physiological processes interact [241, 242]. This has led to the proposal of nine hallmarks of ageing, which consists of a sequence of interrelated physiological processes that produce the aged phenotype in various organ systems. The sequence begins with the accumulation of cell damage, instigating responses such as mitochondrial dysfunction and cell senescence, with end points of inflammation and reduced stem cell turnover affecting biological ageing [243]. This paradigm has changed how ageing, and in turn frailty, mechanisms are perceived, with many researchers now acknowledging multisystem physiological dysregulation as a fundamental biological underpinning of health decline during ageing.

The rationale for considering frailty as a condition comprising simultaneous dysregulation in several systems has been provided by the findings that frailty is concomitant with various pathophysiological syndromes, such as sarcopenia [244], vascular dementia [115], and heart failure [177] (**Figure 1.2**). Similarly, findings from

the Cardiovascular Health Study cohort demonstrated associations between frailty and dysregulation in the cardiac, vascular, and cerebral systems [177], These findings indicate that dysregulation in multiple physiological systems occurs during frailty, thus a research focus has been instigated in this area.

A seminal study first investigated multisystem dysregulation by examining twelve biomarkers in six different physiological systems (anaemia, inflammation, endocrine, micronutrient, adiposity, and fine motor speed) within non-frail and frail older women [245]. Measured biomarker values within these systems were compared against accepted normal ranges to define normal or abnormal values (i.e., greater or lower values compared to the normal range were considered abnormal). This study demonstrated that abnormal values in five systems increased frailty risk by 26-fold (compared to zero abnormal systems) [245]. Importantly, it was also noted that the cumulative number of dysregulated systems, as opposed to any specific system, was the dominating factor predicting frailty severity. Further, the relationship between frailty severity and an increasing number of abnormal systems was nonlinear [245], indicating there may be a threshold beyond which an adverse downward spiral of frailty progression occurs. This would be consistent with the concept of “majority rules” in systems biology [246, 247], whereby the aggregate of impaired systems may adversely affect the function of other unimpaired systems, consequently driving the whole system to a more dysregulated state.

Frailty from a multisystem perspective has also been explored using a statistical approach that quantifies physiological dysregulation by assessing the difference between a discrete biomarker value and the average value for a population mean [241]. Using data acquired from nearly 33,000 individuals, and analysis of 37 biomarkers grouped into six physiological systems (lipids, immune, oxygen transport,

liver function, vitamins, and electrolytes), Li et al., [248] demonstrated dysregulation in several systems and proposed the establishment of a global dysregulation score (collated from estimates on all biomarkers), enabling prediction of the magnitude of frailty presence. Interestingly, no individual system was notably better at predicting frailty than another [248]. Adopting this statistical approach, and similar physiological system groupings for biomarkers, a study of 1,754 volunteers also reported multisystem dysregulation during frailty [249] and similarly concluded that no individual systems were more important than others for predicting frailty. This is particularly relevant as this study assessed a different group of physiological systems than the previous work by Fried et al., [245]. However, some discrepancies between these two studies should be acknowledged. Firstly, the nonlinearity effect of greater frailty risk with an increasing number of dysregulated systems reported by Fried et al., [245] was not corroborated, which was attributed to the low sample size of frail individuals [249]. Secondly, this study did not support the finding that the number of systems dysregulated effectively predicted frailty presence. This discrepancy may be partially explained by the different frailty criteria adopted across studies, which, importantly, has been shown to negatively affect the agreement and predictive ability of the Physical Frailty Phenotype method [250]. Furthermore, the sample adopted by Fried et al., [245] consisted of solely female participants, whereas the cohorts studied by Ghacem et al., [249] incorporated males and females. The widely reported greater prevalence of frailty in females [251] suggests there may be sex-related differences in the physiological characteristics of frailty, which may have contributed to the differential findings between these studies.

Other research groups have also reported physiological dysregulation in multiple systems during frailty. Using previously established cutoff thresholds, against which

measured values for different systems were compared, the prevalence of frailty was reported to be directly related to the number of abnormal organ systems (when considering cardiac, vascular, pulmonary, renal, hematologic, and adipose tissue systems) [180]. Furthermore, this study found that cardiac abnormalities demonstrated the strongest association with frailty relative to the other organ systems measured, reinforcing that dysregulation of the heart may be a key organ contributing to the frailty phenotype.

These observations of multisystem dysregulation support the concept of frailty as a condition comprised of multiple abnormalities in a complex system (i.e., the human body). However, certain considerations should be acknowledged when extrapolating findings from current studies, such as inaccurate assessment methodologies. For example, adiposity was estimated with skinfold thickness [245] and BIA methods [180] in these studies, which are less robust than DEXA- and MRI- derived estimates of fat mass and volume, though were likely adopted because of their feasibility of application within the large participant samples adopted. Furthermore, the physiological systems studied in many of these reports were distinguished based on circulating biomarkers, which may be deemed less representative of the associated organ and tissue functions. Thus, to better understand the contribution of different physiological systems to the frailty phenotype, and to more accurately model and predict frailty development, future studies should employ more robust measurement techniques to assess organ structure and function and expand on these circulating-biomarker-based reports.

1.6 The physiological phenotype of frailty – using a stress stimulus paradigm

The literature described to this point has identified numerous physiological characteristics associated with frailty. Nevertheless, the distinct physiological

phenotype differentiating frail versus non-frail states remains poorly characterised. This lack of clarity may be due to studies being performed under resting-state conditions, thus failing to characterise the disruption of dynamic homeostasis that is central to the definition of frailty [252]. In essence, in the absence of stimuli such as acute infection, illness, and injury, and without the presence of external stressors such as physical activity, the dysregulation of physiological homeostasis in frailty may be subtle or undetectable, particularly without the application of robust and sensitive measurement techniques to quantify physiological resilience. Instead, the phenotypic features of frailty would likely present more overtly than in the resting state if individuals were studied during a physiological stress challenge, such as exercise (**Figure 1.5**). As such, frailty is fundamentally characterised by a reduced ability to cope with and combat stressors [10], i.e., reduced resilience. Appropriately, the measurement of dynamic responses to physiological stressors has been identified as a key next step in frailty research [253]. However, insight into the physiological responses to stressors during frailty remains limited, with markedly less data available relative to findings derived from resting state assessments. Nonetheless, a recent review by Fried and colleagues [254] discussed various physiological responses to stressors within different body systems during frailty, which, promisingly, indicates that this research area is receiving attention. The following section aims to summarise the current evidence and understanding of the physiological responses to stressors during frailty.

Acute exercise is an effective and non-invasive method of inducing physiological stress in vivo, with a bout of exercise instigating rapid and marked changes in physiological function involving multiple organs [255]. For example, **Figure 1.5** depicts the alterations in cardiac output and blood distribution to multiple organ systems when transitioning from rest to vigorous exercise.

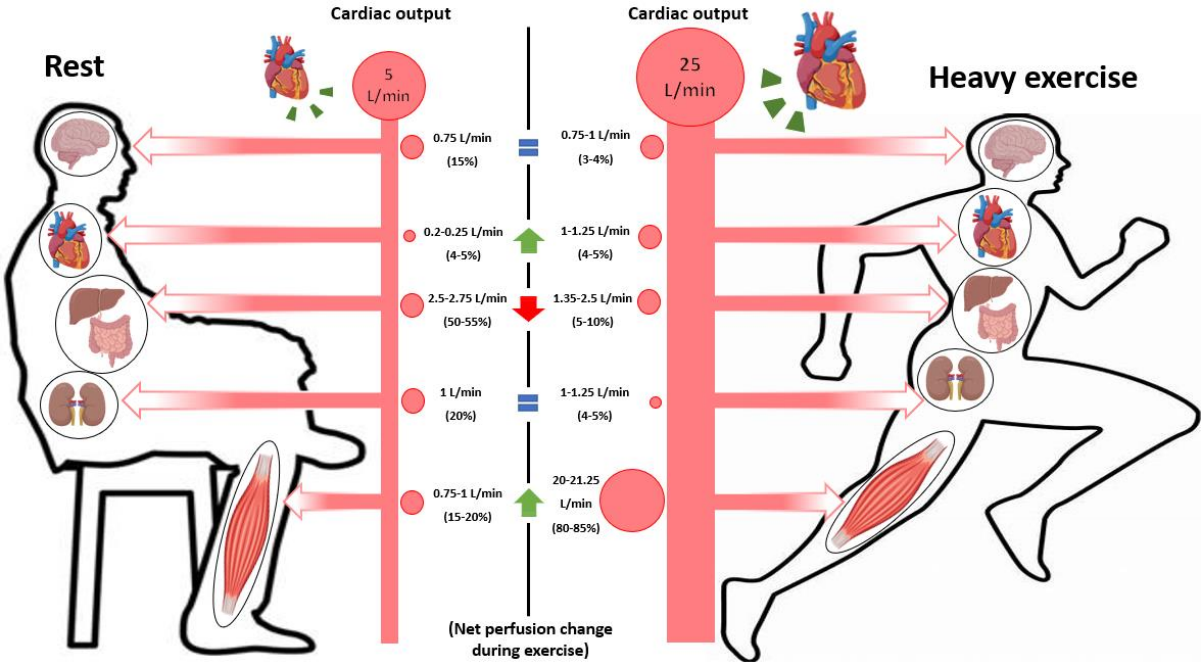

Figure 1.5: *Schematic comparison of cardiac output and blood distribution to organs at rest versus during exercise in a human. Exercise instigates an increase in cardiac output from the resting state along with a redistribution of blood flow from splanchnic organs to skeletal.*

1.6.1 Skeletal muscle energy metabolism

A rapid and sustained increase in muscle ATP turnover is observed during exercise, from ~0.07 mol ATP/min at rest to >2 mol ATP/min during heavy exercise [256]. When the rate of mitochondrial ATP production is exceeded by the rate of ATP demand, energy must be derived from nonmitochondrial sources, i.e., anaerobic glycolysis and PCr hydrolysis (**Figure 1.6**). PCr hydrolysis and lactate accumulation within the muscle are robust markers of mitochondrial dysfunction [257] and skeletal muscle myopathy [257, 258]. Furthermore, in the contexts of ageing and chronic disease, muscle deconditioning and lower mitochondrial content are associated with enhanced nonmitochondrial muscle ATP production during exercise stress [33, 259]. Finally, given post-exercise muscle PCr resynthesis is entirely mitochondrion dependent, the

slowing of PCr resynthesis kinetics during recovery from exercise can be considered as a robust index of mitochondrial function and/or mass [260, 261]. Alterations in muscle energy metabolism during exercise and recovery are therefore likely to provide valuable insight into metabolic and functional decline of the muscle during frailty.

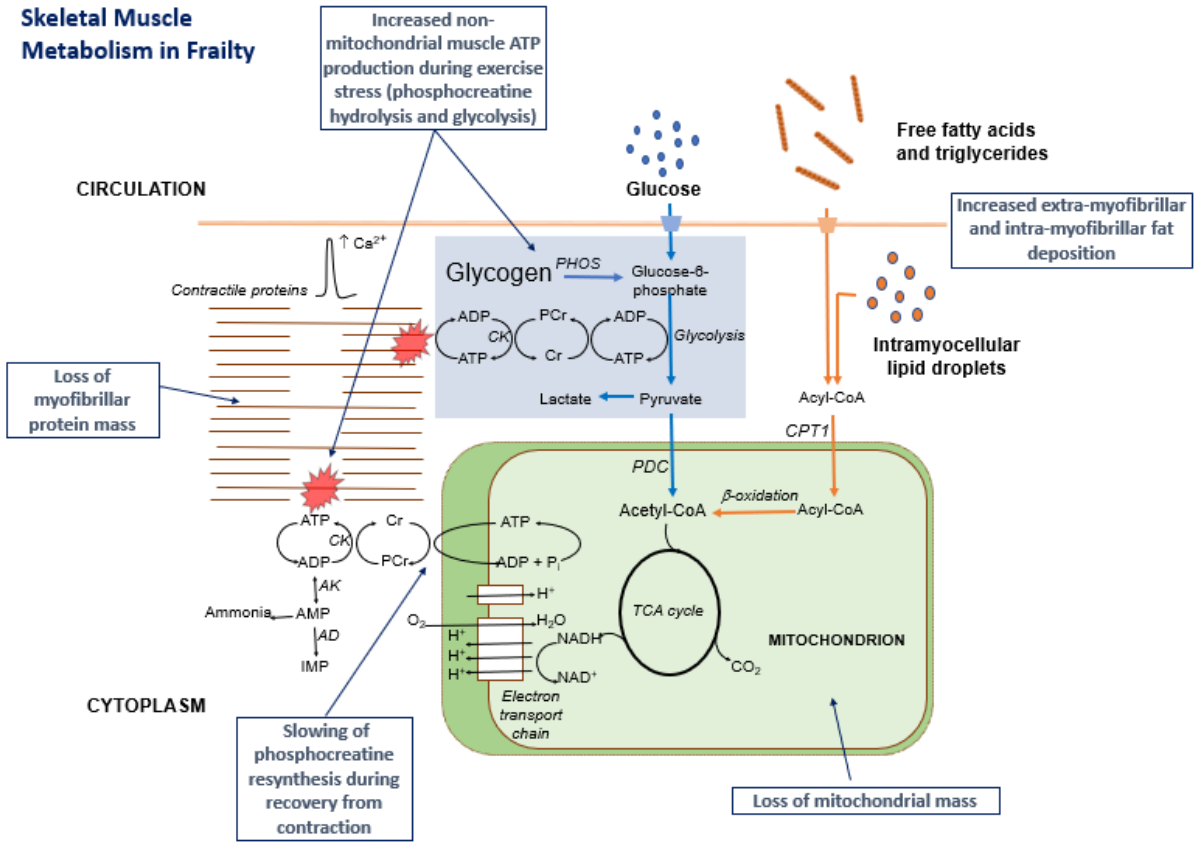

Figure 1.6: *Schematic illustration of the effect of frailty on substrates and pathways involved in skeletal muscle energy turnover. When the rate of ATP demand during muscle contraction exceeds that of mitochondrial ATP production, ATP turnover is maintained from non-mitochondrial routes, namely glycolysis and phosphocreatine (PCr) hydrolysis. ATP, adenosine triphosphate; ADP, adenosine diphosphate; AMP, adenosine monophosphate; Ca^{2+}, calcium; CK, creatine kinase; CPT1, carnitine palmitoyltransferase I; Cr, creatine; H^+, hydrogen ion; H_2O, water; IMP, inosine monophosphate; NADH, reduced nicotinamide adenine dinucleotide; NAD^+, oxidised nicotinamide adenine dinucleotide; PDC, pyruvate dehydrogenase complex; PCr, phosphocreatine; Pi, inorganic phosphate; TCA cycle, tricarboxylic acid cycle. Figure reproduced with permission from Professor Paul Greenhaff.*

^{31}Phosphorus (^{31}P) MRS represents a robust, non-invasive method enabling the quantification of muscle PCr and pH changes during exercise and recovery in vivo, making it well suited to study age- and frailty-related pathophysiology. This approach has been employed in a recent study in age-matched non-frail and frail older adults who performed graded multistage plantar flexion exercise within the bore of a 3-Tesla MRI scanner, whilst a ^{31}P MRS coil was focused on the gastrocnemius and soleus muscles of the calf [53]. When normalised to the work of activity performed, muscle PCr hydrolysis was fourfold greater in the frail participants (and 10-fold greater than middle-aged control participants) during exercise. In addition, this higher rate of PCr hydrolysis was inversely correlated with oxygen uptake ($r = -0.58$; $P < 0.001$) and distance covered on a 6-min walk test ($r = -0.63$; $P < 0.0001$) [53]. These results identify potential physiological mechanisms underpinning the reduced physical function and greater subjective sense of fatigue traits of frailty [17]. Interestingly, this study also reported no difference in MRI-derived calf muscle CSA when comparing frail and non-frail individuals, whereas muscle fat fraction CSA (expressed as a proportion of total muscle area) was greater in the frail individuals [53]. Fat fraction was also positively associated with greater PCr hydrolysis during exercise ($r = 0.38$; $P < 0.05$), indicating that differences in muscle metabolic quality, rather than mass, can differentiate non-frail versus frail phenotypes. It also raises the question as to whether increasing habitual physical activity with interventions in frail people can improve muscle metabolic resilience and thereby functionality in everyday living.

Regarding exercise recovery kinetics, Andreux et al., [262] compared recovery of PCr in the calf muscle following plantar flexion exercise in non-frail versus pre-frail older individuals using ^{31}P MRS at 7 Tesla. Longer PCr recovery times were evident in pre-frail participants compared to physically active non-frail counterparts, suggesting that

reduced mitochondrial respiration/content is a feature of the pre-frail state. However, this study did not report the concentration of PCr within the muscle immediately after exercise cessation, making it difficult to interpret the findings, i.e., the slower recovery may have been a consequence of differences in the rate of ATP turnover, and thereby PCr degradation, during exercise. Considering cellular ADP concentration is a primary driver mitochondrial resynthesis following exercise, this is a pivotal question to resolve.

A consideration of the studies described above is the lack of normalisation of PCr recovery kinetics to total mitochondrial content across the muscle of interest. In the absence of this normalisation, mitochondrial dysfunction cannot be inferred, as a lower mitochondrial content may also underpin slower PCr recovery kinetics. As such, the available data indicate that dysfunction in mitochondrial respiration, demonstrated in ageing [33] and chronic disease (e.g., COPD [263], diabetes [264]), fails to persist when muscle mitochondrial respiration is corrected correct for mitochondrial content. Accordingly, supposed “mitochondrial dysfunction” in older people can be reversed by increasing mitochondrial content with exercise training [33]. In the context of frailty, a study using succinate dehydrogenase as a marker highlighted lower mitochondrial content in pre-frail compared with non-frail men in all fibre types of the vastus lateralis [265]. Pre-frail and frail women have also been shown to exhibit lower vastus lateralis muscle mitochondrial content compared with young inactive participants [266]. Although the lack of a non-frail group for comparison in this study limits insight. Nonetheless, large cohort studies have reported inverse associations between mtDNA copy number (an index of mitochondrial number) and polymorphisms in mtDNA with frailty [267, 268]. Furthermore, lower abundance and maximal activity of mitochondrial respiratory complexes has been shown in the skeletal muscle of pre-frail and frail versus non-frail adults [262, 269].

Overall, these findings point to the need for further research to differentiate between the relative contribution of mitochondrial dysfunction and decline in mitochondrial content to the reduction of metabolic resilience during frailty. Nonetheless, the emerging evidence outlined above implies that altered muscle energy metabolism is a key underlying feature of generalised physiological decline and fatigue in frailty (**Figure 1.6**). Moreover, as alterations in tissue energy metabolism are seemingly associated with dysregulation across numerous different organ systems, this may be a common biological feature of frailty-related decline.

1.6.2 Responses to feeding

Alternative to the stimulus of exercise stress, feeding can also elicit a marked physiological response. Following carbohydrate ingestion, plasma glucose concentrations are elevated, stimulating pancreatic insulin secretion. Insulin facilitates skeletal muscle and hepatic glucose uptake for storage and/or utilisation; thus, the secretion and action of insulin are key responses mediating glucose tolerance. Ageing is associated with alterations in the response to feeding, with older adults exhibiting diminished insulin sensitivity and elevated blood glucose levels after an oral glucose challenge [270, 271]. Despite many studies demonstrating insulin resistance in healthy older participants, few studies have controlled for typical physiological characteristics of ageing that may influence the interpretation of results, such as muscle mass, changes in liver size, a decline in habitual physical activity, and delays in carbohydrate absorption of the gut. These limitations make it difficult to determine whether impaired glucose tolerance is a feature of normal ageing per se or a consequence of age-related changes in lifestyle factors that vary in presence and magnitude between individuals.

A common method utilised in research studies to study the physiological responses to feeding is an OGTT, which has been employed studies of frailty. Kalyani et al., [272]

reported no differences in fasted serum glucose and insulin concentrations between healthy and frail individuals. However, following an OGTT, frail females demonstrated exaggerated increases in blood glucose and insulin concentrations over 180 min compared with pre-frail and non-frail women, indicating impaired glucose tolerance [272]. These findings are consistent with the previous observations of elevated glucose concentrations two hours after oral glucose ingestion in frail volunteers compared with non-frail individuals, but not in the baseline fasted state [236]. Similarly, following a standardised 700-kcal liquid mixed-meal test, elevated area under the curve values were evident in frail versus non-frail women for five hours after consumption of glucose and insulin [273]. Despite these findings appearing to reinforce a reduction in glucose tolerance in frail individuals, frailty in this study was defined using only the slow gait speed and low physical activity criteria of the Physical Frailty Phenotype [17] and thus may be deemed a reductionist assessment of frailty. Although, there is evidence that these two frailty criteria are the most predictive components of the physical frailty phenotype method [274], potentially supporting the assessment of frailty in this way.

The studies outlined above indicate that frailty is associated with impaired glucose tolerance. However, nutrient absorption in the gastrointestinal tract often deteriorates with age [275] and therefore will influence glucose absorption following a meal test or OGTT. Additionally, when a fixed dose of carbohydrate is administered (e.g., with an OGTT), body size will affect the blood glucose response. For this reason, researchers may instead employ an intravenous glucose tolerance test or the euglycemic insulin clamp technique, with these methods controlling for the effects of gut absorption and body size/lean mass on blood glucose disposal (and insulin action in the case of the insulin clamp technique). When this standardisation has been done in previous

studies, the rate of glucose disposal normalised to body surface area (and across a range of steady-state insulin infusion rates) was observed as reduced in healthy, nonobese older volunteers compared with younger volunteers [276]. The same is apparent when comparing older lean versus obese individuals in regard to whole body and leg glucose uptake [240]. Despite the lack of equivalent data in frail volunteers, these lower rates of normalised whole body and leg glucose disposal in older versus young people demonstrate that insulin resistance with age is a real phenomenon, and likely to be multifactorial. In studies of frailty, the quantitative insulin sensitivity check index and homeostasis model assessment scores have been most frequently adopted to assess insulin sensitivity [277-279]. However, these approaches represent estimates based on fasting blood glucose and insulin concentrations and therefore do not reflect the dynamic gluco-regulatory response to feeding. Accordingly, in the Baltimore Longitudinal Study of Aging, blood glucose level at 2 hours after OGTT was a better predictor of mortality risk than fasting glucose alone [271, 280], with similar findings evident in the Cardiovascular Health Study in relation to incident cardiovascular events [281]. Although not specific to frailty, these findings reinforce the importance and efficacy of studying physiological characteristics under conditions of stress to manifest differences between non-frail and frail states.

1.7 Summary

Based on the evidence outlined in this Chapter, it is clear that the current literature fails to adequately characterise the physiological phenotype of frailty. From a physiological standpoint, the most important considerations concern the majority of previous studies assessing the characteristics of individual organs with imprecise measurement techniques. This does not seem optimal for understanding the phenotype of frailty given the emerging evidence of dysregulation in multiple

physiological systems as concomitant with frailty. Despite the improved insight provided by investigations into multisystem dysregulation in frail individuals, the studies in this area have adopted indirect measures to investigate organ structure and function, such as blood biomarkers. Therefore, there is large potential for improving insight into the phenotype of frailty with the application of robust multi-organ physiological techniques in studies of frail individuals.

1.8 Thesis aims and structure

The overarching aim of this thesis was to provide novel insight into the physiological phenotype of frailty by employing multi-organ assessment techniques and measures of physical function in older human volunteers. Particular focus was applied to investigations of the heart, skeletal muscle, adipose tissue, neuromuscular system and brain, as these systems have been shown to be key mediators of age-related physiological change and have been implicated within the frailty phenotype. This multi-organ approach aimed to highlight distinct physiological characteristics of frailty, which may be viewed as areas for further research into mechanisms of frailty development and targets for future interventions aiming to mitigate the syndrome's development.

One physiological and functional phenotyping study was performed in older non-frail, pre-frail and frail female volunteers during the course of this thesis. Chapter Two described the protocol and experimental methods employed within this study. The findings of this study were then explored in three experimental Chapters focussing on characteristics of specific physiological systems and physical function characteristics in non-frail, pre-frail and frail volunteers. Chapter Three focused on characteristics of cardiac structure and function with the novel application of cardiac MRI within the context of frailty. Chapter Four detailed the investigations into body composition characteristics and neuromuscular function using MRI and iEMG techniques.

Furthermore, these physiological measures were combined with assessments of physical function to provide insight into the physiological underpinnings of functional decline during frailty. Chapter Five explored brain morphometry, haemodynamic and oxygenation following MRI assessments, and performed regression analyses to determine associations between brain morphometry and physical function measures. Chapter Six considered the collective findings from Chapters Three, Four and Five in an attempt to integrate and identify interactions between organ structure and function and physical function outcomes, thus providing insight into the whole body physiological phenotype of frailty. Chapter Seven concluded the thesis by summarising and integrating the findings from the experimental Chapters before discussing strengths and considerations of the work and proposing directions for future research.

Chapter Two: General Methods

2.1 Introduction

This Chapter describes the study protocols and experimental methods employed for the Physiological PHENOtyping of FRailty Using Magnetic Resonance IMaging (PHENOFRIM) study. The PHENOFRIM study involved the recruitment of older non-frail, pre-frail and frail female volunteers for two study visits. Study Visit One involved functional phenotyping which consisted of assessments of frailty status, neuromuscular characteristics and knee extensor strength, peak torque and work output. Study Visit Two comprised multi-organ MRI for physiological phenotyping, primarily of the brain, heart, skeletal muscle and adipose tissue. This included structural (e.g., brain volumes, left ventricular mass, skeletal muscle volume, visceral adipose tissue volume) and haemodynamic (e.g., cerebral blood flow, cardiac output) measures. **Figure 2.1** provides an outline of the experimental protocol of Study Visits One and Two. All abbreviations used in this Chapter are outlined on pages 13-17.

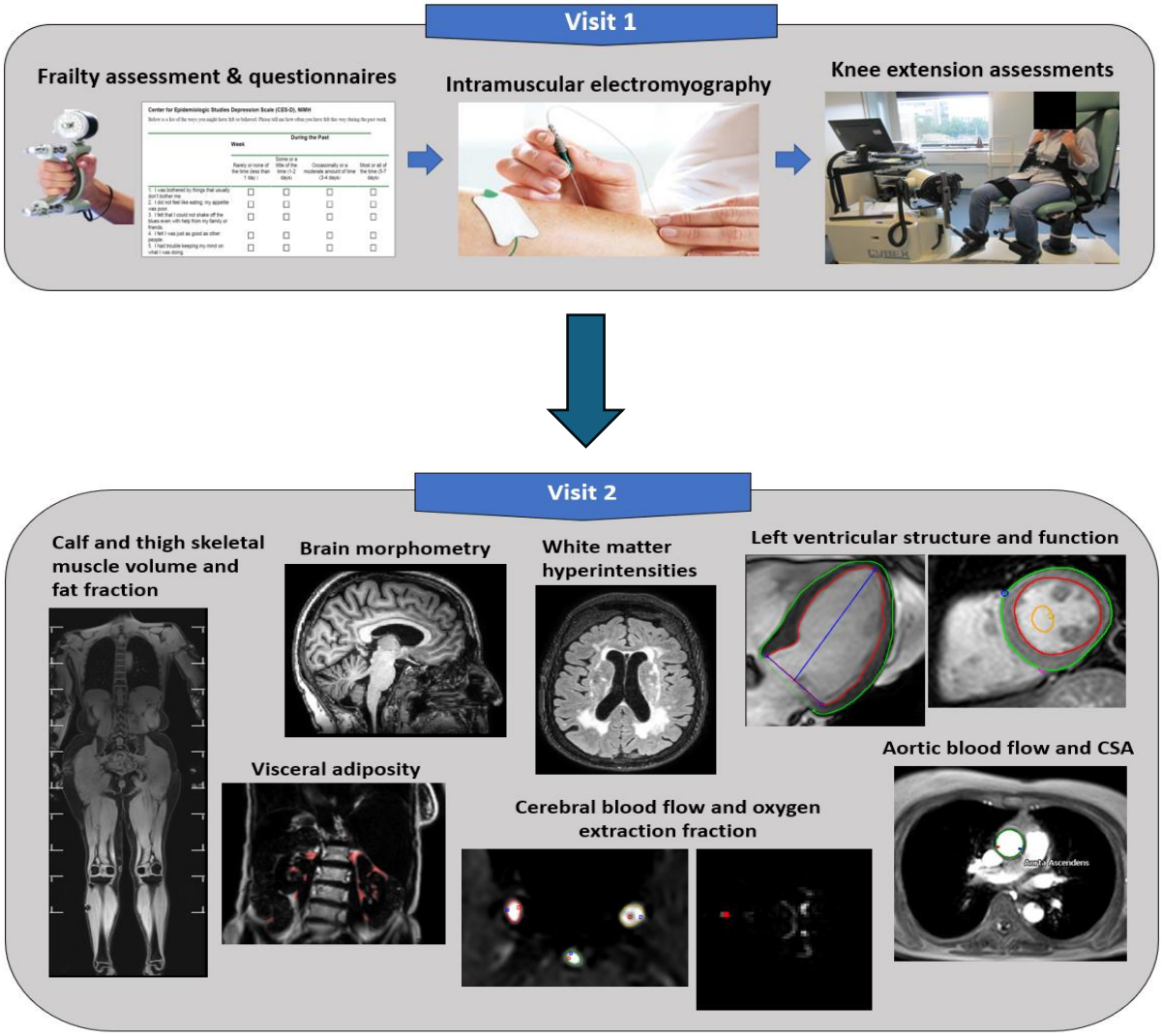

Figure 2.1: *Overview of experimental study visits for the non-frail, pre-frail and frail volunteers. Visit 1: Functional phenotyping at the David Greenfield Human Physiology Unit (DGHPU). Visit 2: Multi-organ MRI collected at the Sir Peter Mansfield Imaging Centre (SPMIC).*

2.2 Ethical approval

Upon completion of the Integrated Research Application System application (Project ID: 278613), the study received approval from the Health Research Authority on 02.09.2020 (Research ethics committee reference: 20/SW/0121). The study conformed to the recognised standards of the Declaration of Helsinki and all volunteers gave informed consent.

2.3 Recruitment

Female outpatients were recruited from clinics for older people within Nottingham University Hospitals NHS Trust. Clinic consultants first approached potential patient volunteers to determine their eligibility and interest in the study. Eligible and interested patients were then directed to a member of the research team who was present in clinic, or contacted and provided with a Participant Information Sheet at a later date. Inclusion and exclusion criteria for participation were as follows:

Inclusion criteria:

- Females aged 65+ attending Nottingham University Hospitals NHS Trust falls and bone health and general geriatric clinics;
- Ability to provide informed consent;
- Good understanding of written and spoken English.

Exclusion criteria

- Metal within the body which could be affected by the magnetic field produced by MRI scanner;
- Any other contraindications for MRI scan (e.g., brain aneurysm clips, permanent pacemaker);
- Over 190.5 cm in height (height limit for MRI scanner);
- Inability to lie on back in MRI scanner;
- Mobility limitations which would prevent the individual transferring onto equipment (e.g., Cybex dynamometer, MRI scanner);
- Unable to speak or understand English;
- In receipt of end of life care;

- Lacking the mental capacity to understand the requirements of study participation and provide consent;
- Diagnosis or history of Dementia.

Using handgrip strength as the primary endpoint, a sample size calculation was performed to quantify the number of participants needed to achieve statistical power. Hand grip strength is currently acknowledged to be a valid physiological component of frailty and previous studies have observed an average difference in grip strength of 12.35 kg between frail and non-frail individuals, with a standard deviation of 11.6 kg [54, 282]. Based on these data, a total of 14 participants (α: 0.05 β: 0.8) in each group was required to detect a significant difference in grip strength between frail and non-frail volunteers.

In the early stages of recruitment, all potential participants referred by the clinic consultants were contacted by telephone to determine eligibility for participation using the inclusion and exclusion criteria. 14 non-frail participants were recruited and completed the study approximately 6 months prior to the end of the recruitment period, following which recruitment was restricted to the pre-frail and frail groups only. At this stage of recruitment, consultants used the Electronic Frailty Index (if available in the patient's medical records) or the Clinical Frailty Scale score to identify pre-frail and frail individuals only.

2.4 Participant demographics

In total, 258 patients were approached, 37 potential participants were screened, and 35 participants (aged 65-91 years, BMI 15.3-35.3 kg/m^2) were recruited into and completed the study. Participant demographic data are presented in **Table 2.1**. Following frailty status assessment (detailed in Section 2.6.1), the sample sizes for the three groups were: *n* = 14 non-frail, *n* = 15 pre-frail and *n* = 6 frail.

Table 2.1: Demographic, comorbidity and medication data for non-frail, pre-frail and frail females recruited to the PHENOFRIM study. Demographic data are mean ± SD. Comorbidity and medication data represent the *n* presentations (and percentage of) of participants in each group. BMI = body mass index. * = significantly different to non-frail. ^ = trend for difference compared to pre-frail.

Demographic parameter	**Non-frail (*n* = 14)**	**Pre-frail (*n* = 15)**	**Frail (*n* = 6)**
Age (years)	71 ± 5	79 ± 8*	78 ± 8^
Height (m)	1.58 ± 0.07	1.55 ± 0.07	1.59 ± 0.08
Body mass (kg)	58.1 ± 6.0	62.8 ± 9.2	59.0 ± 19.6
BMI (kg/m^2)	23.3 ± 2.6	26.3 ± 4.5	23.3 ± 6.9
Body surface area (m^2)	1.59 ± 0.1	1.61 ± 0.12	1.59 ± 0.24
Comorbidities - n (%)			
Osteoporosis	9 (64%)	12 (80%)	3 (50%)
Hypertension	4 (29%)	5 (33%)	3 (50%)
Arthritis	3 (21%)	3 (20%)	2 (33%)
Depression	1 (7%)	1 (7%)	2 (33%)
Lymphedema	1 (7%)	1 (7%)	0 (0%)
Atrial fibrillation	1 (7%)	1 (7%)	1 (17%)
Leaky heart valve	0 (0%)	2 (13%)	2 (33%)
Medications - n (%)			
Alendronic acid	6 (43%)	7 (47%)	0 (0%)
Zoledronic acid	0 (0%)	3 (20%)	0 (0%)
Beta blockers	3 (21%)	2 (13%)	1 (17%)
Vitamin D	8 (57%)	8 (53%)	4 (66%)
Calcium supplement	7 (50%)	5 (33%)	1 (17%)
Amitriptyline	2 (14%)	2 (13%)	1 (17%)

Atorvastatin	3 (21%)	3 (20%)	2 (33%)
Levothyroxine sodium	2 (14%)	0 (0%)	2 (33%)
Aspirin	1 (7%)	2 (13%)	2 (33%)
Omeprazole	2 (14%)	2 (13%)	2 (33%)
Lansoprazole	3 (21%)	4 (27%)	3 (50%)

2.5 General study briefing and informed consent

Potential volunteers were invited to visit the MRC/Versus Arthritis Centre for Musculoskeletal Ageing Research laboratory, David Greenfield Human Physiology Unit (DGHPU), University of Nottingham Medical School, Queen's Medical Centre, Nottingham. Upon arrival volunteers were briefed on the study protocol by a member of the research team and if they were willing to take part in the research, they provided written informed consent to the research team.

2.6 Study Visit One: health screening, frailty assessment and functional phenotyping

After providing written informed consent, all volunteers underwent routine health screening. Height, weight, and lying and standing blood pressure were recorded, along with demographic data on self-reported health and fitness status, smoking and alcohol history, diet history and previous surgeries. All volunteers were screened for pre-existing health conditions and medications that were deemed a contraindication to study participation. Results from this health screening were reviewed by clinical staff to confirm the eligibility of each volunteer to participate. The SPMIC MRI safety screening questionnaire was also completed to determine contraindications to MRI scanning (e.g., non-MR-compatible metal implants within the body).

Following health screening, volunteers began the experimental protocol for the first study visit at the DGHPU. An overview of the study protocol for Study Visit One is provided in **Figure 2.2**.

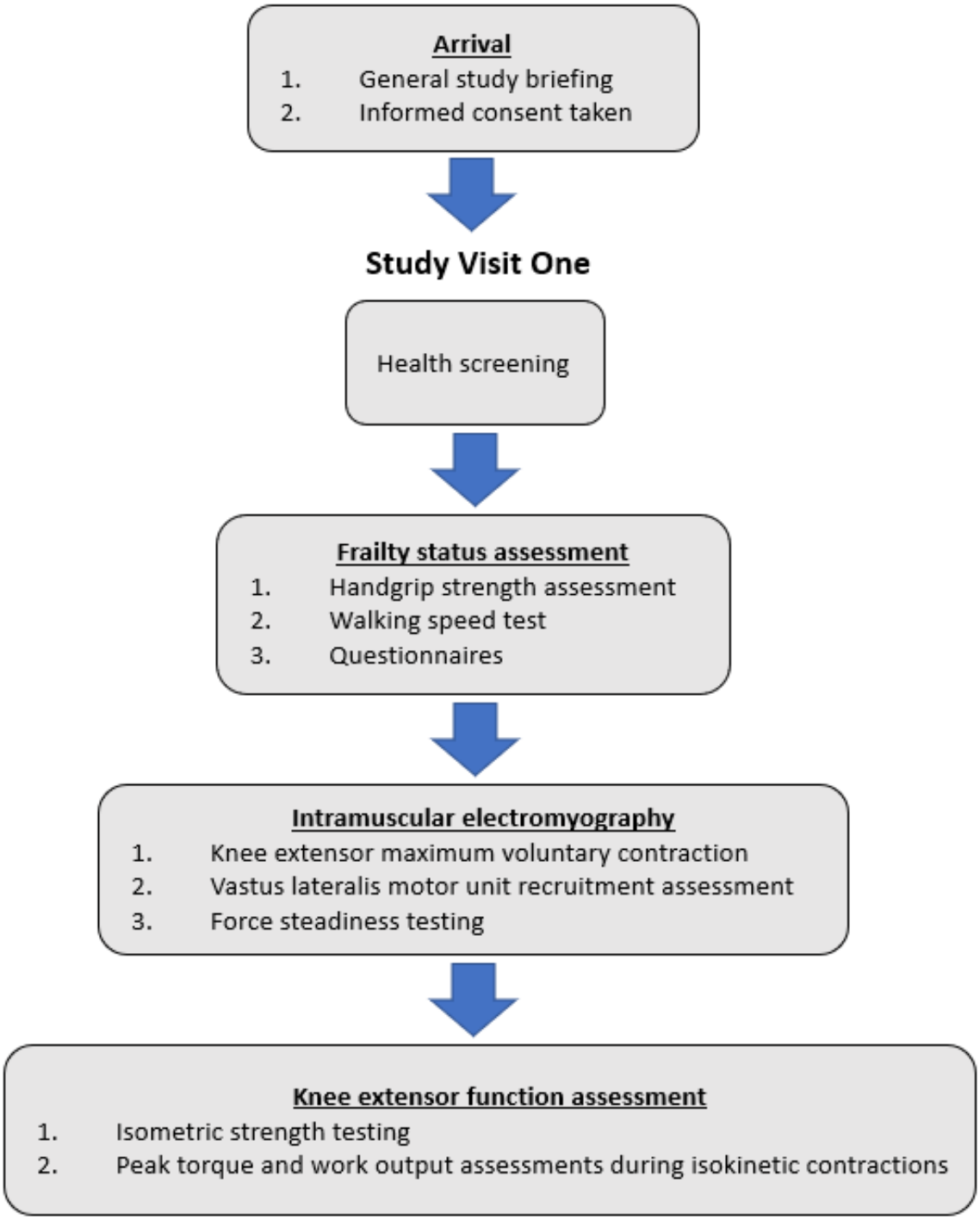

***Figure 2.2**: Overview of experimental protocol for Study Visit One.*

2.6.1 Frailty assessment

The frailty status of volunteers was assessed using the Fried Physical Frailty Phenotype Assessment [17]; frailty status being determined from five assessment components: slowness, weakness, weight loss, exhaustion and physical activity levels. ‘Slowness’ was measured with a timed 15 feet (4.57m) walk, with ‘slowness’ classed as volunteers ≤ 159 cm in height completing in ≥ 7 seconds, and volunteers > 159 cm in height completing in ≥ 6 seconds. ‘Weakness’ was assessed by hand grip strength. Handgrip strength measurements were performed with the dominant hand using a handheld dynamometer (Digital Pinch/Grip Analyser, MIE Medical Research Ltd, Leeds, UK). All measurements were made seated with the upper arm adducted, the elbow at ~90°. The forearm rested on a flat chair arm with the wrist in neutral rotation. The dynamometer was adjusted for each volunteer so that the middle joint of the index finger formed a right angle. The participant then performed 3 warm up repetitions, whereby they were instructed to squeeze the dynamometer at 50% of the perceived maximum effort. After the performance of warm up repetitions, 3 separate maximal voluntary grip measurements were recorded, with > 1 minute rest provided between trials. For each repetition, the volunteer was given a countdown then instructed to squeeze as hard as possible. Trials in which the volunteer compromised the required position (e.g., upper arm held against body, lifting forearm off the arm rest) were discarded and repeated. The peak maximal voluntary grip force (in kg) was recorded for each repetition and the mean of the 3 repetitions used for analysis. The cutoff thresholds (presented in **Table 2.2**) for defining weakness were stratified by BMI. Weight loss was defined as unintentional weight loss of ≥ 5% or ≥ 4.5 kg of total body weight in the previous year (obtained from the participant’s self-report). Perceived exhaustion was assessed by self-reported exhaustion using the Center for

Epidemiologic Studies Depression Scale, based on agreement to the statements: 'I felt that everything I did was an effort' and 'I could not get going'. Participants were asked: 'How often in the last week did you feel this way?'. The exhaustion criterion was deemed present if participants answered 'a moderate amount of the time (3–4 days)' or 'most of the time (5-7 days)' to either statement. Physical activity levels were estimated by self-report with the Minnesota Leisure Time Activity Questionnaire [283], with a shortened list of activities used, based on a previous study [284]. Participants with calculated activity-related energy expenditure < 270 kcal per week in the previous 12 months were classed as frail for the physical activity criterion.

Participants who did not exhibit any of these frailty components were classed as non-frail, those showing one or two frailty components were classified as pre-frail, and those presenting three or more components were classed as frail [17].

Table 2.2: Cutoff thresholds to define weakness criterion of frailty assessment (thresholds stratified by BMI) [17].

BMI ≤ 23 kg/m^2	≤ 17 kg
BMI 23.1 - 26 kg/m^2	≤ 17.3 kg
BMI 26.1 – 29 kg/m^2	≤ 18 kg
BMI > 29 kg/m^2	≤ 21 kg

2.6.2 Intramuscular electromyography

Peripheral motor unit size of the VL muscle was estimated using iEMG. to record individual motor unit potentials during 10%, 25% and 40% of MVC. Initially, iEMG testing was performed using a Cybex Isokinetic dynamometer (Cybex Norm, Rosemont, Illinois, USA), set up for isometric knee extension testing. An image of volunteer set up in the chair ergometer is provided in **Figure 2.5**. However, after

several assessments using the Cybex setup, it became clear that there was significant electrical interference affecting the sampled EMG signals, most likely originating from the electric motor in the Cybex Norm dynamometer, which made the EMG signals unanalysable. Therefore, the testing apparatus was changed to a custom-built chair and force cell setup, built for isometric knee extension assessment. Development work revealed this setup for iEMG testing resulted in markedly less noise within the sampled EMG signal, hence this setup was used for all consequent iEMG procedures.

For iEMG testing using the custom-built chair, the volunteer was first made comfortable in a semi supine position with the ankle of the dominant leg fixed in position with Velcro straps connected to a custom-built force cell. Adjustable screws were fixed both sides of the knee (and padded for participant comfort) to prevent lateral knee movement during knee extensions and the knee was fixed at 90º. Straps were placed over the thigh and hips to prevent limbs lifting off the chair during contraction. Images of the participant setup is provided in **Figure 2.3**. Following a warm-up of the knee extensors, a MVC was performed. The volunteer was instructed to kick out as hard as possible until instructed to stop. Verbal encouragement was provided throughout. When the researcher was satisfied that a maximum force output had been achieved, typically within 2-3 seconds, the volunteer was instructed to relax.

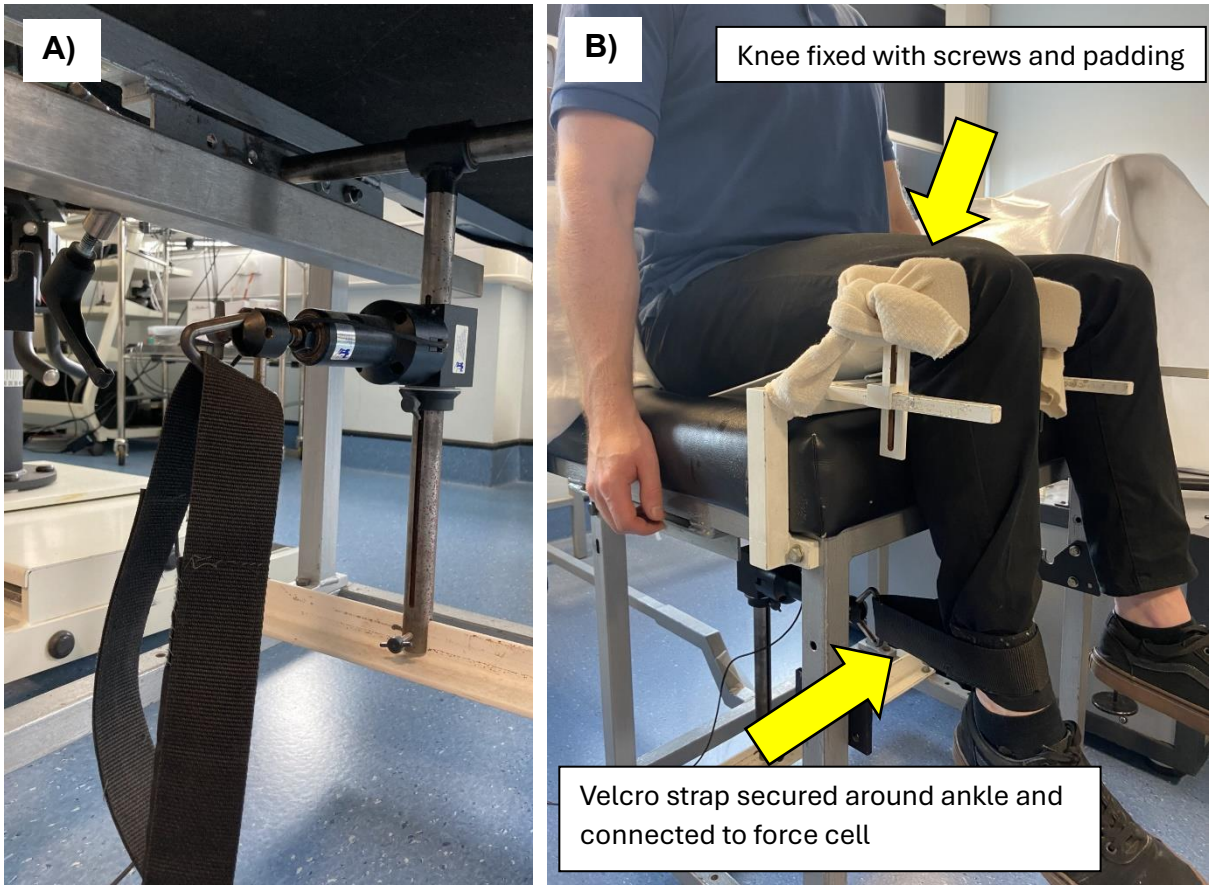

Figure 2.3: *Participant setup on the custom-built chair and force cell for iEMG testing during isometric knee extensions.* ***A)*** *Force cell strapped to the ankle of the dominant leg while testing. Force cell was connected to force amplifier and laptop for signal recordings.* ***B)*** *Full view of participant setup, showing participant in semi-supine position with ankle strapped to force cell and fixing of knee with screws and padding.*

Following MVC testing and iEMG protocol familiarisation, a 25 mm disposable concentric needle electrode (Teca, Hawthorne, New York, USA), with a recording area of 0.07 mm^2, was inserted into the VL of the dominant leg by a trained research nurse or clinical member of the research team. An earth electrode was placed on the surface of the same knee. Once an appropriate depth was reached (0.5-2.5cm; depending on muscle size and amount of subcutaneous tissue), participants underwent sustained isometric knee extensions at 10%, 25% and 40% of their MVC force, which was sustained for 12-15 seconds with real-time feedback from a visual display (**Figure 2.4**). iEMG signals were sampled at 25 kHz and bandpass filtered at 10 Hz to 10 kHz (CED

1902 amplifier; Cambridge Electronics Design Ltd, Cambridge, UK). In between contractions, the needle was repositioned using combinations of 180° needle rotations and needle withdrawals of roughly 3 mm. This was repeated until roughly six recordings from spatially distinct areas had been obtained. Participants had 20-30 seconds rest between each contraction. Motor unit potential (the compound potential generated by the muscle fibres of the motor unit during contraction; MUP) data were recorded using Spike2 software (v.8.1; Cambridge Electronic Designs) and stored for offline analysis (**Figure 2.4**).

Force steadiness was also measured during the isometric knee extensions during iEMG testing. Force steadiness is a measure of neuromuscular control, with poorer force steadiness associated with ageing [285] and lower mobility in older adults [286]. Force steadiness was assessed by quantifying the variation in the force generated in comparison to a target line (representing 10%, 25% or 40% MVC) during a sustained contraction at each contraction level. A computer screen provided real-time feedback to participants regarding force output. Force steadiness was measured as the CV at each contraction level, calculated as:

CV = (standard deviation/mean) x 100

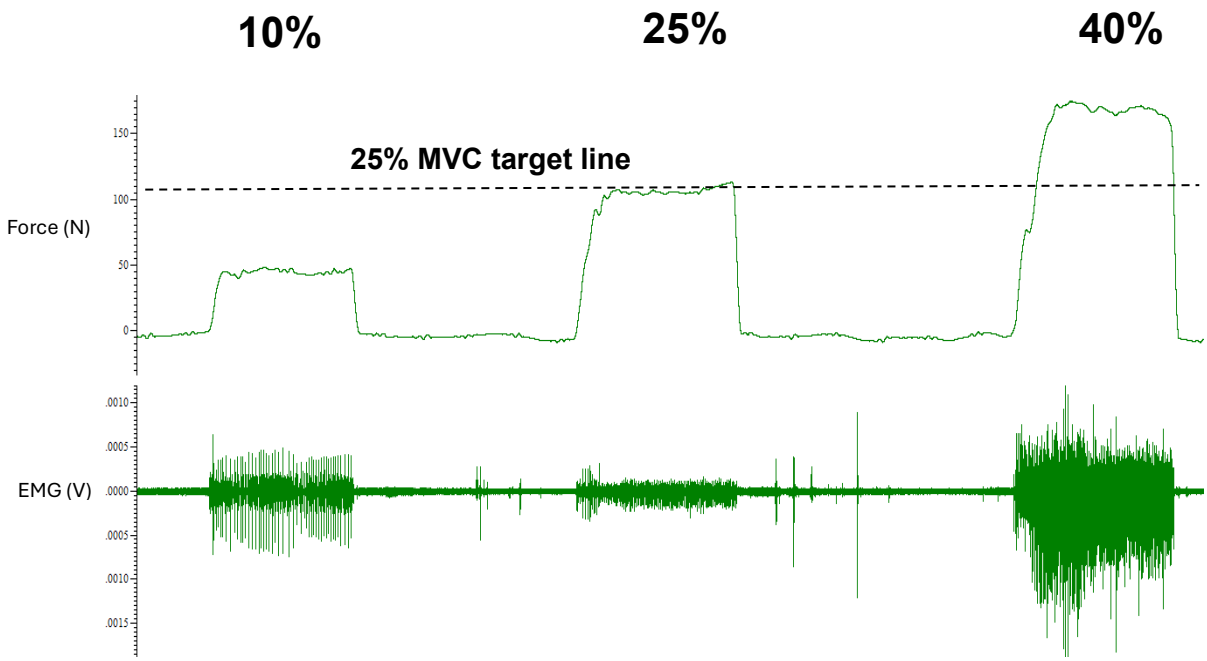

Figure 2.4: *Force and EMG display in Spike2 software during a sustained contraction at each designated contraction intensity: 10%, 25% and 40% of maximal voluntary contraction (MVC). Real time feedback was provided for participants to apply a consistent effort and keep the force at the designated contraction level during isometric knee extensions (top axes). A target line was superimposed on to the screen as a guide regarding required force output. Force steadiness was measured as the coefficient of variation at each contraction level. iEMG signals (MUP data) were sampled via the needle electrode during all contraction intensities (bottom axes) before offline analysis.*

Quantification of force steadiness and MUP data is described in detail in Chapter Four – Section 4.2.

2.6.3 Knee extensor isometric strength, peak torque and work output

The final procedure at Study Visit One involved the assessment of knee extensor isometric strength, isokinetic peak torque and work output during repeated knee extensions using a Cybex Isokinetic dynamometer (Cybex Norm, Rosemont, Illinois, USA). Firstly, a calibration procedure was performed, and the volunteer was secured into the ergometer with a seat belt and Velcro straps placed over the thigh of the dominant leg and around the hips. An image of volunteer set up in the chair ergometer

is provide in **Figure 2.5**. Volunteers were then taken through a familiarisation and warm-up protocol. For knee extension testing, volunteers performed two isometric MVCs with the same instructions provided as those provided for the MVC performed for iEMG testing (Section 2.6.2). Volunteers then performed ten isokinetic repetitions at 90˚/s (speed) as a warmup and familiarisation for isokinetic testing. Warm up sets of five repetitions were then performed at 60˚/s and 180˚/s to familiarise participants with the two speeds measured during the experimental protocol. Upon completion of the warm-up and familiarisation protocol, volunteers rested for 3 minutes and the set-up of the Cybex dynamometer was re-evaluated to ensure correct positioning. It was confirmed that the volunteers understood that the experimental protocol was to be performed under test conditions whereby knee extensions would be performed at maximal effort. After 3 minutes of resting, volunteers performed ten maximal knee extensions at a constant angular velocity of 60˚/s. Following completion another 3 minutes of rest was provided before 10 maximal contractions were performed at 180˚/s. Isokinetic torque was assessed at 60˚/s as this velocity ensures recruitment of all muscle fibre types during contraction, whereas there is preferential recruitment of fast twitch muscle fibres during contractions at 180˚/s. Therefore, considering preferential atrophy of fast twitch muscle fibres is observed during ageing [287, 288], assessing torque at both speeds enabled the assessment of function across all muscle fibres versus specifically fast twitch fibres. Volunteers were encouraged to push hard during all contractions. Each knee extension manoeuvre was initiated from a position of 90˚ knee flexion and continued through to the point of full knee extension. Volunteers were instructed to work as hard as possible on the concentric phase, whilst allowing passive return of the leg to the start position during the eccentric phase.

***Figure 2.5**: Volunteer setup on the Cybex Norm isokinetic dynamometer for knee extension assessments.*

Analyses of data derived from knee extension testing are detailed in Chapter Four – Section 4.2.

2.7 Study Visit Two: MRI physiological phenotyping

On a separate day to Study Visit One, volunteers attended the Sir Peter Mansfield Imaging Centre for a MRI scan. A briefing on the MRI study protocol was provided and the MRI safety screening questionnaire completed at health screening was completed again to confirm potential contraindications to MRI.

2.7.1 MRI study protocol

The MRI study protocol was collected on a Philips 3T Ingenia wide-bore (70 cm) scanner. MRI scans were performed while volunteers were at rest in a supine position to quantify body composition, and morphometric and dynamic cardiac and brain parameters. A schematic of the MRI scan protocol is presented in **Figure 2.6** and

images of the scanner setup are presented in **Figure 2.7**. Heart rate was continuously measured throughout all scans using a VCG or PPU device and respiration using a pneumatic belt, with the physiological data exported as log text files. In total, the MRI scan lasted for approximately 55 minutes, with approximate times for each component being: 10 minutes for the whole-body mDIXON scan, 20 minutes for the cardiac scans and 25 minutes for the brain scans.

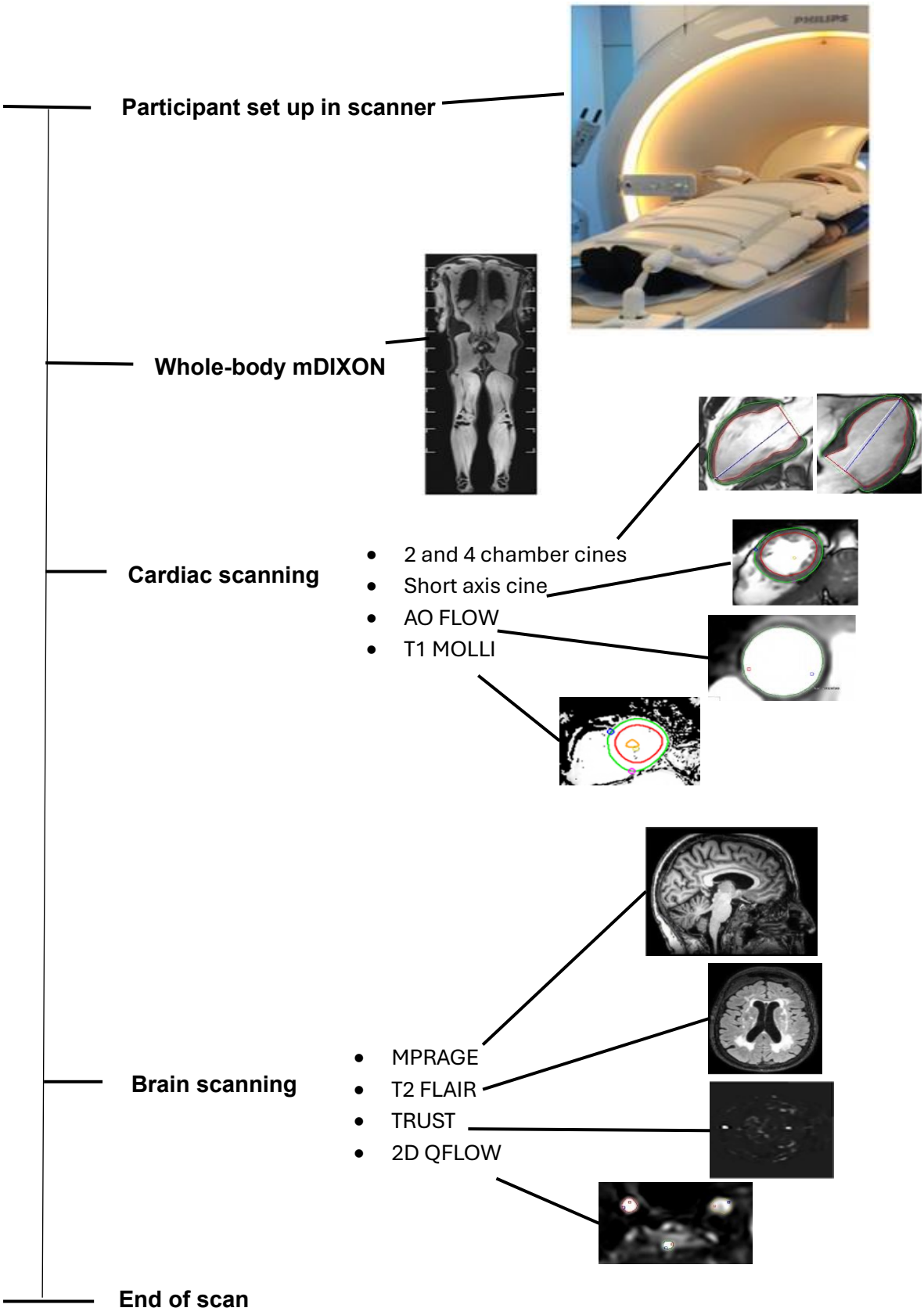

Figure 2.6: *Schematic overview of the MRI protocol collected in Study Visit Two.*

Figure 2.7: *Philips 3T Ingenia MRI scanner shown with the 15-channel head coil and upper and lower anterior body coils - used in conjunction with the integrated FlexCoverage Posterior coils in the scanner bed for whole body mDIXON scan acquisition (left). Scanner set up for cardiac scanning, with lower anterior coil removed and plastic frame used to support the upper anterior coil (right).*

Volunteers were first scanned using a whole-body mDIXON protocol to assess skeletal muscle volume and intramuscular fat fraction of the lower limbs and visceral adiposity of the abdomen. For this the 15-channel head coil, as well as two upper and lower anterior body coils, were used, as shown in **Figure 2.7**. The upper anterior coil was supported with a plastic frame, where possible, for participant comfort. mDIXON images were collected at six table positions covering the head to the toes.

Following the whole-body mDIXON protocol, scanning was briefly stopped whilst the head and lower anterior coils were removed by the scanner operator. The upper anterior coil remained covering the volunteer's torso (**Figure 2.7**). The cardiac scanning protocol was then commenced to assess morphometric and dynamic cardiac parameters including, EDV and ESV, SV, EF, CO, LV mass, circumferential strain,

longitudinal strain, LV MOLLI T1, and the CSA and blood velocity of the aorta. Parameters were indexed to BSA where applicable.

Scanning was then stopped again upon completion of the cardiac protocol. The upper anterior and 15-channel head coils were removed, and the 32-channel head coil was fixed to the scan bed for dedicated brain scanning (**Figure 2.8**). The brain scanning protocol included a structural MPRAGE scan to measure global and regional grey matter volume, white matter volume, cerebrospinal fluid volume, cortical thickness, gyrification index and sulcus depth, and T2-FLAIR to assess white matter hyperintensity volume. In addition, measures were collected of venous oxygenation in the sagittal sinus, as well as velocity of blood flow and CSA of basilar and carotid arteries for global cerebral blood flow, and from this oxygen extraction fraction, cerebral oxygen derived metabolic rate could be assessed.

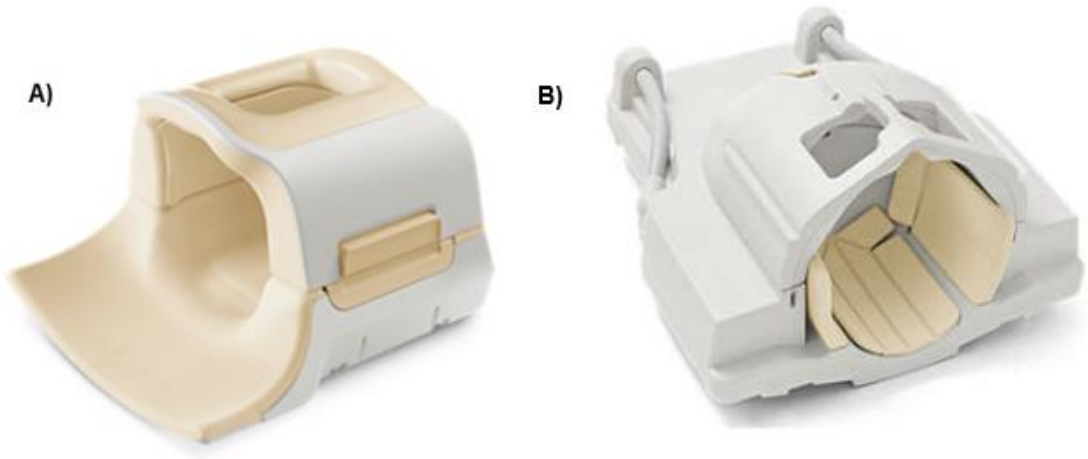

Figure 2.8: A) *Philips 15-channel head coil used to scan the head during the whole-body mDIXON scan.* ***B)*** *Philips 32-channel head coil used for dedicated measurement of brain morphometry, cerebral blood flow and oxygenation.*

2.8 MRI sequences

This section outlines the MRI sequences collected within the Study Visit Two. The processing of MRI data to derive end-point measures are detailed in the relevant

Methods section of each experimental Chapter. At the start of whole-body, cardiac and brain sections of the MRI scan protocol, a survey scan was performed to aid in planning of the final image. In essence, a survey scan provides an initial low spatial resolution image focussed on the area of interest onto which planning of slices (e.g., identifying an ROI within the head for brain scanning) was performed. Example images of the planning scans and final generated images from each MRI sequence are provided in the subsequent sections.

2.8.1 Multipoint DIXON (mDIXON) scanning: skeletal muscle volume, fat fraction and visceral adipose tissue volume endpoints

An mDIXON scan was employed to generate a whole-body image, from which body composition measures can be assessed. Here the chosen metrics were those of skeletal muscle volume and intramuscular fat fraction of the lower limbs, and visceral adipose tissue volume of the abdomen. The DIXON technique exploits the different precession frequency of water and fat [289]. As a result, over time, protons within the water and fat will alternate between being in-phase and opposed-phase, thus allowing images to be generated which are specific to fat and water content, as well as the fat fraction image (**Figure 2.9**). The whole body mDIXON sequence, developed by [290], was collected in six stacks of 1 mm in-plane and a 6 mm slice thickness, reconstructed to 1.92 x 1.92 x 3 mm voxels, FA = 3, TR = 10 ms, TE = 2 ms with 6 echoes (also allowing a T2* image to be generated). The two abdominal stacks are collected in a breath-hold.

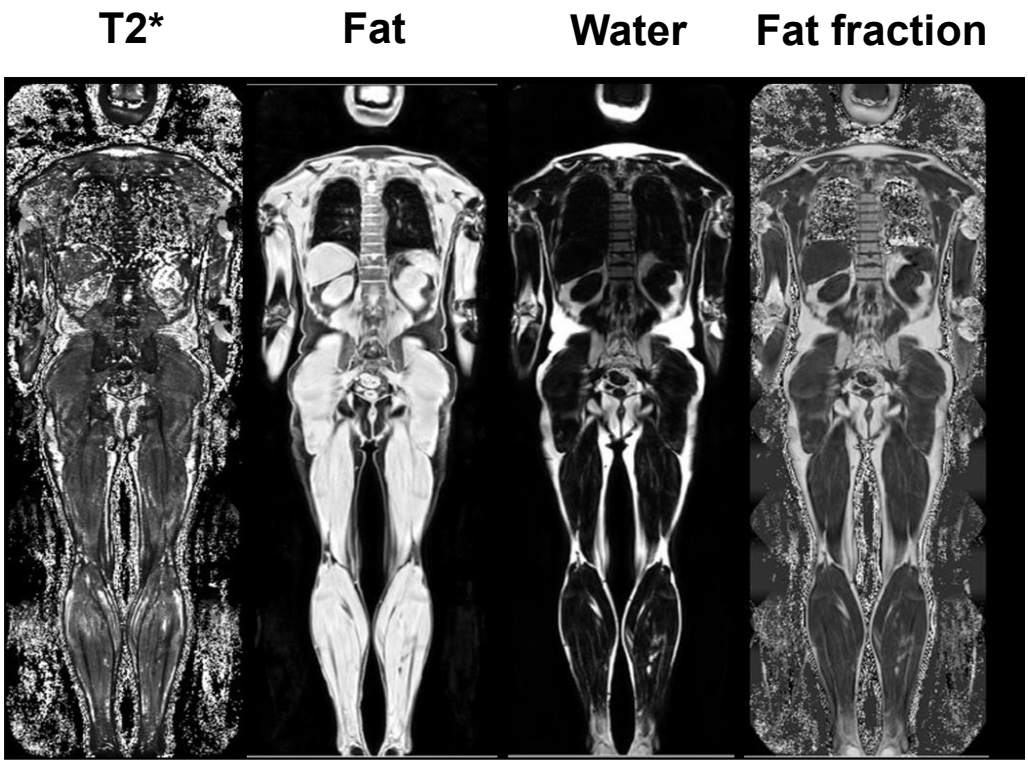

Figure 2.9: *Example whole body mDIXON images. Water and fat images shown in the middle along with fat fraction images. Collecting data at a range of echo times also provides a T2* image.*

2.8.2 Cardiac MRI

Long axis (LAX) 2-chamber and 4-chamber cardiac MR scans were used to assess LV structure and functional parameters. The scans were collected in an expiration breath hold and were triggered by heart rate (i.e., using information from continuously tracking heart rate using the PPU, such that the scan was initiated automatically by the start of the heartbeat and terminated upon completion of the beat). Long axis cine images were acquired with balanced fast-field echo with a typical TR of 3.4 ms, TE = 1.7 ms, FA = 45º, acquisition matrix = 195 x 195 mm, 20-30 phases per cardiac cycle. Scans were performed in a single ten second breath hold at FOV of 300 x 300 x 8 mm, with 2 x 1.6 mm voxels in-plane, and an 8 mm slice thickness. Planning and resultant LAX cine scans are shown in **Figure 2.10**.

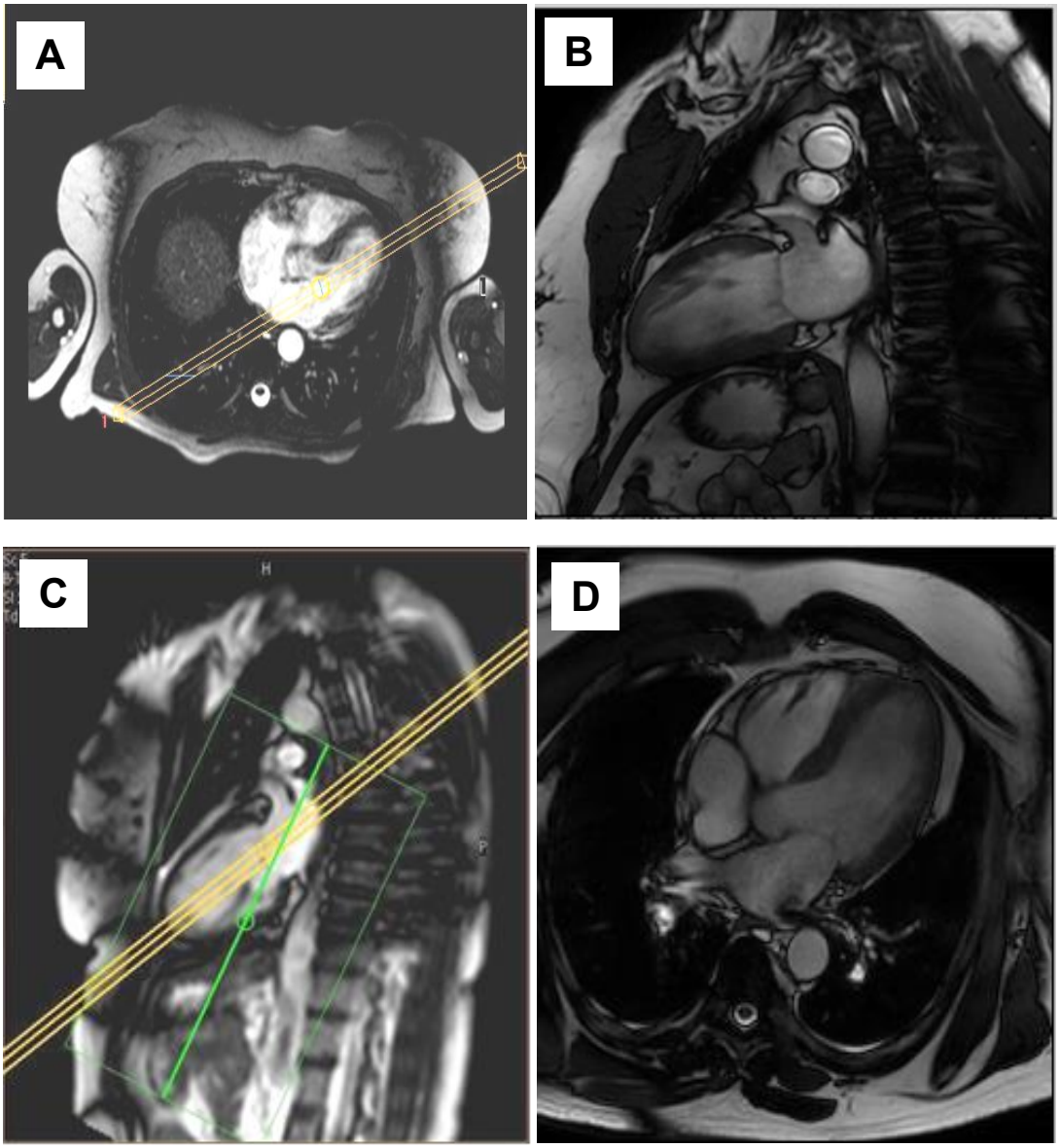

Figure 2.10: *Planning of scans and resultant images for 2 chamber and 4 chamber LAX cine scanning.* ***A)*** *Planning of scans performed on axial survey scan of the chest to produce* ***B)*** *final 2 chamber view of the left ventricle and left atrium.* ***C)*** *2 chamber view used in planning the 4 chamber view.* ***D)*** *Final 4 chamber view of heart, showing left ventricle, left atrium, right ventricle, right atrium.*

Short axis (SAX) cine scans provided an identical set of measures, concerning LV structure and function, to the long axis scans. These scans were taken axially across the left ventricle, capturing the whole heart. Short axis cine images were acquired using balanced fast-field echo with a typical TR of 3.4 ms, TE = 1.7 ms, FA = 45º, 20-

30 phases per cardiac cycle, with one slice per breath hold. Scans were captured with FOV = 300 x 200 x 118 mmm, voxel size = 2 x 1.6 mm and 8 mm slice thickness. The entire short axis stack of scans required six breath holds. Planning and images for short axis cine scans shown in **Figure 2.11**.

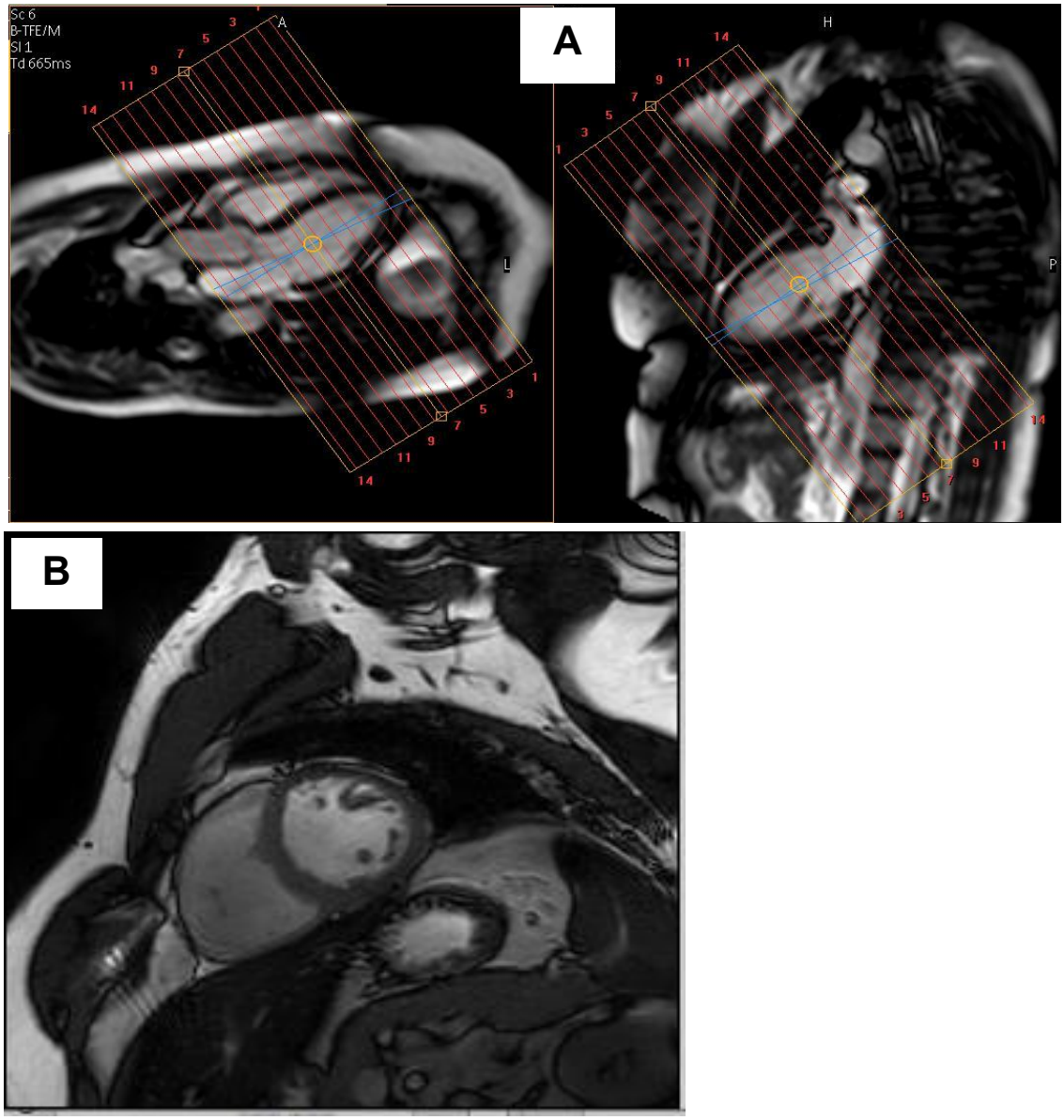

Figure 2.11: *Planning of scans and final images for short axis cine scanning.* ***A)*** *Scan set up and planning utilising 4 chamber (left) and 2 chamber (right) views. Slices stacked through entire left ventricle.* ***B)*** *Example image from one slice of stack. Axial slice of mid left ventricle shown.*

In conjunction with the SAX cine, the 2-chamber and 4-chamber LAX scans provided a 3D representation of the left ventricle and facilitated identification of apical and basal segments as well as end diastolic and end systolic phases. Parameters derived from these scans were correlated against measures acquired from the short axis scans to validate the measurements (described in Chapter Three). The use of both SAX and LAX scans provided a robust method of assessing cardiac function.

2.8.3 Aortic flow (AOFLOW)

Phase contrast MRI (PC-MRI) was used to measure aortic blood flow. The basic premise of PC-MRI relates to the measurement of the net phase shift of moving spins due to flow within a blood vessel during the application of a bipolar magnetic field gradient, with this phase shift being directly proportional to blood velocity. PC-MRI acquires two data sets, with flow sensitivity varied between these acquisitions, and controlled by the strength of an applied bipolar gradient pair of equal magnitude and opposite polarity. The first data set is acquired without flow sensitivity while the second is acquired with a flow sensitive sequence of a defined velocity encoding. Stationary tissue spins will therefore experience no phase shift, while moving blood spins experience a non-zero phase shift. The two data sets are subtracted, producing a phase contrast image. Since the phase shift is proportional to the spin's velocity, quantitative assessment of flow velocity is achieved. This is illustrated in **Figure 2.12**. PC-MRI is collected at 30 time points over a cardiac cycle using the VCG/PPU, and if the cross-section area of the vessel is also measured then this allows blood flow over the cardiac cycle to be measured.

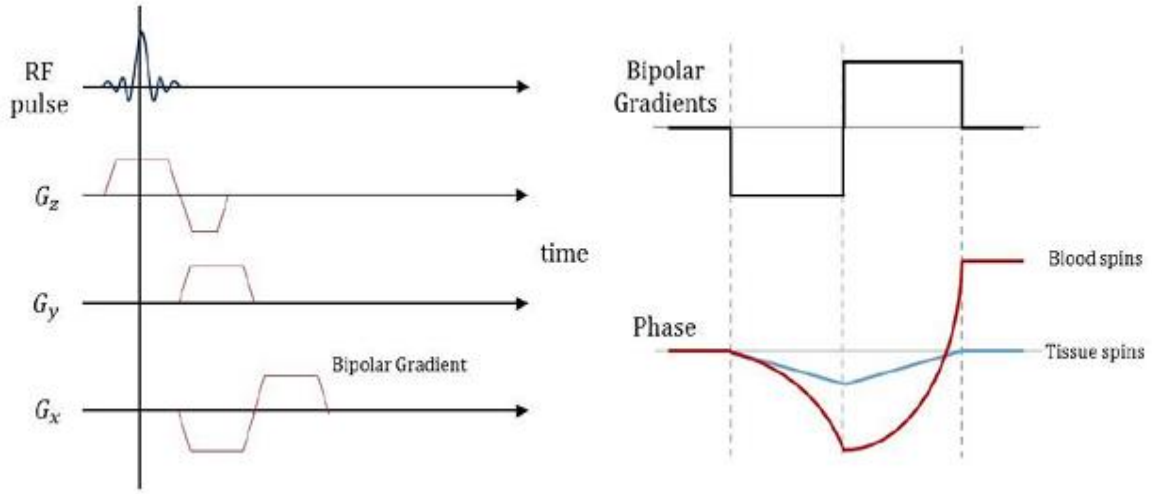

Figure 2.12: *Pulse sequence diagram for PC-MRI sequence, demonstrating the effect of bipolar gradient application on the phase of spins. This is shown for stationary tissue spins (blue line) and blood moving through a vessel (red line).*

PC-MRI has become a popular method quantitation of aortic blood flow in the ascending aorta [291]. In this study, aortic flow was acquired using a free breathing PC-MRI measure with scan parameters of FOV = 280 x 264 mm, voxel size = 2 x 2 mm, FA = 15º and slice thickness of 10 mm. **Figure 2.13** shows the planning scans and final image of AOFLOW scan. AOFLOW scans were triggered by heart rate.

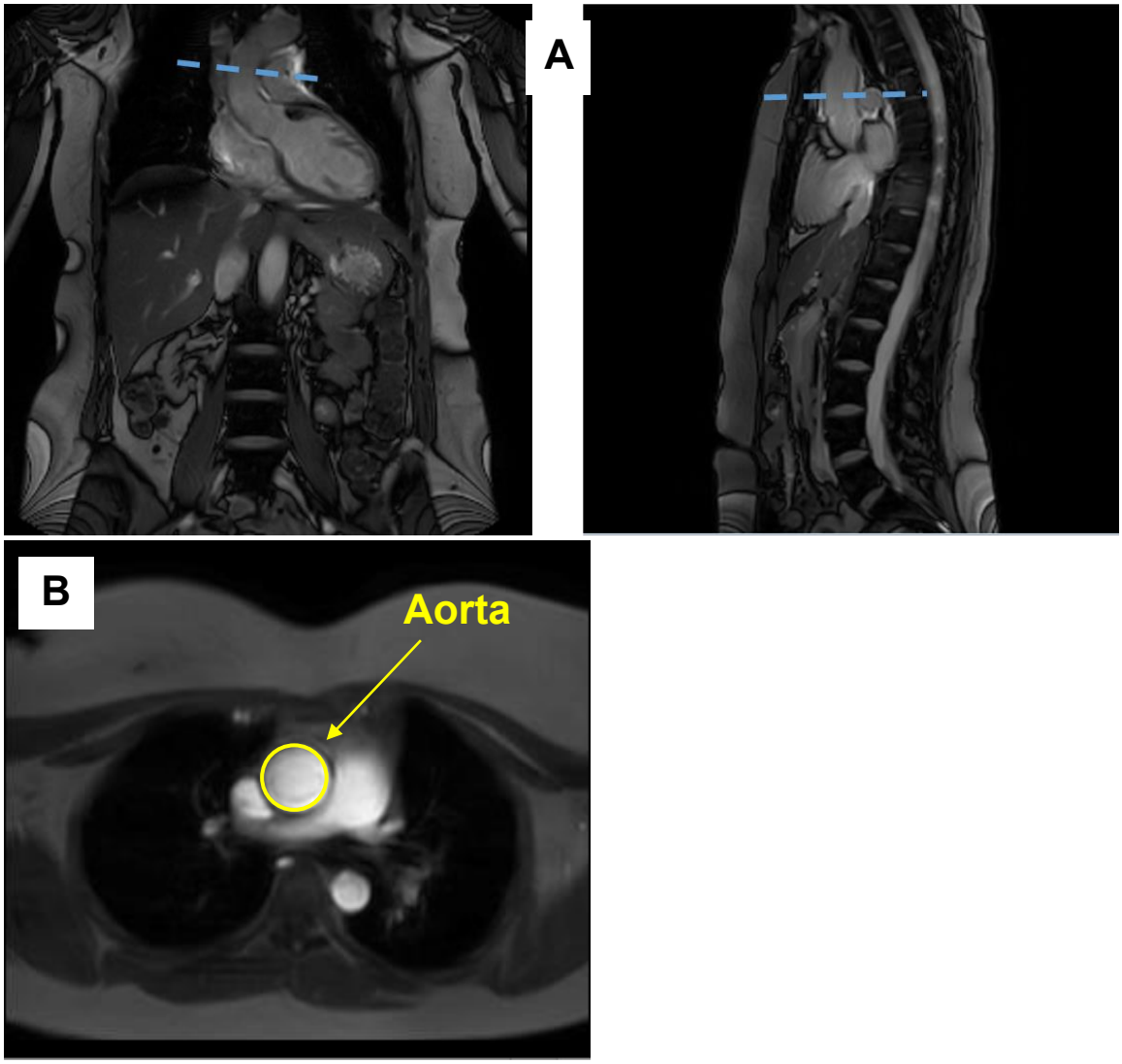

Figure 2.13: *Planning of scans and final images for aortic flow scanning.* ***A)*** *Imaging slice (blue dashed line) placed perpendicular to ascending aorta using coronal and sagittal localiser scans.* ***B)*** *Final axial cross section image of aorta through which PC-MRI measures are collected to measure changes over a cardiac cycle.*

2.8.4 Cardiac Modified Look-Locker Inversion Recovery (MOLLI) T1 mapping

A MOLLI sequence [292] using a 5(3)3 scheme was performed to collect a T1 map in a single midventricular SAX slice of the heart to assess myocardial fibrosis. Planning for this short axis cine scanning is as shown in **Figure 2.11**. This single stack was acquired in a single inspiration breath hold, triggered by the heart rate in the sagittal orientation. TR = 2.4 ms, TE = 1.11 ms, NSA = 1, flip angle = 35°, FOV = 360 × 8 x

273.6 mm, in the foot-head directions x right-left × anterior-posterior directions, voxel size = 1.8 x 1.8 mm and slice thickness = 8 mm. **Figure 2.14** shows the T1 maps generated from these scans.

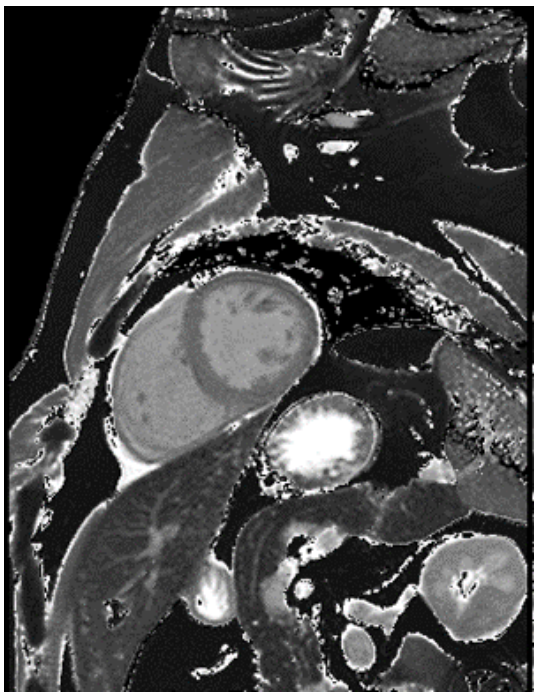

Figure 2.14: *T1 maps of the left ventricle (axial view) generated from MOLLI sequence.*

2.8.5 Brain three-dimensional magnetization prepared rapid gradient-echo (MPRAGE)

A MPRAGE is a common sequence utilised for high-spatial resolution brain imaging with T1-weighting. The sequence provides whole brain images with excellent grey matter/white matter/cerebrospinal fluid (GM/WM/CSF) tissue contrast. The MPRAGE sequence was used to compute global and regional volumes of GM, WM and CSF, and measures of cortical thickness, gyrification index and sulcus depth. The sequence was acquired in the axial-oblique plane along the AC-PC line with 1 mm isotropic resolution; TE = 8.3 ms, TR = 3.8 ms, FA = 8°, 160 slices, FOV = 256 x 256 x 162 mm.

The sequence has wide-ranging clinical application, particularly in disease diagnosis [293] and assessing disease course [294]. The planning of scans and generated images from the MPRAGE sequence are highlighted in **Figure 2.15**.

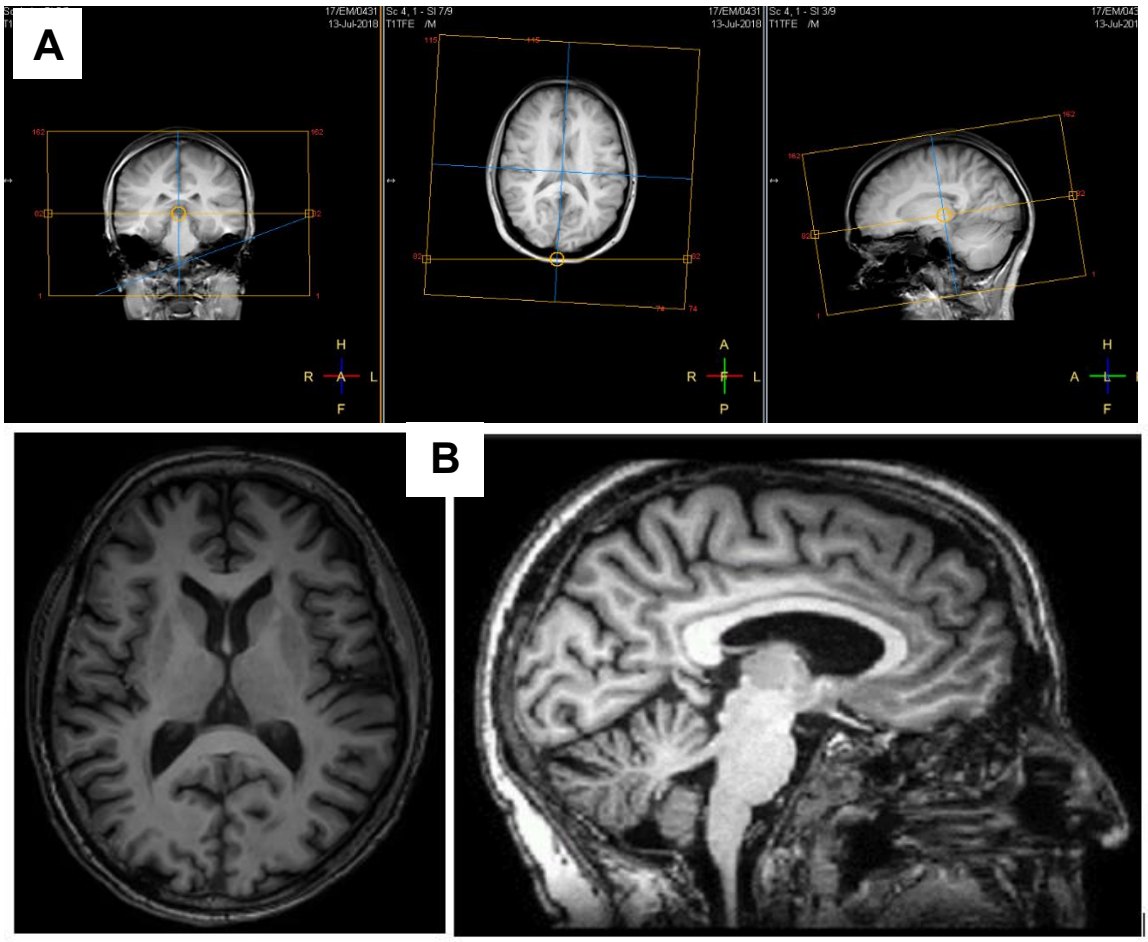

Figure 2.15: A) *Planning of MPRAGE sequence using brain survey scans.* ***B)*** *Example images resulting from MPRAGE scan showing high resolution T1-weighted image in axial (left) and reconstructed in the sagittal (right) orientation.*

2.8.6 Brain T_2-weighted-Fluid-Attenduated Inversion Recovery (T_2-FLAIR)

A T_2-FLAIR sequence was used to assess the presence and volume of brain white matter hyperintensities. The T_2-FLAIR incorporates T_2-weighting to enhance signal intensity from water in the brain. With the fluid attenuation sequence supressing the signal from CSF, the higher water content of WMHs relative to healthy white matter

tissue owes to the brighter appearance of lesions within the image. This is highlighted by the bright lesion appearance on the resulting image (**Figure 2.16**). The T2-FLAIR scan was collected with a FOV of 256 x 256 x 162 mm, 1 mm isometric voxels, 162 slices, a TR of 5000 ms and TE of 0.35 ms.

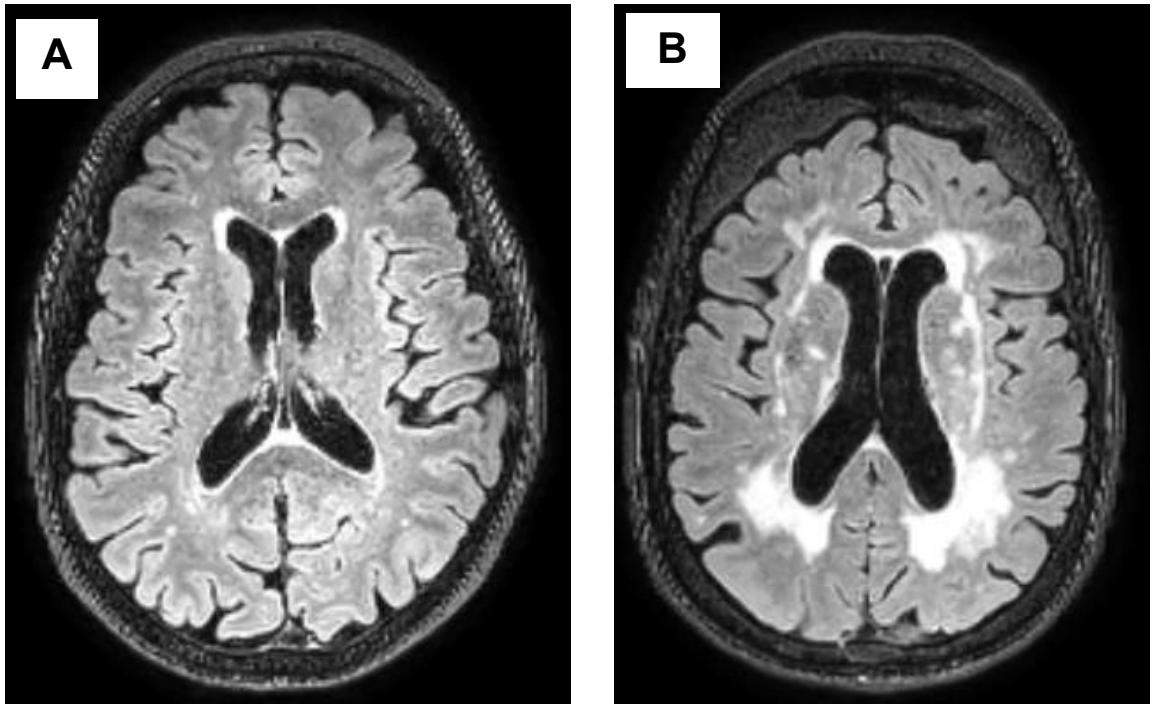

Figure 2.16: *Example image generated from T2-FLAIR sequence, with white matter hyperintensities (WMHs) appearing bright. Examples of volunteers with low* ***(A)*** *and high* ***(B)*** *number and volume of WMHs.*

2.8.7 Cerebral haemodynamics using PC-MRI

Similarly to aortic flow measures, PC-MRI is used for the non-invasive quantitation of cerebral haemodynamics to assess blood flow in the brain through the internal carotid and basilar arteries [295] with a cardiac triggered 2D-QFLOW sequence. In this work, blood flow in the left and right internal carotid arteries and the basilar artery was assessed from a T1FFE planning scan, with slices positioned perpendicular to the direction of flow in the vessel of interest (**Figure 2.17**). Scan parameters were FOV =

150 x 178 mm, spatial resolution = 1.15 x 1.15 mm, slice thickness = 3 mm, SENSE factor 3, TE = 6.5 ms, TR = 15 ms, FA = 20°, VENC 140 cm/s. The sequence was cardiac triggered using the PPU with the data acquired at 30 time points across the cardiac cycle. The duration of the scan was thus dependant on the participant's heart rate.

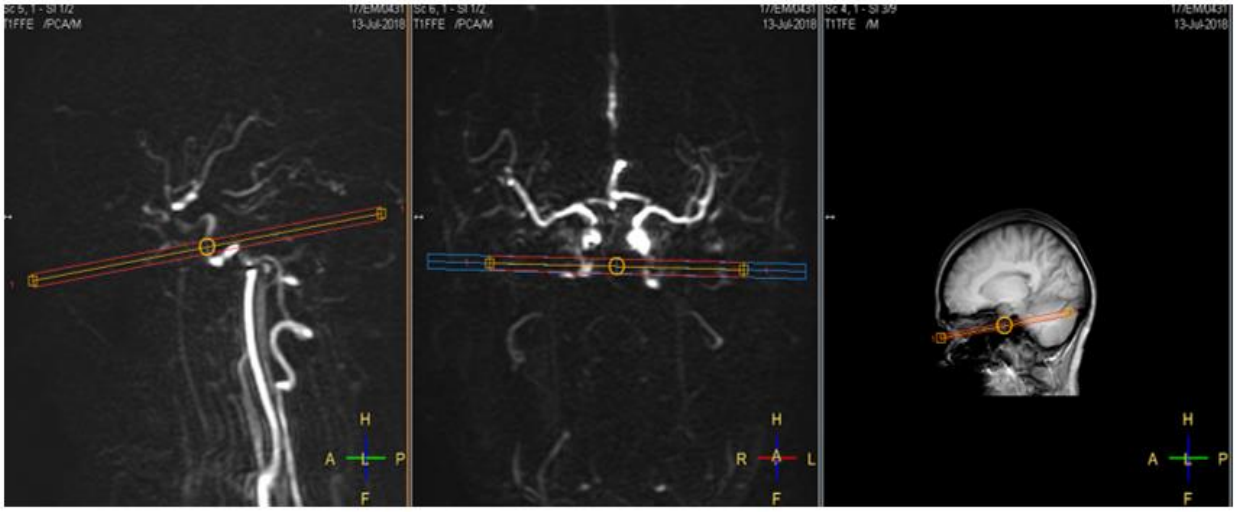

Figure 2.17: *Planning scans for phase contrast MRI sequence assessing blood flow through the basilar and internal carotid arteries.*

2.8.8 Brain T2-Relaxation-Under-Spin-Tagging (TRUST-MRI)

TRUST-MRI is a more recently developed method for quantitative measurement of cerebral oxygenation [296]. Application of the TRUST method to the brain utilises the spin labelling principle, but here it is used to isolate venous blood signal in the sagittal sinus [297]. Following a FAIR labelling pulses (with alternating non-selective and selective inversions for flow labelling) a flow-insensitive T2-preparation pulse scheme is applied, and from this the sagittal sinus can be isolated and the T2 relaxation time of the venous blood within this computed. This T2 relaxation time is then converted into blood oxygenation using a calibration plot [298] which enables quantification of

venous oxygenation and the oxygen extraction fraction percentage. Scan parameters for the TRUST sequence used had an in-plane FOV of 220 x 220 x 5 mm, spatial resolution = 3.44 x 3.44 mm, slice thickness = 5 mm, FA = 90°, TI = 1022 ms, and TR = 3000 ms per label/control pair. Four eTEs were collected at 1, 40, 80, 160 ms corresponding to 0, 4, 8 and 16 refocussing pulses in the T2 preparation with an interval τcpmg = 10 ms (Carr-Purcell-Meiboom-Gill). The scheme comprised a FAIR labelling scheme with selective/nonselective thickness of 25/300 mm. **Figure 2.18** shows planning of TRUST sequence over the sagittal sinus.

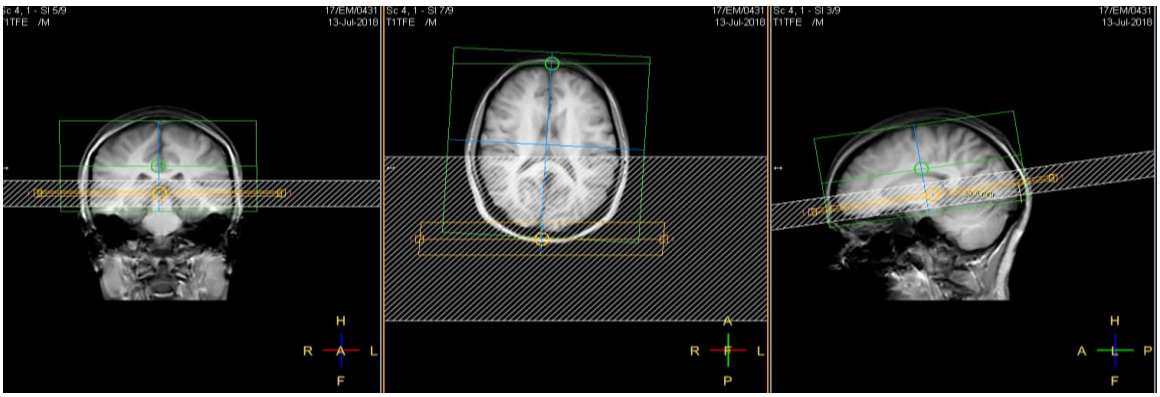

Figure 2.18: *Planning process of TRUST sequence using brain survey scans. Yellow box represents the imaging plane placed through the sagittal sinus. White box shows the FAIR selective slab. Shim box shown in green.*

2.8.9 Unanalysed brain MRI sequences

In addition to the MRI sequences outlined above, this study also collected data from several MRI sequences that were not analysed for inclusion in this thesis, therefore were not described in this Chapter or the associated experimental Chapters. The sequences not included were: Arterial Spin Labelling (measuring global cerebral perfusion), Diffusion Tensor Imaging (assessing brain white matter microstructural integrity) Time-of-Flight Angiography (quantifying the number and radii of arterial blood

vessels within the brain), abdominal T1 mapping (measuring inflammation and fibrosis in the kidney, liver and spleen). The analysis of these data is discussed as a direction for further research in Chapter Six.

2.9 Statistical analysis

Statistical analyses were conducted using GraphPad Prism V.9 (GraphPad Software, Boston, Massachusetts, USA). One way ANOVA with Tukey's post hoc test was used to compare groups (non-frail vs pre-frail vs frail) of continuous parametric variables. Correlation between continuous variables was performed using Pearson's linear correlation analysis. Significance was accepted on all occasions at $P < 0.05$. Values in the text, Tables and Figures represents mean ± standard deviation. Given the low number of frail individuals recruited ($n = 6$), for several analyses data from the pre-frail and frail groups were collapsed and compared to the non-frail group. Student's independent T-test was performed on the collapsed groups (i.e., non-frail vs collapsed pre-frail and frail) for parametric data. In experimental Chapters, data comparing all three groups (i.e., non-frail vs pre-frail vs frail) are presented first, followed by comparison of data from the non-frail versus collapsed pre-frail and frail group. All data were tested for normality using the Shapiro-Wilk test. For data with a non-normal distribution, non-parametric statistical tests were used for analysis. To analyse non-parametric data, the Kruskall-Wallis test was used to compare the 3 groups (non-frail, pre-frail and frail) the, and the Mann-Whitney U test was used when comparing the 2 groups (non-frail versus the collapsed pre-frail and frail group).

Chapter Three: Cardiac Structure and Function in Non-frail, Pre-frail and Frail Females

3.1 Introduction

The importance of investigating cardiac structure and function as components of the frailty phenotype was outlined in Chapter One - Section 1.5.4, with a summary of potential cardiac characteristics present during frailty shown in **Figure 1.2**. In brief, a rationale for investigating cardiac structure and function in the context of frailty was provided by a study of 6,000 non-frail, 7,000 pre-frail and 1,500 frail individuals which reported that frail (odds ratio = 3.4) and pre-frail (odds ratio = 1.5) volunteers were at higher risk of cardiovascular disease and all-cause mortality compared to non-frail counterparts [173]. Despite this increased risk, relationships between cardiac structure and function and frailty status remain equivocal. For example, lower LV ejection fraction has been reported in frail versus non-frail individuals in some studies [179, 180], but not others [181, 182].

Disparity may be underpinned by several factors, including the older age of volunteers in some studies [179] versus others [181], differences in frailty assessment methods (e.g., the 'slowness' frailty criterion measured by a sit-to-stand test [179] or by slow walking speed [180]), and mixed sex samples [177, 179-181] which may have imparted variance into the data due to sex-related differences in cardiovascular parameters [299]. As such, improving and standardising study designs would likely benefit consensus regarding the possible interaction of cardiac deterioration and frailty development. Furthermore, given the use of echocardiography in many previous study protocols, it would also be efficacious to employ cardiac MRI methods to improve the

reliability and validity of results, considering this method is less patient- and investigator-dependent than echocardiography [183-185].

Cardiac MRI also permits the assessment of unique parameters that cannot be quantified with other methodologies. For example, native T1 mapping of the myocardium quantifies the longitudinal relaxation (T1) time taken for protons (primarily in water) within the cardiac tissue to return to equilibrium following perturbation with a radiofrequency pulse (usually an inversion pulse) during MRI. Longer T1 relaxation times in cardiac muscle are indicative of inflammation and fibrosis [300]. This is because native T1 reflects a composite signal from both the intracellular (predominantly myocytes) and extracellular spaces (which includes the interstitial and intravascular compartments). T1 detects free water and increased free water content in tissue, such as oedema or water collecting in expanded interstitial spaces. T1 does not directly detect collagen fibres, but it does detect the accumulation of water around fibrotic tissue which prolongs native T1 relaxation times. Cardiac T1 mapping has been shown to be predictive of all-cause mortality [301, 302], and may therefore be associated with frailty. However, reports of MRI being used to investigate associations between cardiac T1 parameters and frailty status are scarce, with only preliminary data available from a study of a small number of participants in which statistical analysis was not performed [303].

Given the equivocal nature of the published literature to date regarding cardiac structure and function and frailty status, and the lack of frailty studies using robust cardiac MRI methods, the aim of the present Chapter was to utilise multi-modal cardiac MRI to compare structural and functional cardiac measures between non-frail, pre-frail and frail volunteers. The hypothesis was that the use of highly accurate MRI assessments would provide novel insight. Based on epidemiological associations

between cardiovascular disease and all-cause mortality and frailty status outline above, it was hypothesised that pre-frail and frail individuals would exhibit differences in cardiac structure and function compared to non-frail counterparts. To test this hypothesis, non-frail, pre-frail and frail females underwent resting state supine cardiac MRI to assess the multiple measures of structure (e.g., LV mass and T1 relaxation time), and function (e.g., cardiac output, ejection fraction) of the heart.

3.2 Methods

Cardiac MRI parameters were assessed using the scan protocol outlined in Chapter Two – **Figure 2.6**, with descriptions of the scan parameters for all cardiac sequences provided in Chapter Two, Section 2.8. The following section outlines the analysis of the cardiac MRI data performed using cvi42 software (Circle Cardiovascular Imaging Inc; version 5.14.2) to quantify structural and functional variables of the heart in the non-frail, pre-frail and frail female volunteers. All abbreviations used in this Chapter are outlined on pages 13-17.

3.2.1 Cardiac structure and function using cine measures

In this work cardiac MR cine scans have been collected of both the long and short axes (LAX and SAX), The analysis of each of these measures and their comparison is provided below.

3.2.1.1 Long axis (LAX) 2- and 4- chamber and 4 cine measures

Segmentation of the LAX 2- and 4-chamber cine images was performed using the cvi42 automatic segmentation tool to superimpose ROIs on to the borders of the left ventricle epicardium and endocardium for each image over the cardiac cycle. This was used to identify end diastolic and end systolic cardiac phases for both 2- and 4-chamber views (**Figure 3.1**). Manual adjustments to contours were made following the

automatic segmentation, where necessary. Papillary muscles were included in the blood pool. From the delineated endocardial contours, EDV and ESV were calculated (**Figure 3.1**). SV, EF and CO were also computed for LV function assessment. SV was computed from (EDV-ESV), EF from SV/EDV, and CO was computed from (SV x heart rate). LV mass was calculated as the total epicardial volume minus the endocardial volume multiplied by the specific density of the myocardium (1.05 g/ml). Longitudinal strain on the left ventricle was calculated by measuring the deformation of the contours over the phases (i.e., over the complete course of diastole and systole). EDV, ESV, SV, LV mass and CO were adjusted for BSA.

LV volume parameters were determined using a combination of measurements from the 2-chamber and 4-chamber scans using the biplane approach:

$$LV\ volume\ =\ 0.85\ \times\ (LVarea1\ x\ LVarea2)\ /\ LV\ length$$

where LV area1 is the area in the 4-chamber view and LV area2 is the area in the 2-chamber view.

The left ventricular global function index (LVGFI) calculated from:

$$LVGFI = SV\ /\ [LV\ mass/q + (ESV + EDV)/2] \qquad [304]$$

where q = myocardial density and is assumed to be 1.05 g/ml. LVGFI is a relatively novel metric that integrates LV structure and function, and has been shown to be a strong predictor of incident heart failure and cardiovascular events [305].

The intra-rater CV of analysis was calculated for each parameter to determine the reliability of the contour analyses of long axis images. Three repeat measures were performed on 1 participant's set of long axis images and the mean and standard deviation of measures calculated. CV was calculated from:

*CV = (standard deviation/mean) * 100*

For all measures, CV was less than 5% (**Table 3.1**). Raw data for the three CV calculations are presented in **Appendix 3.1**.

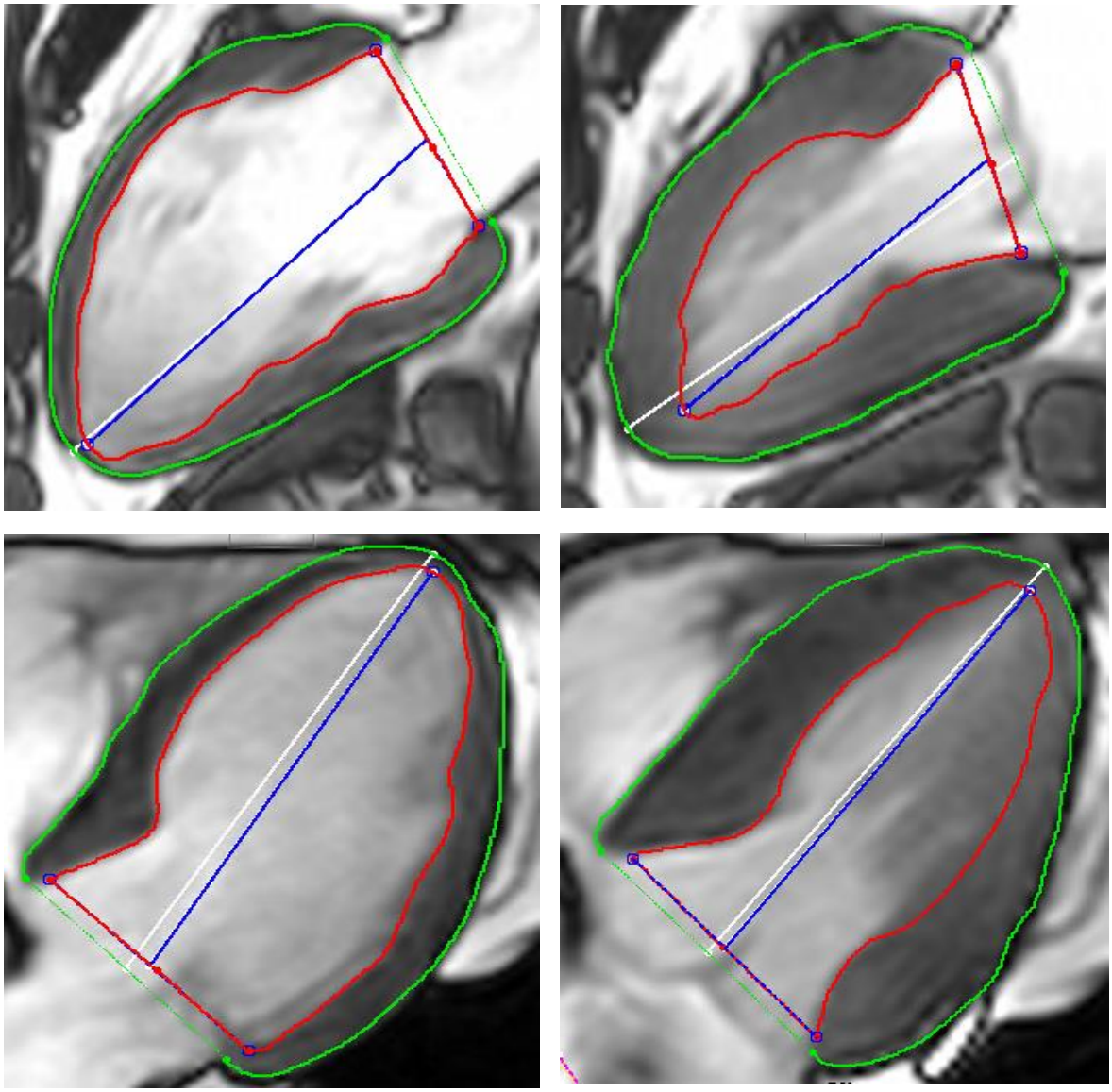

Figure 3.1: *Example of the long axis 2 chamber (top images) and 4 chamber (bottom images) views with the respective epicardial (green) and endocardial (red) contours drawn around the left ventricle within the end diastolic (left hand side images) and end systolic (right hand side images) phases.*

Table 3.1: Intra-rater coefficient of variance (CV) for repeated analysis of long axis (LAX) cine images.

LAX cardiac parameter	CV (%)
End diastolic volume index (ml/m^2)	2.6 %
End systolic volume index (ml/m^2)	2.4 %
Stroke volume index (ml/m^2)	4.8 %
Ejection fraction (%)	2.3 %
Cardiac index (L/min/m^2)	4.8 %
Left ventricular mass index (g/m^2)	1.1 %
Longitudinal strain (%)	1.4 %

3.2.1.2 Cardiac structure and function - short axis (SAX) cine

Epicardial and endocardial segmentation of the LV in the short axis cine was performed by identifying the most apical and basal segments, in accordance with the current guidance on cardiac MRI post processing analysis [306]. The corresponding LAX 2-chamber and 4-chamber images were also used to aid identification of apical and basal segments. An automatic segmentation tool in cvi42 was used to superimpose ROIs on to the epicardial and endocardial borders in all phases, from the base to apex of the left ventricle, to identify end diastolic and end systolic phases (**Figure 3.2**). Manual adjustments to contours were made where necessary. Papillary muscles were included in the blood pool. Analysis of these scans yielded EDV, ESV, SV, EF, LV mass and circumferential strain. Images were excluded from the analysis if they did not include the full set of LV slices from base to apex - for example, due to inappropriate breath holding.

The intra-rater CV for analysis of each short axis parameter was calculated to determine the reliabilty of the contour analyses of cine images. For CV calculations, three repeat measures were performed on 1 set of short axis cine images. All SAX measures had an intra-rater CV of less than 2% (**Table 3.2**). Raw data for CV calculations are presented in **Appendix 3.1**.

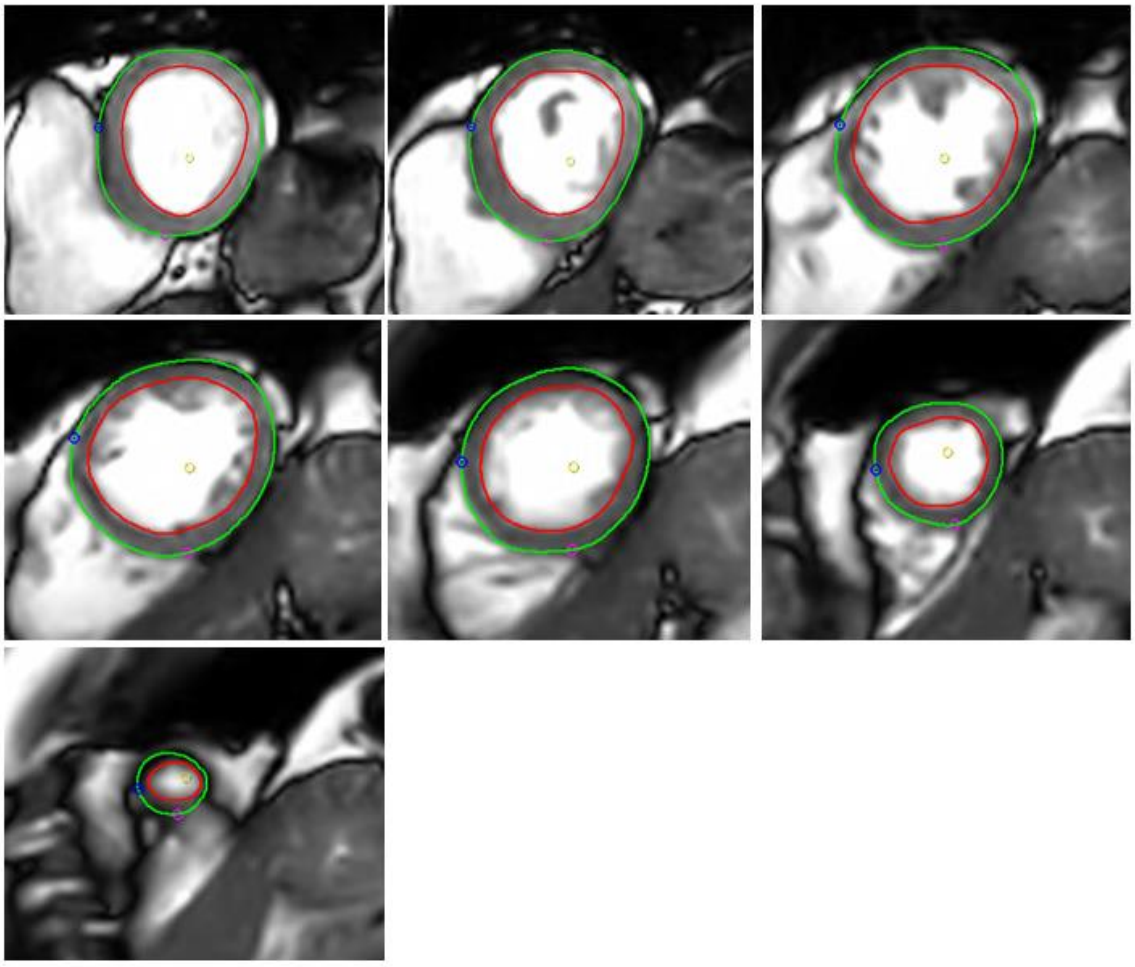

Figure 3.2: *Example of left ventricle short axis cine analysis in cvi42 software. Epicardial (green) and endocardial (red) contours drawn on the image for each slice. Superior (blue) and inferior (pink) short axis reference points added. Slices are shown from basal slice (top left) in descending order (left to right) to apical slice (bottom left).*

Table 3.2: Coefficient of variance (CV) results for repeated analysis of short axis (SAX) cine images.

SAX cardiac parameter	CV (%)
End diastolic volume index (ml/m^2)	0.4 %
End systolic volume index (ml/m^2)	1.7 %
Stroke volume index (ml/m^2)	1.4 %
Ejection fraction (%)	0.6 %
Cardiac index (L/min/m^2)	1.6 %
Left ventricular mass index (g/m^2)	0.9 %
Circumferential strain (%)	1.5 %

3.2.1.3 Correlation between short axis and long axis cine LV measures

Given the short and long axis scans generated an identical set of parameters, with the exceptions of longitudinal strain and circumferential strain quantified by long and short axis scanning, respectively, Pearson's linear correlation analyses was performed to determine the level of agreement in measures across subjects for the SAX and LAX scans. All measures showed highly significant positive correlations (r value range: 0.73-0.9) between SAX and LAX scans (**Figure 3.3**).

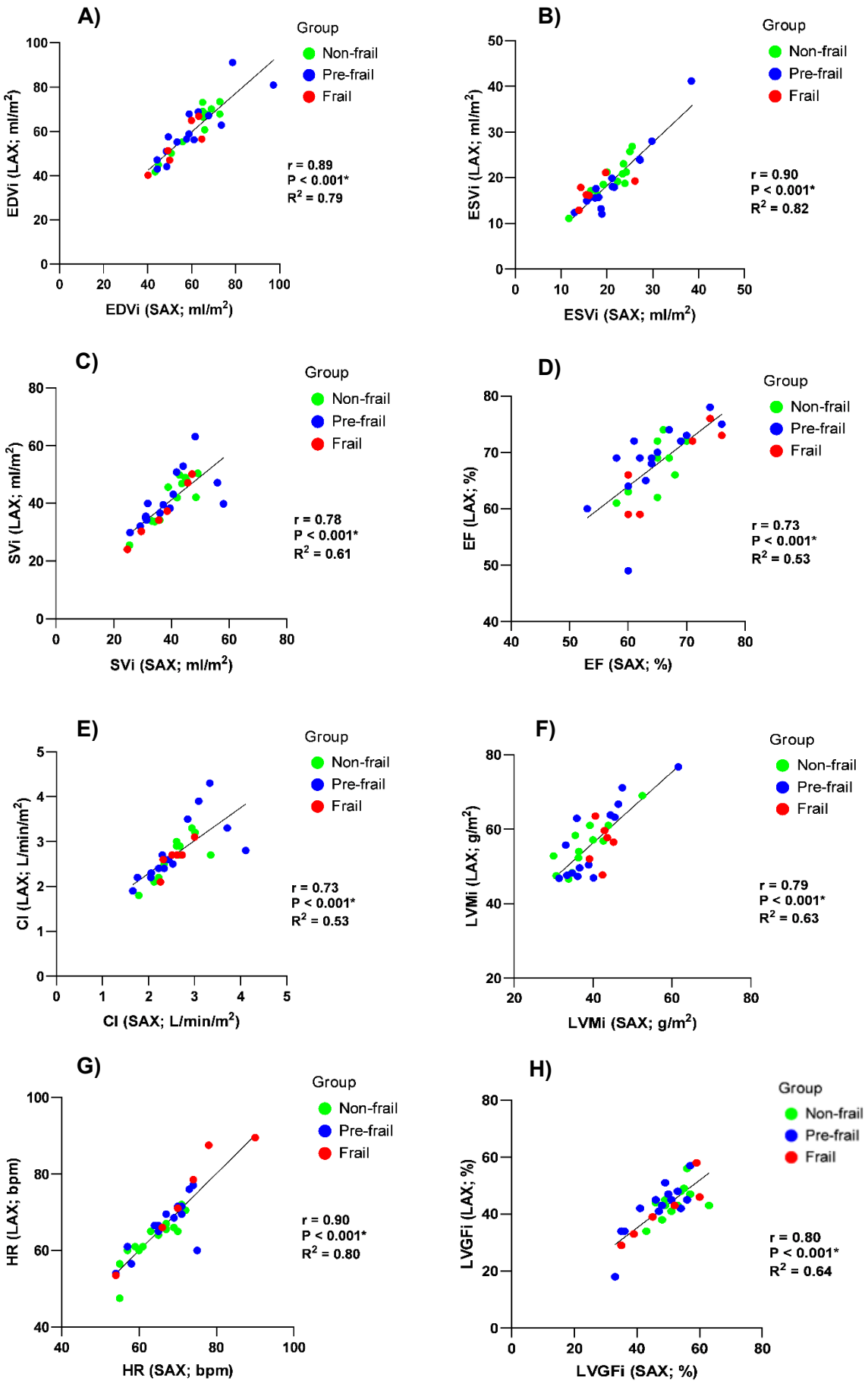
A)
EDVi (LAX; ml/m²)
EDVi (SAX; ml/m²)
r = 0.89
P < 0.001*
R² = 0.79
B)
ESVi (LAX; ml/m²)
ESVi (SAX; ml/m²)
r = 0.90
P < 0.001*
R² = 0.82
C)
SVi (LAX; ml/m²)
SVi (SAX; ml/m²)
r = 0.78
P < 0.001*
R² = 0.61
D)
EF (LAX; %)
EF (SAX; %)
r = 0.73
P < 0.001*
R² = 0.53
E)
CI (LAX; L/min/m²)
CI (SAX; L/min/m²)
r = 0.73
P < 0.001*
R² = 0.53
F)
LVMi (LAX; g/m²)
LVMi (SAX; g/m²)
r = 0.79
P < 0.001*
R² = 0.63
G)
HR (LAX; bpm)
HR (SAX; bpm)
r = 0.90
P < 0.001*
R² = 0.80
H)
LVGFi (LAX; %)
LVGFi (SAX; %)
r = 0.80
P < 0.001*
R² = 0.64
Group
Non-frail
Pre-frail
Frail

Figure 3.3: *Correlation analyses of cardiac parameters assessed by long axis and short axis scans. Figures show long axis (y axes; LAX) versus short axis (x axes; SAX) analysis methods for* ***A)*** *End diastolic volume index (EDVi),* ***B)*** *End systolic volume index (ESVi),* ***C)*** *Stroke volume index (SVi),* ***D)*** *Ejection fraction (EF),* ***E)*** *Cardiac index (CI),* ***F)*** *Left ventricular mass index (LVMi),* ***G)*** *Heart rate (HR),* ***H)*** *Left ventricular global function index (LVGFi) for non-frail, pre-frail and frail volunteers. Pearson correlation coefficient (r), P value, and r squared (R^2) values presented.*

3.2.2 Aortic blood flow - AOFLOW

Post-processing of the AOFLOW images was performed by drawing an ROI around the border of ascending aorta using the magnitude image and propagating the ROI across the cardiac cycle (**Figure 3.4**). Manual adjustments were made to contours, where necessary. The computed heart rate and stroke volume was used to calculate cardiac output. Cardiac output was termed ‘effective’ as measurements included small amounts of blood backflow. These measurements were normalised to BSA to compute aortic cardiac index. Peak velocity of the blood, aortic forward flow and aortic CSA were also calculated.

Intra-rater CV for analysis of each parameter was calculated to determine the reliabilty of the contour analyses of AOFLOW images. For CV calculations, three repeat measures were performed on 1 set of AOFLOW images. The CV of all AOFLOW measures was less than 1% (**Table 3.3**). Raw data for CV calculations are presented in **Appendix 3.1**.

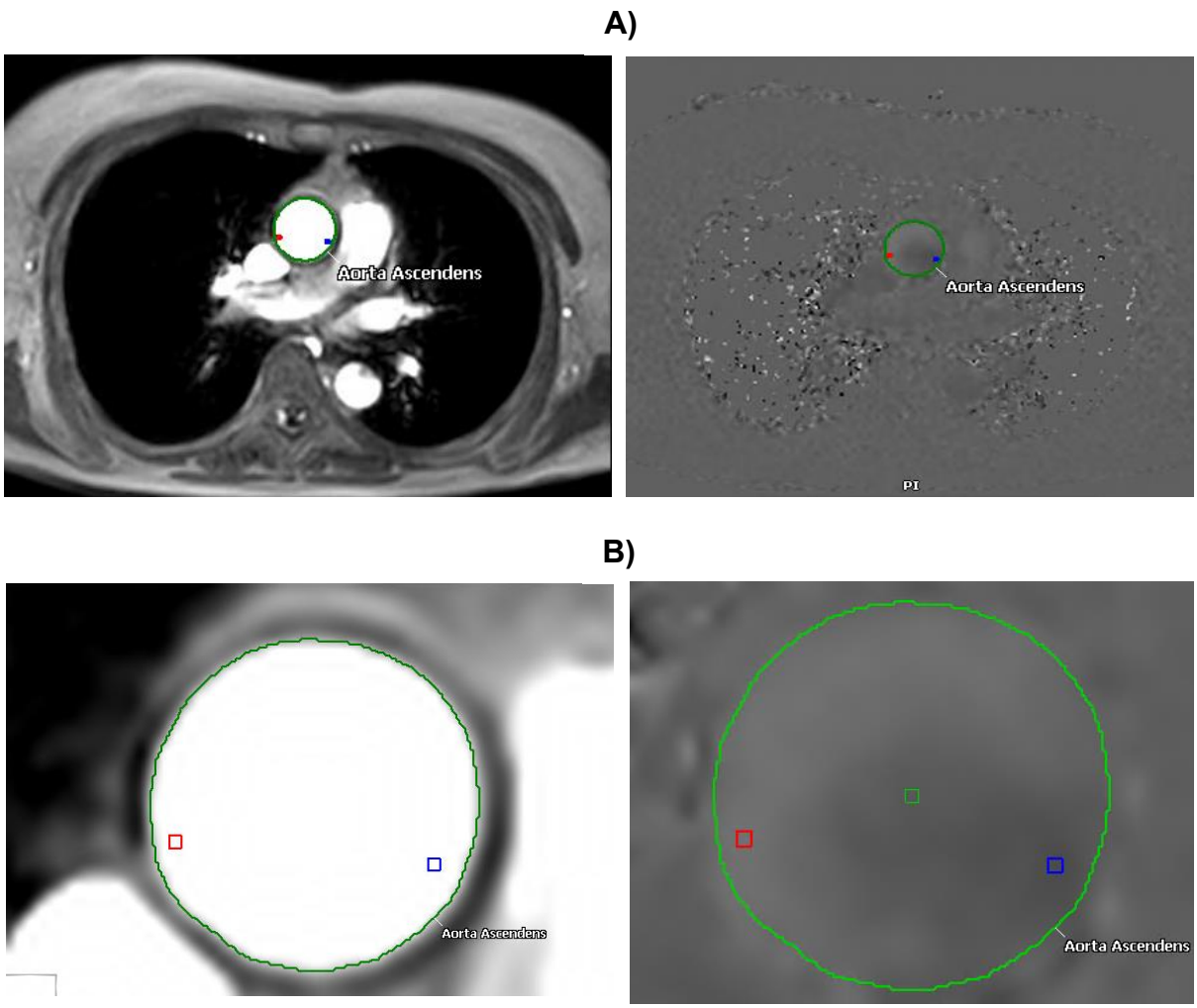

Figure 3.4: *Example PC-MRI analysis of AOFLOW sequence in cvi42 software. ROIs drawn around ascending aorta on magnitude image (left). ROI can be adjusted on corresponding phase image (right).* ***A)*** *Full view magnitude and phase images in axial cross section of body* ***B)*** *magnitude and phase mages zoomed in and focused on aorta.*

Table 3.3: Coefficient of variance (CV) results for repeated analysis of aortic flow (AOFLOW) images.

AOFLOW cardiac parameter	CV (%)
Peak blood velocity (m/s)	0.2%
Cardiac index (effective; L/min/m^2)	0.2%
Effective forward flow (ml)	0.3%
Aortic vessel area (mm^2)	0.6%

3.2.3 Cardiac T1 mapping

Cardiac T1 maps were generated on the scanner from the MOLLI sequence on a pixel-by-pixel basis, where the signal intensity of each pixel reflected the absolute T1 value in milliseconds. However, due to significant motion artefacts in some image sets, caused by inadequate breath holds from volunteers, the raw data from each volunteer was motion corrected during analysis within the cvi42 software (Circle Cardiovascular Imaging Inc; version 5.14.2).

For each image and phase, epicardial, endocardial and blood pool contours were automatically segmented with the inbuilt tool, with manual adjustments to contours made where necessary. Superior and inferior reference points were manually identified in each phase. Motion corrected images with overlayed contours were then used to create T1, R^2 and T1* maps (**Figure 3.5**), where T1* reflected T1 time with the additional influence of magnetic field inhomogeneities. T1 MOLLI sequences have previously been adopted in numerous studies to assess cardiac fibrosis across a large age range of healthy adults [307] and during ageing [308].

The intra-rater CV for each parameter was calculated to determine the reliabilty of the contour analyses of cardiac T1 map images. For CV calculations, three repeat

measures were performed on 1 participant's set of cardiac MOLLI images, all were less than 4% (**Table 3.4**). Raw data for CV calculations are presented in **Appendix 3.1**.

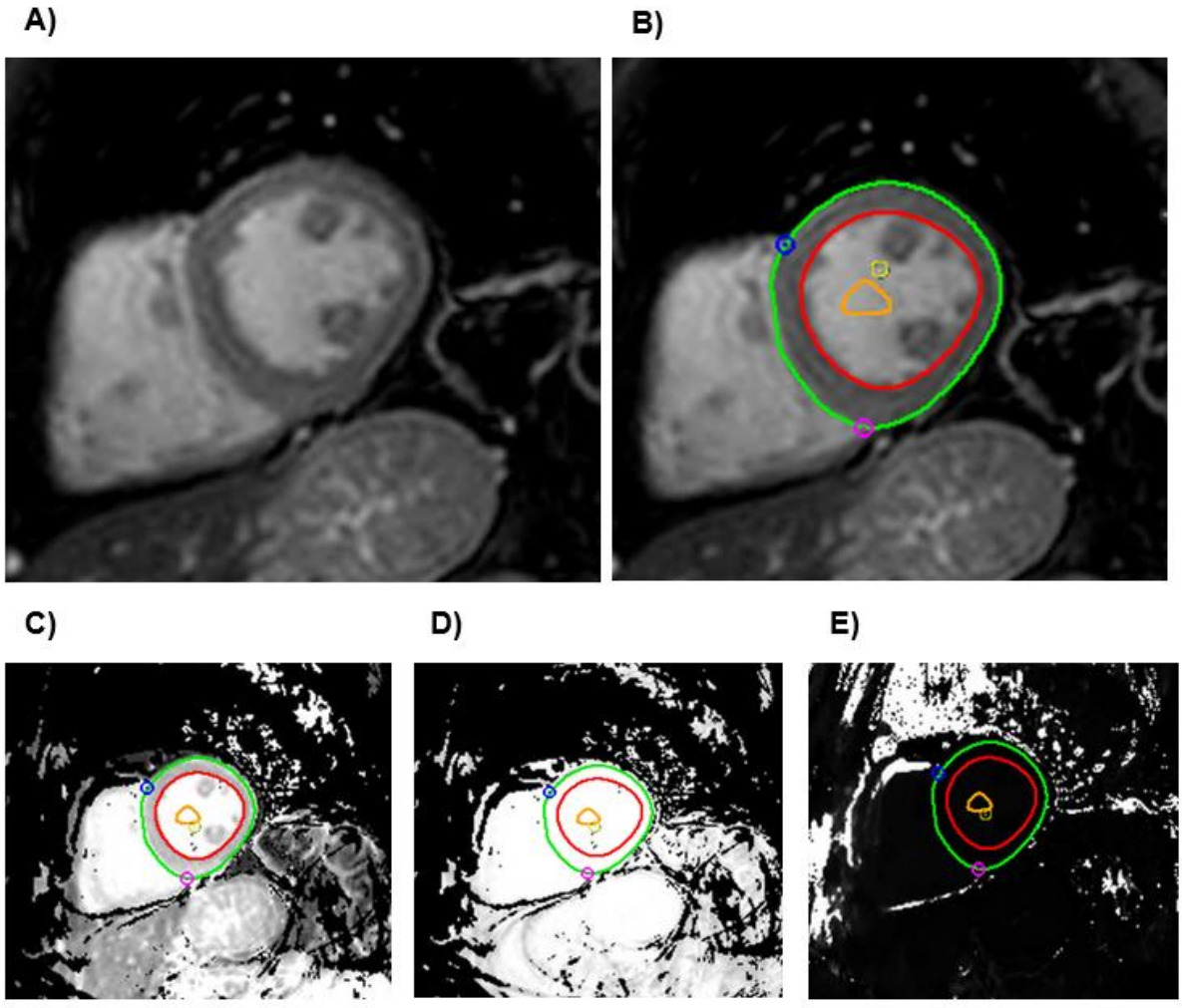

Figure 3.5: *Example T1 mapping image (MOLLI) postprocessing in cvi42 software.* ***A)*** *Raw image from scanner without contours.* ***B)*** *Epicardial (green), endocardial (red) and blood pool (orange) contours drawn on left ventricle. Superior (blue) and inferior (pink) short axis reference points added. Following motion correction of the images, T1 (**C**), R^2 (**D**) and T1* (**E**) maps were generated.*

Table 3.4: Coefficient of variance (CV) results for repeated analysis of cardiac T1 mapping (MOLLI) images.

T1 mapping parameter	CV (%)
Myocardial T1 time (ms)	1.4%
Myocardial T1* time (ms)	2%
Blood pool T1* time (ms)	3.2%

3.2.4 Statistical analysis

Statistical analysis methods are described in Chapter Two – Section 2.9. Data normality testing revealed non-normal distributions of: LAX derived EF, LVMi (3 group comparisons) and CI (two group comparisons), SAX derived LVMi (2 and 3 group comparisons), AFLOW derived peak blood velocity and vessel area (2 and 3 group comparisons) T1 MOLLI derived T1 (3 group comparisons) and T1* (2 and 3 group comparisons. Therefore, non-parametric equivalent statistical tests (detailed in Chapter Two – section 2.9) were used for analysis of these parameters. Values in the text, Tables and Figures represents mean ± standard deviation.

3.3 Results

The following outlines the results for the LAX cine, SAX cine, AOFLOW and MOLLI T1 mapping measures, results are presented for the non-frail, pre-frail and frail groups, and the non-frail versus the collapsed group of pre-frail and frail to allow further scrutiny. One frail participant's data was removed from HR analysis due to a large discrepancy in HR measurements between long axis and short axis scanning. One pre-frail participant's data was removed from EDVi, ESVi, LVMi and LVGFi analysis due to an enlarged heart (i.e., this participant had a LVMi of 172 g/m^2, which was markedly higher than each group average: non-frail: 55.5 g/m^2, pre-frail: 56.9 g/m^2, frail: 56.2 g/m^2), causing abnormally high values for these metrics.

3.3.1 Left ventricular LAX measures in non-frail, pre-frail and frail females

Results from LAX analysis are presented in **Figure 3.6**. Resting state EDVi, ESVi and SVi were no different when comparing non-frail (EDVi: 62 ± 11 ml/m^2; ESVi: 20 ± 4 ml/m^2; SVi: 42 ± 8 ml/m^2) pre-frail and frail volunteers (**Figure 3.6 A-C**). Similarly, EF, CI and LVMi did not differ between the non-frail (EF: 69 ± 5 %; CI: 2.6 ± 0.5 L/min/m2; LVMi: 56 ± 6 g/m^2) pre-frail or frail groups (**Figure 3.6 D-F**). There were also no differences in longitudinal strain and LVGFi in non-frail (longitudinal strain: -16.8 ± 3.4%; LVGFi: 45 ± 5 %) females in comparison to pre-frail and frail females (**Figure 3.6 H-I**). Heart rate in the pre-frail-frail volunteers was 67 ± 7 bpm, which was no different to the non-frail or frail groups (**Figure 3.6 G**). However, there was a trend for greater heart rate in the frail compared to non-frail volunteers (*P* = 0.087; **Figure 3.6 G**).

3.3.2 Left ventricular LAX measures in non-frail versus the collapsed group of pre-frail and frail females

The pre-frail and frail groups were collapsed to allow further scrutiny of the left ventricular structural and functional data. This analysis also revealed no significant differences existed between groups (**Figure 3.7 A-I**), but there was a trend for heart rate to be greater in the collapsed pre-frail and frail group (68 ± 9 bpm) compared to the non-frail group (*P* = 0.076; **Figure 3.7 H**).

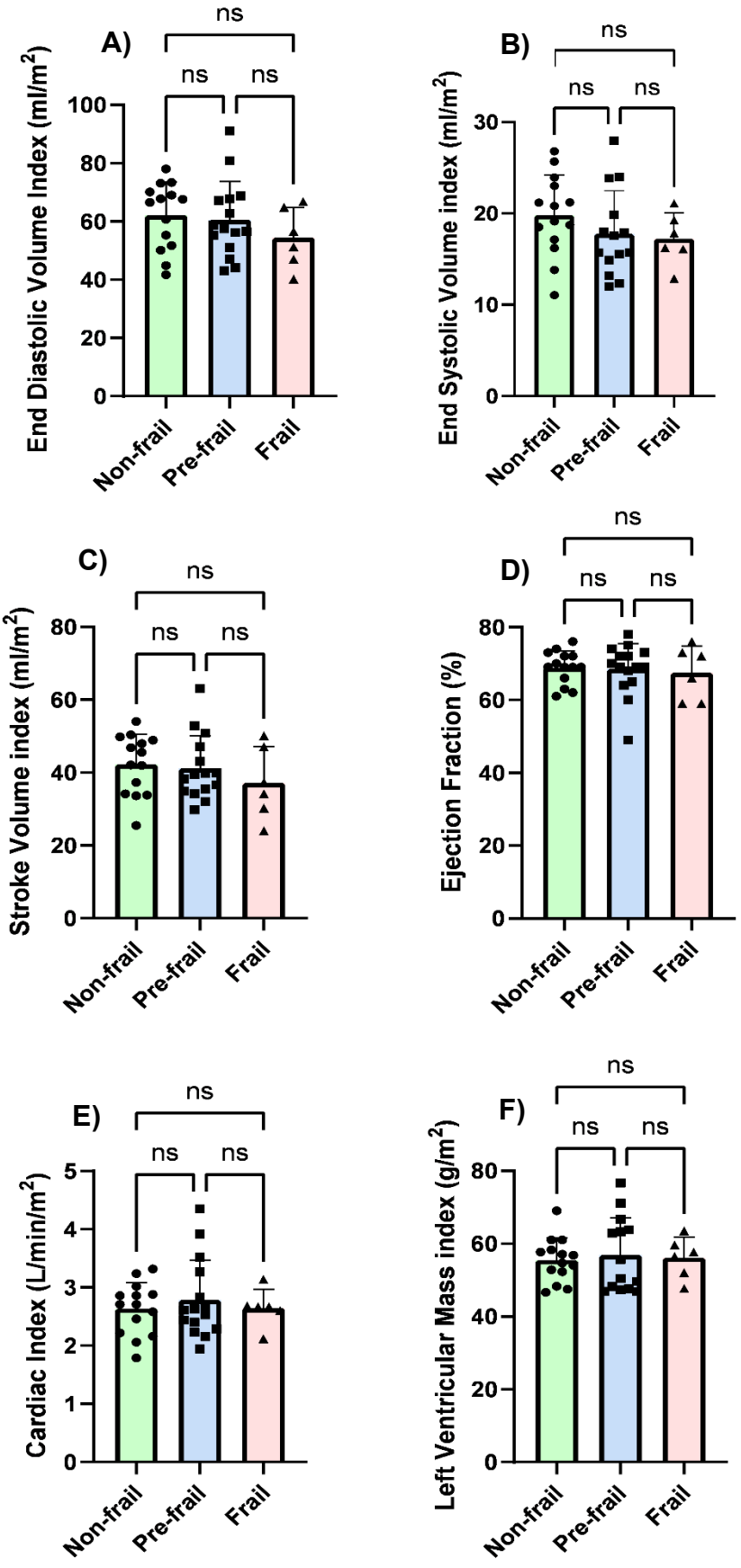
A)
End Diastolic Volume Index (ml/m2)
ns
ns
ns
100
80
60
40
20
0
Non-frail
Pre-frail
Frail
B)
End Systolic Volume index (ml/m2)
30
20
10
C)
Stroke Volume index (ml/m2)
D)
Ejection Fraction (%)
E)
Cardiac Index (L/min/m2)
5
4
3
2
1
F)
Left Ventricular Mass index (g/m2)

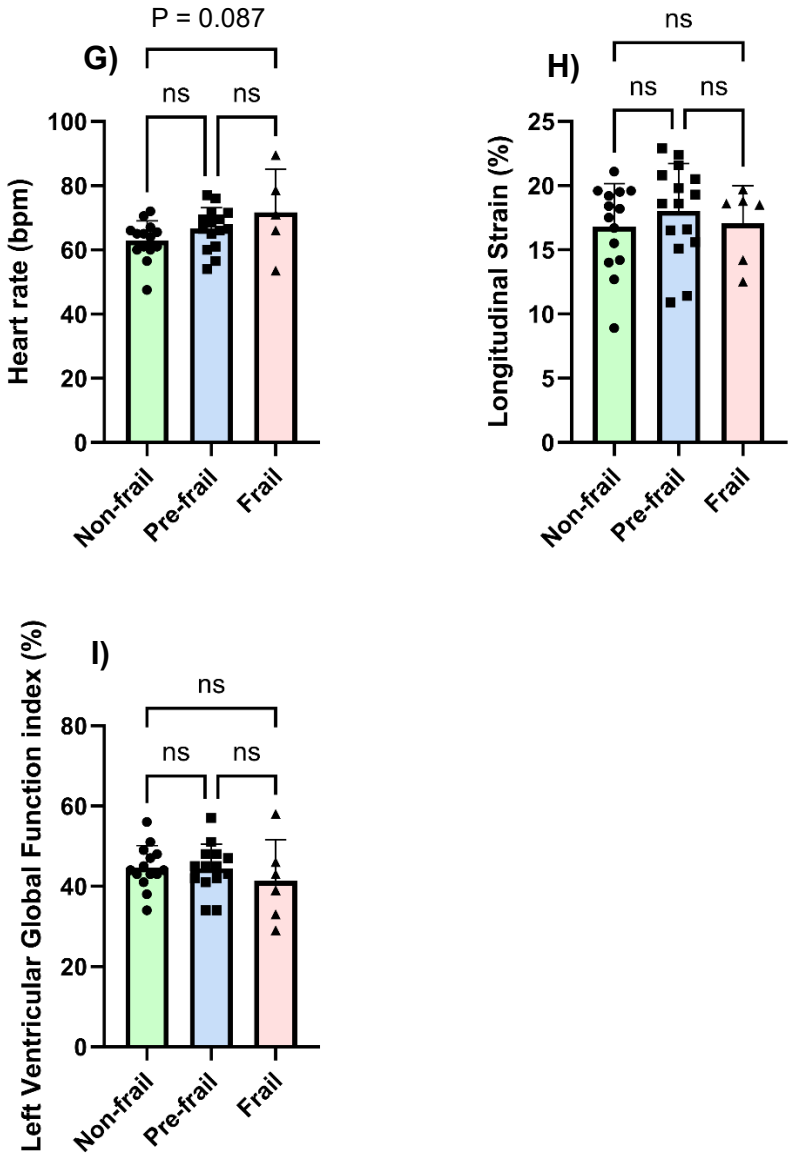

Figure 3.6: *Long axis (LAX)* ***A)*** *End diastolic volume index,* ***B)*** *End systolic volume index,* ***C)*** *Stroke volume index,* ***D)*** *Ejection fraction,* ***E)*** *Cardiac index,* ***F)*** *Left ventricular mass index,* ***G)*** *Heart rate,* ***H)*** *Longitudinal strain,* ***I)*** *Left ventricular global function index for non-frail, pre-frail and frail volunteers. Values are mean ± standard deviation and individual values.*

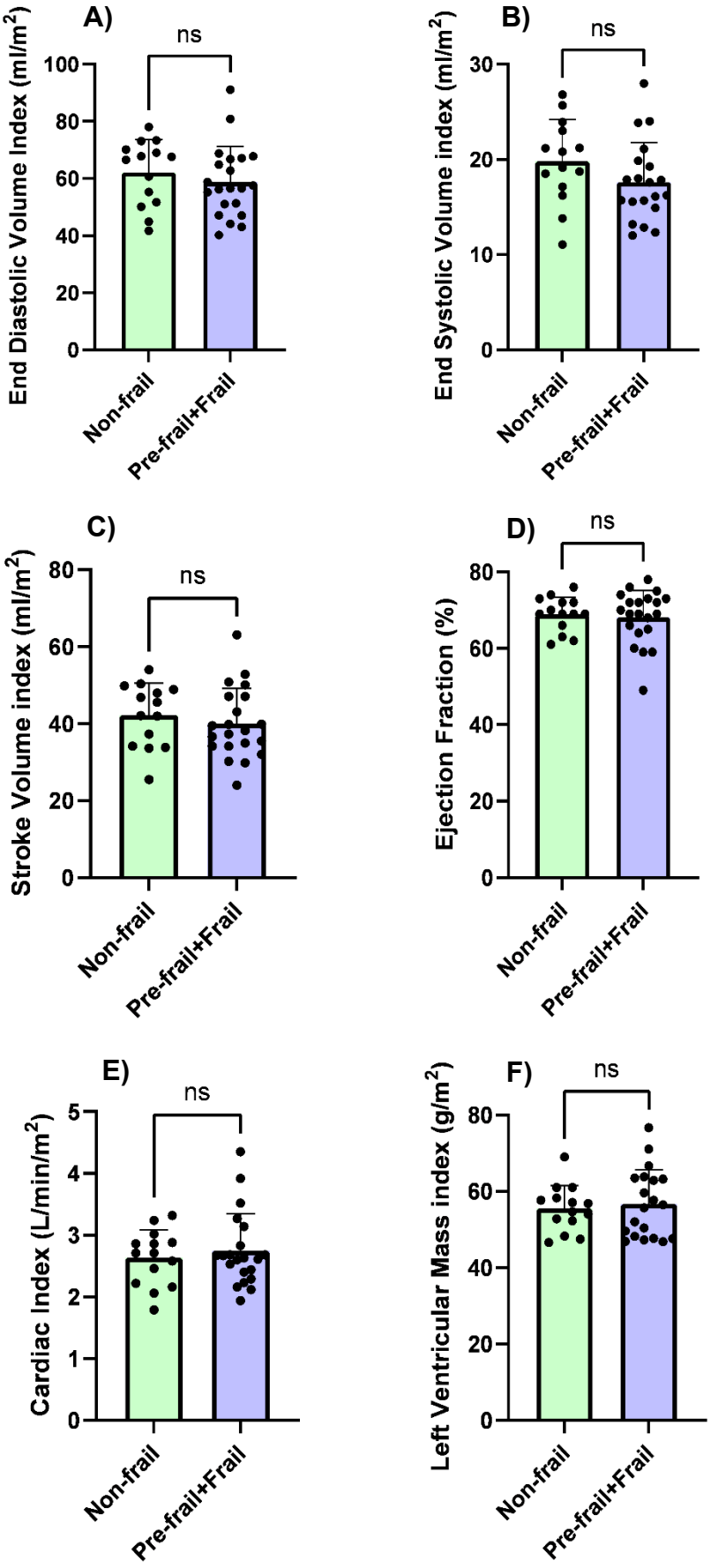
A)
ns
End Diastolic Volume Index (ml/m2)
100
80
60
40
20
0
Non-frail
Pre-frail+Frail
B)
ns
End Systolic Volume index (ml/m2)
30
20
10
0
Non-frail
Pre-frail+Frail
C)
ns
Stroke Volume index (ml/m2)
80
60
40
20
0
Non-frail
Pre-frail+Frail
D)
ns
Ejection Fraction (%)
80
60
40
20
0
Non-frail
Pre-frail+Frail
E)
ns
Cardiac Index (L/min/m2)
5
4
3
2
1
0
Non-frail
Pre-frail+Frail
F)
ns
Left Ventricular Mass index (g/m2)
80
60
40
20
0
Non-frail
Pre-frail+Frail

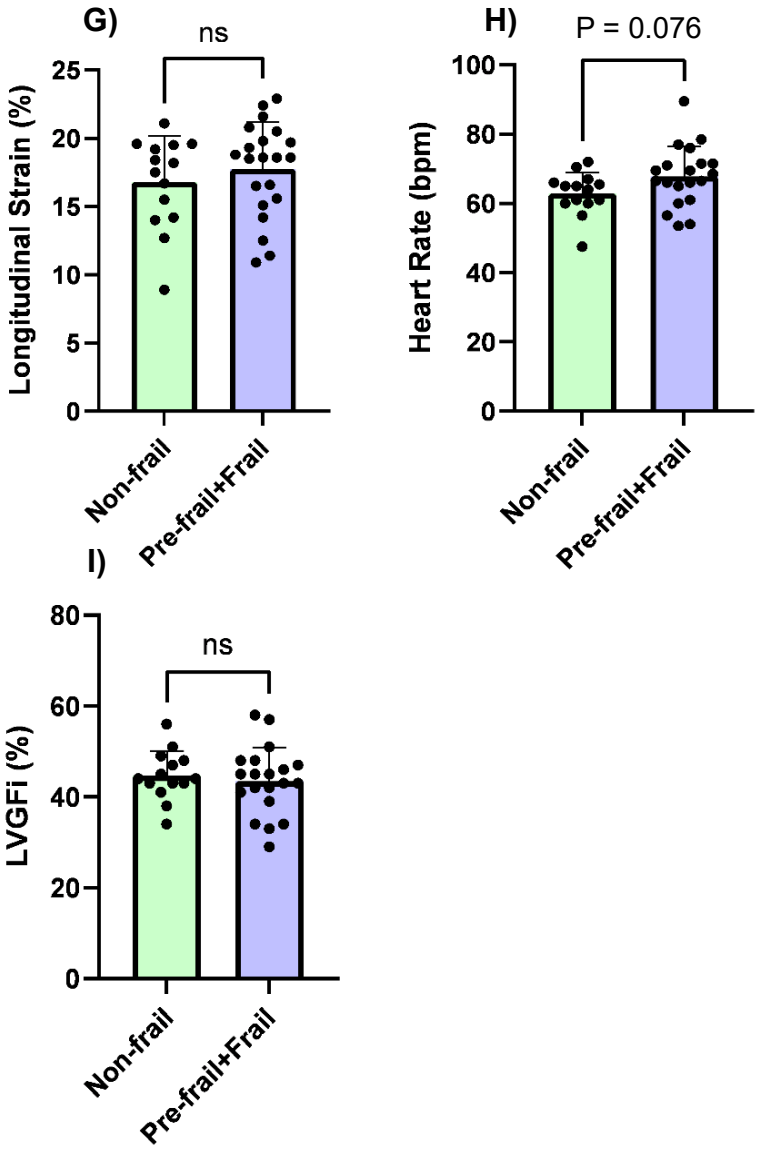

Figure 3.7: *Long axis (LAX)* ***A)*** *End diastolic volume index,* ***B)*** *End systolic volume index,* ***C)*** *Stroke volume index,* ***D)*** *Ejection fraction,* ***E)*** *Cardiac index,* ***F)*** *Left ventricular mass index,* ***G)*** *Heart rate,* ***H)*** *Longitudinal strain,* ***I)*** *Left ventricular global function index (LVGFi) for non-frail and combined pre-frail and frail volunteers. Values are mean ± standard deviation and individual values.*

3.3.3 Left ventricular SAX measures in non-frail, pre-frail and frail females

Analysis of the SAX cine images generated an identical set of measures to the LAX data. In addition, SAX analysis yielded circumferential strain data which are presented in **Figure 3.8**. Circumferential strain was -19.4 ± 2.6% in non-frail volunteers, which was not different to pre-frail or frail females (**Figure 3.8 A**). While there was a trend (*P* = 0.067) for greater heart rate in the frail (72 ± 12 bpm) versus non-frail (64 ± 6 bpm) groups (**Appendix 3.2** - **Figure 3.14 G**), there were no significant differences evident in any of the other SAX derived measures across non-frail, pre-frail and frail groups. These results are presented in **Appendix 3.2**. Two participant's short axis cine datasets were inadequate for analysis due to insufficient breath holds during scanning.

3.3.4 Left ventricular SAX measures in non-frail versus the collapsed group of pre-frail and frail females

There were no differences in circumferential strain between the non-frail group and the collapsed pre-frail and frail group (**Figure 3.8 B**). However, there was a trend (*P* = 0.096) for greater heart rate in the collapsed pre-frail and frail group (68 ± 8 bpm) versus the non-frail group (**Appendix 3.3** - **Figure 3.15 G**). Although, no differences were observed between the non-frail group and the collapsed pre-frail and frail group for any of the other SAX derived cardiac measures (**Appendix 3.3**).

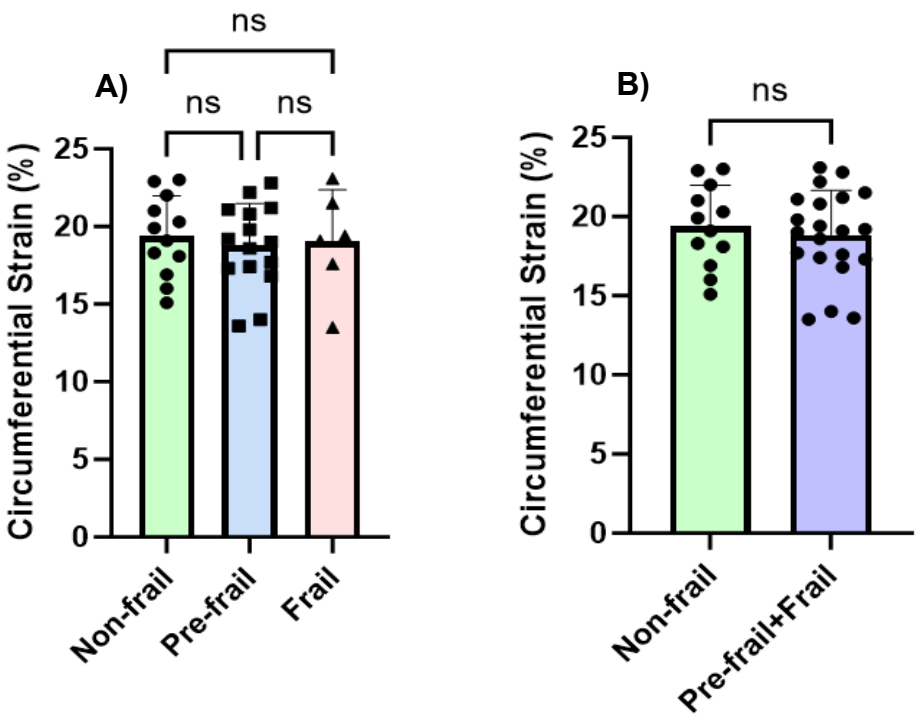

Figure 3.8: *Circumferential strain results in **A)** non-frail, pre-frail and frail volunteers, **B)** non-frail versus the collapsed group of pre-frail and frail females. Values are mean ± standard deviation and individual values.*

3.3.5 Aortic blood flow and cross-sectional area in non-frail, pre-frail and frail females

Peak blood velocity within the aorta was 1.12 ± 0.46 m/s in the non-frail group, which was no different to the pre-frail or frail groups (**Figure 3.9 A**). Similarly, no differences in effective forward flow of the aorta were observed between non-frail (63 ± 12 ml), pre-frail or frail groups (**Figure 3.9 B**). Cardiac index in the non-frail females was 2.5 ± 0.5 L/min/m^2, which was similar to pre-frail and frail subjects (**Figure 3.9 C**). Non-frail, pre-frail and frail volunteers also exhibited no differences in aortic cross-sectional area (non-frail: 706 ± 172 mm^2; **Figure 3.9 D**).

3.3.6 Aortic blood flow and cross-sectional area in non-frail versus the collapsed group of pre-frail and frail females

In the additional analyses in which the pre-frail and frail groups data were collapsed, no significant differences were seen between peak blood velocity of the aorta in non-frail females and the collapsed pre-frail and frail group (1.10 ± 0.47 m/s; **Figure 3.10 A**). Similarly, no differences were evident in effective forward flow when comparing the non-frail volunteers to the collapsed group of pre-frail and frail females (59 ± 14 ml; **Figure 3.10 B**). Cardiac index in the combined pre-frail and frail group was 2.5 ± 0.5 L/min/m^2, which was also not different in comparison with the non-frail group (**Figure 3.10 C**). Finally, aortic cross-sectional area was no different between the collapsed group of pre-frail and frail participants (743 ± 141 mm^2) in comparison to the non-frail group (**Figure 3.10 D**).

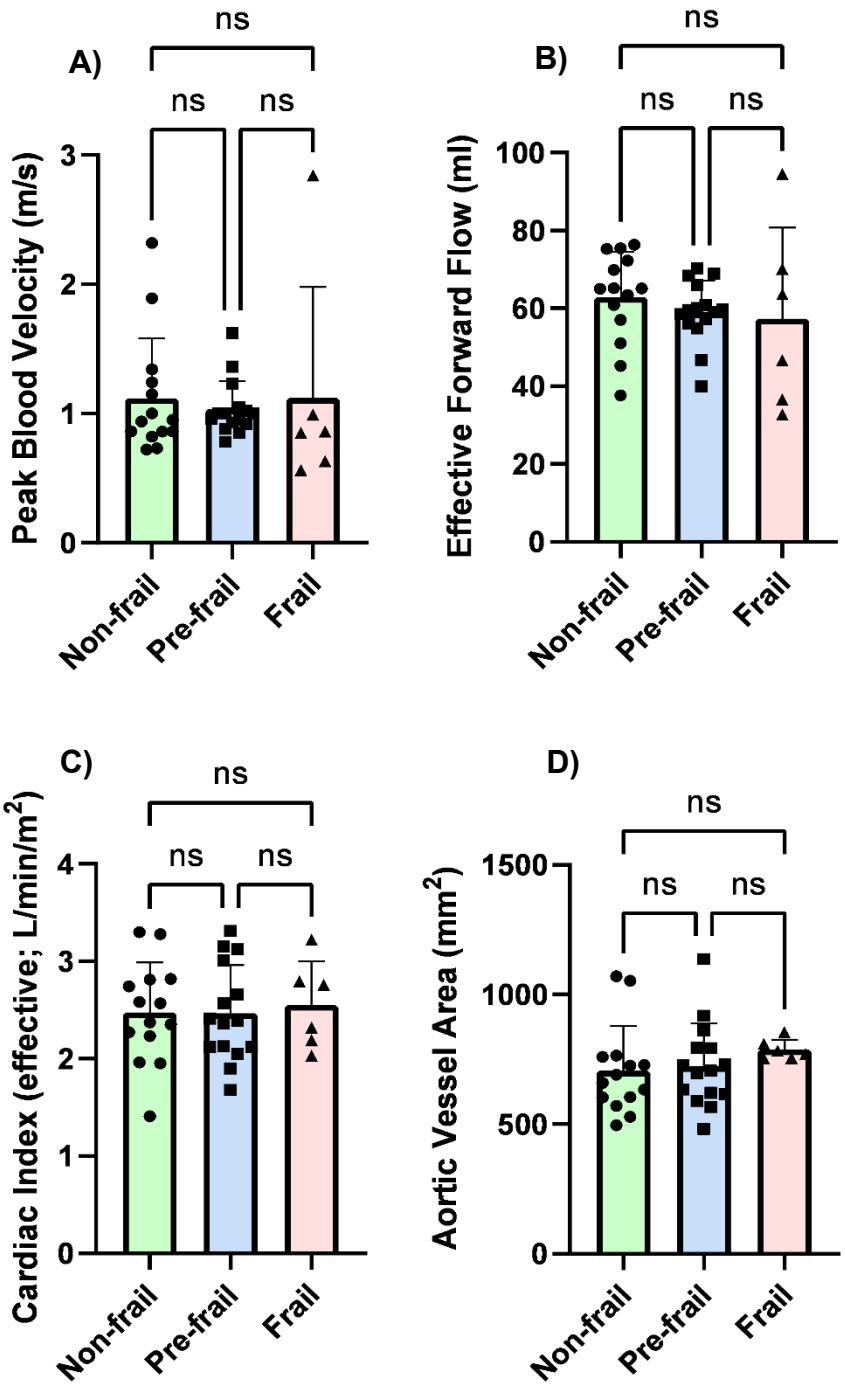

Figure 3.9: *Aortic flow (AOFLOW) phase contrast MRI results.* ***A)*** *Peak blood velocity,* ***B)*** *Effective forward flow,* ***C)*** *Cardiac index* ***D)*** *Aortic vessel CSA for non-frail, pre-frail and frail volunteers. Values are mean ± standard deviation and individual values.*

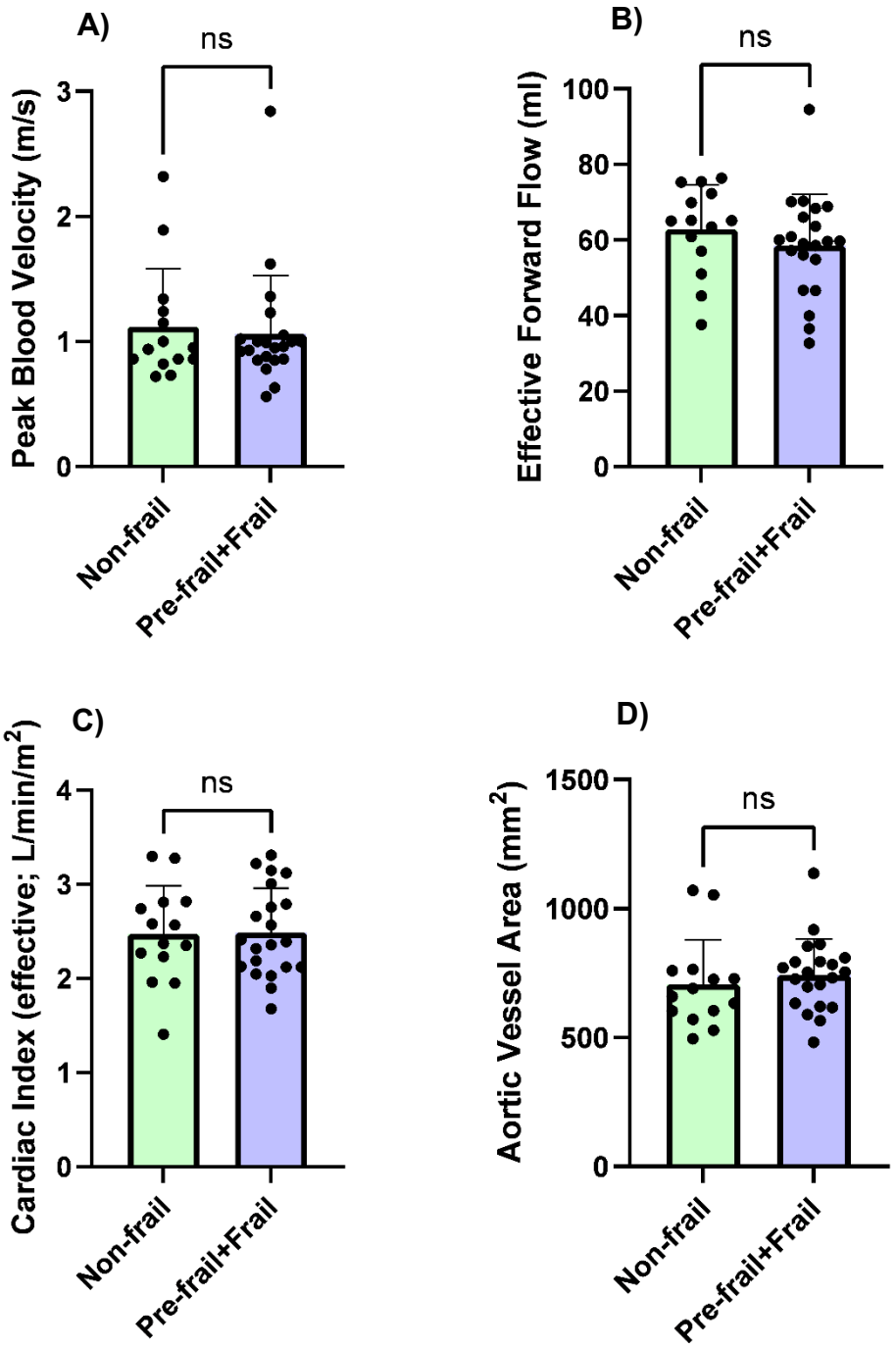

Figure 3.10: *Aortic flow (AOFLOW) phase contrast MRI results.* ***A)*** *Peak blood velocity,* ***B)*** *Effective forward flow,* ***C)*** *Cardiac index (CI)* ***D)*** *Aortic vessel CSA for non-frail and combined pre-frail and frail volunteers. Values are mean ± standard deviation and individual values.*

3.3.7 Cardiac MOLLI T1 mapping in non-frail, pre-frail and frail females

Myocardial T1 in non-frail females was 1280 ± 56 ms, which was no different to pre-frail and frail females (**Figure 3.11 A**). Similarly, no differences were evident following assessment of myocardial T1* time in non-frail (994 ± 271 ms), pre-frail and frail groups (**Figure 3.11 B**). There were also no differences in blood pool T1* time when comparing non-frail (1937 ± 142 ms), pre-frail and frail females (**Figure 3.11 C**). One pre-frail participant's myocardial T1* data was removed from analysis due to an enlarged heart causing abnormally high T1 values.

3.3.8 Cardiac MOLLI T1 mapping in non-frail versus the collapsed group of pre-frail and frail females

Analysis of data from the collapsed pre-frail and frail group (1305 ± 40 ms) revealed no significant differences in myocardial T1 time when compared to the non-frail group (**Figure 3.12 A**). Similarly, myocardial T1* time in the collapsed group of pre-frail and frail females was 959 ± 157 ms, which was no different to the non-frail group (**Figure 3.12 B**). There were also no differences in blood pool T1* time when comparing the non-frail females to the collapsed group of pre-frail and frail females (1879 ± 129 ms; **Figure 3.12 C**).

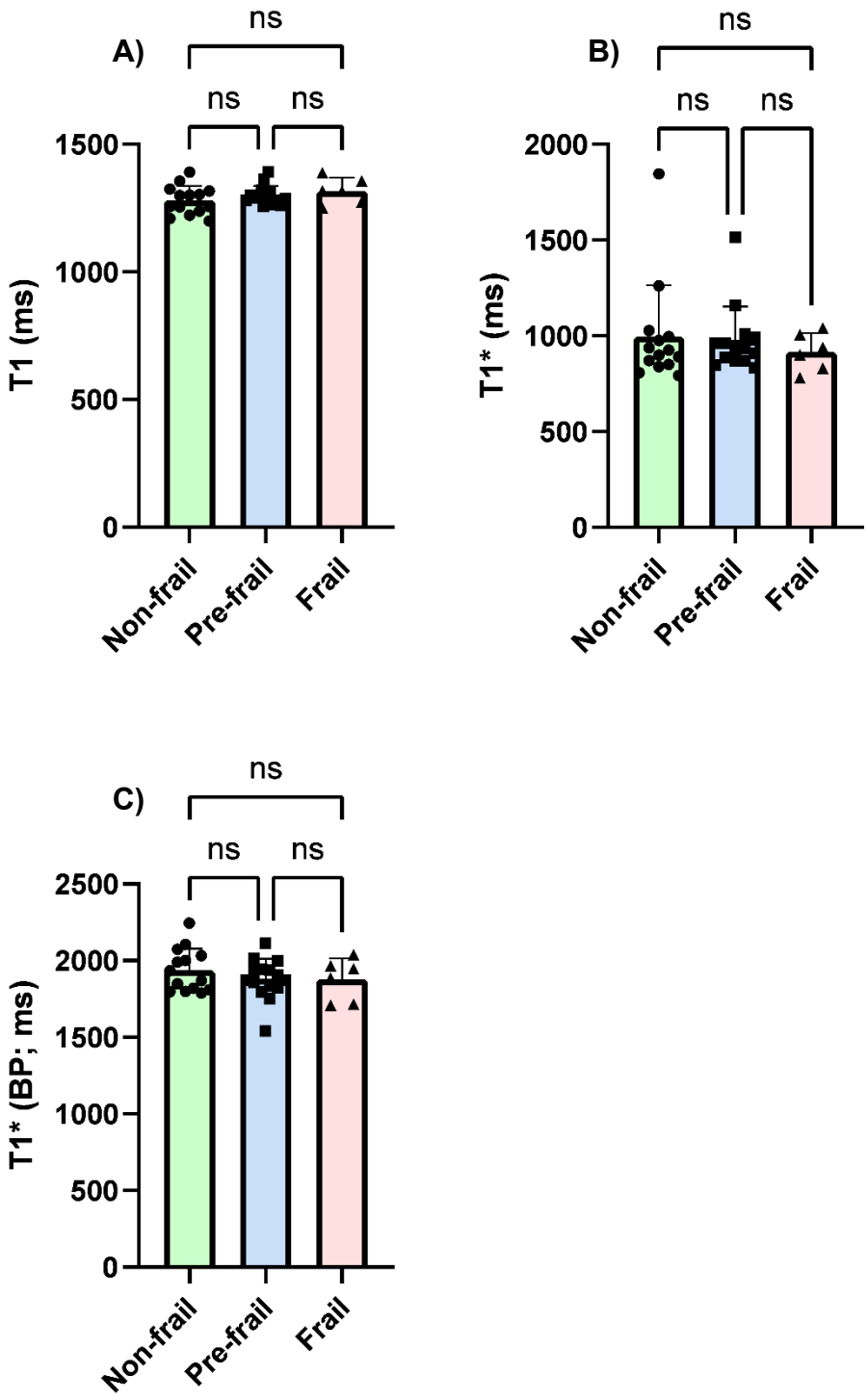

Figure 3.11: *Cardiac T1 mapping (MOLLI) results for non-frail, pre-frail and frail females.* ***A)*** *Myocardial T1 time,* ***B)*** *Myocardial T1* time,* ***C)*** *Blood pool (BP) T1* time. Values are mean ± standard deviation and individual values.*

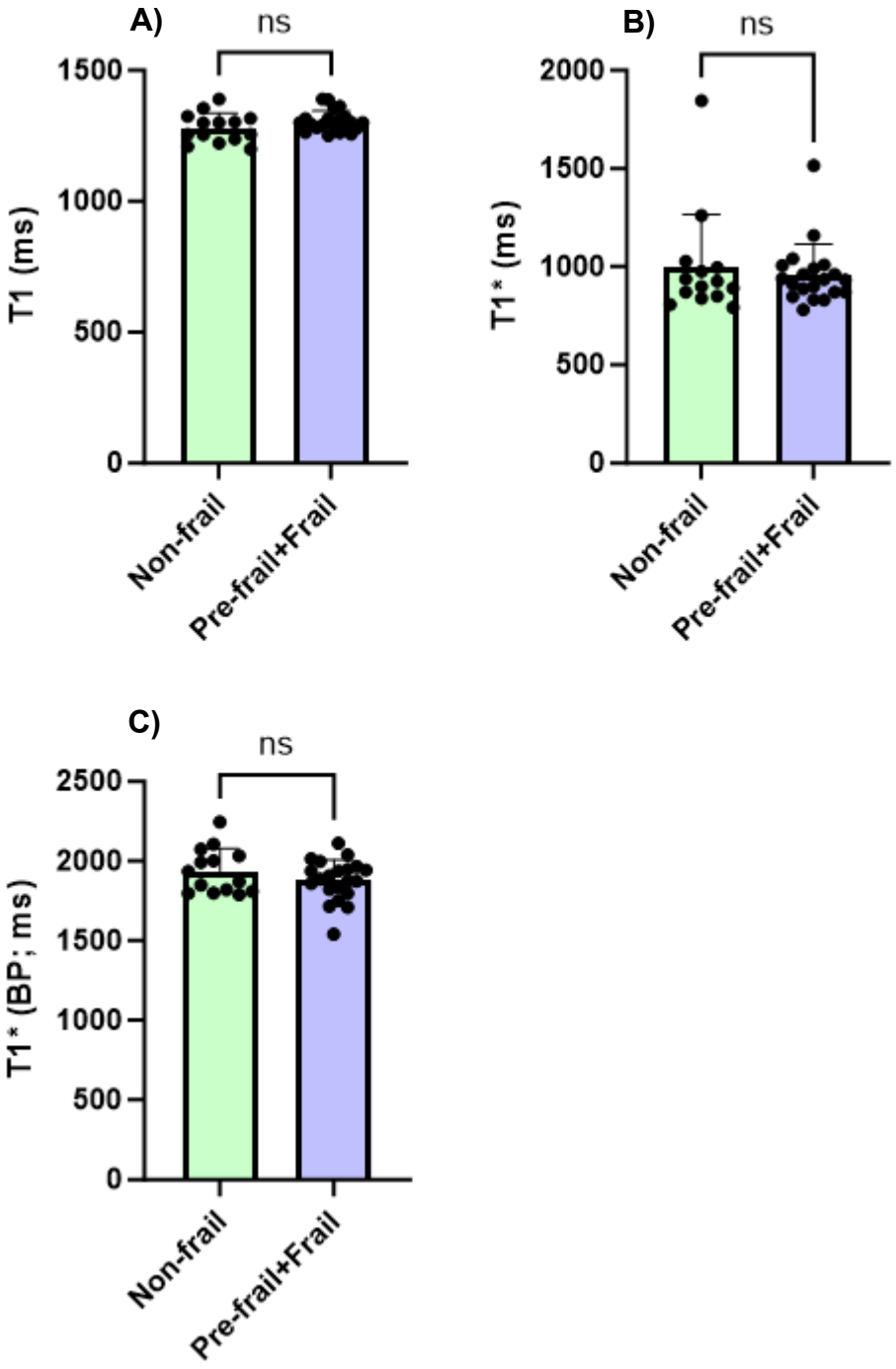

Figure 3.12: *Cardiac T1 mapping (MOLLI) results for non-frail versus pre-frail and frail groups combined.* ***A)*** *Myocardial T1 time,* ***B)*** *Myocardial T1* time,* ***C)*** *Blood pool (BP) T1* time. Values are mean ± standard deviation and individual values.*

3.4 Discussion

The present study represents the first investigation of cardiac parameters with MRI within the context of frailty and demonstrates the feasibility of utilising multiparametric cardiac MRI in the study of pre-frail and frail individuals. The volunteers in this study were of mean age 70-78 years and left ventricular structure and function data are seen to agree with published reference values derived from previous meta-analyses of women aged 60-69 years following cardiac cine MRI at 1.5 T and 3 T [309]. For example, similar values were observed in the present study and previous reference values for EDVi (current study: 60 ± 12 ml/m^2; reference value: 68 ± 12 ml/m^2), ESVi (current study: 19 ± 4 ml/m^2; reference value: 25 ± 5 ml/m^2) SVi (current study: 41 ± 9 ml/m^2; reference value: 44 ± 7 ml/m^2), EF (current study: 69 ± 6 %; reference value: 65 ± 6 ml/m^2) and LVMi (current study: 56 ± 8 g/m^2; reference value: 65 ± 6 g/m^2) [309].

The main findings of this Chapter were that non-frail, pre-frail and frail females exhibited no differences in structural and functional cardiac characteristics when assessed at rest in a supine state using MRI assessments. Furthermore, collapse of pre-frail and frail groups to enhance statistical power did not change these study outcomes.

The lack of differences in cardiac structure and function between groups in the present study (**Figure 3.6, Figure 3.7**) is consistent with a previous report demonstrating no differences in echocardiography-derived LV mass index, ejection fraction and cardiac index between non-frail, pre-frail and frail individuals [181]. This previous study also performed measures in the resting state in volunteers of a similar age to the current work (age range 70-78 years), supporting a lack of differences in cardiac parameters in healthy versus pre-frail and frail states under resting conditions. Given this previous

data was gathered using echocardiography methods [181], these findings are strengthened by data from the current study through the enhanced validity and reliability of the MRI methods used.

The cardiac MRI methods employed herein may also underpin the differential findings to previous studies adopting less precise resting-state echocardiographic assessments within the context of frailty, which observed differences in cardiac structure and function, such as greater LV mass [177, 179] and lower ejection fraction [179, 180], in frail versus non-frail individuals. Whilst less accurate methods potentially underpin these discrepancies, several other methodological limitations in earlier work must also be acknowledged. For example, all of these previous studies adopted mixed sex participant samples [177, 179-181], with the proportion of males in some samples being markedly higher than others (e.g., 51% of frail sample being male [179] vs 30% of frail sample being male [180]). Data derived from these mixed sex samples were therefore likely prone to variance based on the reported sex-related differences in cardiac morphology and function [299], which may have resulted in erroneous differences between healthy and frail states. Furthermore, an older mean age of volunteers and an indirect assessment of ejection fraction, with the authors acknowledging that this parameter was ‘not quantitatively’ measured, may contribute to different findings between some studies [179]. These considerations reflect the limited nature of the current evidence regarding cardiac structure and function characteristics during frailty and emphasise the need for further assessments by MRI in sex-stratified samples. Whilst the greater accuracy and reliability of MRI may give precedence to the findings of this study, the low number of frail individuals recruited (n = 6) should be considered when extrapolating the findings, particularly as some prior studies adopted well powered samples of frail individuals (e.g., n = 211 [180]). Low

statistical power in the current study may have obscured differences due to large data variance within the frail group for some parameters, such as the effective forward flow of aortic blood (**Figure 3.9 B**). To overcome this, data were also presented from the collapsed group of pre-frail and frail females to improve statistical power, which supported a lack of differences in all cardiac parameters between frailty states compared to the non-frail condition. The low analytical variation of measures (evidenced by low CVs – **Tables 3.1-3.4**) reported in this study reinforces the reliability of the present data. Furthermore, high scan-rescan reproducibility and low intra-observer variation (CVs of 3.1%, 3.8% and 5.4% for EDV, LV mass and EF, respectively) have been reported by previous work analysing data with the same analysis software as the present study (cvi42 software) following 1.5 T and 3T MRI [310]. Thus, the present study provides robust evidence of a lack of differences in cardiac parameters in pre-frail and frail versus non-frail females.

With no differences observed in LV longitudinal strain (**Figure 3.6 H, Figure 3.7 H**), the current work contradicts previous echocardiographic data demonstrating lower LV longitudinal strain in frail versus non-frail individuals [180, 311]. Despite the larger samples of frail individuals in these previous reports (*n* = 157 [311] and *n* = 211 [180]), LV strain assessment by echocardiography has been shown to be more susceptible to observer variability compared to MRI methods [312], which may support the lack of differences in LV longitudinal strain observed following MRI assessment in the present study. Further, the persistent issue of mixed sex participant samples in these two previous studies potentially contributed to variance in the data [180, 311]. The lack of differences observed herein may be explained by the dynamic nature of LV strain as a cardiac parameter, thus similar investigations during conditions of acute exercise stress may be more appropriate to delineate differences between frailty and healthy

states, particularly as acute exercise has been shown to impart a lowering in myocardial strain in middle aged adults [313]. However, these results are not specific to frailty. Therefore, to improve insight into associations between frailty and myocardial strain, future work should employ cardiac MRI measurements during conditions of physiological stress.

In addition to being the only MRI-derived quantification of LV strain in frail individuals, this study provides the first statistical analysis of aortic flow imaging and cardiac T1 mapping data within the context of frailty. Previous preliminary work comparing n = 4 frail and n = 2 non-frail individuals has observed a higher atheroma score and greater aortic tortuosity in the frail participants [303]. However, the small sample size and absence of statistical analysis in this preliminary work prevents direct comparisons to the present study. Cardiac T1 mapping provides markers of inflammation and fibrosis within the myocardium, which has utility in the prognosis of cardiac disease (e.g., transthyretin amyloidosis) and mortality [305, 314]. The data presented herein portray no differences in T1 or T1* time of the myocardium between non-frail, pre-frail and frail females (**Figure 3.11, Figure 2.12**), suggesting myocardial inflammation and fibrosis were not different between groups. Without previous data in frail individuals, comparisons are difficult to make, but data within the context of ageing suggest older age is associated with increased T1 times [308]. Importantly, this study demonstrates the feasibility of performing cardiac T1 mapping, in conjunction with a large battery of cardiac scanning, with MRI in older frail volunteers. Moreover, despite some participants experiencing difficulty performing the required breath holds for accurate scanning (and thus causing motion artefacts in the resulting images) in this study, motion correction during image post-processing was able to rectify this issue and thus

enhances the feasibility of applying these measures in future studies recruiting frail volunteers.

In this study, a trend for greater heart rate was observed in the frail and collapsed of pre-frail and frail groups versus the non-frail group (**Figure 3.6 G, Figure 3.7 H**). This may be deemed consistent with a previous study of 442 older adults which observed higher resting heart rate in frail compared to non-frail individuals, when also measured in the supine position [315]. Higher resting heart rate during frailty may be attributable to functional impairments in the sinoatrial node, with this notion evidenced by associations between changes in sinoatrial action potential morphology and frailty in a frail mouse model [316]. As such, these processes may underpin the increased risk of CVD in frail and pre-frail individuals [173], given sinoatrial node dysfunction has been associated with cardiac pathologies, such as heart failure [317]. However, this level of mechanistic insight is far from being achieved considering the associational nature of evidence provided in the present and previous studies. Furthermore, not all studies of frailty have observed differences in resting heart rate, with ECG data illustrating no differences in heart rate between non-frail and frail individuals [318]. Whilst the use of MRI in the present work in comparisons to ECG data in this previous study may explain these differential findings, it is clear more research is needed to clarify potential differences in heart rate in healthy and frail individuals, with dynamic assessments perhaps key for elucidating these associations.

As alluded to above, a noteworthy consideration of the present study and previous work, concerns the assessment of cardiac parameters in the resting state. As discussed in Chapter One – Section 1.6, measurements made in the resting state may not be effective at highlighting differences in physiological characteristics between frail and non-frail individuals, considering frailty is defined by a dysregulation in

homeostasis [252]. This may underpin the lack of differences shown in dynamic cardiac parameters (e.g., ESV, EDV, cardiac index) in this study and previous work [179, 180]. Instead, the administration of a physiological stressor, such as exercise, may better delineate physiological differences in cardiac function between healthy and frail states. Accordingly, the exercise stimulus of walking has been applied in a previous study to elicit a dynamic cardiac response in pre-frail and frail individuals [318]. These authors showed that these dynamic measures of heart rate exhibited stronger associations with frailty status compared to resting-state measures [318], suggesting differences in cardiac variables are best manifested under conditions of physiological stress. Furthermore, given the well-established profound increase in cardiac output and heart rate shortly following the commencement of exercise [319], it seems reasonable to infer that potential differences in cardiac function may be best viewed under conditions of cardiovascular stress. The combination of pre-frail and frail groups in subsequent analyses in this study further reinforces this notion, by indicating that the lack of differences between healthy and frail states may not have been an issue of statistical power, rather a physiological stressor could be needed to disrupt homeostasis and manifest differences in cardiac function. However, dynamic measurements of cardiac parameters within the context of frailty are scarce, with further research fundamental in elucidating the cardiac response to physiological stress in frail versus healthy states.

In conclusion, the current study indicates that non-frail, pre-frail and frail females do not exhibit differences in cardiac structure and function following assessment with MRI in the resting state. Given the reliance on echocardiography methods in the limited number of previous studies of frailty, this study provides much greater insight into cardiac structure and function characteristics in frail individuals through the novel

application of robust cardiac MRI. The functional characteristics of the heart during frailty may be best investigated under conditions of physiological stress to effectively delineate potential differences between non-frail and frail individuals, which should be explored in future research. Importantly, this study demonstrates the feasibility of applying multi-modal cardiac MRI within frail individuals, reinforcing the use of this modality to investigate cardiac parameters during frailty.

Chapter Three Appendices

Appendix 3.1 – Calculations of coefficient of variation of cardiac parameters

Raw data used to calculate CV for analysis of long axis (**Table 3.5**), short axis (**Table 3.6**), aortic flow (**Table 3.7**) and cardiac T1 mapping (**Table 3.8**) scans.

Table 3.5: Data used to generate coefficient of variation for repeated analysis of long axis scans.

Cardiac parameter	Measurement #1	Measurement #2	Measurement #3
EDVi (ml/m^2)	78.0	74.9	74.3
ESVi (ml/m^2)	23.9	24.9	25.1
SVi (ml/m^2)	54.0	49.7	49.7
EF (%)	69	67	66
CI (L/min/m^2)	2.6	2.4	2.4
LVMi (g/m^2)	57.7	58.3	58.9
HR (bpm)	47.5	47.5	47.5
Longitudinal strain (%)	-18.4	-17.9	-18.1

Table 3.6: Data used to generate coefficient of variation for repeated analysis of short axis scans.

Cardiac parameter	Measurement #1	Measurement #2	Measurement #3
EDVi (ml/m^2)	95	95.7	95.6
ESVi (ml/m^2)	20	19.8	19.4
SVi (ml/m^2)	35.9	36.5	36.9
EF (%)	65	64.8	65.6
CI (L/min/m^2)	2.1	2.2	2.2
LVMi (g/m^2)	34.7	34.1	34.3
HR (bpm)	59	59	59
Circumferential strain (%)	-19.9	-20.1	-20.5

Table 3.7: Data used to generate coefficient of variation for repeated analysis of aortic flow (AOFLOW) scans.

Cardiac parameter	Measurement #1	Measurement #2	Measurement #3
Peak blood velocity (m/s)	0.73	0.728	0.728
Effective forward blood flow (ml)	65.2	65.1	64.9
CI (L/min/m^2)	1.96	1.96	1.95
Aortic CSA (mm^2)	1053	1060	1066

Table 3.8: Data used to generate coefficient of variation for repeated analysis of cardiac T1 mapping (MOLLI) scans.

Cardiac parameter	Measurement #1	Measurement #2	Measurement #3
Myocardial T1 (ms)	1238	1272	1266
Myocardial T1* (ms)	899	930	933
Blood pool T1* (ms)	2073	1947	1999

Appendix 3.2 - Short axis (SAX) cine data in non-frail pre-frail and frail females

Cardiac structure and function in non-frail, pre-frail and frail females derived from short axis cine scans (**Figure 3.13**).

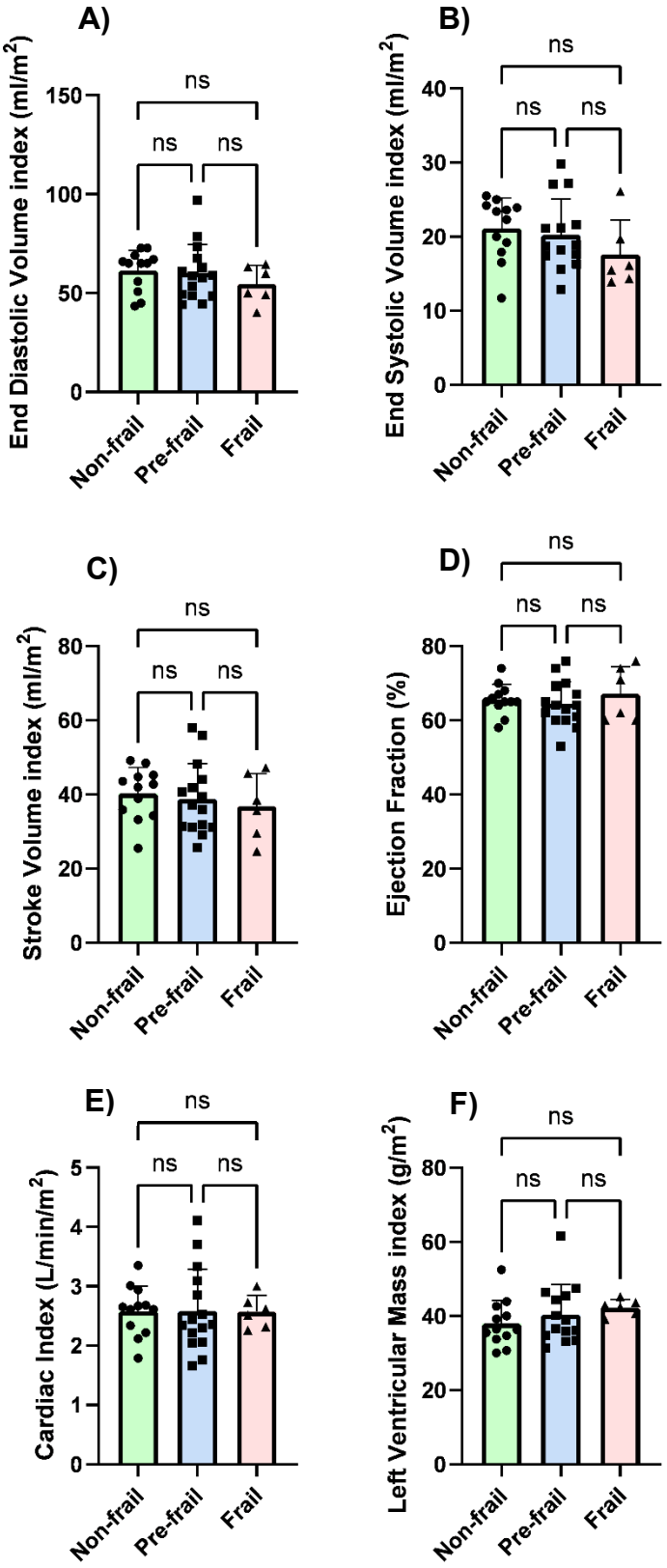

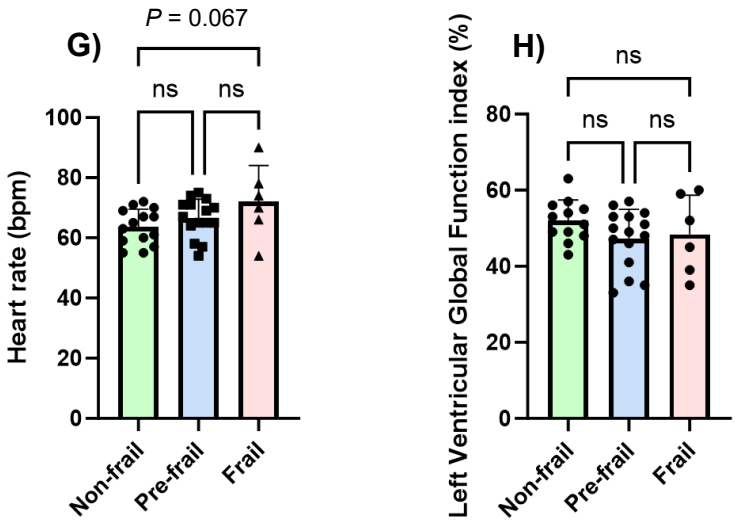

Figure 3.13: *Short axis **A)** End diastolic volume index (EDVi), **B)** End systolic volume index (ESVi), **C)** Stroke volume index (SVi), **D)** Ejection fraction, **E)** Cardiac index, **F)** Left ventricular mass index (LVMi), **G)** Heart rate (HR), **H)** Left ventricular global function index (LVGFi) for non-frail, pre-frail and frail volunteers. Mean and individual values ± standard deviation presented.*

Appendix 3.3 - Short axis (SAX) cine data in non-frail versus combined pre-frail and frail females

Cardiac structure and function in non-frail versus combined pre-frail and frail females derived from short axis cine scans (**Figure 3.14**).

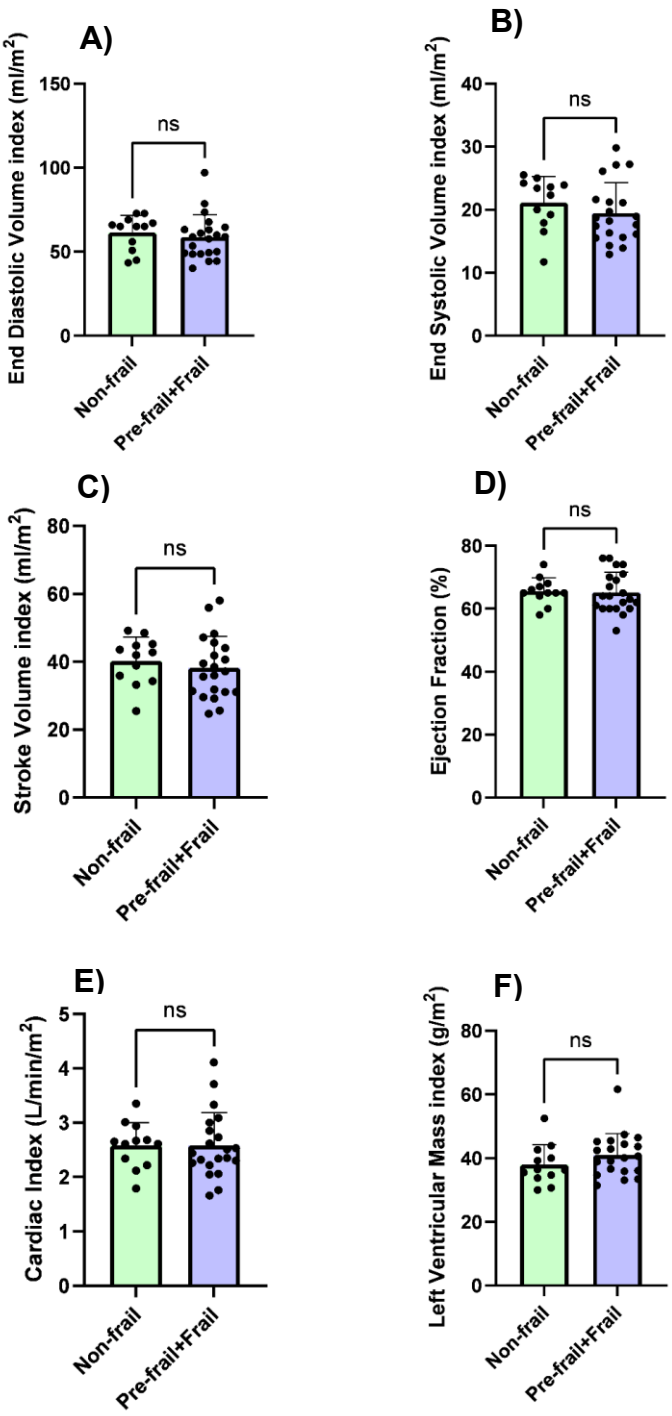

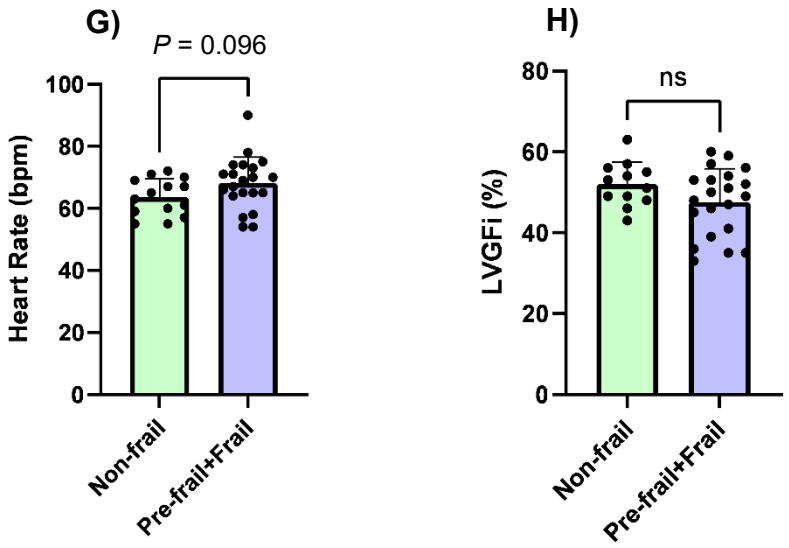

Figure 3.14: *Short axis* ***A)*** *End diastolic volume index (EDVi),* ***B)*** *End systolic volume index (ESVi),* ***C)*** *Stroke volume index (SVi),* ***D)*** *Ejection fraction,* ***E)*** *Cardiac index,* ***F)*** *Left ventricular mass index (LVMi),* ***G)*** *Heart rate (HR),* ***H)*** *Left ventricular global function index (LVGFi) in non-frail versus combined pre-frail and frail groups. Mean and individual values ± standard deviation presented.*

Chapter Four: Body Composition, Neuromuscular Characteristics and Physical Function in Non-frail, Pre-frail and Frail Females

4.1 Introduction

Physical function decline is considered the hallmark characteristic of frailty [9, 10]. However, the physiological underpinnings of functional decline during the syndrome are poorly understood. As outlined in Chapter One – Section 1.5, physiological alterations within the skeletal muscle, adipose tissue and motor unit may promote functional deterioration during frailty. For example, the significant overlap observed in the presence of sarcopenia (the age-related loss of muscle mass and quality [27]) and frailty [37] suggests deterioration in the quantity and quality of skeletal muscle may be traits of frailty and physiological underpinnings of diminished functional capacity in frail individuals [54]. Thus, investigating body composition and neuromuscular characteristics in combination with physical function measures is fundamental for the characterisation of the frailty phenotype and developing strategies to mitigate frailty development.

Regarding skeletal muscle quantity, only a limited number of studies have compared lean mass estimates across healthy and frail states, with studies utilising BIA [44] and DEXA [42, 45] reporting mixed results. Discrepancies may be underpinned by the fact that these methods do not directly quantify muscle mass, thus contributing to variance in study outcomes. MRI, on the other hand, permits the direct assessment of muscle volume and has greater accuracy than DEXA, particularly in the measurement of discrete muscle groups (e.g., muscles of the thigh) [320], which is important given the evidence of greater atrophy of the lower versus upper limbs during ageing [28]. The

small number of studies utilising MRI and CT methods in studies of frailty have highlighted smaller thigh and calf skeletal muscle CSA in frail versus non-frail individuals [49, 51, 52]. Although, differences in muscle CSA between healthy and frail states are not universally observed [53], which may be attributed to mixed sex sampling and differing frailty assessments across studies. Furthermore, CSA measurements may not be reflective of whole muscle volume as analysis is performed on a partial cross section of the muscle. As such, there is a requirement for more direct assessments of whole muscle volume with imaging techniques in improved study designs to further insight into the associations between frailty and skeletal muscle atrophy.

Improved functional capacity has been induced through exercise intervention in older adults, but these gains were not mediated by changes in skeletal muscle CSA [55]. This suggests that the quality of skeletal muscle (i.e., the force generating capacity per unit of muscle mass or volume), contributes to changes in physical function, which may also present during frailty. As such, a lower functional muscle quality of the knee extensors has been observed in frail versus non-frail adults [59]. Physiological underpinnings of this attenuation of muscle quality may include a greater lipid infiltration of the skeletal muscle, considering IMAT has been reported as the strongest predictor of mobility in older adults, when compared against measurements of lean tissue and strength of the quadriceps muscles [321]. Accordingly, previous studies have observed greater calf and thigh muscle IMAT in frail versus healthy adults [49, 53, 57]. However, these estimations were limited to CSA measurements, thus would benefit from further exploration of intramuscular fat volume across whole muscles. Furthermore, the relationship between IMAT and functional muscle quality during frailty was not assessed in these studies. In other work, a larger proportion of high-

density muscle fibres (indicative of lower IMAT based on greater attenuation values of muscle tissue versus adipose tissue) has been associated with better gait kinematics and greater muscle power output in frail individuals using CT scanning [322, 323]. Although, CT attenuation is deemed an indirect measure of IMAT, given it is based the principle of X-ray transmission changes during passage through tissues of different density (i.e., skeletal muscle versus adipose tissue) which does not directly measure of lipid mass or volume. Therefore, further studies of frailty incorporating direct measurements of IMAT in conjunction with assessments of functional capacity are required to improve physiological insight.

Alterations within the neuromuscular junction and MU are also postulated to influence physical function, with smaller MU size associated with lower muscle strength and power output [97], and sarcopenia [81]. Prior studies have observed a smaller MU size in frail versus healthy older adults [95], suggesting neuromuscular degeneration during frailty. However, evidence of lower MU size is at present limited to frail males [95]. Considering MU characteristics, such as MU firing rate and firing rate variability, have been shown to be different between males and females [96], further investigations of MU characteristics in pre-frail and frail females are required.

Associations between frailty and other body composition characteristics such as visceral adiposity are also poorly understood. Investigations of visceral adiposity during frailty are important, given greater visceral fat is a powerful indicator of poor metabolic health associated with all-cause mortality in older adults [324]. Previous BIA and CT data have demonstrated associations between frailty and greater visceral adipose tissue mass [325, 326] and CSA [327]. A prospective study adopting DEXA assessments has also demonstrated that individuals with greater baseline visceral adiposity had higher odds of frailty development (odds ratio: 2.47) after an 8 year follow

up [328]. Whilst this longitudinal data improves insight, these DEXA estimates were likely a composite of both subcutaneous and visceral adipose tissue mass. Direct measurements of visceral adipose tissue, in particular the volume of visceral fat, using imaging techniques are therefore required in studies of frailty.

To further clarify the relationships between frailty, body composition, neuromuscular characteristics and physical function, the aim of this Chapter was to directly quantify and compare body composition characteristics, including: skeletal muscle volume and fat fraction of the calves and whole legs and abdominal visceral adipose tissue volume; neuromuscular characteristics, including: MU size, firing rate and firing rate variability of the VL; and measures of physical function, including: isometric strength, power output, work output, force steadiness and functional quality of the knee extensors, handgrip strength and gait speed; in non-frail, pre-frail and frail females using MRI, iEMG and knee extensor dynamometry techniques. By combining these physiological measures with assessments of physical function, it was hoped that the highly accurate methods would provide a more robust characterisation of body composition and neuromuscular characteristics than previous studies of frailty and provide insight into the physiological underpinnings of physical function deterioration during the syndrome. It was hypothesised that, when compared to non-frail females, pre-frail and frail counterparts would exhibit lower physical function, muscle volume, smaller motor unit size, and greater IMAT and visceral adipose tissue volume.

4.2 Methods

All abbreviations used in this Chapter are outlined on pages 13-17.

4.2.1 Physical function measures

Testing protocols for knee extensor (isometric strength, isokinetic peak torque, work output and force steadiness), handgrip strength and gait speed data acquisition are detailed in Chapter Two – Section 2.6. The following section outlines the data analysis methods used to quantify these physical function measures.

4.2.1.1 Knee extensor isometric strength, isokinetic peak torque, work output and functional quality

Knee extensor isometric strength, isokinetic peak torque and work output during ten repeated contractions were automatically quantified by the Humac Norm software (Humac Norm, Rosemont, Illinois, USA) and saved for offline analysis. Maximal knee extensor isometric strength was taken as the peak torque value (in Nm) achieved following two isometric MVCs. Maximal knee extensor isokinetic peak torque was taken as the peak torque value achieved during each set of ten consecutive isokinetic knee extension repetitions at 60˚/s and 180˚/s. Total work output (in J) was taken as the sum of the work values completed during each of the ten repetition sets at 60˚/s and 180˚/s.

Using the isometric strength data, functional quality of the dominant leg knee extensors was also quantified following normalisation to muscle volume of the thigh (muscle volume analysis detailed in Section 4.2.3.1), which was done by dividing isometric strength (measured in Nm) by thigh muscle volume (measured in cm^3). Whilst force output is proportional to muscle quantity [329], there is a dissociation between the loss of muscle mass and the corresponding reduction in force output and functional capacity in older adults. For example, loss of muscle mass explained only 5% of the corresponding reduction in muscle strength in older individuals in a 10-year

longitudinal study [330]. This suggests force output is also largely influenced by muscle quality characteristics, such as energy metabolism, mitochondrial mass and neural input [35]. Therefore, by normalising isometric strength to muscle volume, a measure of the muscle quality is provided by negating the effect of muscle size on force production. Muscle functional quality was calculated using BSA corrected muscle volume, which represented the final values. For reference, absolute muscle functional quality data are presented in **Appendix 4.2.**

Analysis of knee extension data with the Humac Norm software was fully automated, therefore analytical CV data were not generated for this measure. Previous work has shown high reliability for knee extensor peak torque and work output testing using a Cybex dynamometer [331].

4.2.1.2 Knee extensor force steadiness measures

For force steadiness data analysis, signals recorded in Spike2 software (v.8.1; Cambridge Electronic Designs) were analysed offline by superimposing cursors at the start and end of each sustained contraction (**Figure 4.1**). To avoid corrective actions when reaching the target line, the first two passes of the target (<1s) were excluded from the calculation. The Spike2 software enabled the quantification of mean and SD of the force output between the two cursor points, from which CV was calculated (CV = (SD/mean) × 100). CVs were generated for each contraction and the mean of these CVs represented the final force steadiness value for each contraction intensity (i.e., 10%, 25% or 40% MVC).

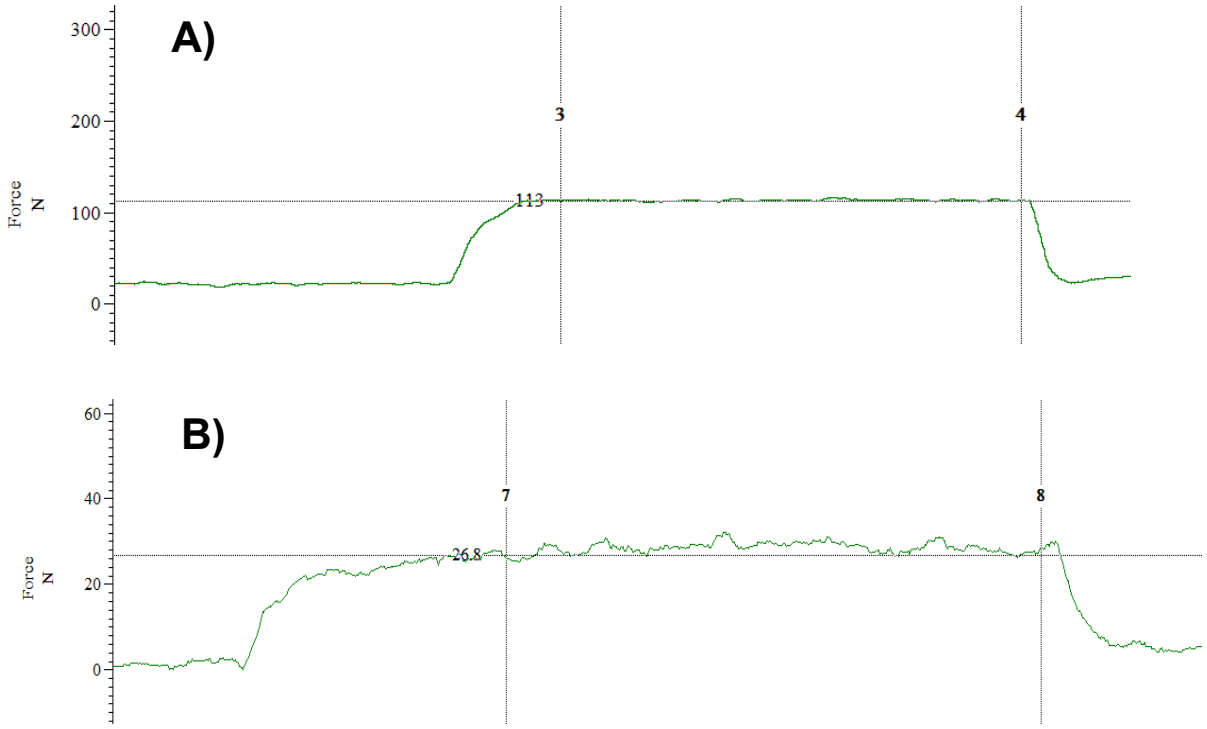

Figure 4.1: *Examples of force steadiness analysis with Spike2 software. During testing, the participant attempted to sustain knee extension force for 12-15 seconds along a target line (horizontal black line) representing 10%, 25% or 40% MVC. For analysis, cursors (vertical lines) were placed at the beginning and end of the force trace (green line) for each contraction to calculate mean, SD and CV.* ***A****) Example of good force steadiness with small fluctuations around the target line (low CV).* ***B****) Example of poor force steadiness - large fluctuations from the target line (high CV).*

CV was calculated to determine the reliability of force steadiness analysis methods, when analysed in the Spike2 software, and all CVs were less than 4% (**Table 4.1**). For CV calculations, three repeat measures were performed on 1 participant's set of force steadiness data at 10%, 25% and 40% MVC. These CV values represent solely the analytical variance, separate to the biological variance between participants, as a measure of the reproducibility of the force steadiness analysis method. Raw data for CV calculations are presented in **Appendix 4.1**.

Table 4.1: Coefficient of variance (CV) results for repeated analysis of force steadiness data using the Spike2 software. MVC = maximum voluntary contraction.

Force steadiness contraction level	CV (%)
10% MVC	2.46 %
25% MVC	3.26 %
40% MVC	3.25 %

4.2.1.3 Handgrip strength and gait speed assessments

Assessments of handgrip strength and gait speed were performed as part of the frailty assessment (detailed in Chapter Two - Section 2.6.1). The raw data generated from these assessments were also analysed as measures of physical function. Final values for handgrip strength represented the mean of three measurements, whilst the mean of two measurements was used as the final value for gait speed (i.e., the time taken to complete the 4.57 metre walk test).

4.2.1.4 Independence in activities of daily living questionnaire

The NEADL scale was used to assess self-reported independence in ADLs. Participants ranked their independence when performing 22 activities, including mobility, kitchen activities and leisure activities (**Figure 4.2**). Higher scores reflected greater independence in ADLs.

Nottingham Extended ADL Scale

The following questions are about everyday activities. Please answer by ticking ONE box for each question. Please record what you have ACTUALLY done in the last few weeks.

DID YOU…….	Not at all	with help	on your own	on your own with difficulty
1. Walk around outside?	☐	☐	☐	☐
2. Climb stairs?	☐	☐	☐	☐
3. Get in and out of a car?	☐	☐	☐	☐
4. Walk over uneven ground?	☐	☐	☐	☐
5. Cross roads?	☐	☐	☐	☐
6. Travel on public transport?	☐	☐	☐	☐
7. Manage to feed yourself?	☐	☐	☐	☐
8. Manage to make yourself a hot drink?	☐	☐	☐	☐
9. Take hot drinks from one room to another?	☐	☐	☐	☐
10. Do the washing up?	☐	☐	☐	☐
11. Make yourself a hot snack?	☐	☐	☐	☐

Figure 4.2: *Example questions from the Nottingham Extended Activities of Daily Living (ADLs) scale, used to rank participant's independence in ADLs.*

4.2.2 Intramuscular electromyography (iEMG) analysis

The iEMG testing protocol is described in Chapter Two – Section 2.6.2. For analysis, iEMG signals were decomposed using custom-written DQEMG software (Decomposition-based Quantitative EMG; v4, http://www.QEMG.org) [332, 333]. Individual MUPs were isolated to assess measures of peripheral function (MUP size) and central function (MU firing rate (FR) and FR variability; **Figure 4.3**). MUP area (i.e., MU size) was taken as the total area under the curve within the MUP duration [88]. MU FR was assessed as the rate of MUP occurrences within a MUP template,

expressed as the number of occurrences per second (measured in Hertz). MU FR variability was reported as the CV for the interspike interval (the time between subsequent action potentials) displayed as a percentage.

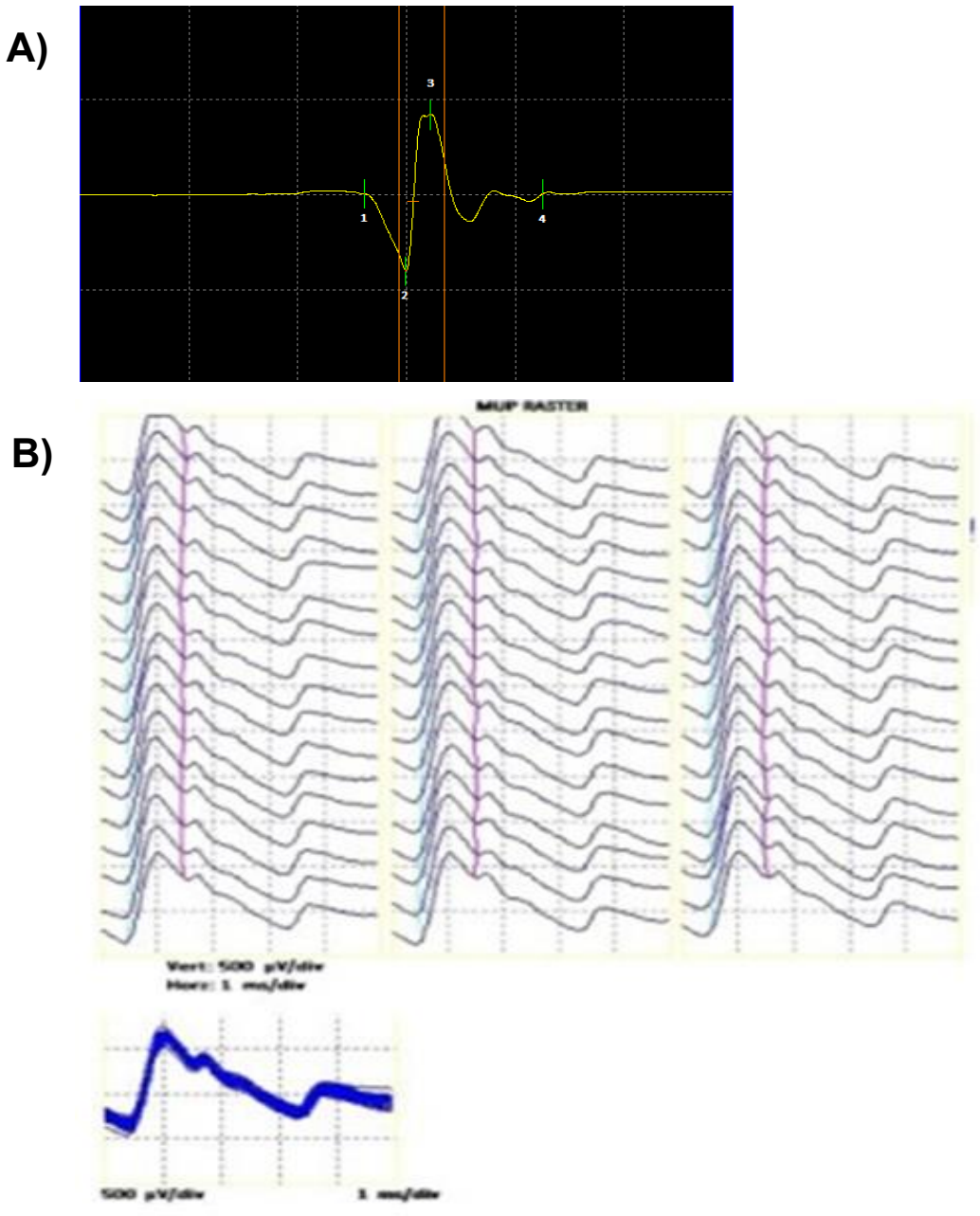

Figure 4.3: *Analysis of motor unit potentials (MUPs) carried out in DQEMG software application.* ***A)*** *Example MUP recorded following action potential depolarisation during contraction of the VL.* ***B)*** *Image display of near-fibre (NF) MUP analysis in DQEMG software.*

Analysis of MUP data with DQEMG software was fully automated, therefore CV data were not generated for this analysis. Previous work using intraclass correlations has shown moderate to high intra- and inter-operator reliability of MUP data analysis using DQEMG [334, 335].

4.2.3 Post processing of MRI images for analysis of body composition parameters

The MRI scan sequence parameters utilised for body composition imaging were detailed in Chapter Two – Section 2.6.3. The following section outlines the post processing analysis techniques used to quantify skeletal muscle volume and fat fraction of the dominant calf and leg, and visceral adipose tissue volume of the abdomen.

4.2.3.1 Segmentation of leg skeletal muscle volume and intra/intermuscular fat fraction

An in-house MATLAB algorithm was developed for analysis of skeletal muscle volume and intramuscular fat fraction of the lower limbs. This algorithm was developed at the University of Nottingham and used as a faster and reliable method of segmentation compared to manual segmentation. Firstly, the MATLAB script stitched together the 6 individual mDIXON image stacks (segments of the body) and bias corrected the resulting image using FMRIB's software library's automated segmentation tool (FAST) (**Figure 4.4**). Bias correction was performed to remove the intensity variability in the image caused by the automatic stitching of the scanner of the 6 segments and resulted in the generation of a water image which could be segmented based on an intensity threshold.

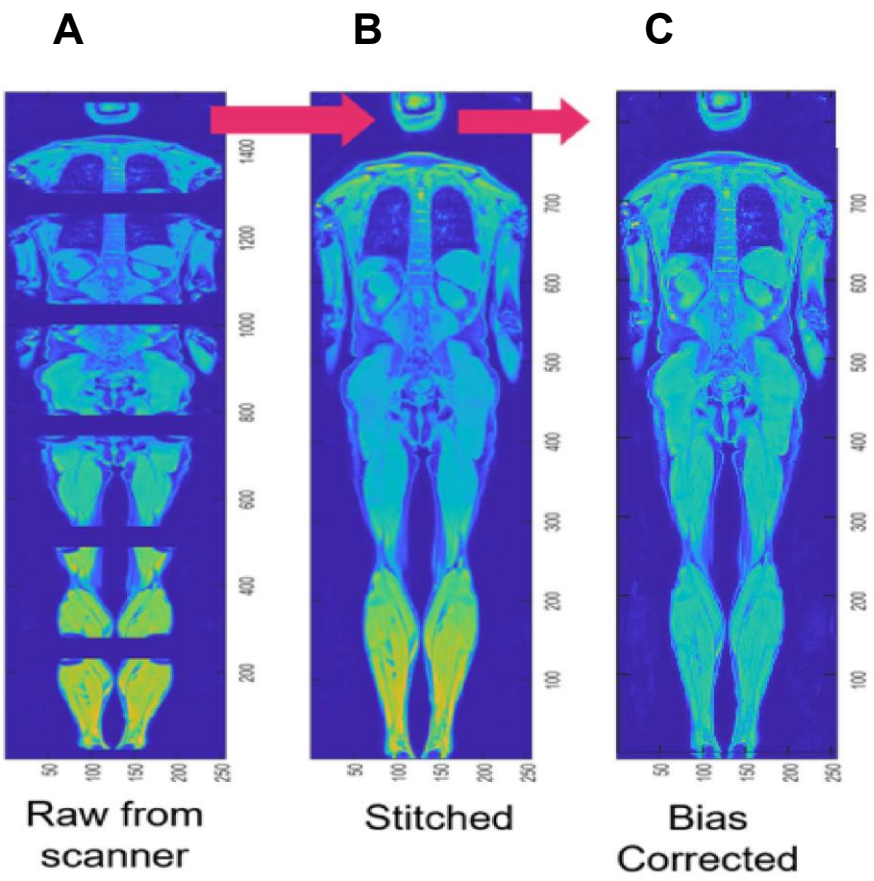

Figure 4.4: *The first three pre-processing steps within the pipeline for semi-automatic segmentation – presented for the water image.* ***A)*** *The six stacks of raw data following export from the scanner.* ***B)*** *The stitched image (all 6 stacks stitched together).* ***C)*** *The bias corrected and stitched image.*

Given the skin's large water content, the skin was then removed from the image as it would remain in FAST segmentation of the water image. This was achieved by generating a skin mask using the 'bwperim' function in MATLAB (a function enabling identification of the perimeter of an image), with the skin mask then applied to the water image. The generated perimeter was labelled as the skin (**Figure 4.5**) and this mask was removed from the whole-body water image prior to further segmentation.

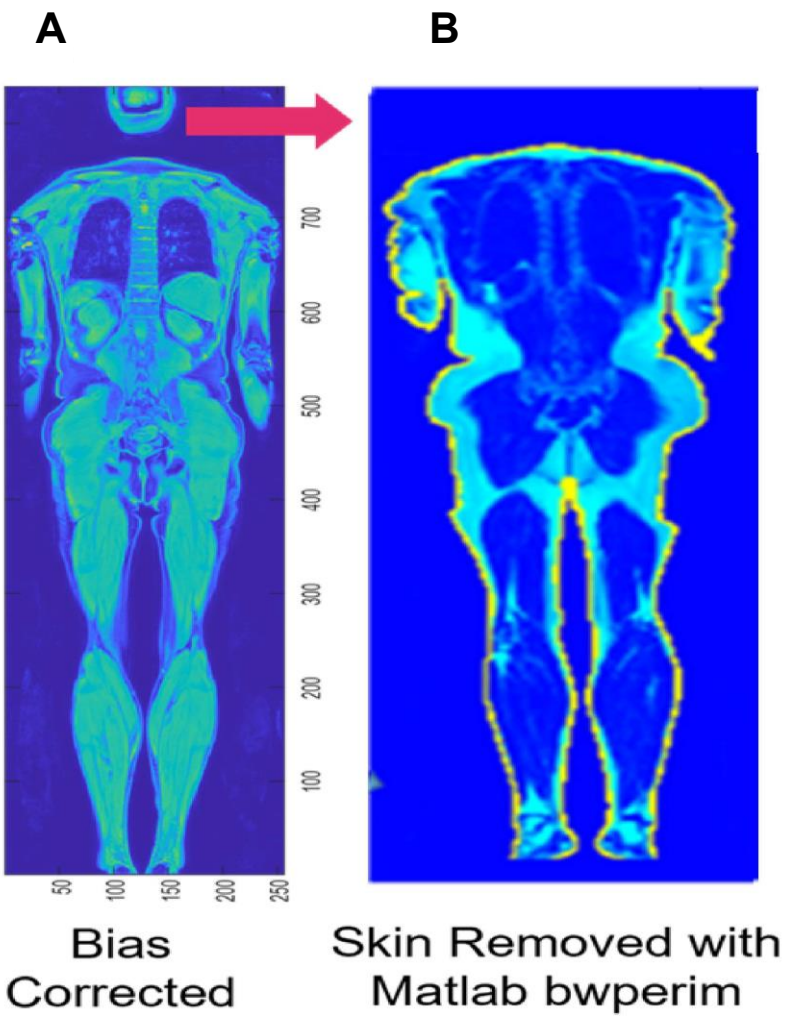

Figure 4.5: A) *Bias corrected water image. Removal of the perimeter of the fat image which represents the skin.* ***B)*** *Skin to be removed shown in yellow.*

The FAST segmentation tool was then used for calf and thigh muscle segmentation using the PVE function. The PVE function calculates the proportion of tissue type in a given voxel (and multiple voxels) based on the voxel's intensity - represented as a value in the range of 0-1. The FAST function was therefore used to separate, and create subsequent images of, subcutaneous and intra/intermuscular adipose tissue, muscle and image noise. Initial testing revealed that running FAST on the whole-body image produced poor results due to large variations in voxel intensities caused by various differing tissue types within internal organs. Therefore, the script was

developed to perform a cropping of the area of within the image, which was divided into 4 segments – right thigh, left thigh, right thigh and right calf. Example thigh ROI segment (following cropping) shown in **Figure 4.6**.

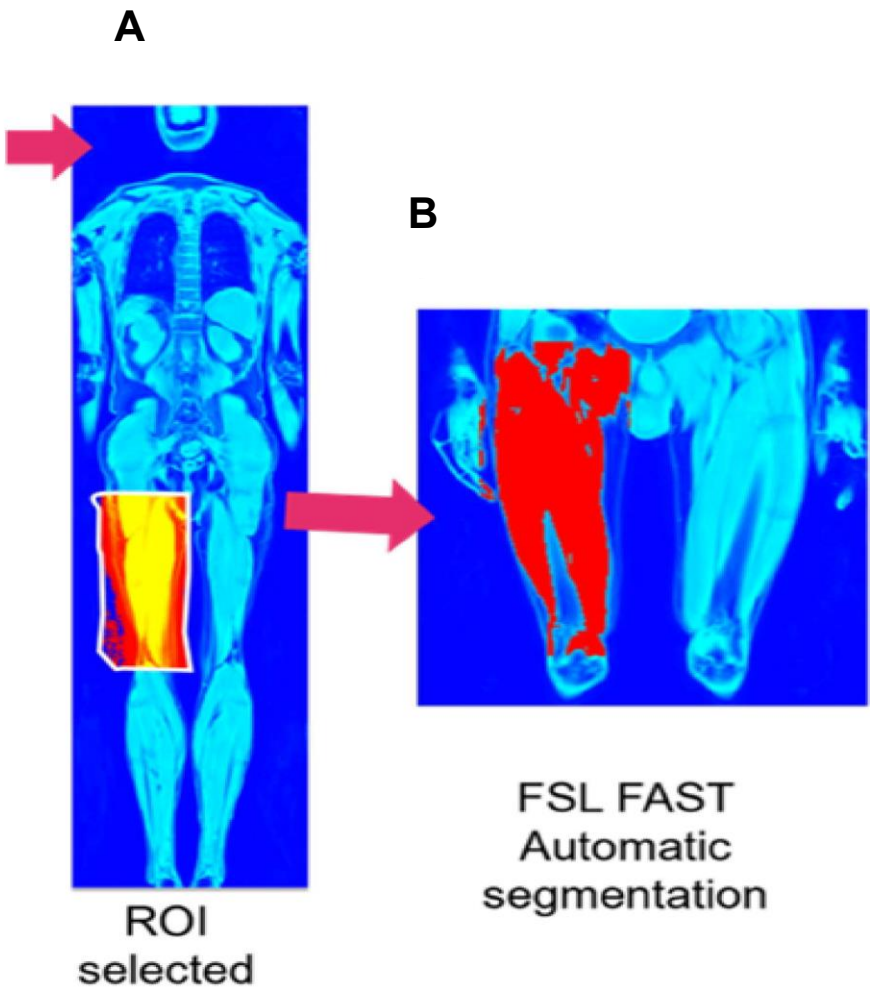

Figure 4.6: *Example of polygonal manual crop of the thigh.* ***A****) Polygon ROI cropped manually from whole body image (shown in white outline).* ***B****) Resulting muscle mask following FSL FAST automatic segmentation (shown in red).*

A single ROI for each calf was drawn around the coronal slice of the image whereby the calf was widest, with the ROI then extended to the rest of the image and applied to the fat and fat fraction images to extract the same ROI from all. Thigh ROIs required cropping with multiple ROIs in order to exclude the gluteus maximus from the

segmentation. Rough polygons were drawn on the water image, firstly on slices where the tissue was visible and contained under 20000 voxels, then every 10 slices once the slice contained above 200 voxels. These regions were then applied to the fat and fat fraction images (**Figure 4.7**).

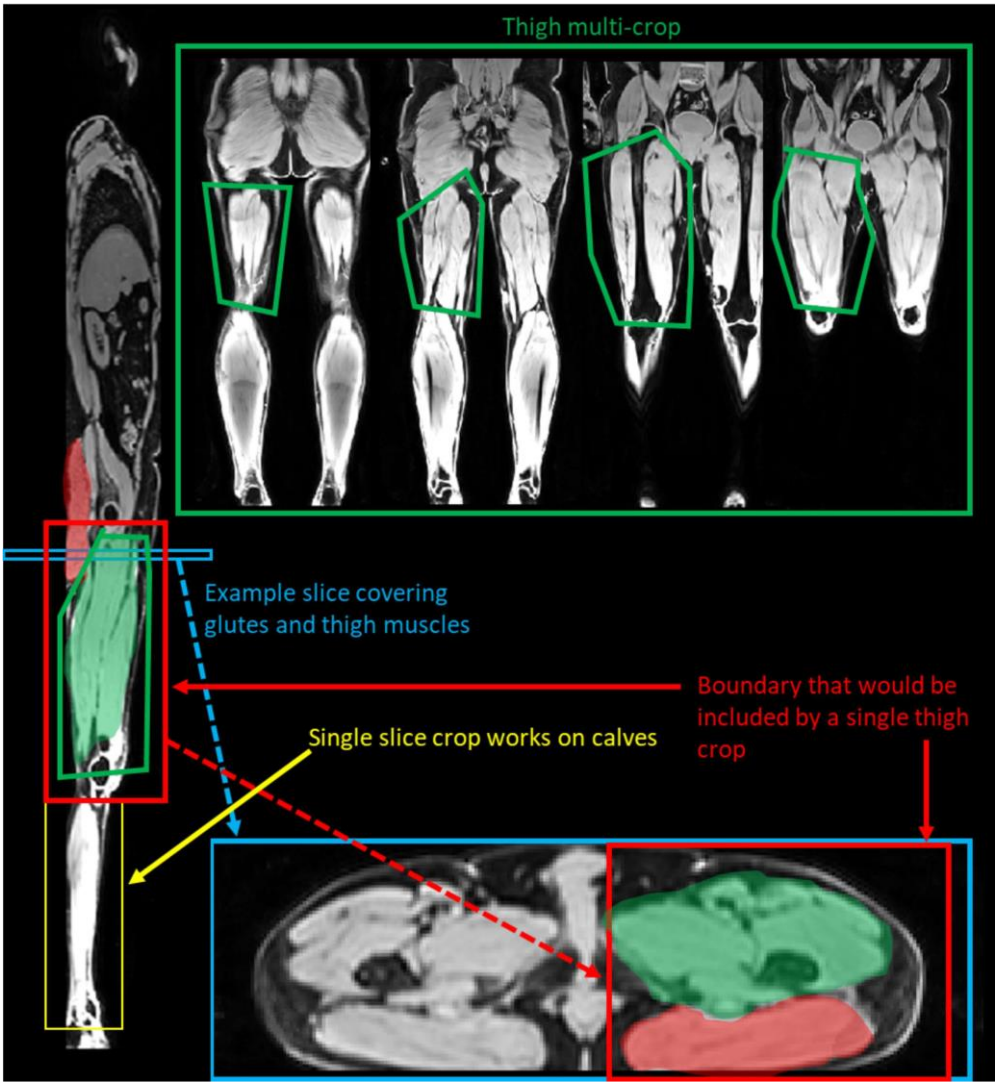

Figure 4.7: *Segmentation of lower limbs using polygon ROIs. A single crop was suitable for the calves (shown in yellow). Depiction of why the single crop method was unsuitable for thigh segmentation (shown in red box with undesired tissue shaded red). Green box highlights the multicrop method for thigh segmentation and exclusion of gluteus maximus.*

The MATLAB script then pushed the cropped ROIs through the FAST function to segment the image into the three PVE components of subcutaneous and intra/intermuscular adipose tissue, muscle and image noise - shown in **Figure 4.8**.

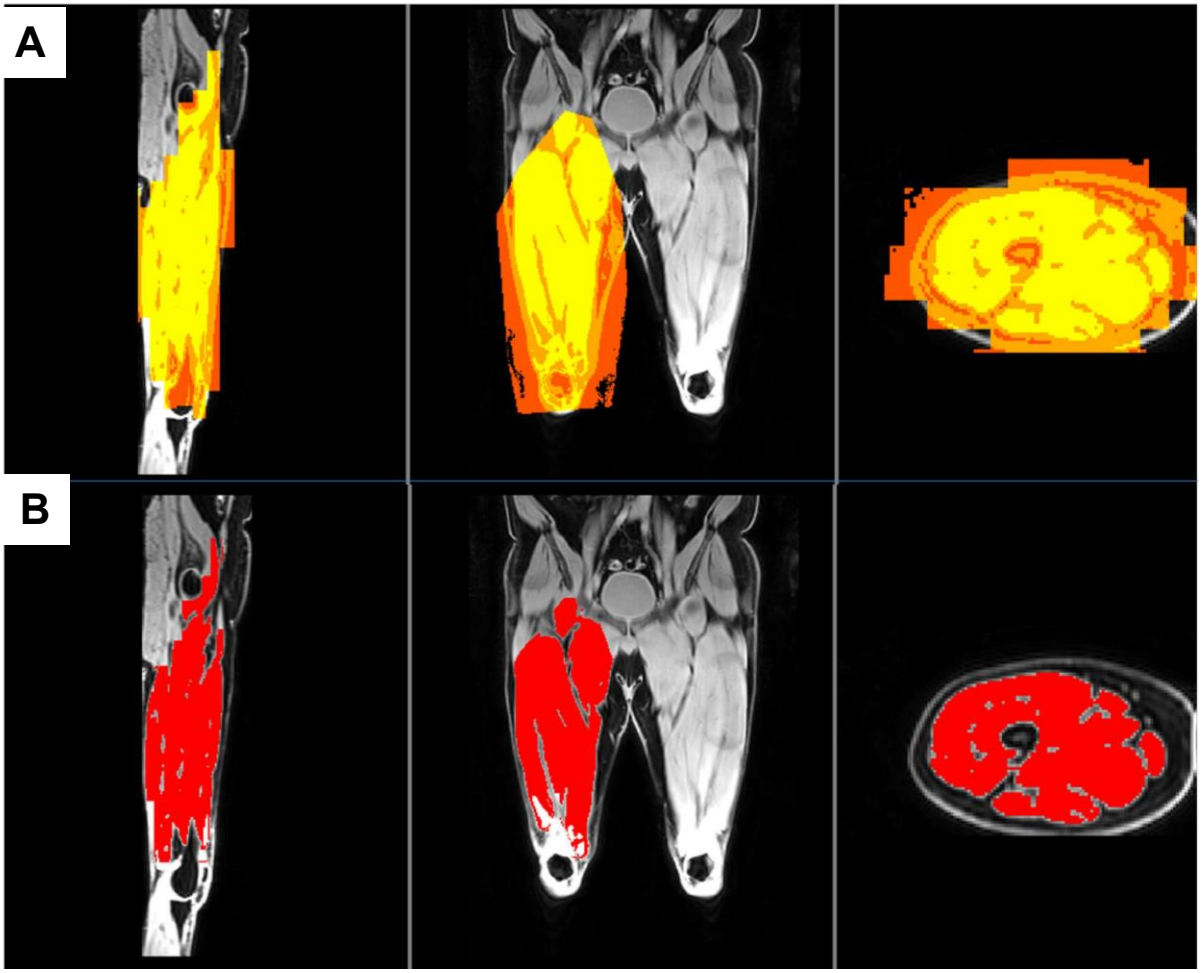

Figure 4.8: *Example PVE map of thigh segment using FSL FAST command.* ***A)*** *The 3 PVE components of muscle (yellow), subcutaneous and intra-/inter-muscular adipose tissue (light orange), and noise (dark orange).* ***B)*** *The red areas represent the final muscle mask following pipeline completion.*

Following segmentation using FAST, the resultant image consisted primarily of the desired muscle tissue but often included small regions of noise, skin or muscle from an undesired muscle group. To discard erroneous regions in segments, the script utilised numerous functions to isolate and remove these areas (**Figure 4.9**). Firstly, a

EDT was applied to the binary mask, with a distance value of 2 used to separate out disparate objects – any values below the distance value were removed from the EDT map. A connectivity function (the 'bwconncomp' MATLAB function) was then applied to the EDT map to facilitate greater object separation. The erroneous objects were then identified based on size to create a mask of solely the large, highly connected objects. This mask was then dilated outwards 5 times and then applied to the segmentation mask to remove any areas where the dilation expanded the mask beyond the initial segmentation mask.

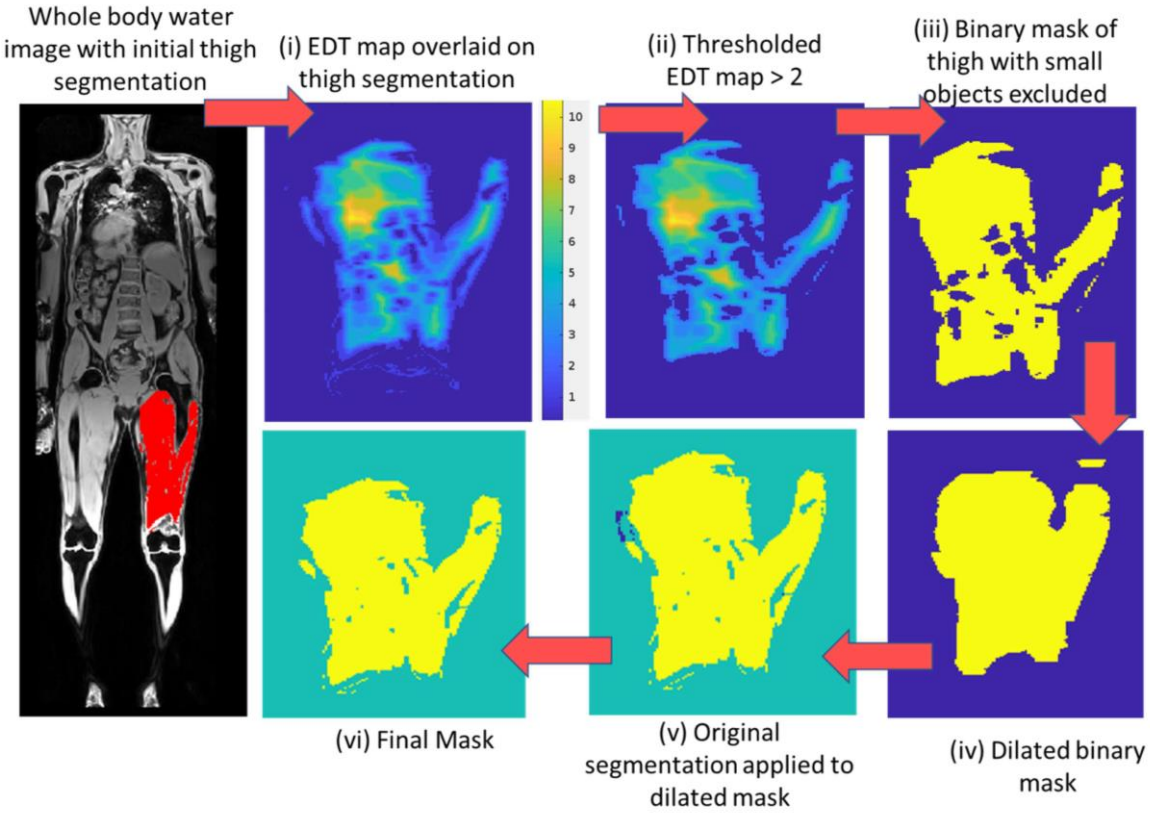

Figure 4.9: *Euclidean Distance Transform (EDT) and connectivity cleaning of thigh muscle mask during segmentation.*

To ensure areas of erroneous fat were excluded from tissue, a threshold of greater than 60% was applied to the fat fraction image to generate a fat mask, which was

subsequently applied to the water mask. This enabled thresholding out of areas of extremely high fat fraction that were subcutaneous adipose tissue or physiologically implausible for intermuscular fat (**Figure 4.10**).

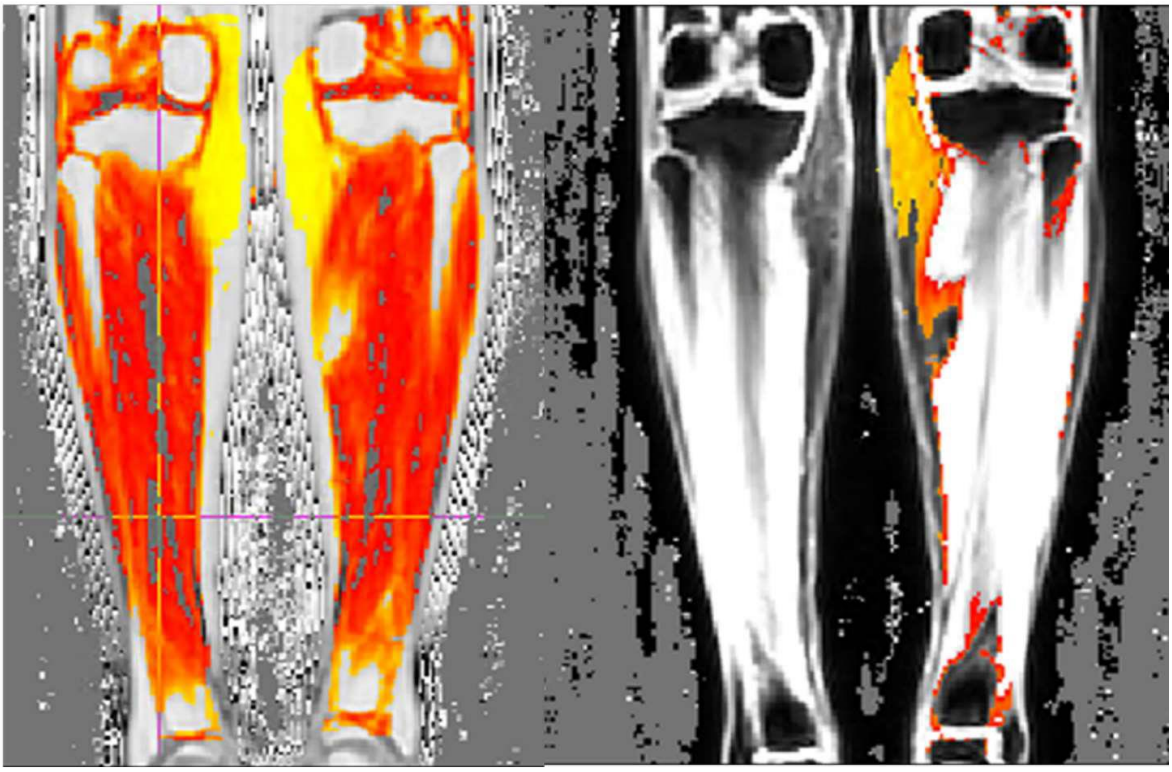

Figure 4.10: *Threshold of fat content greater than 60% applied to the fat fraction image (left). This generated fat mask which was then applied to water mask to visualise and remove areas of very high fat fraction.*

Some generated muscle masks contained artefacts which caused an exclusion of small areas of muscle within the mask. These muscle masks were manually corrected using the MRIcron software package (v1.0.20190902, https://www.nitrc.org/projects/mricron) to correct areas whereby muscle was erroneously excluded, with the masks overlayed on to the stitched whole body water image in the background as a guide. Examples of manual corrections of muscle masksare highlighted in **Figure 4.11**.

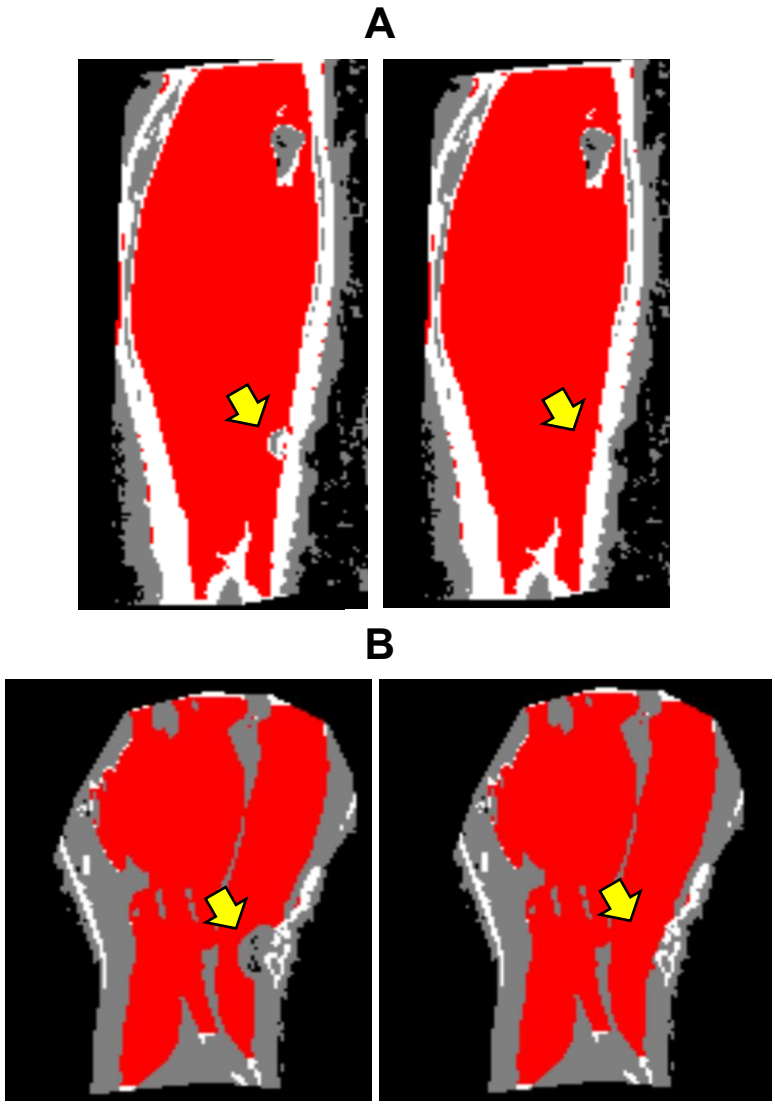

Figure 4.11: *Examples of manual corrections made to muscle masks using MRIcron software. Muscle masks shown in red, overlayed onto stitched mDIXON water image.* ***A)*** *Artefact in calf muscle mask highlighted by yellow arrow (left image). Same calf muscle mask following manual correction (right image).* ***B)*** *Artefact in thigh muscle mask highlighted by yellow arrow (left image). Same thigh muscle mask following manual correction (right image).*

Skeletal muscle volume values were normalised to BSA. For reference, absolute muscle volume data are presented in **Appendix 4.3**. Results were presented for the dominant calf muscle. Additionally, muscle volume of the calf and thigh segments of the dominant leg were also summed to generate whole leg volume (e.g., in a participant with a dominant left leg – left leg volume = left calf + left thigh). Fat fraction

of the muscle was generated by quantifying the mode of the gaussian distribution of fat content across all voxels of the muscle mask. Fat fraction represented a combination of the intra- and inter-muscular volume of fat content, expressed as a percentage of the whole muscle for each of the four lower limb segments. Fat fraction results are presented for the dominant calf and fat fraction of the dominant leg represented the average percentage of intra- and intermuscular fat across the dominant calf and thigh.

CVs were calculated for skeletal muscle volume and fat fraction measures to determine the reliability of the semi automatic pipleline analysis of mDIXON images and all were less than 2% (**Table 4.2**). For CV calculations, three repeat measures were performed on 1 participant's set of mDIXON images. CV values represented the analytical variance as a measure of the reproducibility of the muscle volume and fat fraction analysis method, which is distinct from the biological variance between participants. Raw data for CV calculations are presented in **Appendix 4.1**.

Table 4.2: Coefficient of variance (CV) results for repeated analysis of mDIXON images using the semi-automatic pipepline.

Parameter	CV (%)
Left calf skeletal muscle volume (cm^3)	0.89 %
Right calf skeletal muscle volume (cm^3)	1.44 %
Left leg skeletal muscle volume (cm^3)	1.23 %
Right leg skeletal muscle volume (cm^3)	0.78 %
Left calf fat fraction (%)	0.7 %
Right calf fat fraction (%)	1.0 %
Left leg fat fraction (%)	0.56 %
Right leg fat fracion (%)	0.56 %

4.2.3.2 Visceral adipose tissue volume of the abdomen

The wholebody fat image generated from the mDIXON sequence also enabled the analysis of visceral adispose tissue volume, which was performed following stitching of the six image stacks (described in previous section; **Figure 4.4**) of fat weighted images. The stitched fat images were then ran through a custom in-house MATLAB code to generate a mask of visceral adipose tissue. The MATLAB script firstly read in the wholebody mDIXON stitched fat image and enabled the manual identification of a ROI of the abdomen from the coronal view of the image, which was defined as the bottom of the sternum to the top of the pelvis. The fat image was then binarised, which entailed all fat voxels within the ROI being converted from grey scale to white (with the basis of this being the higher intensity of fat-containing voxels compared to other tissue in the fat weighted image) and all other tissue and noise in the image being converted to black. Black voxels within areas surrounded by white fat voxels were filled in white with a flood-fill function (im_fill). A connectivity function (bwconncomp) was then used to remove unconnected objects and Gaussian filtering (using a 3-D smoothing kernal with a standard deviation of 2) was performed to calculate a weighted average of neighbouring fat voxels (based on the Gaussian distribution) to remove image noise. The flood-fill function was then applied again to fill holed encompassed within the mask.The resultant mask was then multiplied by the original fat image to remove any non-fat areas included in the mask. A line extraction function was then used to define the internal perimeter of the subcutaneous fat to generate a mask that does not extend into the visceral vat, thus excluding subcutaneous fat, and the Gaussian filtering process was repeated on the final visceral adipose tissue mask.

Following the automatic segmentation, generated masks were manually corrected to remove erroneous regions (such as the spine; **Figure 4.12**) included in the mask.

Manual adjustments to masks were performed with the MRIcron software package (v1.0.20190902, https://www.nitrc.org/projects/mricron). Finally, the visceral fat mask was ran through separate in-house MATLAB code to calculate the absolute volume (cm^3) of the mask by multiplying the voxel number by the voxel dimensions. Visceral adipose tissue volume was corrected for BSA, which represented the final values. For reference, absolute visceral adipose volume data are presented in **Appendix 4.4.**

A CV of 1.6% was calculated for visceral adipose tissue volume analysis, following three repeat measures performed on 1 participant's set of mDIXON images using the MATLAB code and manual corrections. CV values represented the analytical variance as a measure of the reproducibility of the visceral adipose tissue volume analysis method, which was separate to the biological variance between participants. Raw data for CV calculations are presented in **Appendix 4.1**.

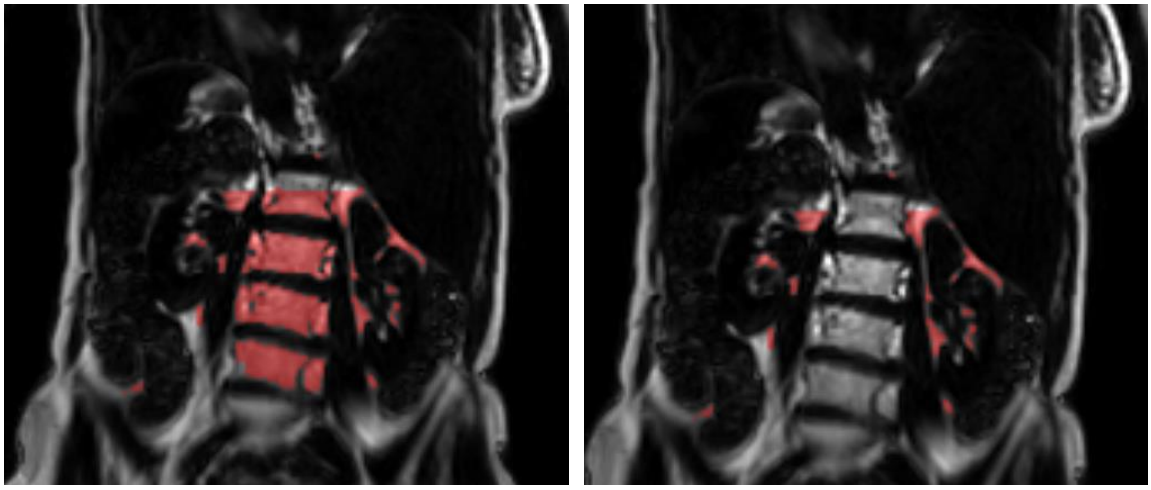

Figure 4.12: *Example images of visceral adipose tissue mask from the abdomen and manual correction performed to remove erroneous regions of mask. Original mask (shown in red) generated from MATLAB code shown on left with erroneous areas such as the spine included in mask. Right image shows the mask following manual correction in MRIcron software to remove spine.*

4.2.4 Statistical analysis

Statistical analysis methods were described in Chapter Two – Section 2.9. Values in the text, Tables and Figures represents mean ± standard deviation.

4.3 Results

4.3.1 Physical function measures

Functional assessments were not completed in a small number of participants due to pre-existing injuries and functional impairments preventing completion of the testing protocols. **Table 4.3** outlines the sample size of participants with available data for each physical function assessment. Normality testing revealed non-normal distributions of the following data sets: force steadiness at 40% MVC (2 and 3 group comparisons), time taken to complete the walking test (2 and 3 group comparisons), dominant calf fat fraction (2 and 3 group comparisons), dominant leg fat fraction (2 group comparisons). For non-normally distributed data, *P* values are derived from the Kruskall-Wallis test (for 3 group comparisons) and Mann-Whitney U test (for 2 group comparisons).

Table 4.3: Available physical function data in non-frail, pre-frail and frail participants. NEADL = Nottingham Extended Activities of Daily Living questionnaire.

Physical function assessment	**Data analysed in non-frail (*n*)**	**Data analysed in pre-frail (*n*)**	**Data analysed in frail (*n*)**
Knee extensor isometric strength	12	12	5
Knee extensor peak torque (60°/s)	13	12	5
Knee extensor peak torque (180°/s)	13	12	4

Knee extensor work output (60°/s)	13	12	5
Knee extensor work output (180°/s)	13	12	4
Knee extensor functional quality	12	12	5
Knee extensor force steadiness	13	10	4
Handgrip strength	14	15	6
Time to complete walk test	14	15	6
NEADL questionnaire	14	15	6

4.3.1.1 Knee extensor isometric strength in non-frail, pre-frail and frail females

Isometric strength of the knee extensors in the pre-frail (80 ± 18 Nm) and frail (64 ± 14 Nm) females was significantly lower compared to non-frail counterparts (non-frail vs pre-frail: $P = 0.011$; non-frail vs frail: $P = 0.002$; **Figure 4.13 A**). However, there were no differences in isometric strength between the pre-frail and frail groups (**Figure 4.13 A**).

4.3.1.2 Knee extensor isometric strength in non-frail versus the collapsed group of pre-frail and frail females

Knee extensor isometric strength in the collapsed group of pre-frail and frail females was also significantly lower compared to the non-frail (105 ± 23 Nm) group ($P < 0.001$; **Figure 4.13 B**).

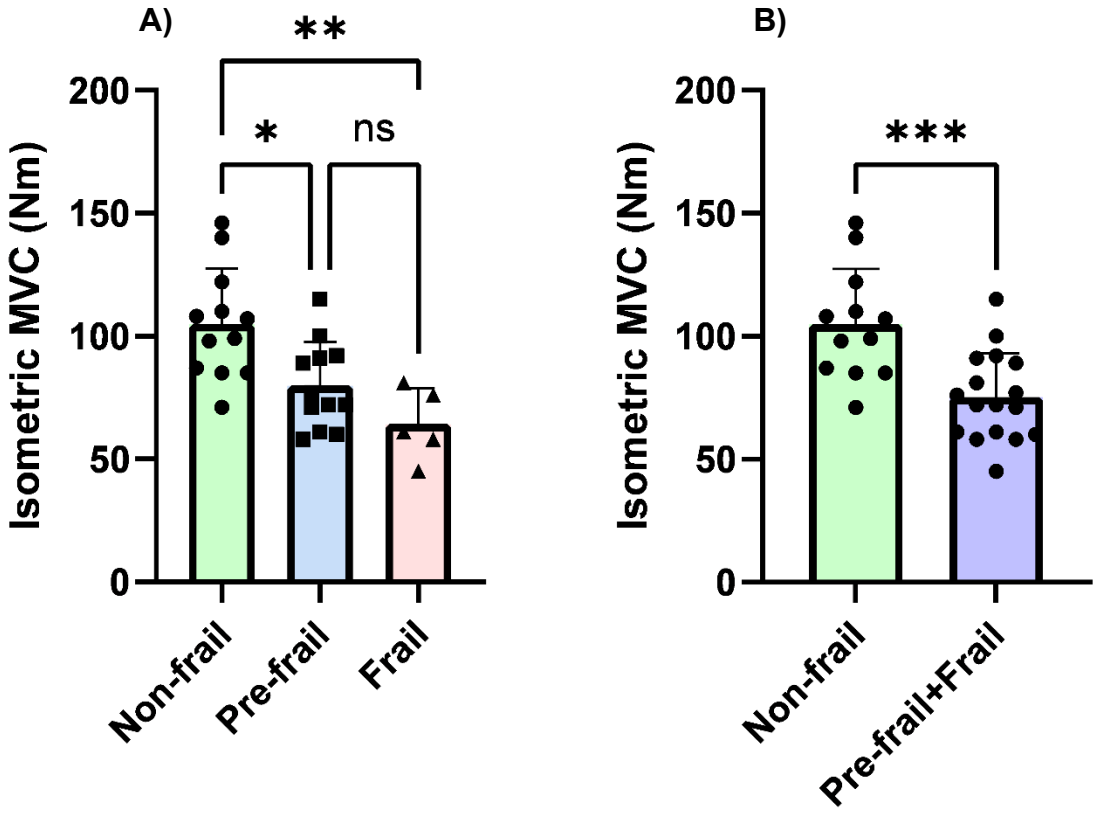

Figure 4.13: *Isometric strength of the knee extensor muscles in **A)** non-frail, pre-frail and frail females, and **B)** non-frail versus the collapsed group of pre-frail and frail females. MVC = maximum voluntary contraction; Nm = Newton metres. Values are mean ± standard deviation and individual values. * = P < 0.05; ** = P < 0.01, *** = P < 0.001.*

4.3.1.3 Knee extensor isokinetic peak torque in non-frail, pre-frail and frail females

Peak torque during knee extensions at 60°/s was significantly lower in pre-frail (65 ± 12 Nm) and frail (54 ± 21 Nm) females compared to non-frail females (non-frail vs pre-frail: $P = 0.042$; non-frail vs frail: $P = 0.01$; **Figure 4.14 A**). However, no differences in peak torque at 60°/s were evident between pre-frail and frail females (**Figure 4.14 A**).

Knee extensor peak torque at 180°/s was also significantly less in pre-frail (41 ± 8 Nm) and frail (38 ± 17 Nm) compared to non-frail females (non-frail vs pre-frail: $P = 0.01$; non-frail vs frail: $P = 0.03$; **Figure 4.14 B**). However, peak torque at 180°/s was no different between pre-frail and frail females (**Figure 4.14 B**).

4.3.1.4 Knee extensor isokinetic peak torque in non-frail versus the collapsed group of pre-frail and frail females

Peak torque during knee extensions at 60°/s was significantly lower in the collapsed group of pre-frail and frail females compared to non-frail (81 ± 17 Nm) females ($P = 0.003$; **Figure 4.14 C**). The collapsed group of pre-frail and frail females also exhibited significantly less knee extensor peak torque at 180°/s in comparison to the non-frail (53 ± 10 Nm) group ($P = 0.001$; **Figure 4.14 D**).

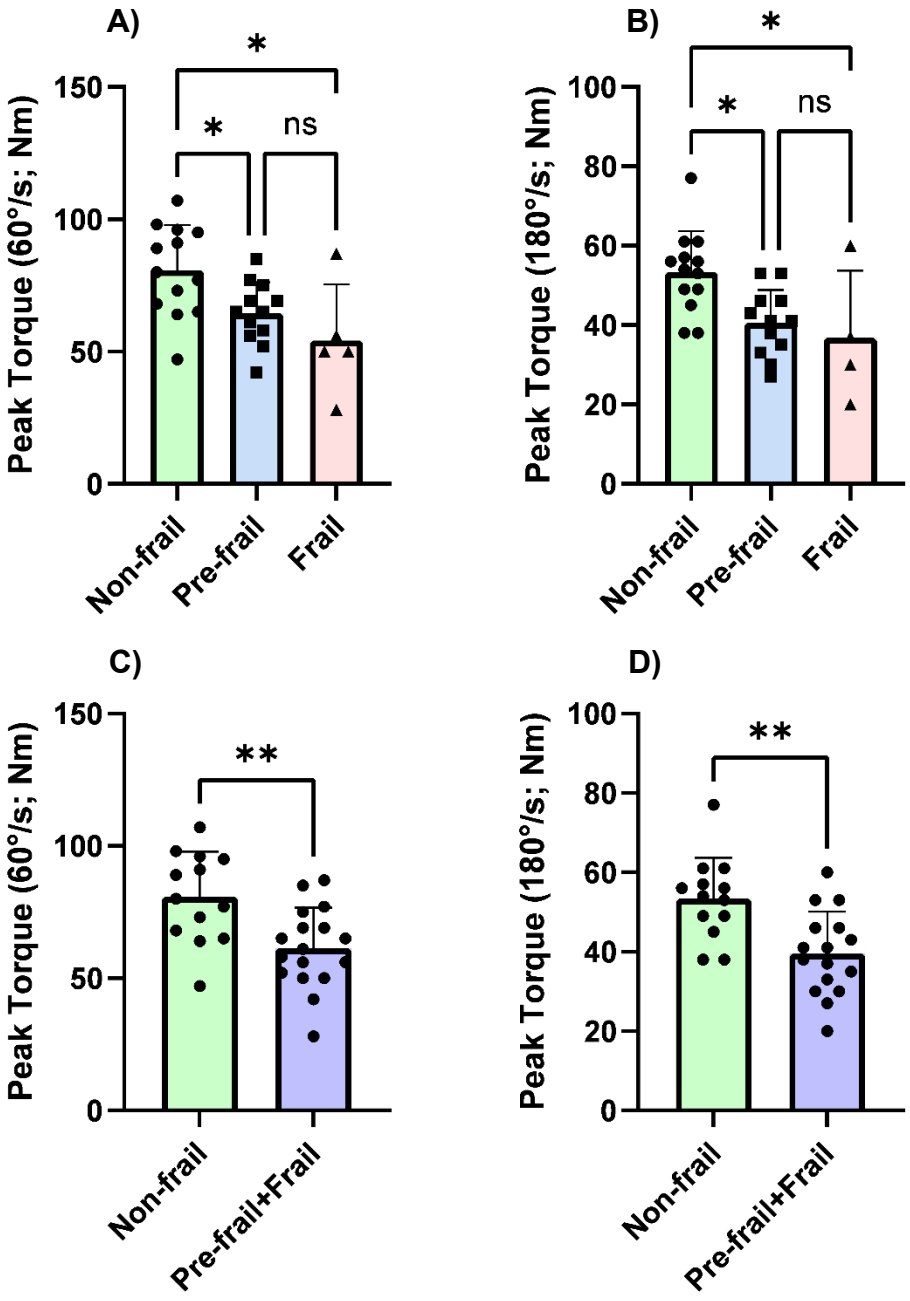

Figure 4.14: *Peak torque of the knee extensor muscles during contractions at 60°/s (**A**) and 180°/s (**B**) in non-frail, pre-frail and frail females. Knee extensor peak torque during contractions at 60°/s (**C**) and 180°/s (**D**) in non-frail versus the collapsed group of pre-frail and frail females. Nm = Newton metres. Values are mean ± standard deviation and individual values. * = P < 0.05; ** = P < 0.01.*

4.3.1.5 Knee angle at peak torque during isokinetic contractions of the knee extensors in non-frail, pre-frail and frail females

During isokinetic contractions at 60°/s, pre-frail (40.4 ± 10.1°) and frail (37.6 ± 6.2°) females achieved peak torque at a significantly smaller knee angle compared to non-frail females (non-frail vs pre-frail: $P = 0.028$; non-frail vs frail: $P = 0.032$; **Figure 4.15 A**). No differences in knee angle at peak torque during contractions at 60°/s were observed between pre-frail and frail groups (**Figure 4.15 A**).

During contractions at 180°/s, pre-frail (39.6 ± 9.6°) and frail (31.3 ± 12.3°) females also achieved peak torque at significantly smaller knee angles versus non-frail females (non-frail vs pre-frail: $P = 0.036$; non-frail vs frail: $P = 0.004$; **Figure 4.15 B**). No differences in knee angle at peak torque during contractions at 180°/s were observed between pre-frail and frail groups (**Figure 4.15 B**).

4.3.1.6 Knee angle at peak torque during isokinetic contractions of the knee extensors in non-frail versus the collapsed group of pre-frail and frail females

Knee angle at peak torque was significantly lower in the collapsed group of pre-frail and frail females compared the non-frail group (50.2 ± 8.5°) during contractions at 60°/s ($P = 0.003$; **Figure 4.15 C**). Similarly, knee angle at peak torque during contractions at 180°/s was significantly lower in the collapsed group of pre-frail and frail females versus the non-frail group (48.9 ± 6.3°; $P = 0.002$; **Figure 4.15 D**).

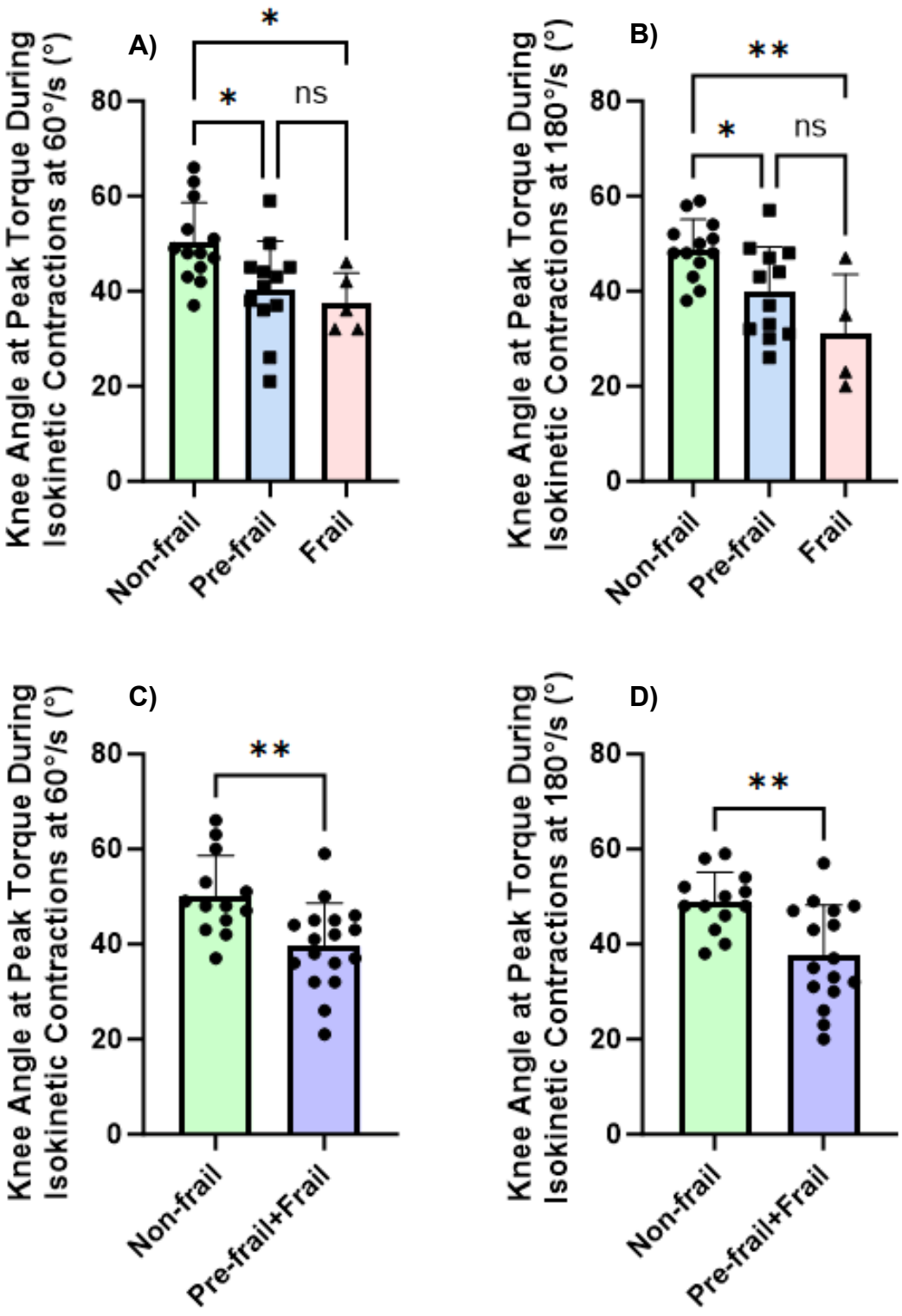

Figure 4.15: *Knee angle at peak torque during contractions at 60°/s (**A**) and 180°/s (**B**) in non-frail, pre-frail and frail females. Knee angle at peak torque during contractions at 60°/s (**C**) and 180°/s (**D**) in non-frail versus the collapsed group of pre-frail and frail females. Values are mean ± standard deviation and individual values. ° = Degrees. * = P < 0.05; ** = P < 0.01.*

4.3.1.7 Knee extensor work output in non-frail, pre-frail and frail females

Pre-frail (560 ± 100 J) and frail (461 ± 208 J) females performed a significantly lower amount of work compared to non-frail females at 60°/s (non-frail vs pre-frail: $P = 0.03$; non-frail vs frail: $P = 0.005$; **Figure 4.16 A**), whereas the amount of work performed at 60°/s was not different between pre-frail and frail groups (**Figure 4.16 A**).

During contractions at 180°/s, the pre-frail (347 ± 72 J) and frail (321 ± 151 J) groups also performed significantly less work compared to non-frail counterparts (non-frail vs pre-frail: $P = 0.01$; non-frail vs frail: $P = 0.03$; **Figure 4.16 B**). However, no differences in work output at 180°/s were observed between pre-frail and frail groups (**Figure 4.16 B**).

4.3.1.8 Knee extensor work output in non-frail versus the collapsed group of pre-frail and frail females

The collapsed group of pre-frail and frail females performed significantly lower amounts of work compared to non-frail (710 ± 134 J) females at 60°/s ($P = 0.001$; **Figure 4.16 C**). Similarly, significantly lower work output at 180°/s was exhibited by the collapsed group of pre-frail and frail females versus the non-frail (462 ± 94 J; $P = 0.001$; **Figure 4.16 D**).

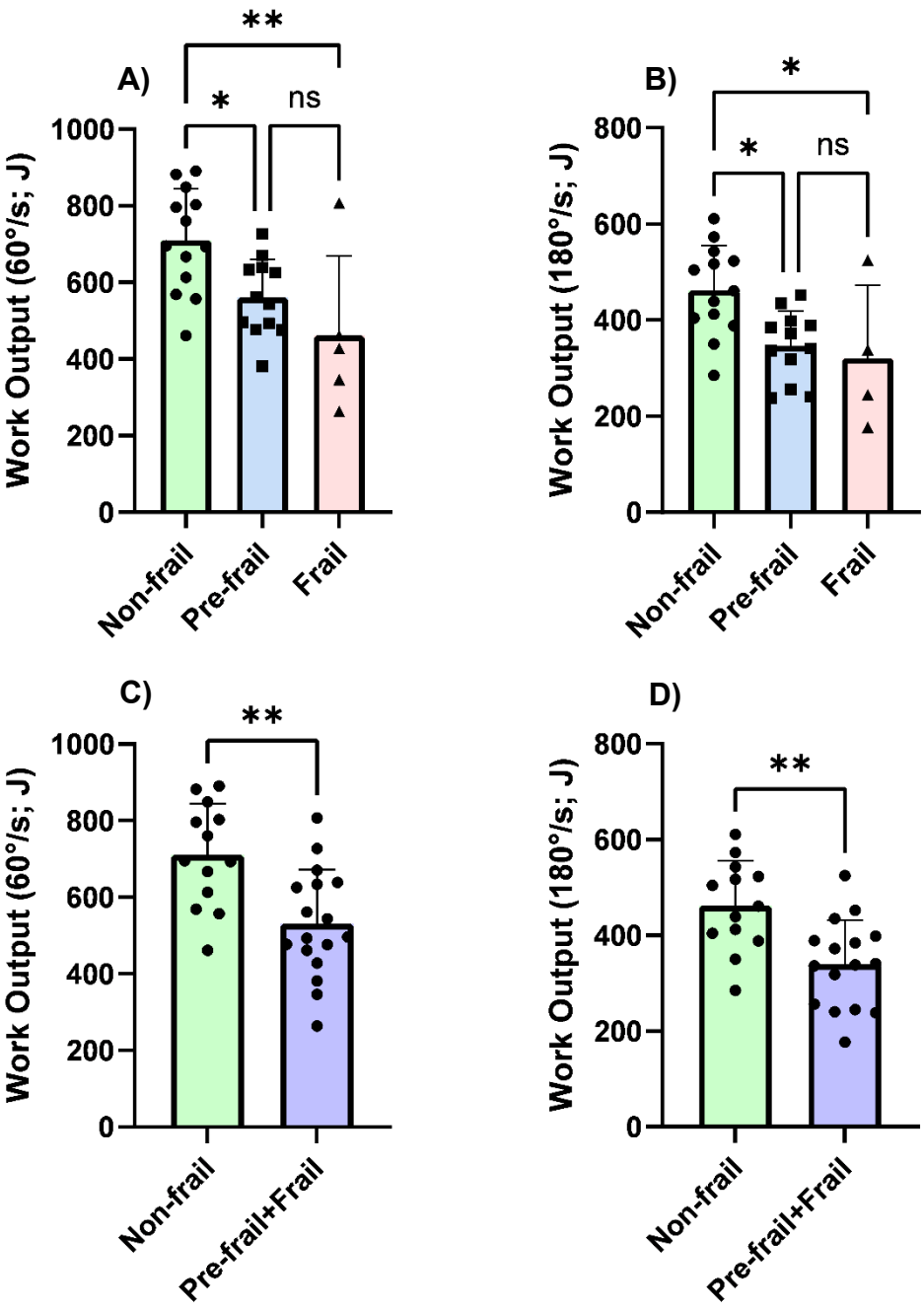

Figure 4.16: *Knee extensor work output during contractions at 60°/s (**A**) and 180°/s (**B**) in non-frail, pre-frail and frail females. Knee extensor work output during contractions at 60°/s (**C**) and 180°/s (**D**) in non-frail versus the collapsed group of pre-frail and frail females. Values are mean ± standard deviation and individual values. J = Joules. * = P < 0.05; ** = P < 0.01.*

4.3.1.9 Knee extensor muscle functional quality in non-frail, pre-frail and frail females

Pre-frail (0.064 ± 0.01 Nm/cm^3/m^2) and frail (0.053 ± 0.009 Nm/cm^3/m^2) females exhibited significantly lower muscle functional quality compared to non-frail females (non-frail vs pre-frail: P = 0.04; non-frail vs frail: P = 0.006; **Figure 4.17 A**). However, functional muscle quality was not different between pre-frail and frail groups (**Figure 4.17 A**).

4.3.1.10 Knee extensor muscle functional quality in non-frail versus the collapsed group of pre-frail and frail females

Knee extensor functional quality in the collapsed group of pre-frail and frail females was also significantly lower versus the non-frail (0.079 ± 0.017 Nm/cm^3/m^2) females (P = 0.003; **Figure 4.17 B**).

For reference, absolute knee extensor functional quality data are presented in **Appendix 4.2**.

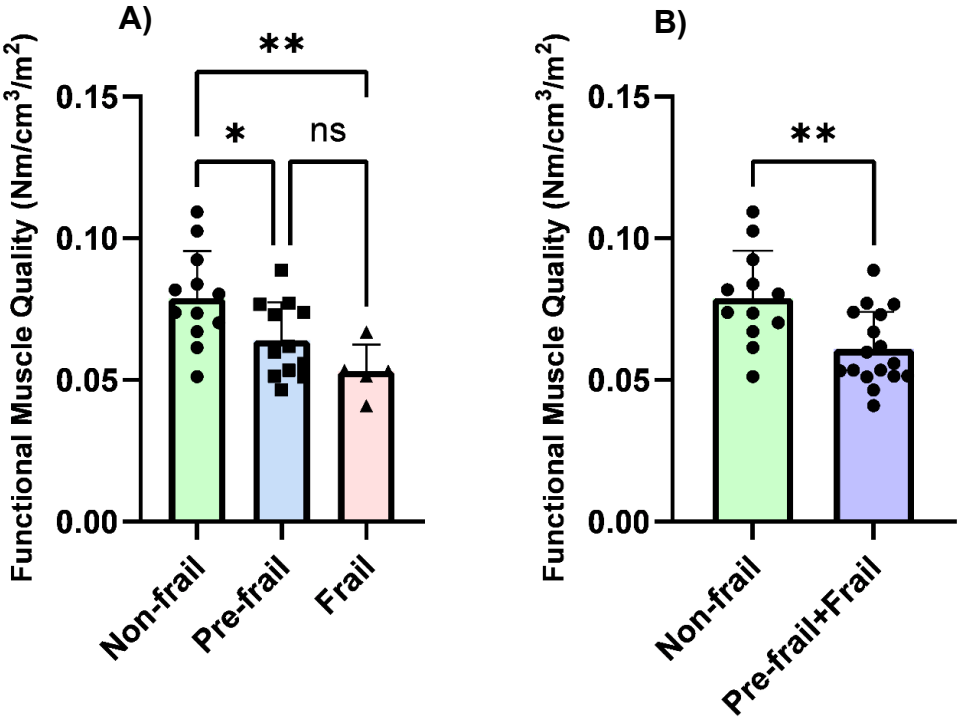

Figure 4.17: *Functional quality of the knee extensor muscles of the dominant leg in non-frail, pre-frail and frail females (**A**). Knee extensor functional quality in non-frail versus the co*llapsed *group of pre-frail and frail females (**B**). Computed by dividing knee extensor isometric strength (measured in Newton metres (Nm)) by BSA corrected thigh muscle volume (in cm^3/m^2). Values are mean ± standard deviation and individual values. * = P < 0.05; ** = P < 0.01.*

4.3.1.11 Force steadiness of the knee extensors in non-frail, pre-frail and frail females

During sustained contractions at 10% MVC, pre-frail (9.2 ± 2.9 %) and frail (10.1 ± 4.3 %) females displayed poorer force steadiness (presented as CV (%)) compared to non-frail females (non-frail vs pre-frail: *P* = 0.004; non-frail vs frail: *P* = 0.008; **Figure 4.18 A**). Although, pre-frail and frail females exhibited no differences in force steadiness at 10% MVC (**Figure 4.18 A**).

At 25% MVC, pre-frail (4.7 ± 1.4 %) females displayed worse force steadiness versus non-frail (2.5 ± 0.8 %) volunteers ($P < 0.001$; **Figure 4.18 B**). However, no differences in force steadiness at 25% MVC were evident when comparing non-frail or pre-frail to frail females (**Figure 4.18 B**).

Force steadiness during contractions at 40% MVC was also significantly worse in the pre-frail (3.9 ± 1.2 %) group compared to non-frail (1.8 ± 0.8 %) counterparts ($P < 0.001$; **Figure 4.18 C**). However, force steadiness at 40% MVC was not different when comparing non-frail or pre-frail to frail females (**Figure 4.18 C**).

4.3.1.12 Force steadiness of the knee extensors in non-frail versus the collapsed group of pre-frail and frail females

The collapsed group of pre-frail and frail females displayed poorer force steadiness during sustained contractions at 10% MVC compared to non-frail (5.2 ± 1.6 %) females ($P < 0.001$; **Figure 4.19 A**). At 25% MVC, pre-frail and frail volunteers also exhibited worse force steadiness in comparison to non-frail (2.5 ± 0.8 %) females ($P < 0.001$; **Figure 4.19 B**). Similarly, in comparison to non-frail (1.8 ± 0.8 %) females, pre-frail and frail females showed poorer force steadiness during contractions at 40% MVC ($P < 0.001$; **Figure 4.19 C**).

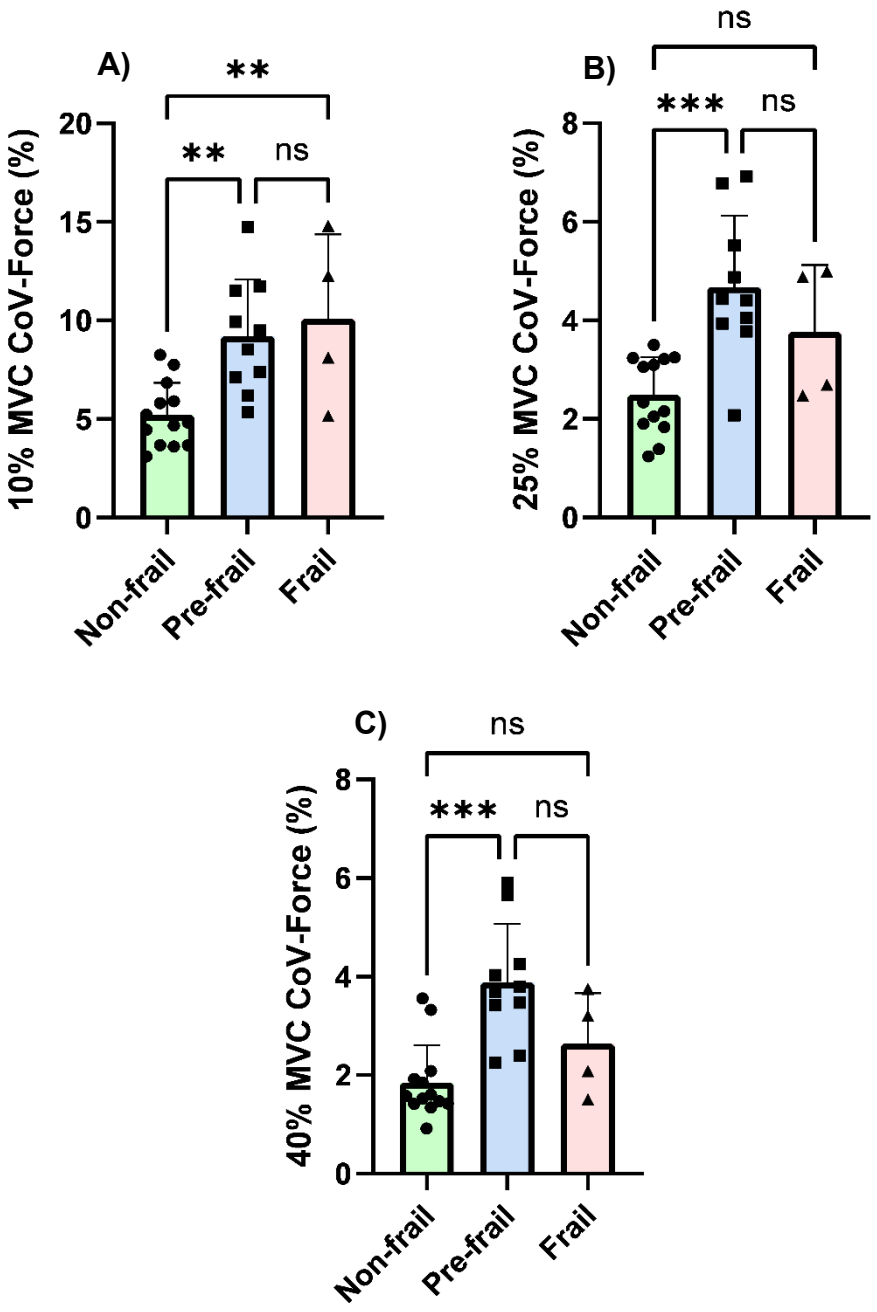

Figure 4.18: *Force steadiness of the knee extensors in non-frail, pre-frail and frail females. Force steadiness defined as the coefficient of variation (CoV) of applied force when performing a sustained contraction at 10% (**A**), 25% (**B**) and 40% (**C**) of maximum voluntary contraction (MVC). Values are mean ± standard deviation and individual values. ** = P < 0.01; *** = P < 0.001.*

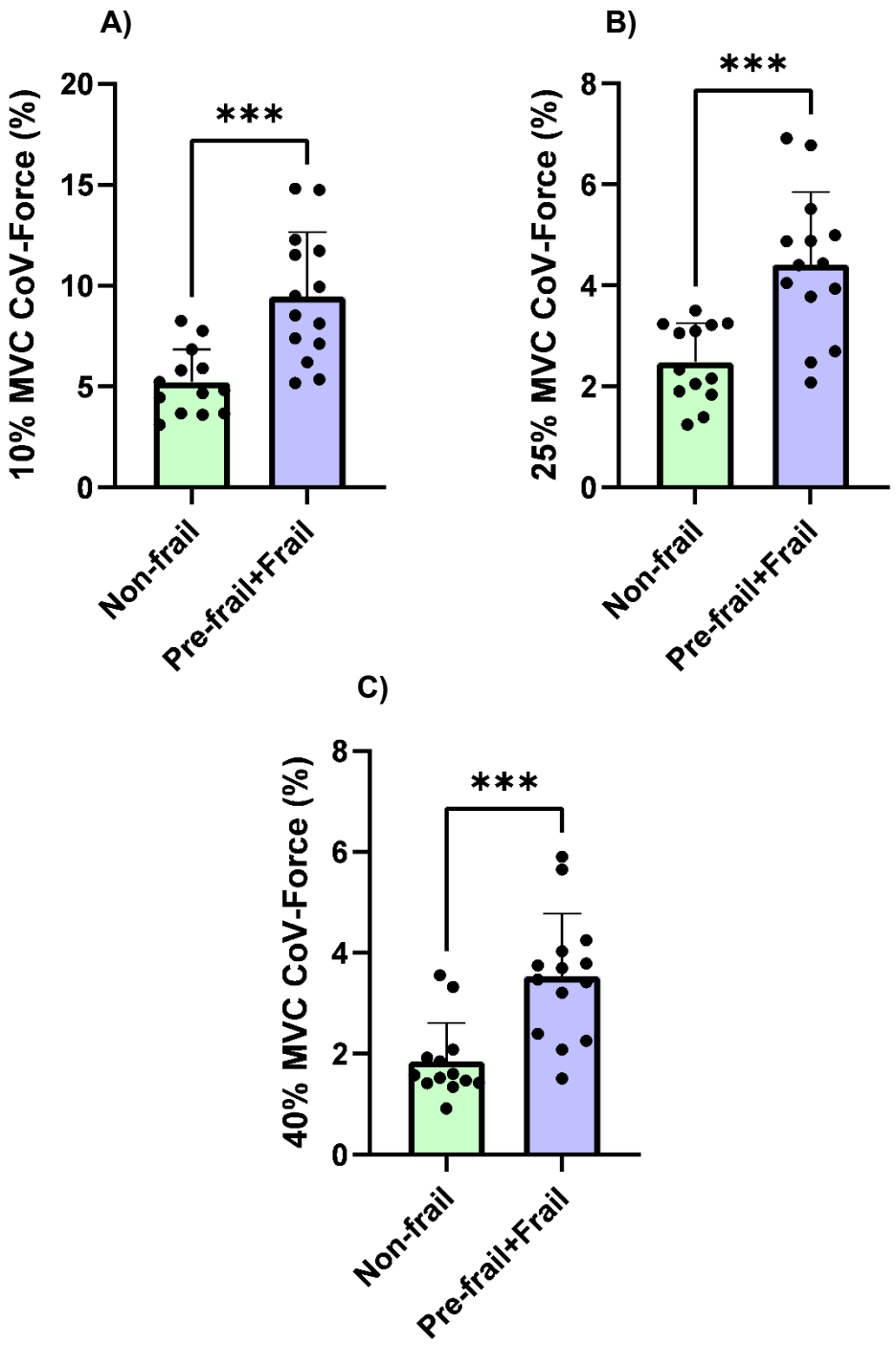

Figure 4.19: *Force steadiness of the knee extensors in non-frail versus the collapsed group of pre-frail and frail females. Force steadiness defined as the coefficient of variation (CoV) of applied force when performing a sustained contraction at 10% (**A**), 25% (**B**) and 40% (**C**) of maximum voluntary contraction (MVC). Values are mean ± standard deviation and individual values. *** = P < 0.001.*

4.3.1.13 Handgrip strength in non-frail, pre-frail and frail females

Handgrip strength was significantly lower in the pre-frail (15.1 ± 4.1 kg) and frail (11.9 ± 4.2 kg) versus non-frail females (non-frail vs pre-frail: $P = 0.0003$; non-frail vs frail: $P < 0.0001$; **Figure 4.20 A**). However, no differences in handgrip strength were evident when comparing pre-frail and frail females (**Figure 4.20 A**).

4.3.1.14 Handgrip strength in non-frail versus the collapsed group of pre-frail and frail females

The collapsed group of pre-frail and frail females also exhibited significantly lower handgrip strength compared to the non-frail (21.2 ± 3.0 kg) group ($P < 0.001$; **Figure 4.20 B**).

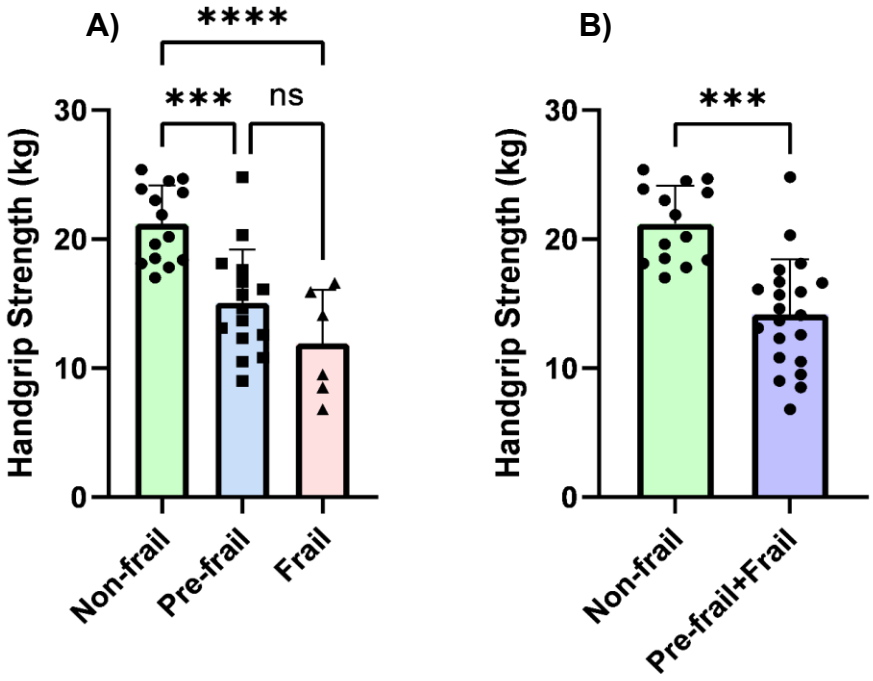

Figure 4.20: *Handgrip strength in non-frail, pre-frail and frail females (**A**) and in non-frail versus the collapsed group of pre-frail and frail females (**B**). kg = kilograms. Values are mean ± standard deviation and individual values. *** = P < 0.001; **** = P < 0.0001.*

4.3.1.15 Time taken to complete the walk test (gait speed) in non-frail, pre-frail and frail females

Frail females (7.3 ± 3.1 s) took significantly longer to complete the 4.57 metre walk test compared to pre-frail (4.8 ± 1.2 s) and non-frail counterparts (frail vs pre-frail: $P = 0.034$; frail vs non-frail: $P < 0.001$; **Figure 4.21 A**). Although, the time taken to complete the 4.57 metre walk was not different between non-frail and pre-frail groups (**Figure 4.21 A**).

4.3.1.16 Time taken to complete the walk test (gait speed) in non-frail versus the collapsed group of pre-frail and frail females

The collapsed group of pre-frail and frail females took significantly longer to complete the 4.57 metre walk compared to non-frail (3.7 ± 0.5 s) females ($P < 0.001$; **Figure 4.21 B**).

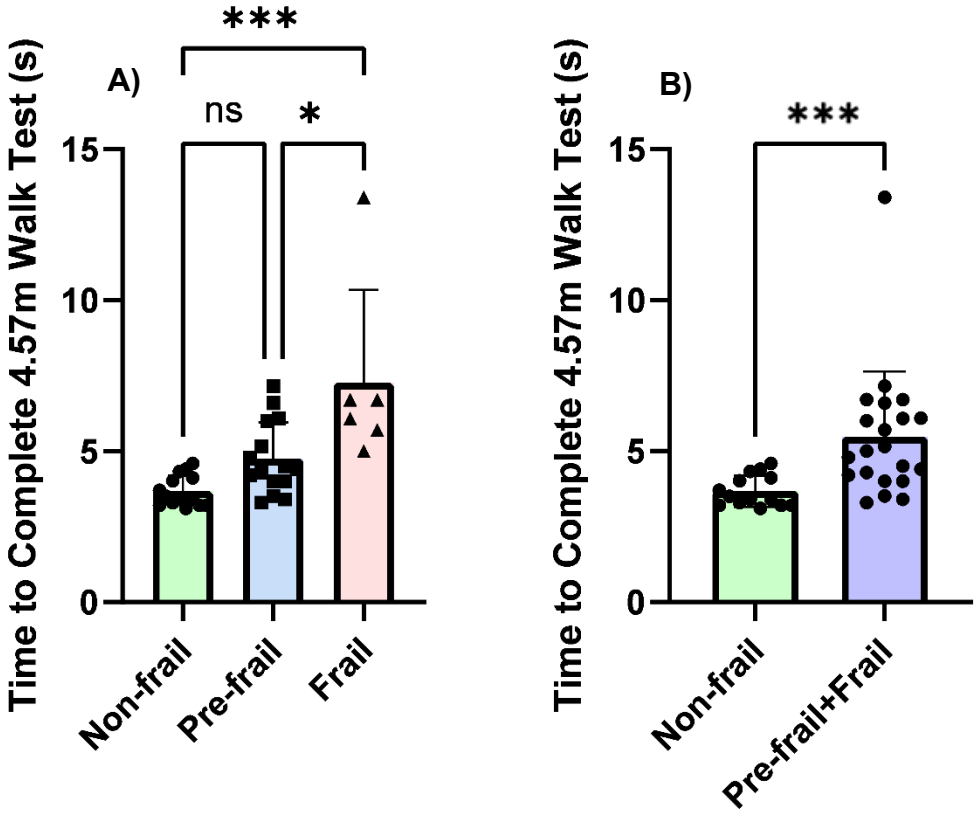

Figure 4.21: *Time taken to complete the 4.57 metre (m) walk test in non-frail, pre-frail and frail females (**A**) and in non-frail versus the collapsed group of pre-frail and frail females (**B**). s = seconds. Values are mean ± standard deviation and individual values. * = P < 0.05; *** = P < 0.001.*

4.3.1.17 Independence in activities of daily living questionnaire in non-frail, pre-frail and frail females

Self-reported independence in ADLs was significantly lower in frail (15.5 ± 3.2 score) versus pre-frail (21.3 ± 1.0 score) and non-frail females (frail vs pre-frail: P = 0.003; frail vs non-frail: P < 0.001; **Figure 4.22 A**). However, no differences in self-reported independence in ADLs were apparent between non-frail and pre-frail groups (**Figure 4.22 A**).

4.3.1.18 Independence in activities of daily living questionnaire in non-frail versus the collapsed group of pre-frail and frail females

Self-reported independence in ADLs was also significantly lower in the collapsed group of pre-frail and frail females in comparison to the non-frail (21.8 ± 0.6 score) group (*P* = 0.004; **Figure 4.22 B**).

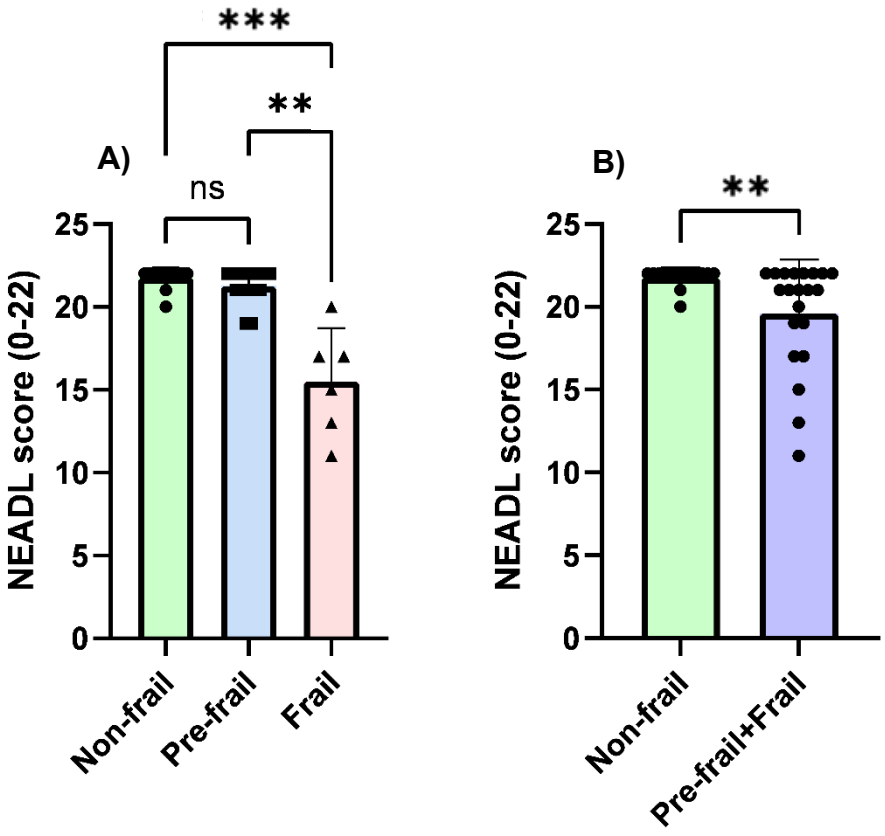

Figure 4.22: *Self-reported independence in activities of daily living assessed by the Nottingham Extended Activities of Daily Living (NEADL) questionnaire in non-frail, pre-frail and frail females (**A**) and in non-frail versus the collapsed group of pre-frail and frail females (**B**). Higher scores reflect greater independence. Values are mean ± standard deviation and individual values. ** = P < 0.01; *** = P < 0.001.*

4.3.2 Neuromuscular measures

Difficulties in the acquisition of iEMG data, mainly due to low signal production during muscle contractions of volunteers, entailed data analysis was only available and

performed on *n* = 10 non-frail, *n* = 4 pre-frail and *n* = 4 frail. An inadequate amount of data was also collected at 40% MVC. Therefore, to increase statistical power, pre-frail and frail female's data were combined for iEMG data analysis at 10% and 25% MVC. Therefore, analysis was performed on *n* = 10 non-frail versus *n* = 8 pre-frail and frail.

For MRI data analysis, one non-frail participant's data was excluded from muscle volume and fat fraction analyses due to inadequate image acquisition. Therefore, muscle volume and fat fraction analyses were performed on *n* = 13 non-frail, *n* = 15 pre-frail and *n* = 6 frail participants.

4.3.2.1 Motor unit potential size, firing rate and firing rate variability in non-frail versus the collapsed group of pre-frail and frail females

At 10% MVC, MUP size in the non-frail females was 772 ± 317 $\mu V.ms^{-1}$, which was no different to the collapsed group of pre-frail and frail females (**Figure 4.23 A**). Similarly, no differences were observed in motor unit firing rate between non-frail (8.3 ± 1.5 Hz) and the collapsed pre-frail and frail group (**Figure 4.23 B**). Firing rate variability was also not different between groups (non-frail = 0.09 ± 0.01 %, combined pre-frail and frail = 0.09 ± 0.02 %; **Figure 4.23 C**) at 10% MVC.

At 25% MVC, no significant differences were evident between non-frail females and the collapsed group of pre-frail and frail females in MUP size (non-frail = 919 ± 341 μV .ms, combined pre-frail and frail = 876 ± 420 $\mu V.ms^{-1}$; **Figure 4.23 A**). Likewise, motor unit firing rate in the non-frail was 8.2 ± 1.0 Hz, which was no different to the collapsed pre-frail and frail group (**Figure 4.23 B**). Firing rate variability was also no different in the non-frail (0.09 ± 0.02 %) versus the collapsed group of pre-frail and frail females (**Figure 4.23 C**) at 25% MVC.

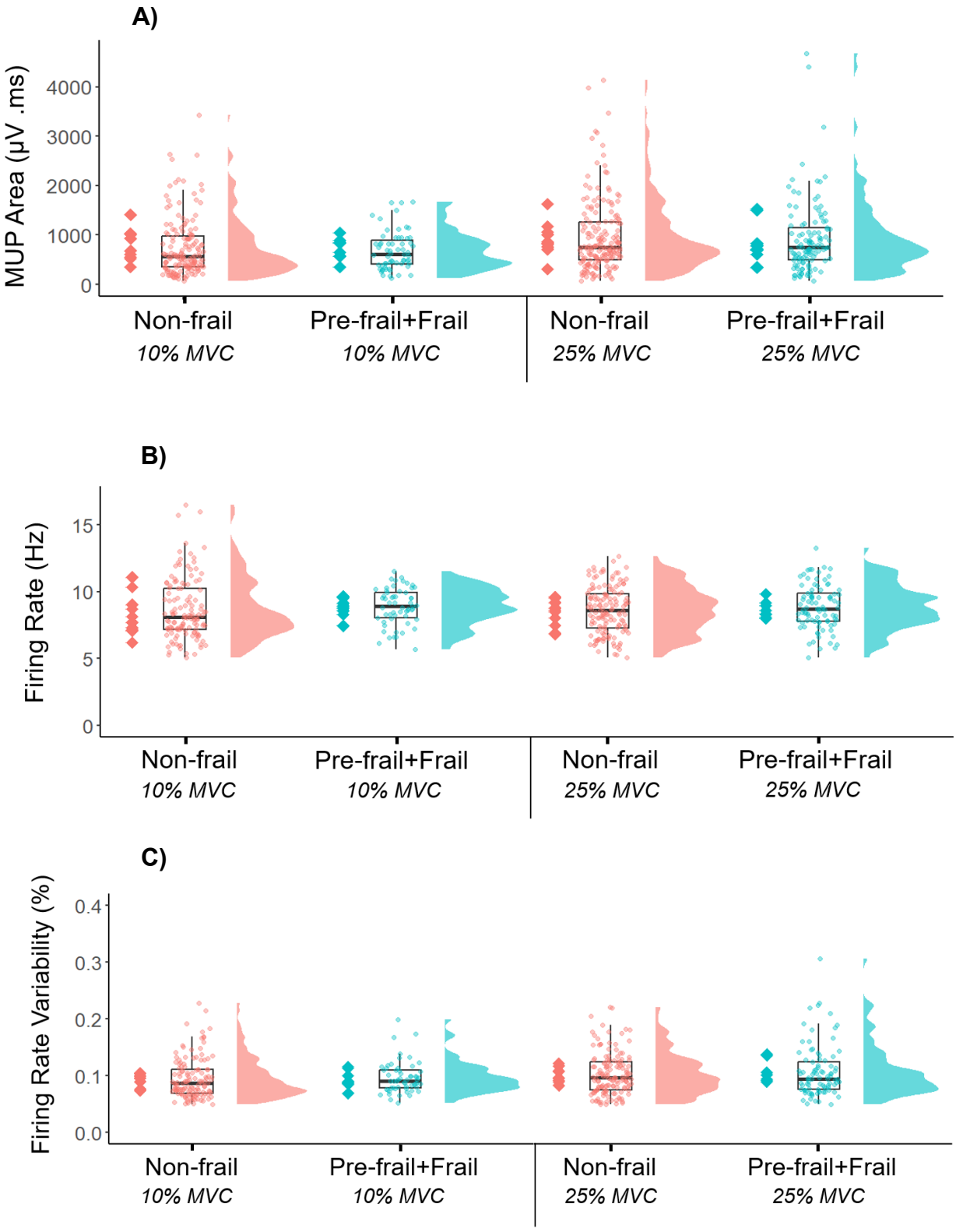

Figure 4.23: Motor unit potential size (MUP area; (**A**)), firing rate (**B**) and firing rate variability (**C**) in the non-frail versus the collapsed group of pre-frail and frail females at 10% and 25% of maximum voluntary contraction (MVC). For each group and contraction level, individual means (red and green diamonds), violin plots and box plots with overlayed individual recordings and standard deviation are presented. MUP area (i.e., MU size) was taken as the total area under the curve within the MUP

duration. MU FR was assessed as the rate of MUP occurrences within a MUP template, expressed as the number of occurrences per second (measured in Hertz). MU FR variability was reported as the CV for the interspike interval (the time between subsequent action potentials) displayed as a percentage.

4.3.3 Body composition

4.3.3.1 Calf and whole leg skeletal muscle volume in non-frail, pre-frail and frail females

BSA corrected muscle volume of the dominant calf was significantly lower in the pre-frail (736 ± 105 cm^3/m^2) and frail (667 ± 86 cm^3/m^2) groups compared to the non-frail group (non-frail vs pre-frail: P = 0.036; non-frail vs frail: P = 0.006; **Figure 4.24 A**). However, no differences were evident in BSA corrected dominant calf muscle volume between the pre-frail and frail groups (**Figure 4.24 A**).

The pre-frail (1979 ± 177 cm^3/m^2) and frail (1893 ± 169 cm^3/m^2) females also exhibited significantly less BSA corrected muscle volume of the dominant leg compared to the non-frail females (non-frail vs pre-frail: P = 0.026; non-frail vs frail: P = 0.011; **Figure 4.24 B**). Although, BSA corrected muscle volume of the dominant leg was not different between the pre-frail and frail groups (**Figure 4.24 B**).

4.3.3.2 Calf and whole leg skeletal muscle volume in non-frail versus the collapsed group of pre-frail and frail females

BSA corrected muscle volume of the dominant calf was significantly lower in the collapsed group of pre-frail and frail females compared to the non-frail (840 ± 112 cm^3/m^2) group (P = 0.002; **Figure 4.24 C**).

The collapsed group of pre-frail and frail females also exhibited significantly lower BSA corrected muscle volume of the dominant leg versus the non-frail (2162 ± 175 cm^3/m^2) group (P = 0.002; **Figure 4.24 D**).

For reference, absolute muscle volume data are presented in **Appendix 4.3**.

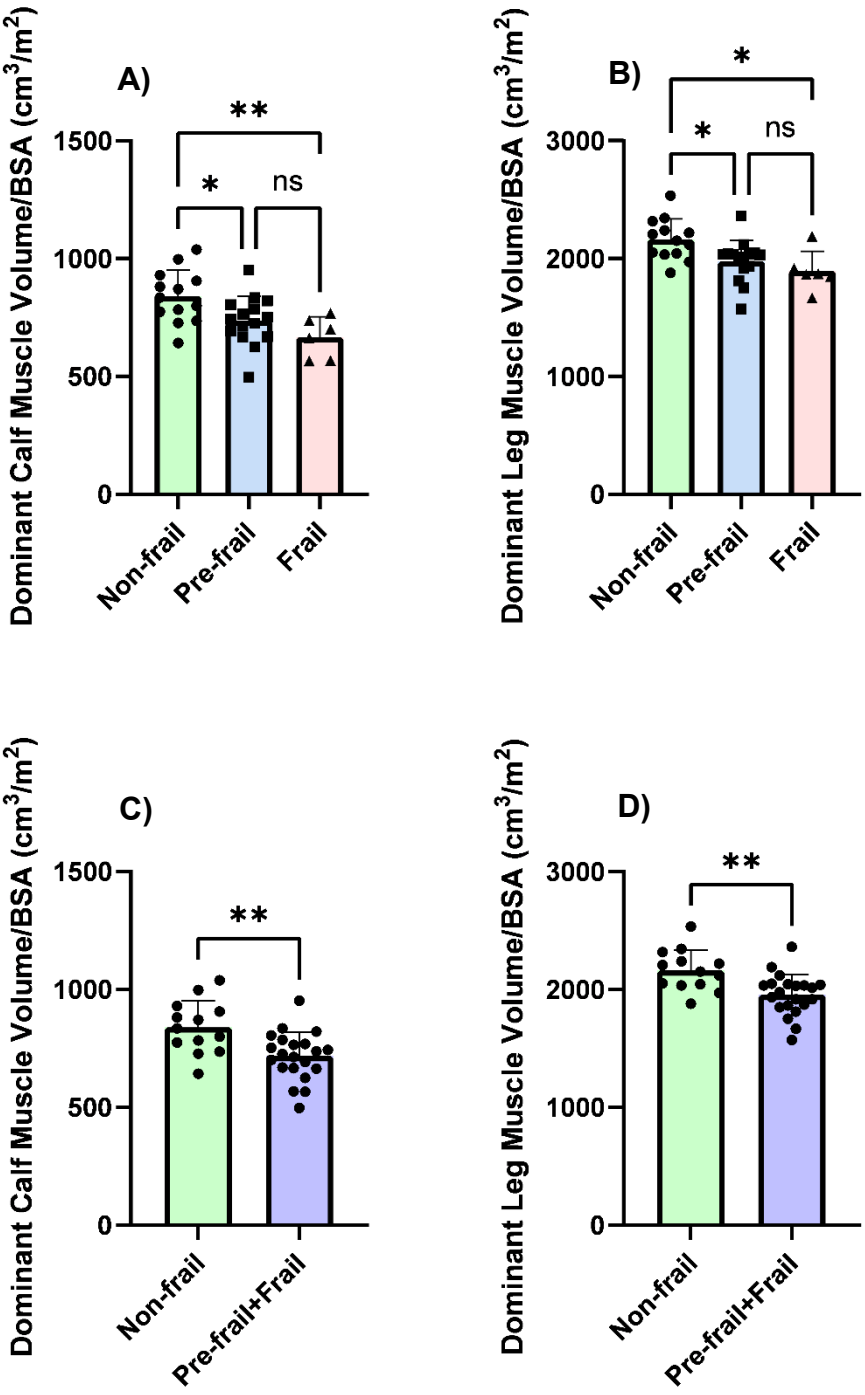

Figure 4.24: *Body surface area (BSA) corrected muscle volume of dominant calf (**A**), and leg (**B**) muscles in non-frail, pre-frail and frail females. Dominant calf (**C**) and leg (**D**) BSA corrected muscle volume in non-frail versus the collapsed group of pre-frail and frail females. Values are mean ± standard deviation and individual values. * = P < 0.05; ** = P < 0.01.*

4.3.3.3 Intra- and inter-muscular fat fraction of the dominant calf and leg muscles in non-frail, pre-frail and frail females

Dominant calf fat fraction in the non-frail group was 5.2 ± 2.2 %, which was no different to the pre-frail and frail females (**Figure 4.25 A**). There were also no significant differences in dominant leg fat fraction between non-frail, pre-frail (6.4 ± 2.4 %) and frail (7.8 ± 4.7 %) females (**Figure 4.25 B**).

4.3.3.4 Intra- and inter-muscular fat fraction of the dominant calf and leg muscles in non-frail versus the collapsed group of pre-frail and frail females

There were no significant differences in dominant calf fat fraction between non-frail (5.2 ± 2.2 %) females and the collapsed group of pre-frail and frail females (**Figure 4.25 C**). Similarly, dominant leg fat fraction was not different between non-frail females and the combined group of pre-frail and frail (7.8 ± 4.7 %) females (**Figure 4.25 D**).

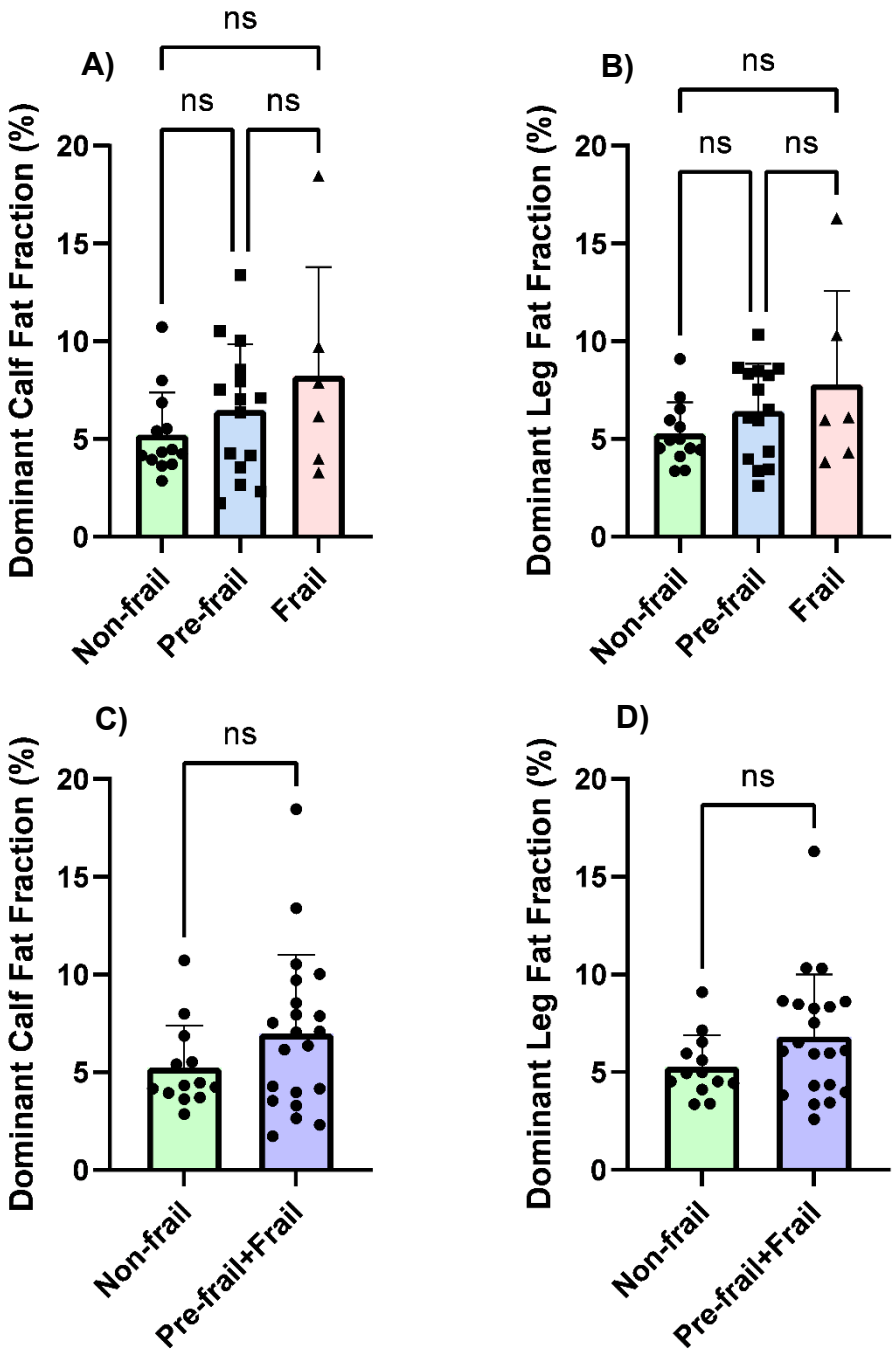

Figure 4.25: *Fat fraction (expressed as a percentage of muscle volume) in the dominant calf (**A**) and leg (**B**) muscles in non-frail, pre-frail and frail females. Fat fraction in the dominant calf (**C**) and leg (**D**) of non-frail versus the collapsed group of pre-frail and frail females. Values are mean ± standard deviation and individual values.*

4.3.3.5 Visceral adipose tissue volume in non-frail, pre-frail and frail females

BSA corrected visceral adipose tissue volume of the abdomen was 547 ± 359 cm^3/m^2 in the non-frail group, which was no different to the pre-frail and frail groups (**Figure 4.26 A**). There were also no differences between the pre-frail and frail groups (**Figure 4.26 A**).

4.3.3.6 Visceral adipose tissue volume in non-frail versus the collapsed group of pre-frail and frail females

Similarly, when data from the pre-frail and frail groups were collapsed, BSA corrected visceral adipose volume was no different between the collapsed pre-frail and frail (628 ± 407 cm^3/m^2) and non-frail groups (**Figure 4.26 B**).

For reference, absolute visceral adipose tissue volume data are presented in **Appendix 4.4**.

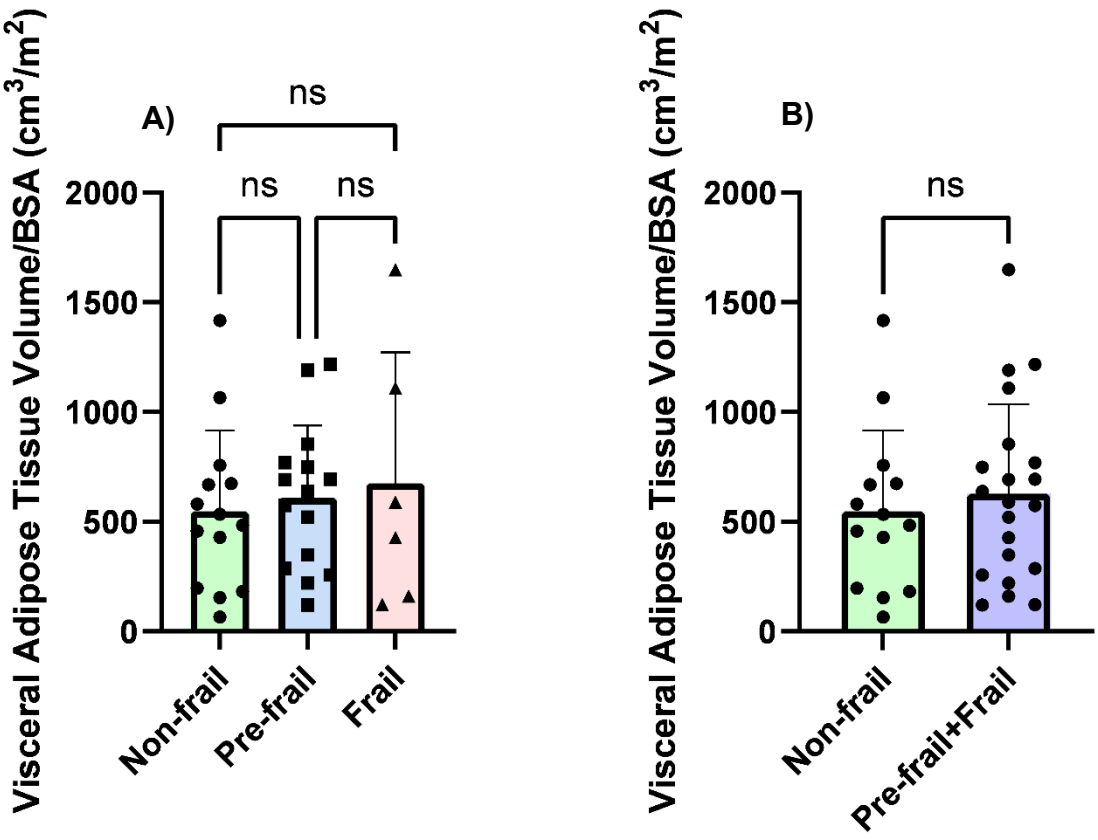

Figure 4.26: *Body surface area (BSA) corrected visceral adipose tissue volume of the abdomen in (**A**) non-frail, pre-frail and frail females, and (**B**) non-frail versus the collapsed group of pre-frail and frail females. Values are mean ± standard deviation and individual values.*

4.4. Discussion

The main findings of this Chapter were that pre-frail and frail females exhibited lower calf and leg skeletal muscle volume, in addition to lower isometric strength, power output functional quality and work output capacity of the knee extensor muscles, compared to non-frail counterparts. As such, muscle atrophy may underpin the impairments in isometric strength during frailty shown in this study, and previous work [54], whilst the findings of lower work output and functional muscle quality are indicative of impairments in metabolic quality in pre-frail and frail versus non-frail

females. Interestingly though, this study found that this evidence of lower muscle metabolic capacity was not underpinned by a greater lipid infiltration of the muscle, with no differences in fat fraction of the calf and leg muscles observed between healthy and frail states. Furthermore, visceral adiposity, another powerful indicator of metabolic health, was no different between groups, reinforcing that greater adipose tissue stores may not contribute to impaired metabolic capacity during frailty. This study is the first assessment of muscle volume and fat fraction of the calf and thigh muscles, and also the first measurement of visceral adiposity, by MRI when comparing non-frail, pre-frail and frail individuals, providing the greater insight into body composition metrics during pre-frailty and frailty. Moreover, by combining these highly accurate body composition measurements with multiple functional assessments indicative of strength, power output, neuromuscular control and metabolic quality of the muscle, this study provides much needed insight into the physiological underpinnings of diminished functional capacity during frailty.

Several previous studies have quantified whole body lean mass [43, 44] and skeletal muscle CSA [49, 52] in frail versus non-frail individuals, providing evidence of lower muscle mass during frailty, which is in agreement with the lower muscle volume of the dominant calf and leg observed in frail versus non-frail volunteers in the current study (**Figure 4.24**). However, numerous improvements in study design in the present work improve the extrapolation of these findings. For example, prior studies have mainly adopted mixed sex participant samples [43, 44, 49, 52], which likely imparted variance into the data due to sex-related differences in muscle mass [28], whereas the present study studied an all-female sample. Furthermore, one report utilised the modified physical performance battery to determine frailty status [49], whereas the Physical Frailty Phenotype method [17] was adopted herein, which is the current recommended

standard [10]. Perhaps the most valid improvement, though, concerns the measurement of whole leg muscle volume with MRI in the present study versus previous measurements of lean mass and muscle CSA [44, 49]. Lean mass estimations are not direct measurements of muscle mass and CSA assessments rely on extrapolation of whole muscle area from a partial two-dimensional cross section of the muscle of interest. The present study performed direct muscle volume measurements of the whole calves and legs using MRI, which also showed low analytical variance in the analysis techniques (**Table 4.2**), thus providing robust and reliable evidence of lower skeletal muscle volume as a physiological feature of pre-frail and frail versus non-frail women. This finding was also reinforced by the lower calf and leg muscle volume observed when the pre-frail and frail groups were collapsed to increase statistical power (**Figure 4.24 C, D**).

Whilst the MRI-derived skeletal muscle volume measurements adopted herein may be considered the gold standard quantification of muscle quantity, muscle architecture characteristics (e.g., physiological CSA and pennation angle) were not assessed. Physiological CSA is defined as the CSA of a muscle when measured perpendicular to its fibres. Since the physiological CSA represents the maximal number of muscle fibres that can be recruited during contraction, the maximal force generating capacity of the muscle is proportional to its physiological CSA. The pennation angle (the angle between the deep aponeurosis and the muscle fascicles) also influences the physiological CSA, as a greater pennation angle allows more fibres to be arranged in parallel, thus increasing physiological CSA and force generation capacity of the muscle [336]. As such, pennation angle of the vastus lateralis has been positively correlated with knee extensor isometric strength in older adults (r = 0.36; $P < 0.05$) [337], and a smaller pennation angle has been observed in frail versus non-frail adults,

although the relationship between pennation angle and functional capacity in frail individuals was not measured [338]. Given physiological CSA and pennation angle are major determinants of force production within skeletal muscle, further investigations of associations between muscle architecture and physical function measurements in frail individuals may provide further insight into the underpinnings of the lower knee extensor isometric strength and power output observed in frail versus non-frail females in the current study.

In addition to lower muscle volume, markedly lower functional capacity was also evident in the pre-frail and frail females compared to non-frail counterparts in this study, such as lower handgrip strength (**Figure 4.20**), slower gait speed (**Figure 4.21**) and lower knee extensor isometric strength (**Figure 4.13**) and power output (**Figure 4.14**). This is in line with previous studies observing lower isometric strength [54] and peak torque [339] of the knee extensors, as well as lower handgrip strength and gait speed [9, 17] in frail versus non-frail individuals, thus further supporting the evidence of functional deterioration as a hallmark characteristic of frailty [9, 340]. The lower muscle volume of pre-fail and frail females showcased in this study may contribute to this lower functional capacity seen in pre-frail and frail individuals, given diminished knee extensor isometric strength and isokinetic peak torque has been correlated with the loss of muscle CSA during ageing [341, 342] and studies of frailty demonstrate positive correlations between lower limb muscle CSA, strength and power output [282]. This would also be consistent with the loss of muscle mass, strength and power output evident in sarcopenic individuals [342], due to mechanisms such as atrophy and loss of individual muscle fibres [288] leading to attenuated strength and force production of the muscle [343]. Furthermore, longitudinal studies have highlighted losses of both thigh muscle CSA and knee extension isokinetic strength during ageing

[342]. However, longitudinal data regarding the relationship between muscle atrophy and functional deterioration during frailty are lacking. Thus, it would be beneficial to determine if functional decline is concomitant with muscle atrophy during frailty progression in longitudinal studies to provide further insight into skeletal muscle atrophy as a potential physiological mechanism of functional deterioration during frailty.

It should be noted that joint angle affects torque production during voluntary contractions, with changes in joint angle influencing the moment arm of external force and thus torque production. Several studies have demonstrated lower torque at shorter and longer muscle lengths (i.e., when the joint angle is either small or large), compared to when torque output is measured in the middle of the muscle length [344, 345]. Therefore, the smaller joint angles at peak torque in the pre-frail and frail groups versus the non-frail group in the present study may have contributed to the lower isokinetic peak torque values seen in the pre-frail and frail groups (**Figure 4.15**). To remove the influence of joint angle on peak torque during isokinetic contractions, angle specific peak torque could have been quantified by identifying the peak torque at a given knee angle (e.g., 60°) across groups. Nonetheless, the pattern of the differences between groups for knee angle at peak torque data was observed to be similar to the majority of other knee extension data. For example, knee angle at peak torque was lower in the pre-frail and frail groups versus non-frail group, but no differences were observed between pre-frail and frail groups (**Figure 4.15**), which is a similar pattern observed for the group differences in knee extensor isometric strength (**Figure 4.13**) and peak torque (**Figure 4.14**). Therefore, differences in knee angle at peak torque between non-frail and frail states may not have heavily influenced torque production.

In the present study, the volume of whole muscles was quantified alongside the isometric strength and power output of the knee extensors. A valuable adjunctive perspective could have been to determine if force production at the single fibre level was also influenced by frailty status. Mechanical properties of individuals muscle fibres, such as force production and power output, can be quantified from the permeabilised single muscle fibre preparation technique (derived from biopsies), which involves inducing contractions in the fibre using a calcium solution. The rationale for performing single fibre assessments is to overcome factors that may influence force production during measurements performed in vivo, such as differences in intramuscular fibre orientation or pennation, potential coactivation of antagonist muscles during strength testing, and variations in participant motivation; factors that may have influenced force production by participants in the present study. Lower force production per unit CSA of single VL muscle fibres has been reported in older versus young individuals [346], alongside lower power output of type I fibres in mobility-limited older adults compared to middle aged counterparts [347]. Following a 10-week resistance training intervention, frail individuals exhibited no changes in force per CSA of individual VL muscle fibres despite 17% and 7% increases in knee extension one repetition maximum and MVC, respectively [348], which may suggest single fibre mechanical characteristics do not influence functional capacity during frailty. However, comparisons of single fibre characteristics between frail and non-frail individuals were not performed in this previous study and have not been undertaken by others. Comparisons of the mechanical properties of individual fibres between non-frail and frail individuals would ascertain whether the lower whole muscle force and power generation capacity of frail individuals in the present study translates to the single fibre level.

The lower isometric strength and power output exhibited by the frail females in the present study may also contribute to the lower self-reported independence in ADLs in the frail group compared to the pre-frail and non-frail groups (**Figure 4.22**). This notion is supported by previous studies demonstrating skeletal muscle power and strength are important for the completion of ADLs (e.g. rising from a chair, climbing stairs) in older people [349, 350]. Similarly, in frail individuals, negative associations have been observed between knee extensor power output and gait speed, whilst positive associations have been shown between muscle power and ability to rise from a chair [282]. Of course, with the exception of gait speed, ADLs were assessed subjectively with a questionnaire in the present study, compared to more robust quantitative measurements performed previously [349], which prevents direct comparisons. Interestingly, this subjective measure of functional capacity in the present study (the NEADL questionnaire) differentiated the groups differently from the majority of other measures of physical function, with no differences evident between the non-frail and pre-frail groups, and lower independence in the frail versus pre-frail group. This suggests that whilst frail individuals perceive their functional capacity to be impaired, which is in parallel with their quantitative performance (e.g., isometric strength), pre-frail individuals perceive their functional performance to be similar to non-frail counterparts, but their quantitative performance is not in line with this. This indicates that the perception of a loss in functional capacity occurs later in the trajectory of frailty.

Considering diminished functional capacity during ageing cannot be fully explained by a loss of muscle mass [208], this study also assessed the functional quality (i.e., the force producing capacity of the knee extensors per unit of muscle volume) and work output capacity of the knee extensor muscles to investigate muscle metabolic quality during frailty. Lower functional quality and work output of the knee extensors was

observed in the pre-frail and frail compared to non-frail females (**Figure 4.17**), which is in agreement with previous work in frail versus non-frail individuals [59]. This earlier study adopted DEXA-derived estimates of lean mass, therefore the current work consolidates these previous findings with a more robust characterisation of muscle functional quality through the assessment of MRI-derived whole muscle volume. By highlighting a lower ability to undertake repeated contractions (i.e., lower work output) and attenuated force production of the muscle per unit volume, these findings point to lower metabolic quality of the skeletal muscle in pre-frail and frail females. Physiological underpinnings of this lower metabolic quality may include a loss of mitochondrial mass, lower capillary to fibre ratio and great lipid infiltration of the muscle [35, 351]. Accordingly, this study quantified a composite measure of intra- and inter-muscular fat fraction within the thigh and calf muscles. However, no differences in muscle fat fraction were noted between non-frail, pre-frail and frail states (**Figure 4.25**), suggesting lower muscle metabolic quality during frailty is not underpinned by a greater lipid infiltration of the skeletal muscle. This lack of differences in muscle fat fraction also contradicts previous studies highlighting greater IMAT content of the thigh muscles [49, 57] and fat fraction of the calves [53] in frail versus non-frail individuals. Whilst the mixed sex samples adopted in these previous studies may have affected the data due to sex-related differences in IMAT in older individuals [58], the main difference explaining this disparity possibly relates to the fat fraction assessment method used in the present work versus prior studies. The current study quantified the fat content of each image voxel within the whole muscle mask (e.g., every voxel of the calf muscle mask). Previous studies also utilising MRI methods quantified IMAT from a partial cross section of the calves or thighs [49, 53], whereas another study using an MRS technique focussed on a 2 cm^3 ROI in the mid portion of each quadriceps muscle

[57]. It may be deemed therefore that the method of fat fraction quantification used herein is a more comprehensive and valid measurement of IMAT than previous methods, given its assessment of whole muscles and muscle groups. Further, the low analytical variation demonstrated for fat fraction measurements (**Table 4.2**) reinforces the reliability of the analysis technique. However, as noted above, this technique encapsulated a composite of both intermuscular as well as intramuscular fat of the whole muscle groups, which reinforces the need for further studies with standardised measures of IMAT to clarify these findings.

It is interesting to note that the lack of differences in skeletal muscle fat fraction between groups suggests that IMAT is not a physiological driver of the loss of metabolic muscle quality during frailty. This may be deemed inconsistent with previous studies using CT scanning whereby lower IMAT has been associated with better gait kinematics and greater muscle power output in frail individuals [322, 323]. However, IMAT was assessed indirectly with CT attenuation measures in these studies, rather than the direct assessments of fat fraction volume in the current study. Regarding alternative mechanisms that may underpin the loss of muscle metabolic quality in pre-frail and frail females, previous studies have investigated the role of mitochondrial content and respiration (i.e., deconditioning) during ageing and frailty. In older women, an index of muscle energetics, derived from a combination of ^{31}P MRS measures of the quadriceps muscles and respirometry analysis of VL biopsies, has shown that up 75% of variation in short physical performance battery scores was explained by lower muscle energetics [352], suggesting deconditioning is strongly associated with lower functional capacity in older women. In the context of pre-frailty, analysis of VL biopsies revealed that mitochondrial content, but not lipid content, was positively correlated with functional capacity (i.e., walking speed and timed up and go test performance) in pre-

frail individuals [265], suggesting mitochondrial content/respiration may be a more potent driver of muscle deconditioning, compared to lipid infiltration, during pre-frailty. Unfortunately, this study did not include frail participants in analyses, restricting insight into frailty. Despite these shortcomings in study design, other studies have evidenced impairments in mitochondrial characteristics during frailty, such as lower abundance and maximal activity of mitochondrial respiratory complexes [262, 269] and inverse associations between mtDNA copy number and polymorphisms in mtDNA [267, 268], which reinforces a need for further investigations into alterations in mitochondrial characteristics as underpinnings of diminished functional capacity during pre-frailty and frailty. In turn, impairments in mitochondrial content/respiration may contribute to the findings of greater rates of PCr hydrolysis during exercise [53], and slower rates of PCr resynthesis following exercise [262], in frail versus non-frail individuals when measured with ^{31}P MRS techniques. Interestingly, Lewsey et al., [53] reported greater calf fat fraction in frail versus non-frail participants and positive associations between fat fraction and PCr hydrolysis rates, which, conversely to the present study, suggests greater IMAT may contribute to impaired metabolic muscle quality during frailty. However, with CSA measurements of fat fraction adopted in Lewsey et al., [53] further research would benefit from measurements of whole muscle IMAT volume, similar to the current study. Together these findings stress the need for combined assessments of IMAT, mitochondrial content and PCr hydrolysis in conjunction with measures of functional capacity to clarify the physiological drivers of impaired muscle metabolic quality in pre-frail and frail individuals.

Knee extensor peak torque at 180°/s was also lower in pre-frail and frail groups versus the non-frail group in this study (**Figure 4.14**). Considering contractions performed at this velocity entails a preferential recruitment of fast twitch muscle fibres, this finding

demonstrates a loss of force production, perhaps via atrophy, of fast twitch muscle fibres during pre-frailty and frailty. This would be in line with the selective atrophy of fast twitch muscle fibre types with age [287]. Muscle fibre type analysis was not performed herein, although prior work has demonstrated a lower CSA of type IIa and type IIx muscle fibres of the VL in pre-frail older adults versus young active adults [265]. Although, no differences were observed between the pre-frail group and a group of non-frail older adults when assessing fibre type composition and CSA [265], suggesting atrophy of fast twitch fibres, or a shift from fast twitch to slow twitch, is not evident during pre-frailty compared to normal ageing. Given the absence of a frail participant group in St-Jean-Pelletier et al., [265], and the lack of other studies assessing fibre type specific characteristics of the skeletal muscle during frailty, further study in this area is needed to investigate the drivers of lower peak torque at fast contraction speeds shown within pre-frail and frail females in the current study.

The present study also provided evidence of poorer knee extensor force steadiness (i.e., an impaired ability to maintain a constant force with the knee extensors) in the collapsed group of pre-frail and frail females compared to non-frail counterparts (**Figure 4.19**). This represents the first report of lower neuromuscular control of the knee extensors in frail versus healthy states and further reinforces a deterioration in muscle function during frailty. As such, this diminished neuromuscular control may contribute to other aspects of lower functional capacity in frail individuals, with poorer force steadiness of the quadriceps and calf muscles associated with traits of frailty, including poorer walking performance [286] and greater risk of falls [353] in older adults. This suggests the ability to exert control over the skeletal muscle may contribute to frailty and negative outcomes associated with the syndrome. However, based on the iEMG data gathered in this study, poorer force control during pre-frailty

and frailty does not seem to be explained by smaller motor unit size, FR or FR variability, given no differences were observed between the groups for these neuromuscular measures. Considering force steadiness has been reported to be mediated by motor unit FR and FR variability [354-356], the physiological underpinnings of poorer force steadiness in the current sample of frail females are unclear. The most likely explanation for the lack of differences in motor unit characteristics, however, relates to the low sample size of pre-frail (n = 4) and frail (n = 4) females available for iEMG data analysis. Regarding MU size, this study contradicts one other previous report demonstrating smaller MU size in frail versus non-frail males [95]. However, this previous study [95] adopted an all-male sample which may contribute to discrepancies in findings derived from the all-female sample in the present work, as previous reports have demonstrated sex-related differences in MU characteristics [96]. Therefore, considering the limited evidence available, it is clear further research within larger samples of stratified males and females is needed to effectively characterise MU parameters during frailty.

The lack of differences in neuromuscular characteristics may be attributed to participants being unable to fully recruit all motoneurons during voluntary contractions. This notion is based on the findings from previous studies indicating that skeletal muscle torque produced during voluntary contractions is lower than that produced during contractions evoked during electrical stimulation of the muscle (i.e., involuntary contractions) [357, 358]. The interpolated twitch technique could have been employed in the present study to determine if voluntary skeletal muscle activation is affected by frailty status by determining if torque produced during the voluntary knee extensor MVCs was different to that produced when the muscles were electrically stimulated with surface electrodes. It appears that previous studies have not compared voluntary

muscle activation between non-frail and frail states with the interpolated twitch technique, which could be explored in future investigations. However, twitch interpolation has been applied in a study of frail individuals who underwent 10 weeks of resistance training, which reported no changes in voluntary muscle activation following the intervention [348]. These findings may point to neuromuscular dysfunction in frail individuals, particularly as resistance training has been shown to improve muscle activation measured by twitch interpolation in older adults [359].

This study also found no differences in visceral adipose tissue volume between non-frail, pre-frail and frail states (**Figure 4.26**). In contrast, a small number of prior studies have evidenced positive associations between frailty and greater visceral adipose tissue mass [325, 326] and CSA [327]. A prospective study adopting DEXA assessments has also demonstrated that individuals with greater baseline visceral adiposity had higher odds of frailty development (odds ratio: 2.47) at 8 year follow up [328]. Differential findings may be underpinned by the MRI methods adopted in the present study, which is the first assessment of visceral adipose volume and thus may be deemed the most direct measurement of visceral adiposity during frailty to date. Previous studies assessed visceral adiposity with BIA and DEXA methods, which may be deemed less valid measurement techniques. For example, despite these studies using DEXA to assess visceral adipose tissue mass in an ROI specific to the abdomen, the segmentation methods likely included subcutaneous adipose tissue in analyses [328]. Whilst the direct MRI-derived volume measurements in the present study may therefore point to a lack of differences in visceral adiposity between healthy and frail states, the large variation in values across groups (**Figure 4.26**) indicates a need for further MRI based investigations within larger sample sizes to effectively delineate associations between visceral adiposity and frailty. This characterisation is important

given greater visceral adiposity is a robust marker of poor metabolic health, associated with numerous diseases (e.g., type 2 diabetes [360], coronary heart disease [361]) and all-cause mortality [324]. As such, larger amounts of visceral adiposity may contribute to the multi-morbidity aspect of frailty [362]. For example, as discussed in Chapter One, Section 1.5.5.1, visceral adipose tissue may contribute to the proinflammatory environment observed within pre-frail and frail individuals [363], through the release of inflammatory cytokines [364, 365]. In turn, these inflammatory molecules may influence pathophysiological alterations in other organs and physiological systems, such as skeletal muscle atrophy [65] and greater LV mass (potentially through a TNF-α induced accumulation of ubiquitinated proteins in the left ventricle [199]). Of course, evidence of visceral adipose tissue promoting a heightened inflammatory environment is limited, and therefore further research is required to support this notion.

In conclusion, this study demonstrated that pre-frail and frail females exhibit lower skeletal muscle volume of the calf and whole leg compared to non-frail females, which may underpin the markedly lower performance on functional measures related to muscle volume (i.e., isometric strength and muscle power output). Functional muscle quality and work output was also lower in the pre-frail and frail groups versus the non-frail groups, indicating impaired muscle metabolic quality. However, this lower metabolic quality did not appear to be underpinned by greater lipid infiltration of the muscle or visceral adiposity, with no differences in skeletal muscle fat fraction or visceral adipose tissue volume evident between groups. These findings indicate deconditioning of the muscle as an alternative driver of impaired muscle quality during frailty and future work should further investigate the role of mitochondrial content and respiration in frail individuals. Given the marked improvements in measurement

techniques, such as the direct MRI-derived assessments of whole muscle volume and IMAT, versus earlier work, this study demonstrates powerful evidence of lower muscle quantity and quality in pre-frail and frail individuals, thus providing much needed insight into the physiological underpinnings of diminished functional capacity during frailty.

Chapter Four Appendices

Appendix 4.1

Table 4.4: Raw data used to generate coefficient of variation for repeated analysis of force steadiness data.

Force steadiness contraction level	Measurement #1	Measurement #2	Measurement #3
10% MVC (% CV)	5.81	5.77	5.55
25% MVC (% CV)	3.25	3.17	3.05
40% MVC (% CV)	1.92	1.94	2.04

Table 4.5: Raw data used to generate coefficient of variation for repeated analysis of skeletal muscle volume and fat fraction data form mDIXON images.

Parameter	Measurement #1	Measurement #2	Measurement #3
Left calf skeletal muscle volume (cm^3)	1165.0	1149.5	1169.0
Right calf skeletal muscle volume (cm^3)	1083.4	1114.5	1104.8
Left leg skeletal muscle volume (cm^3)	3119.6	3122.9	3055.5
Right leg skeletal muscle volume (cm^3)	2955.4	2990.6	2946.8
Left calf fat fraction (%)	3.96	3.99	3.97
Right calf fat fraction (%)	4.16	4.15	4.17
Left leg fat fraction (%)	4.21	4.26	4.24
Right leg fat fracion (%)	3.97	3.99	4.01

Table 4.6: Raw data used to generate coefficient of variation for repeated analysis of visceral adipose tissue volume from mDIXON images.

Parameter	Measurement #1	Measurement #2	Measurement #3
Visceral adipose tissue volume (cm^3)	712.7	716.4	734.3

Appendix 4.2

Absolute knee extensor functional muscle quality in non-frail, pre-frail and frail females

Pre-frail (0.040 ± 0.009 Nm/cm^3) and frail (0.033 ± 0.003 Nm/cm^3) females exhibited significantly lower absolute muscle functional quality compared to non-frail females (non-frail vs pre-frail: P = 0.028; non-frail vs frail: P = 0.002; **Figure 4.27 A**). However, functional muscle quality was not different between pre-frail and frail groups (**Figure 4.27 A**).

Absolute knee extensor functional quality in the collapsed group of pre-frail and frail females was also significantly lower versus the non-frail (0.049 ± 0.008 Nm/cm^3) females (P = 0.001; **Figure 4.27 B**).

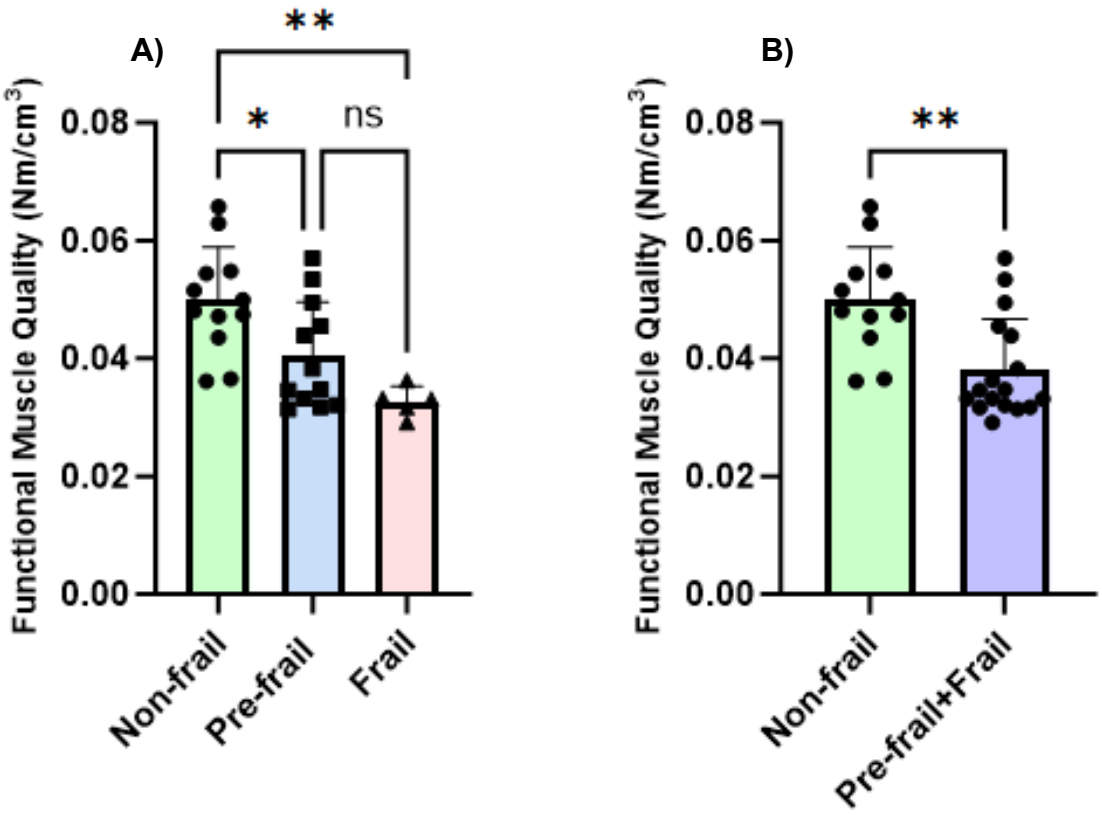

Figure 4.27: *Absolute functional quality of the knee extensor muscles of the dominant leg in non-frail, pre-frail and frail females (**A**). Knee extensor functional quality in non-frail versus the collapsed group of pre-frail and frail females (**B**). Computed by dividing knee extensor isometric strength (measured in Newton metres (Nm)) by thigh muscle volume (in cm^3). Values are mean ± standard deviation and individual values. * = P < 0.05; ** = P < 0.01.*

Appendix 4.3

Absolute calf and leg skeletal muscle volume in non-frail, pre-frail and frail females

Absolute muscle volume of the dominant calf was significantly lower in the frail (1066 ± 228 cm^3) compared to non-frail group (P = 0.017; **Figure 4.28 A**). There was also a trend (P = 0.092) for lower absolute dominant calf muscle volume in the pre-frail (1185 ± 165 cm^3) versus the non-frail. However, no differences were evident in left calf muscle volume between the pre-frail and frail groups (**Figure 4.28 A**).

There was a trend (P = 0.073) for smaller absolute muscle volume of the dominant leg in the frail (3019 ± 555 cm^3) versus non-frail groups (**Figure 4.28 B**), whereas no differences were apparent when comparing absolute muscle volume of the dominant leg in the pre-frail females (3203 ± 345 cm^3) to the non-frail and frail females (**Figure 4.28 B**).

Absolute calf and leg skeletal muscle volume in non-frail versus the collapsed group of pre-frail and frail females

The collapsed group of pre-frail and frail females also exhibited significantly (P = 0.008) lower absolute muscle volume of the dominant calf compared to the non-frail group (1342 ± 202 cm^3; **Figure 4.28 C**). Similarly, significantly (P = 0.033) smaller absolute muscle volume of the dominant leg was also evident in the collapsed pre-frail and frail group versus the non-frail group (3454 ± 345 cm^3; **Figure 4.28 D**).

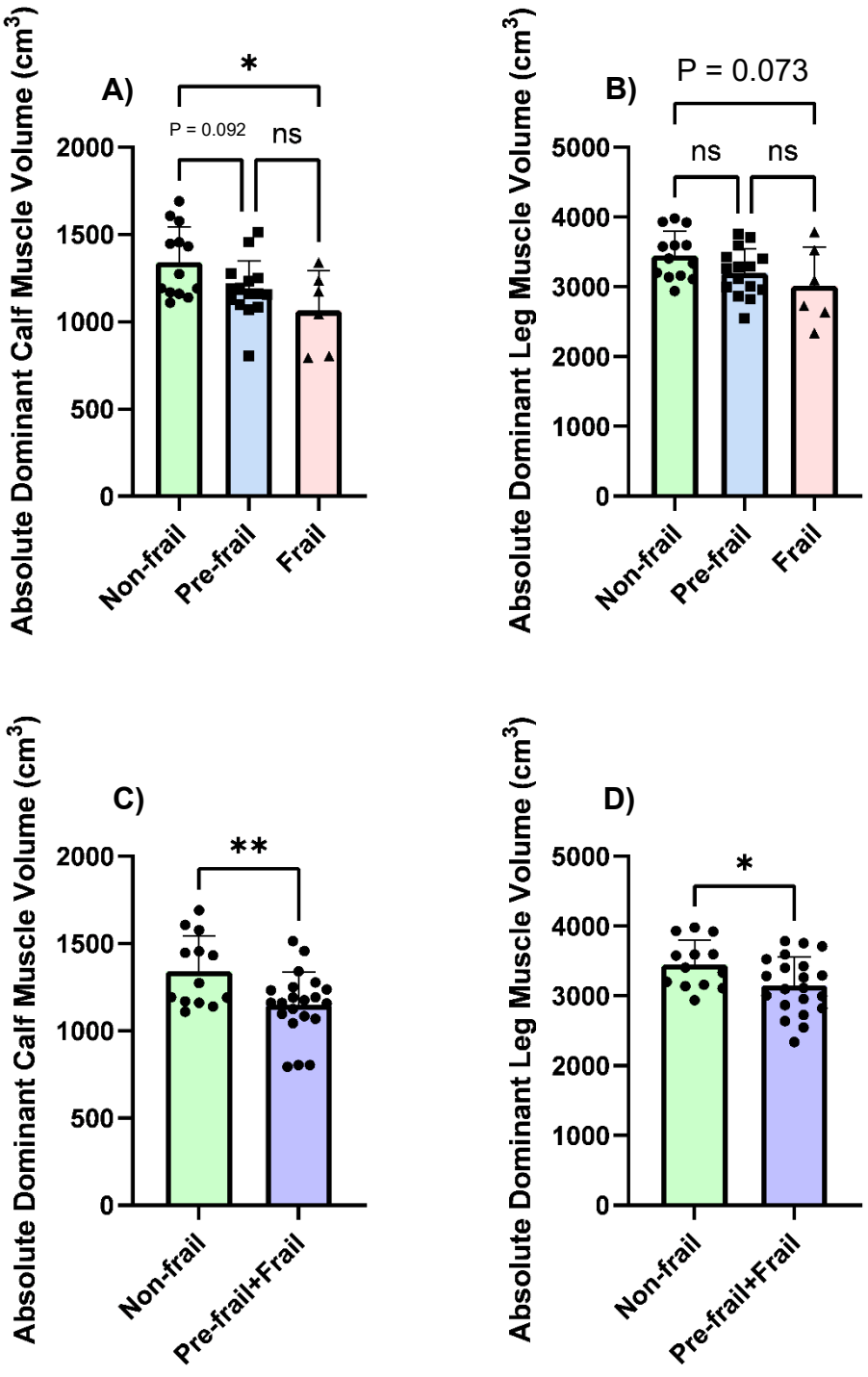

Figure 4.28: *Absolute muscle volume of the dominant calf (**A**) and leg (**B**) in non-frail, pre-frail and frail females. Absolute muscle volume of the dominant calf (**C**) and leg (**D**) in non-frail versus the collapsed group of pre-frail and frail females. Values are mean ± standard deviation and individual values. * = P < 0.05; ** = P < 0.01.*

Appendix 4.4

Absolute visceral adipose tissue volume in non-frail, pre-frail and frail females

Absolute visceral adipose tissue volume of the abdomen was 875 ± 592 cm^3 in the non-frail group, which was no different to the pre-frail and frail groups (**Figure 4.29 A**). There were also no differences between the pre-frail and frail groups (**Figure 4.29 A**).

Absolute visceral adipose tissue volume in non-frail versus the collapsed group of pre-frail and frail females

Similarly, when data from the pre-frail and frail groups were collapsed, absolute visceral adipose volume was no different between the collapsed pre-frail and frail (1052 ± 777 cm^3) and non-frail groups (**Figure 4.29 B**).

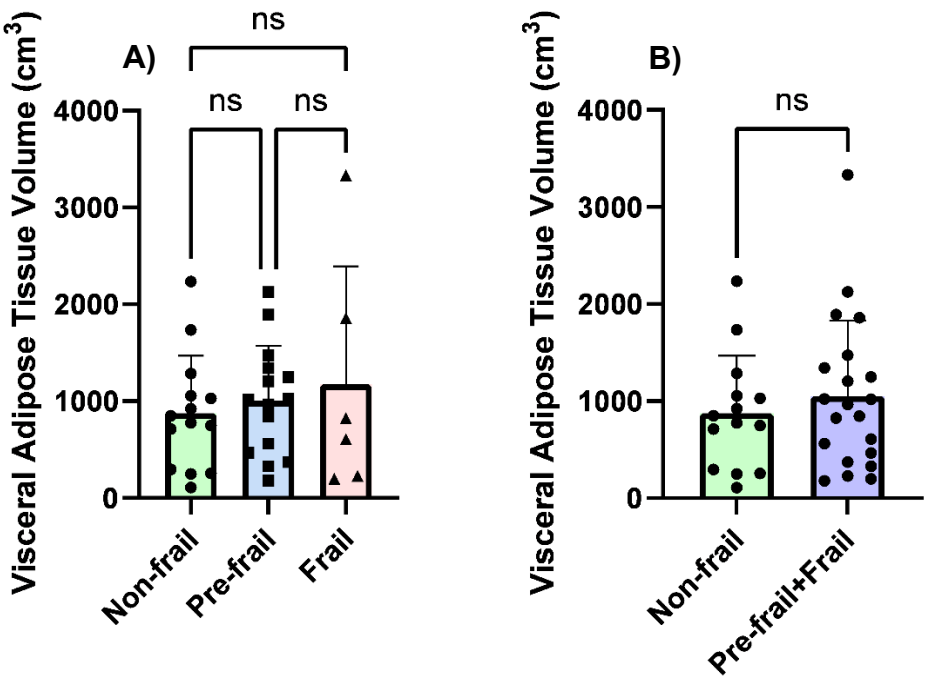

Figure 4.29: *Absolute visceral adipose tissue volume of the abdomen in (**A**) non-frail, pre-frail and frail females, and (**B**) non-frail versus the collapsed group of pre-frail and frail females. Values are mean ± standard deviation and individual values.*

Chapter Five: Brain Morphometry, Haemodynamics and Oxygenation in Non-frail, Pre-frail and Frail Females

5.1 Introduction

Associations between frailty status and brain structural and haemodynamic parameters were outlined in Chapter One – Section 1.5. In summary, studies have largely focussed on brain structural parameters of morphometry which have highlighted lower global brain volume [118, 119] and greater white matter hyperintensity (WMH) volume [143, 144] in frail versus non-frail individuals. The most robust evidence to date was derived from a study using the UK Biobank data in over 40,000 adults aged 44-82 (mean 64 ± 8 years). This study reported frailty severity was negatively associated with GMV in 75 brain regions (Cohen's d = 0.027 – 0.082, P < 0.01), and confirmed a positive association between WMH volume and frailty severity (Cohen's d = 0.084, P < 0.0001) [123].

Whilst there is growing evidence of lower global and regional GMVs with frailty, there appears to be no comparisons of regional white matter volumes between non-frail and frail states. Lower white matter volume in numerous brain regions, such as the hippocampus (t = 3.72, P < 0.001) and precentral gyrus (t = 3.36, P < 0.001), has been associated with older age [124]. However, it is unknown if frailty is associated with this loss of regional white matter volume compared to normal ageing. Previous studies of frailty have instead adopted measures related to white matter integrity from DTI (an MRI technique which assesses the direction of water diffusion in white matter axonal fibres). DTI studies have revealed lower white matter microstructural integrity in frail versus non-frail individuals [146, 366]. For example, greater mean diffusivity (MD, indicating lower structural integrity of white matter tracts that prevent undirected water

diffusion) within the prefrontal cortex has been observed in frail compared to non-frail individuals [151]. Since studies in older versus young individuals have highlighted that age-related impairments of white matter microstructural integrity from DTI can be explained by the loss of white matter volume [367], it is predicted that regional white matter volumes will also be lower in frailty.

To date, there are no previous reports of regional grey matter cortical surface measures such as gyrification (the degree of folding of gyri on the cortical surface) and sulcus depth (the distance between the cortical surface and the cerebral hull) in frail individuals. Studies have demonstrated an inverse association between age and gyrification in brain regions such as the pre-frontal cortex ($r = -0.13$; $P = 0.0004$) and negative associations between regional gyrification and cognitive function ($r = -0.13$; $P < 0.0003$) [135]. Similarly, a reduction in sulcus depth of the parieto-occipital brain region has been observed in a 5 year longitudinal study of older adults [136] and lower sulcus depth has been observed in cognitively impaired older individuals versus healthy controls [137]. Therefore, given the higher prevalence of cognitive impairment in frail versus non-frail individuals [138], frailty may be related to changes in gyrification and sulcus depth.

Brain morphometry differences in frail versus non-frail individuals, such as regional differences in GMV, have also been explored in relation to functional traits of frailty, such as low handgrip strength and slow walking speed [116, 125]. For example, GMV in several brain regions, such as the hippocampus, have been negatively associated with handgrip strength ($t = 4.0$, $P < 0.001$) and walking speed ($t = 5.0$, $P < 0.001$) in a study of non-frail, pre-frail and frail individuals [125]. However, regional volume relationships are currently limited to GMV, leaving associations between other structural indices of the brain, such as white matter volume and cortical thickness, and

functional capacity in frail individuals to be explored. These investigations are important as atrophy of white matter in a 2.5 year longitudinal study of older adults has been associated with greater decline in gait speed (regression coefficient: = 0.25, P < 0.001) [126], suggesting white matter atrophy may be related to functional deterioration in frail individuals. Furthermore, in addition to studies associating brain measures with handgrip strength and walking speed, it would be insightful to investigate associations between brain structure and measures of skeletal muscle strength and fatigability, functional measures also shown to be negatively impacted by frailty [54].

As well as brain structural measures, MRI provides brain functional measures including haemodynamic parameters, such as CBF, and measures of oxygenation, such as OEF, which can be studied in frail individuals. Lower resting CBF [110, 152] and cerebral oxygenation [111] has been demonstrated in older versus young individuals. Furthermore, lower CBF and oxygenation in older versus young individuals has been associated with lower cognitive function (R^2 = 0.46, P = 0.008) [152], and lower cerebral oxygenation has been observed in Alzheimer's Disease patients versus healthy counterparts [153]. Previous work has shown an inverse correlation between frailty severity and cognitive function (r = -0.58; P < 0.05) [154] and a higher prevalence of neurodegenerative diseases in frail versus healthy individuals (40.02 % vs 11.27 %; P < 0.0001) [155]. However, studies assessing haemodynamic and functional measures of the brain in frail individuals are scarce. One study adopting NIRS assessments noted no differences in resting cerebral oxygenation between non-frail, pre-frail and frail states [157]. NIRS has a limited sampling range of 2 cm beneath the skull [158], therefore measurements may not be indicative of whole brain cerebral oxygenation, and this technique does not permit assessments of cerebral oxygen

utilisation. In contrast, TRUST MRI (see Chapter Two, Section 2.8.8) assesses venous oxygenation through the superior sagittal sinus to provide measures of global cerebral OEF and $CMRO_2$, but these measures have not been utilised in studies of frailty. Likewise, measurements of CBF using PC-MRI within the carotid and basilar arteries have also not been employed in frailty studies. Studies of ageing employing TRUST and PC-MRI have revealed lower CBF [152, 159] and a greater $CMRO_2$ [159, 160] at rest in older compared with younger individuals. However, these relationships have not yet been explored in frail versus non-frail individuals.

Overall, further insight into the physiological characteristics of the brain in frail individuals which can be addressed using MRI is needed. In particular, insight into regional white matter volumes and cortical surface measures, cerebral haemodynamic and oxygenation parameters, and the relationships between regional brain structure and physical function. The aim of this current Chapter was to address these gaps, by investigating global and regional brain morphometric measures and WMH volume, haemodynamic and oxygenation measures in the brain, and relationships between brain morphometry indices and physical function measures in non-frail, pre-frail and frail females.

It was hypothesised that frail participants would exhibit lower global and regional grey matter volumes, and these differences in brain morphometry would relate to physical function parameters, including handgrip strength, walking speed, and skeletal muscle strength and fatigability (measures detailed in Chapter Four). Given the lack of investigations into cerebral haemodynamic parameters in frail individuals, functional measurements of CBF, and global cerebral venous oxygenation, OEF, and $CMRO_2$ were also collected in non-frail, pre-frail and frail females to bring further novel insight into the frailty phenotype.

5.2 Methods

Participant demographics were described in Chapter Two – Table 2.1. Structural and functional parameters of the brain were assessed using different MRI sequences. The full MRI scan protocol was outlined in Chapter Two – **Figure 2.6,** with scan parameters for all brain MRI sequences described in Chapter Two, Section 2.8. The following section outlines the post-processing methods used for the brain MRI analysis to quantify brain global and regional morphometry, and cerebral haemodynamic and fractional oxygen extraction parameters in non-frail, pre-frail and frail female volunteers. All abbreviations used in this Chapter are outlined on pages 13-17.

5.2.1 Brain morphometry

5.2.1.1 Voxel-based morphometry (global and regional brain volumes; VBM)

VBM is an automated analysis method used to quantify structural brain parameters on a voxel-by-voxel basis by statistical parametric mapping [368]. During VBM analysis the high-resolution T_1-weighted MPRAGE image undergoes a series of processing steps, including spatial normalisation and segmentation, prior to data smoothing and later statistical parametric mapping [368]. This method provides metrics of global GMV, WMV, CSF volume, which has been shown to allow the delineation of small-scale regional differences in GMV and WMV between experimental groups [369]. In this work, VBM was used to quantify GMV, WMV and CSF volume for non-frail, pre-frail and frail group comparisons.

Pre-processing for VBM was conducted in Computational Anatomy Toolbox (version 12.6 r1450; http://www.neuro.uni-jena.de/cat/; CAT12) within Statistical Parametric Mapping (version 7771; http://www.fil.ion.ucl.ac.uk/spm/softw are/spm12/; SPM12) using MATLAB version 9.7 (R2022a, MathWorks). This included bias-field and noise

removal, skull stripping, segmentation into grey and white matter, and normalisation to MNI space using DARTEL to a 1.5 mm isotropic adult template within the CAT12 toolbox. Intensity modulation of the normalised tissue segments accounts for both global affine transformations and local warping. Image data quality was assessed in all individual images and included basic image properties, noise and geometric distortions (e.g., due to motion) with an image quality rating of 84% (1.5% SD), representing good image quality. GM and WM segments were spatially smoothed using a 12 mm FWHM Gaussian smoothing kernel, and edge effects between tissue types avoided by excluding all voxels with values < 0.1 (absolute threshold masking). Example images of WM, GM and CSF segmentations are shown in **Figure 5.1**. The resulting global volumes of GM, WM, CSF were saved for offline statistical analysis. Of relevance in VBM analysis is the confounding factor of head size, i.e., TIV. To overcome this issue, the global volumes of each tissue type (GM, WM, CSF) were normalised to the TIV.

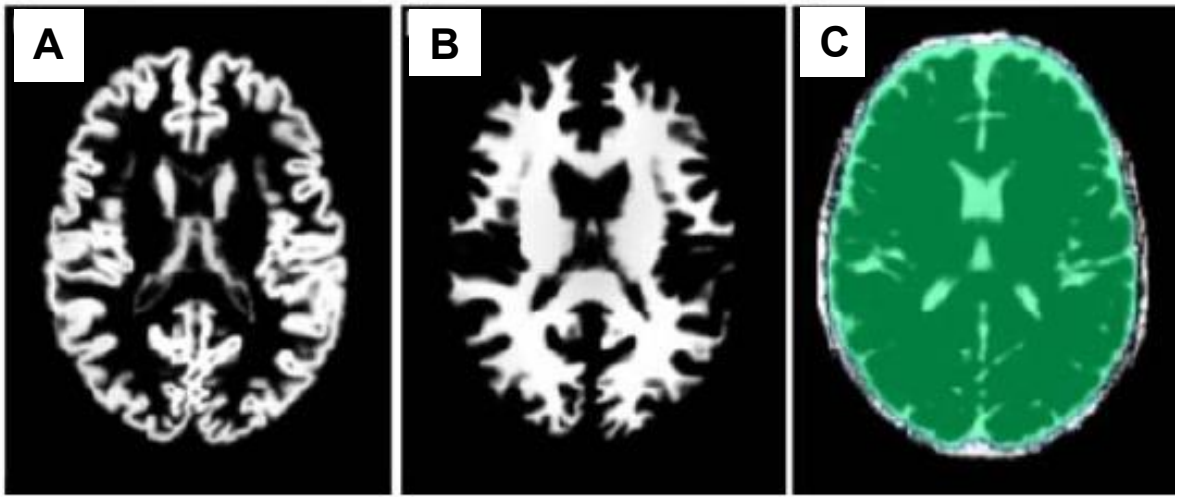

Figure 5.1: Example MPRAGE segmentation into grey matter (GM) **(A)**, white matter (WM) **(B)** and cerebrospinal fluid (CSF) **(C)** and the Total Intracranial Volume (TIV) shown in green using CAT12.

Following analysis of global brain volumes, a first level analysis was performed to assess regional differences in GM, WM and CSF volumes using a GLM implemented in SPM12. For this analysis, data from the pre-frail and the frail groups were collapsed into one group (as the sample size of the frail group alone was too low to meet the requirements for statistical analysis using SPM12). An independent t-test was performed to evaluate differences in regional GM, WM and CSF volume between the non-frail group and the collapsed pre-frail and frail group. In this VBM analysis, TIV and age were included as normalised covariates of no interest in the GLM remove the variations in brain size and age.

Statistical inferences were deduced using nonparametric permutations (set to 5,000), and a Threshold-Free Cluster Enhancement Correction was applied to the t-statistic maps (https://www.fil.ion.ucl.ac.uk/spm/ext/#TFCE). Uncorrected analyses were performed at $P < 0.01$ and $P < 0.001$, with cluster size set to $k > 50$. The value of k represents the number of voxels (i.e., the tissue volume) within each brain region exhibiting significant differences between the non-frail group and collapsed pre-frail and frail group. For this analysis, exact *P*-values of significant differences, except in instances of $P < 0.001$, are tabulated.

Analysis of global and regional brain volume data with CAT12 in SPM12 software was fully automated, therefore CV data were not generated for this analysis. Prior studies have shown a very high Pearson's correlation coefficient (0.99) and very low percent volume difference (<1%) of GM and WM volumes from scan-rescan MPRAGE data analysed using SPM12 [370]. Further, scan-rescan data has been shown to have has excellent intra-scanner repeatability (<1% CV) and inter-scanner reproducibility (<5% CV) [371] in GM, WM and whole brain volume segmentation using SPM12.

5.2.1.2 Surface based morphometry (SBM)

SBM of MPRAGE data was used to construct and analyse cortical surfaces. The preprocessing steps and masks generated from VBM segmentation in CAT12 acted as pre-requisites for SBM analyses. SBM was used to quantify cortical thickness (the width of cortical grey matter), gyrification index and sulcus depth (measures of grey matter folding).

For cortical thickness analysis, MPRAGE images underwent tissue segmentation to estimate white matter distance, i.e., projection-based thickness [372], which handles partial volume information, sulcal blurring, and asymmetries, and topological correction performed based on a spherical harmonics approach [373]. Spherical registration was used to adapt the volume-based diffeomorphic DARTEL algorithm to the cortical surface [374]. Finally, to increase processing speed, all scans were resampled to a higher-resolution 164,000 mesh compatible with FreeSurfer data, followed by smoothing with a gaussian kernel of 15 mm FWHM.

Sulcus depth was quantified based on the Euclidean distance between the central surface and its convex hull (measured in mm). Gyrification was extracted based on the amount of cortical folding relative to the absolute mean curvature of the grey matter (measured in degrees). Both of these measures underwent the same processing steps as cortical thickness analysis with the exception of smoothing with a gaussian kernel of 20 mm FWHM.

Surface maps of mean cortical thickness, gyrification index and sulcus depth were generated, with regional differences in these parameters assessed with an independent T test within a GLM (as used for regional grey and white matter volume analyses) between the non-frail group and collapsed pre-frail and frail group.

Analysis of repeat scan data using CAT12 has shown a very low percentage differences (1.9%) and high intraclass correlation coefficient values (0.83) for cortical thickness quantification [375] and high intraclass correlation coefficient [376].

5.2.1.3 Regression analyses of VBM and SBM measures against physical function measures

A GLM within SPM12 was also used to determine the relationship between regional brain volume measures derived from VBM (GM and WM volumes) and surface-based measures derived from SBM (cortical thickness, gyrification index, sulcus depth), with physical function measures (handgrip strength, walking speed, knee extensor isometric strength and knee extensor work output at 60°/s, as outlined in Chapter Four). TIV and age were included as normalised covariates of no interest in the GLM to remove the variations in head size. The magnitude of associations between measures was determined by the T-statistic, calculated by dividing the correlation coefficient (r value) by its standard error which represents how many standard errors the r value is away from zero (zero representing no correlation). Higher T-statistic values (greater than 0) represent stronger associations between two variables, with a value of 2 or greater considered to be a strong correlation between two variables. For this analysis, exact *P* values are tabulated for significant differences, except in instances of $P < 0.001$.

5.2.1.4 White Matter Hyperintensity (WMH) volume

WMH volume was quantified from the T_2-FLAIR sequence using FSL's BIANCA tool. BIANCA is a fully automated method of WMH detection using the k-nearest neighbour algorithm, which classifies objects (or tissue) based on the feature space of neighbouring objects [377]. BIANCA utilises feature space information of individual

voxels, such as intensity and spatial properties, to delineate WMHs from WM tissue. Delineation in the BIANCA tool is reliant on a training set of previous images whereby tissue has been segmented into WMH and non-WMH classes. The BIANCA algorithm was used to generate masks of WMHs from T_2-FLAIR images (shown in red in **Figure 5.2**). The masks were then run through an in-house MATLAB code to generate WMH volume, and statistical analysis was performed on the mean WMH volume across groups. WMH values are presented as absolute volume and WMH volume normalised to TIV.

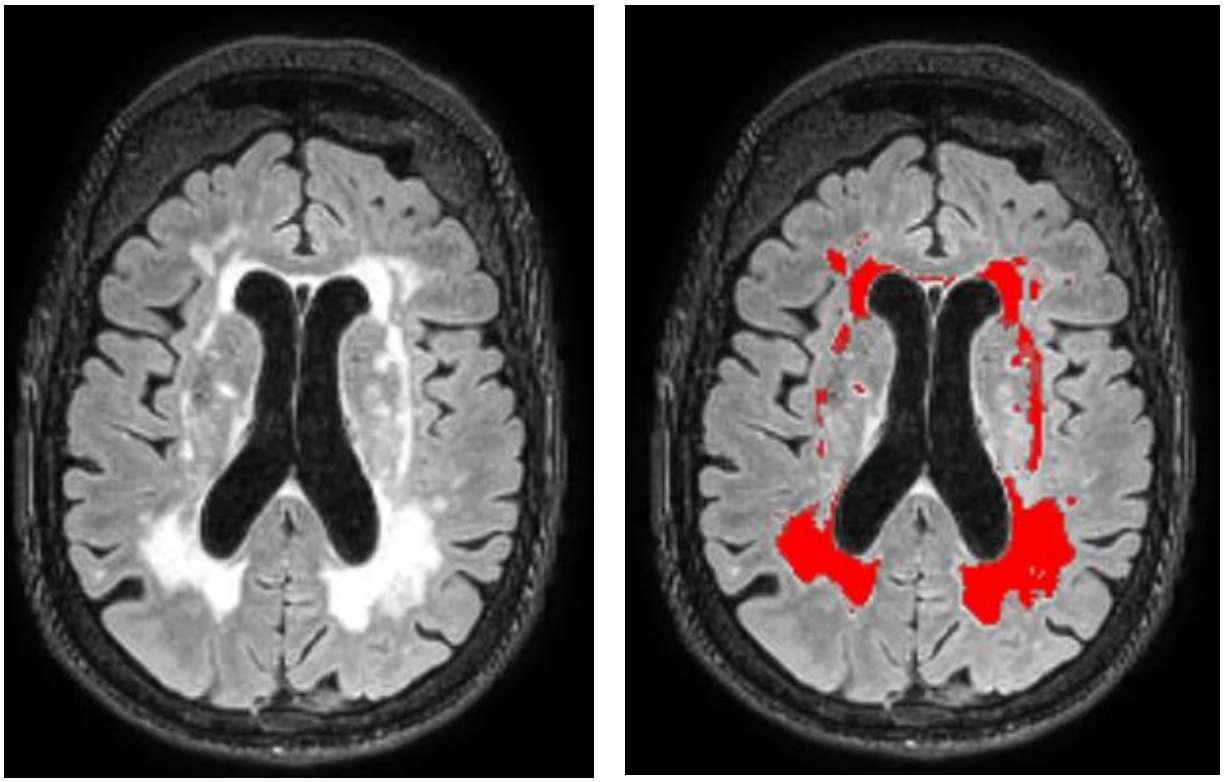

Figure 5.2: Example T_2-FLAIR image and resultant WMH output from the BIANCA tool. Image from the MRI scanner (left) showing WMHs appearing in white. WMH masks (right, shown in red) overlaid on the T_2-FLAIR image from which WMH volume is computed.

Analysis of WMH volume data with the BIANCA algorithm was fully automated, therefore CV data were not generated for this analysis. Previous work has shown

excellent scan-rescan reproducibility of T_2-FLAIR derived WMH volume measures from BIANCA, with intraclass correlation coefficient values reported of 0.99 [377].

5.2.2 Brain haemodynamics and oxygenation

5.2.2.1 Cerebral artery blood flow

PC-MRI 2D-QFLOW data were processed using cvi42 software (Circle Cardiovascular Imaging Inc; version 5.14.2). An ROI was drawn around the walls of the internal carotid arteries and the basilar artery using the magnitude image. The ROI was then propagated across all phases in the cardiac cycle and manually checked and edited to optimise fitting (**Figure 5.3**). The magnitude image was cross-referenced with the phase data to ensure no phase aliasing. The phase data was then used to calculate the mean blood velocity (cm/s), mean flow rate (ml/min) and CSA (mm^2) in each of the cerebral arteries. Mean blood velocity was estimated from computing the mean across all three blood vessels. The mean flow rate across each of the internal carotid arteries and the basilar artery were summed to compute global cerebral blood flow (CBF_{global}). CBF was also normalised to GMV (estimated from MRPAGE data, as detailed in Section 5.2.1.1) to give CBF_{gm} (in units of ml/100g grey matter/min) which accounts for structural atrophy. CBF_{gm} is computed, as derived in [152], from:

$$CBF_{gm} = \frac{CBF_{global}}{r \times (GMV + WMV) \times \rho} \times 100000$$

where *r* is taken to be 1.4 and represents the assumption that white matter flow is approximately 40% that of grey matter and so CBF_{global} = 1.4 CBF_{gm}, whilst ρ is the mass density of tissue (assumed = 1.06 g/ml). CBF_{global} is measured in ml/min, GMV and WMV are tissue volumes measured in ml.

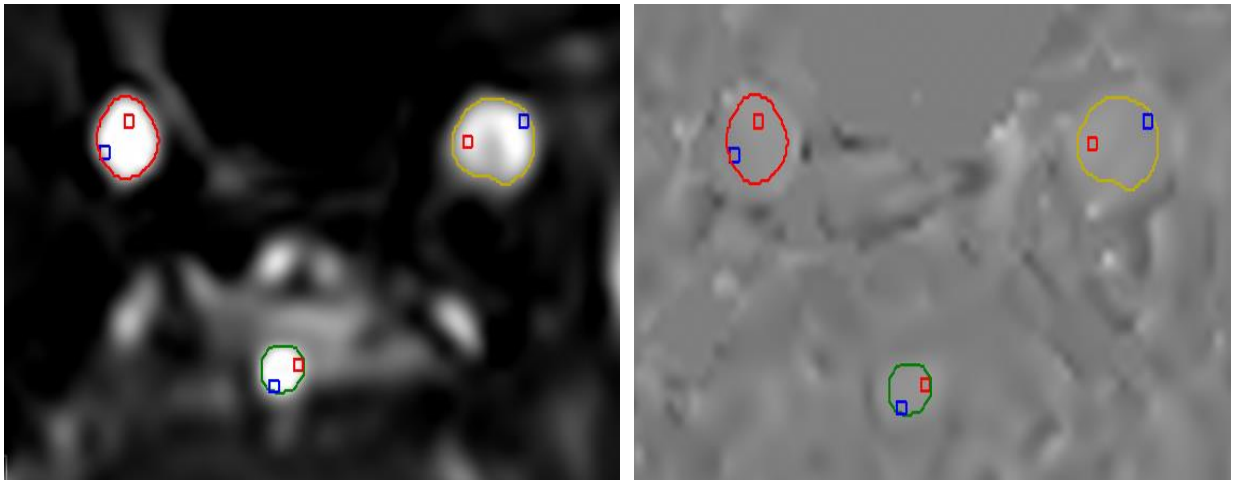

Figure 5.3: Example PC-MRI 2D-QFLOW analysis performed in cvi42 software. ROIs drawn around basilar and internal carotid arteries shown on the magnitude image (left). Corresponding phase image shown on the right.

The intra-rater CV calculated to determine the reliabilty of the contour analyses of 2D-QFLOW images. For CV calculations, three repeat measures were performed on 1 participant's set of 2D-QFLOW images using the cvi42 software. All were less than 3% (**Table 5.1**). Raw data for CV calculations are presented in **Appendix 5.1** – **Table 5.10**.

Table 5.1: Coefficient of variance (CV) results for repeated analysis of 2D-QFLOW images.

2D-QFLOW parameter	CV (%)
Left carotid CSA (mm^2)	1.6%
Right carotid CSA (mm^2)	2.1%
Basilar CSA (mm^2)	2.3%
Mean blood velocity (cm/s)	0.3%
CBF_{global} (ml/min)	1.2 %
CBF_{gm} (ml/100g grey matter/min)	1.2 %

5.2.2.2 Cerebral arterial oxygenation and oxygen metabolism

TRUST data were analysed using in-house MATLAB code as described in [296]. Venous blood signal in the superior sagittal sinus (SSS) was computed from the pairwise subtraction of label and control images to obtain difference images for each effective echo time. In the resultant difference images, an ROI was superimposed onto the four voxels with the highest difference signal to create a mask for spatial averaging of the signal. Blood T_2 relaxation was then calculated within the SSS ROI by fitting to the mono-exponential signal decay (**Figure 5.4**). The blood T_2 relaxation time in the SSS was then converted into venous oxygenation, Y_v, using the calibration plot [378] shown in **Figure 5.5.**

Arterial oxygenation, Y_a, was calculated as described by Peng et al., [295]

$$Ya = 99.77 - 0.036 \times age - 1.235 \times sex + 0.021 \times age \times sex$$

where age is in years and sex is defined as 0 for females and 1 for males [297].

$$OEF = Ya - Yv$$

Global $CMRO_2$ ($gCMRO_{2\_global}$) was calculated as described by Liu et al [379]

$$CMRO_{2\_global} = CBF_{global} \times (Ya - Yv) \times Ch$$

where CBF_{global} is the global cerebral blood flow, and Ch is the capacity of blood to transport oxygen. Since individual haematocrit data was unavailable, Ch was estimated for each subject by adjusting the literature value of (8.34 mmol/L or ~13.4g/dL haemoglobin at an age of 20 years) for age assuming a decline rate of Ch of 0.0079 mmol/L per year [380]. Grey matter $CMRO_2$ ($CMRO_{2\_gm}$) was computed, corrected for brain atrophy to account for any disease or age-related loss of grey and white matter, which could differ between groups [160] using CBF_{gm} computed above.

$$CMRO_{2\_gm} = CBF_{gm} \times (Ya - Yv) \times Ch$$

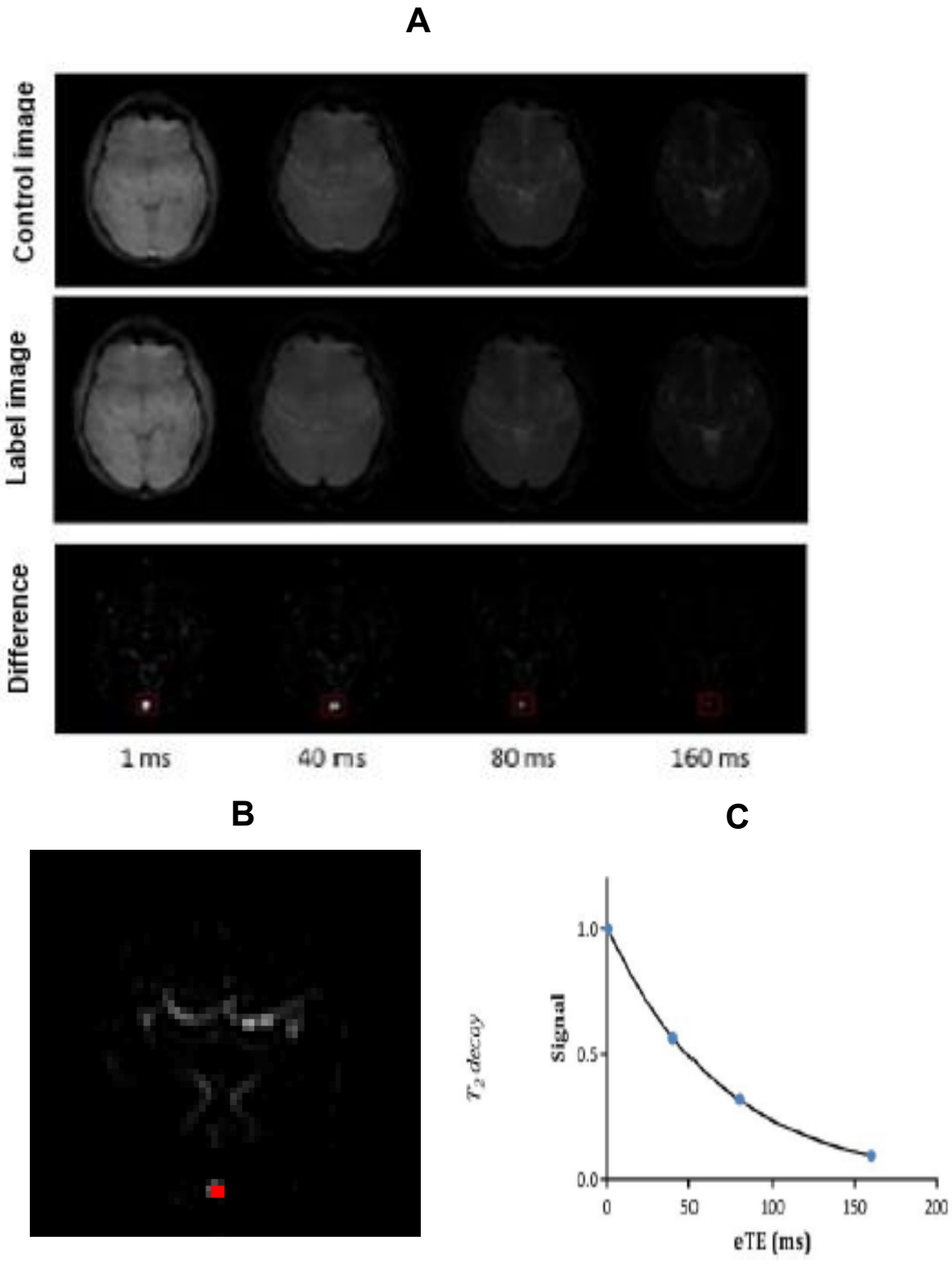

Figure 5.4: *TRUST analysis.* ***(A)*** *Label and control images acquired at 4 effective echo times (TE) of 1, 40, 80 and 160 ms. A difference image is created by the pairwise subtraction of the label from the control images at each TE to isolate the signal in the sagittal sinus.* ***(B)*** *Four voxels in the sagittal sinus with the highest signal intensity (highlighted in red) are interrogated and* ***(C)*** *fit to a T_2 decay curve to estimate the T_2 of venous blood.*

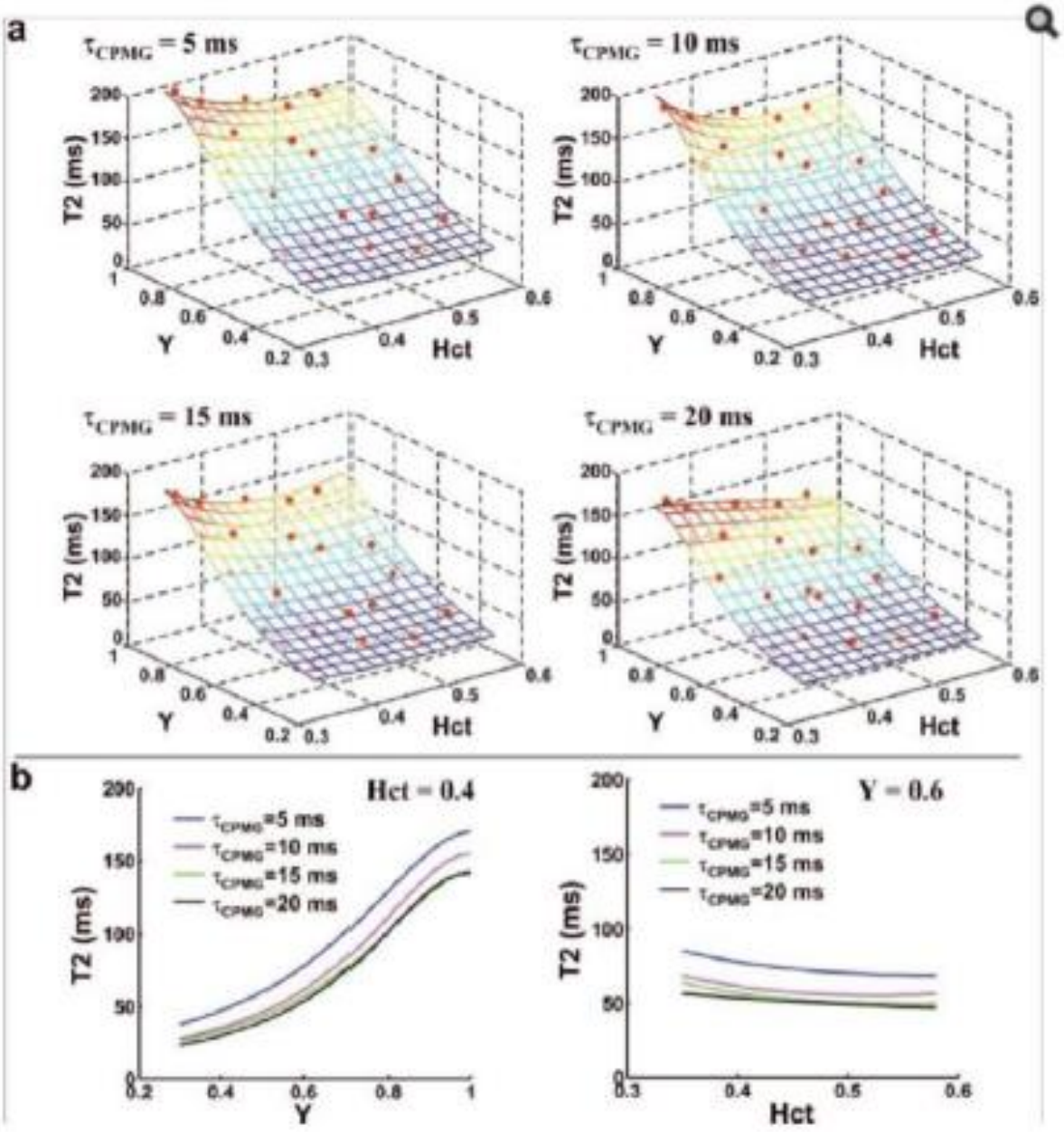

Figure 5.5: *TRUST calibration plots used to convert the venous blood T_2 to venous oxygenation, Y_v [378].*

Analysis of TRUST data was fully automated, therefore CV data were not generated for this analysis. Prior work has demonstrated a <4% CV for scan-rescan repeatability measurements of venous oxygenation, oxygen extraction fraction and $CMRO_2$ using TRUST MRI at 3T [379]. Intra-session (repeating without repositioning participant) and inter-session (scan repeated on separate day after repositioning participant in scanner) reproducibility CVs have also been shown to be 3.3% and 6.8%, respectively, for OEF measurements in a previous TRUST study at 3T [381].

5.2.3 Statistical analysis

In addition to the post-processing methods outlined above, several methods generated data that were analysed offline using statistical analysis methods that were described in Chapter Two – Section 2.9. These methods included global brain volumes and cortical thickness (Section 5.2.1.1), WMH volume (Section 5.2.1.4), CBF, gmCBF, mean blood velocity and CSA of carotid and bailar arteries (Section 5.2.2.1), venous oxygenation, oxygen extraction fraction and $gmCMRO_2$ (Section 5.2.2.2). Data normality testing revealed non-normal distributions of GM volume, cortical thickness (2 group comparisons), absolute and TIV corrected WMH volumes (2 and 3 group comparisons), mean blood velocity of the cerebral arteries (2 group comparisons). For non-normally distributed data, *P* values are derived from the Kruskall-Wallis test (for 3 group comparisons) and Mann-Whitney U test (for 2 group comparisons). The regression analysis of GM and WM volume and surface based measures (described in section 5.2.1.3) represented a multiple linear regression. Values in the text, Tables and Figures represents mean ± standard deviation.

5.3 Results

Results are presented for brain morphometry (MPRAGE derived measures of global whole brain, GM, WM and CSF volume, and cortical thickness, gyrification index and

sulcus depth) differences between groups, WMH volume (derived from T_2-FLAIR), CBF_{global}, CBF_{gm}, mean blood velocity and CSA of the carotid and basilar arteries (derived from PC-MRI 2D-QFLOW), and for venous oxygenation and $CMRO_{2\_gm}$ (derived from TRUST). Comparisons are made between the non-frail, pre-frail and frail groups, and the non-frail group versus the collapsed group of pre-frail and frail to allow further scrutiny. One frail participant was withdrawn from the brain MRI protocol after collection of the MPRAGE scan due to thoracic and cervical kyphosis causing discomfort with the head coil, and so only MPRAGE brain data was available for this participant. One pre-frail and one non-frail participant's PC-MRI 2D-QFLOW data were excluded from analysis due to poor image quality. Two non-frail participant's TRUST data were excluded from analysis due to poor image quality.

5.3.1 Brain morphometry parameters

5.3.1.1 Global brain volumes and cortical thickness in non-frail, pre-frail and frail females

No differences in whole brain volume were evident between non-frail, pre-frail and frail females (**Figure 5.6 A**). Frail females exhibited significantly smaller GM volume compared to non-frail females (36 ± 5.5 % vs 40.0 ± 1.8 %; $P = 0.029$). No differences were apparent when comparing the pre-frail group to the non-frail and frail groups (**Figure 5.6 B**). WM volume was significantly lower in the frail (29.6 ± 3.4 %) and the pre-frail (31.8 ± 2.3 %) females when compared with the non-frail females ($P = 0.002$ and $P = 0.045$, respectively). However, WM volume was not different between pre-frail and frail females (**Figure 5.6 C**). Frail females also exhibited significantly greater CSF volume in comparison to non-frail counterparts (33.2 ± 8.3 % vs 25.8 ± 3.6 %; $P = 0.009$). CSF volume in the pre-frail group was no different to the non-frail and fail

groups (**Figure 5.6 D**). Cortical thickness was no different between non-frail, pre-frail and frail groups (**Figure 5.6 E**).

5.3.1.2 Global brain volumes and cortical thickness in non-frail versus the collapsed group of pre-frail and frail females

There were no differences in whole brain volume between the non-frail group and the collapsed pre-frail and frail group (**Figure 5.7 A**). GM volume in the collapsed pre-frail and frail group (37.7 ± 3.6 %) was smaller than in the non-frail group (P = 0.021; **Figure 5.7 B**). Similarly, the collapsed pre-frail and frail group exhibited a smaller WM volume in comparison to the non-frail group (31.1 ± 2.8 % vs 34.1 ± 2.1 %; P = 0.006; **Figure 5.7 C**). CSF volume was also greater in the collapsed pre-frail and frail group than the non-frail group (30.3 ± 5.6 % vs 25.8 ± 3.6 %; P = 0.012; **Figure 5.7 D**). A smaller cortical thickness was evident in the collapsed pre-frail and frail group when compared to the non-frail group (2.44 ± 0.15 mm vs 2.52 ± 0.06 mm; P = 0.009; **Figure 5.7 E**).

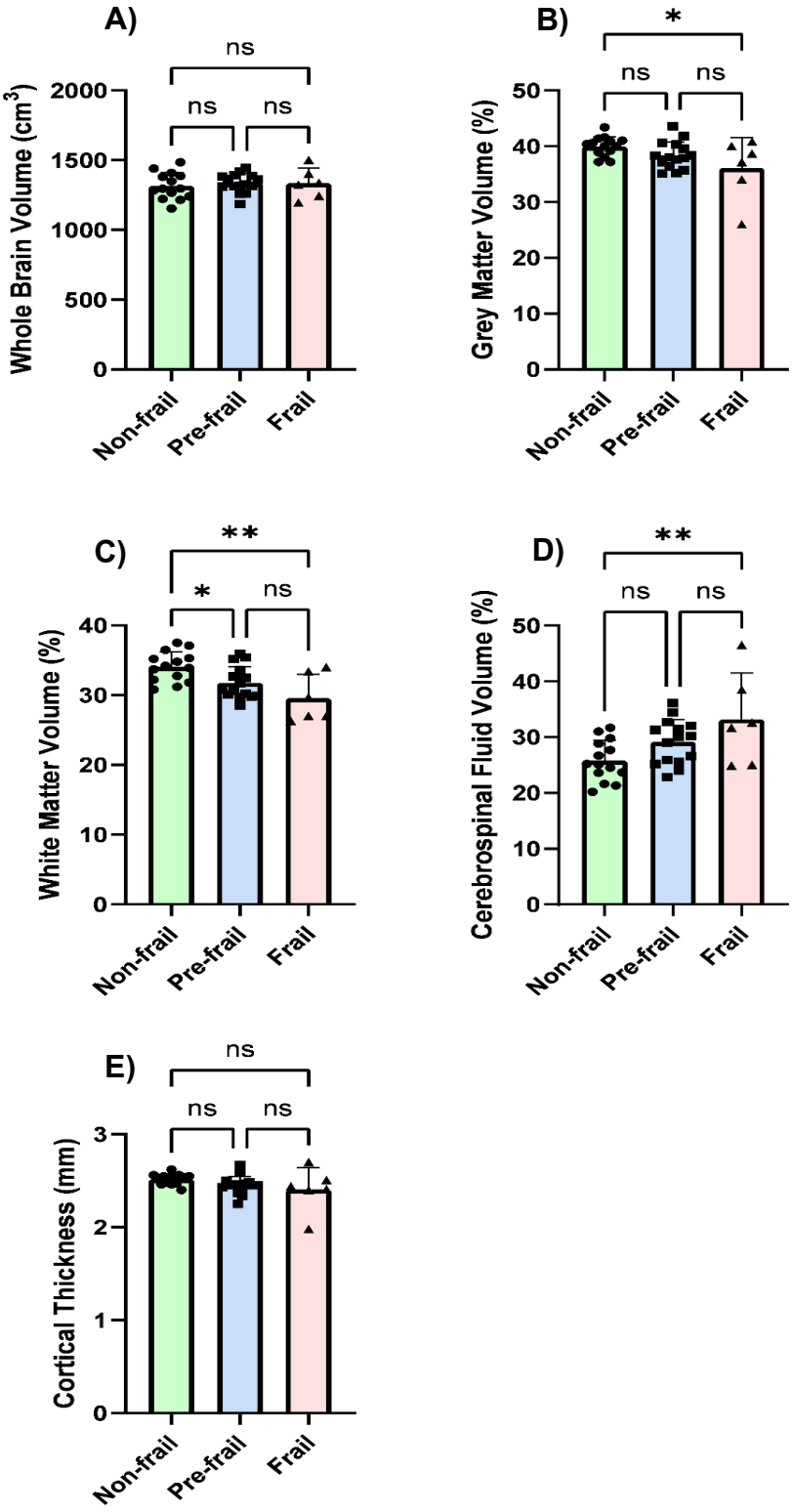

Figure 5.6: *Global brain morphometry results derived from MPRAGE scans in non-frail, pre-frail and frail females.* ***A)*** *Whole brain volume,* ***B)*** *Grey matter volume,* ***C)*** *White matter volume,* ***D)*** *Cerebrospinal fluid volume,* ***E)*** *Cortical thickness. Values are mean ± standard deviation and individual values. * = P < 0.05; ** = P < 0.01.*

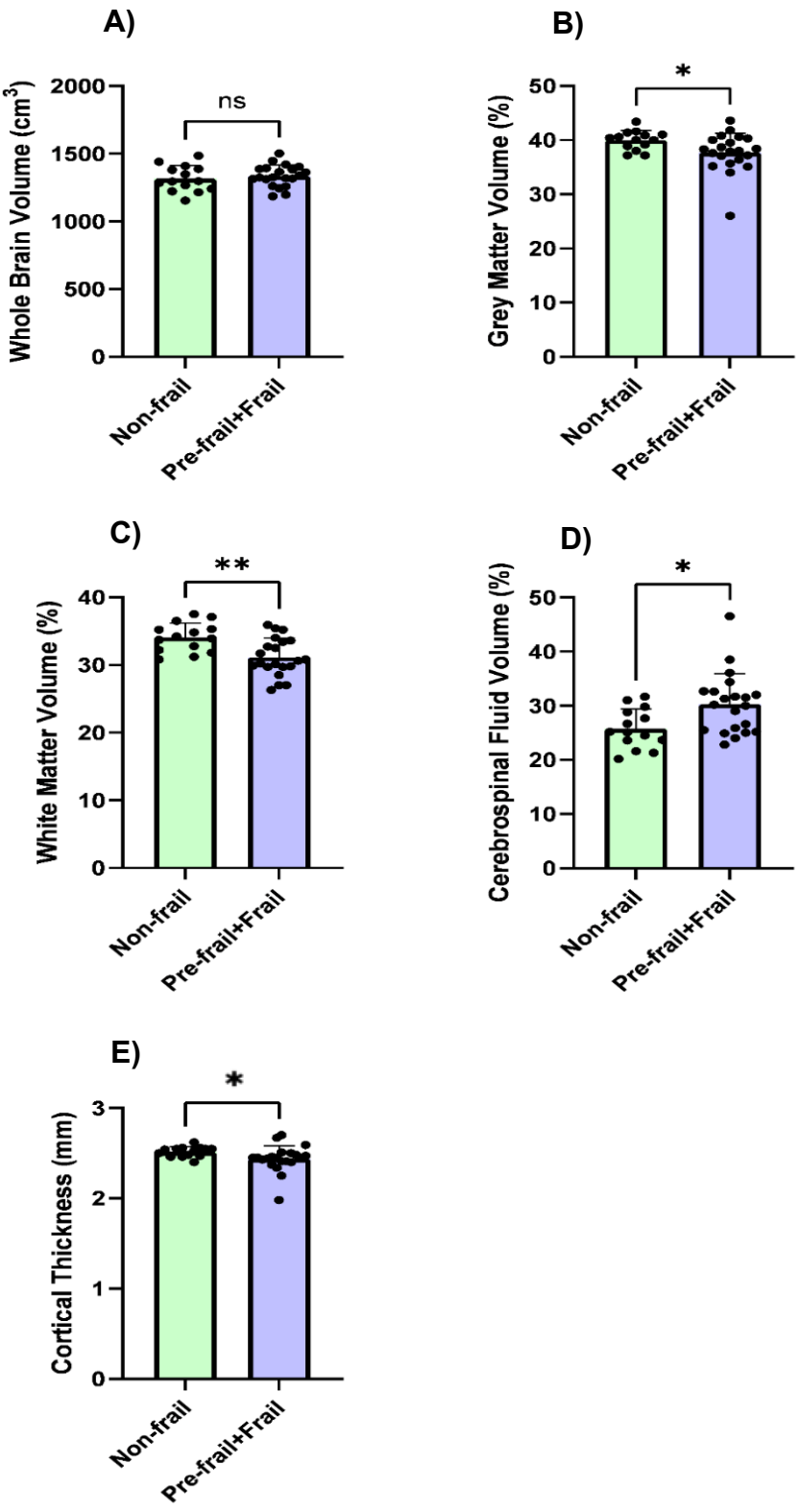

Figure 5.7: *Global brain morphometry results derived from MPRAGE scans in non-frail versus the collapsed group of pre-frail and frail females.* ***A)*** *Whole brain volume,* ***B)*** *Grey matter volume,* ***C)*** *White matter volume,* ***D)*** *Cerebrospinal fluid volume,* ***E)*** *Cortical thickness. Values are mean ± standard deviation and individual values. * = P < 0.05; ** = P < 0.01.*

5.3.1.3 Regional brain volumes in non-frail versus the collapsed group of pre-frail and frail females

For regional volume analysis, data from the pre-frail and the frail groups were collapsed given the sample size requirements for statistical analysis using SPM12.

5.3.1.3.1 Regional brain grey matter volumes in non-frail versus the collapsed group of pre-frail and frail females

13 brain regions exhibited significantly lower GM volume in the collapsed pre-frail and frail group versus the non-frail group as shown in **Figure 5.8** and **Table 5.2**. Regions showing the greatest significant difference included the postcentral gyrus, middle frontal gyrus, frontal pole, angular gyrus, subcallosal cortex, occipital fusiform gyrus and lateral occipital cortex ($P < 0.001$; **Table 5.2**). No brain regions showed greater GM volume in the collapsed pre-frail and frail group compared to the non-frail group.

Grey Matter Volume: Non-frail > Pre-frail+Frail

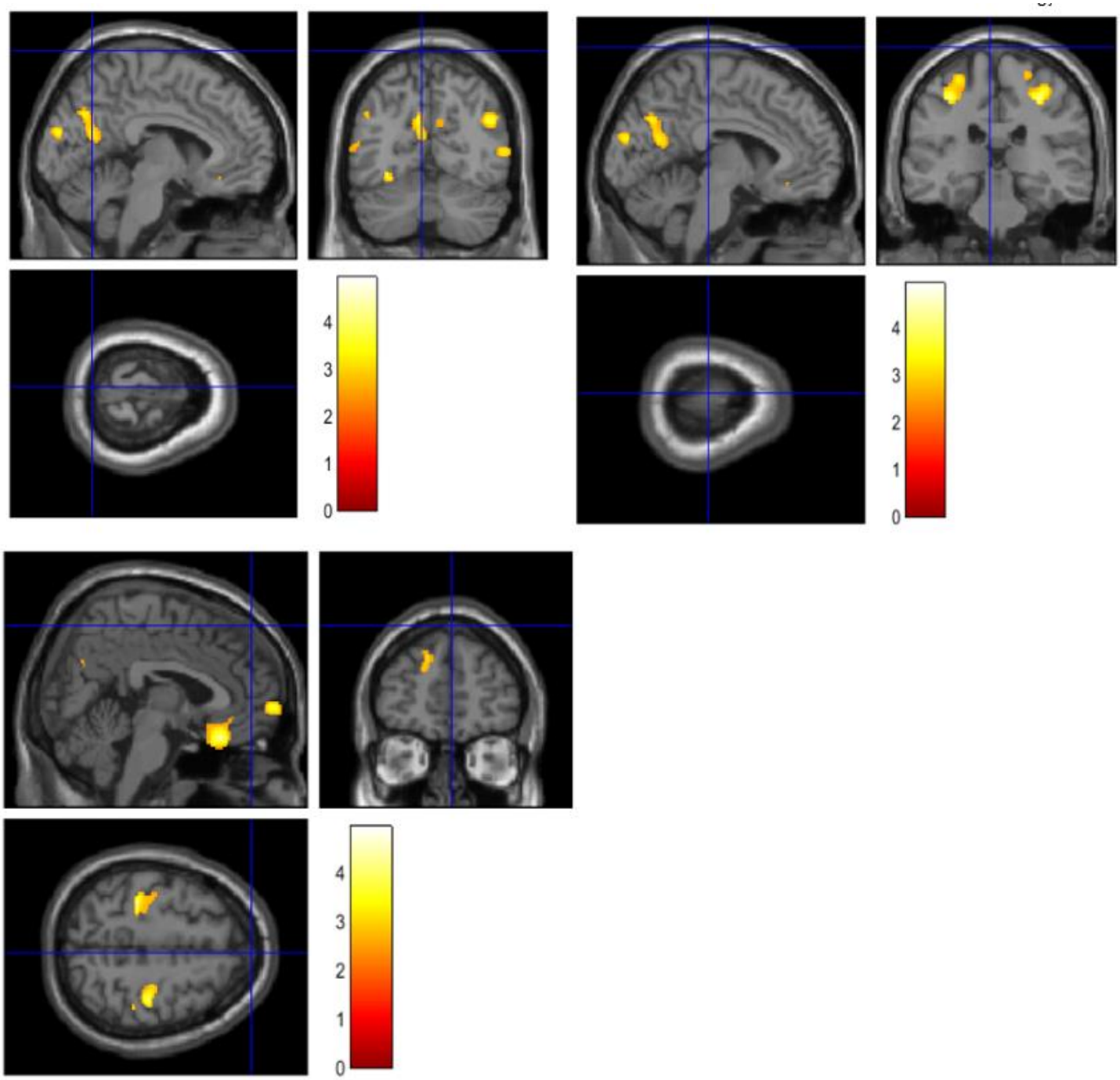

Figure 5.8: Brain regions (yellow-red clusters) exhibiting significantly ($P < 0.01$) lower grey matter volume in the collapsed pre-frail and frail group compared to the non-frail group. Brain regions and associated P values listed in Table 5.2.

Table 5.2: Regions of lower grey matter volume in the collapsed pre-frail and frail group versus the non-frail group. X, Y and Z coordinates refer to Harvard-Oxford Atlas. k denotes the number of voxels (i.e., the volume) exhibiting lower grey matter volume in the collapsed pre-frail and frail group. L = left, R = right hemisphere.

Brain region	X (mm)	Y (mm)	Z (mm)	k	P value
R postcentral gyrus	34	-24	46	323	P < 0.001
L middle frontal gyrus	-26	36	27	187	P < 0.001
R frontal pole	16	63	3	375	P < 0.001
L frontal pole	-12	45	38	84	P < 0.001
L angular gyrus	-44	-58	32	336	P < 0.001
L postcentral gyrus	-32	-32	57	270	P < 0.001
R subcallosal cortex	4	28	-22	119	P < 0.001
L occipital fusiform gyrus	-30	-63	-12	111	P < 0.001
R lateral occipital cortex	45	-60	12	127	P < 0.001
L precuneus cortex	-6	-68	32	615	P = 0.001
L occipital pole	-6	-90	20	211	P = 0.001
R temporal fusiform	34	-18	-33	91	P = 0.003
R precuneus cortex	18	-52	18	84	P = 0.005

5.3.1.3.2 Brain regional white matter volumes in non-frail versus the collapsed group of pre-frail and frail females

In the collapsed group of pre-frail and frail group, significantly lower WM volume was observed in 18 brain regions compared to the non-frail group as shown in **Figure 5.9** and **Table 5.3**. Regions with the greatest statistical significance included the occipital fusiform gyrus, superior frontal gyrus, lateral occipital cortex, frontal pole and postcentral gyrus ($P < 0.001$; **Table 5.3**). No brain regions showed significantly greater WM volume in the collapsed pre-frail and frail group compared to the non-frail group.

White Matter Volume: Non-frail > Pre-frail+Frail

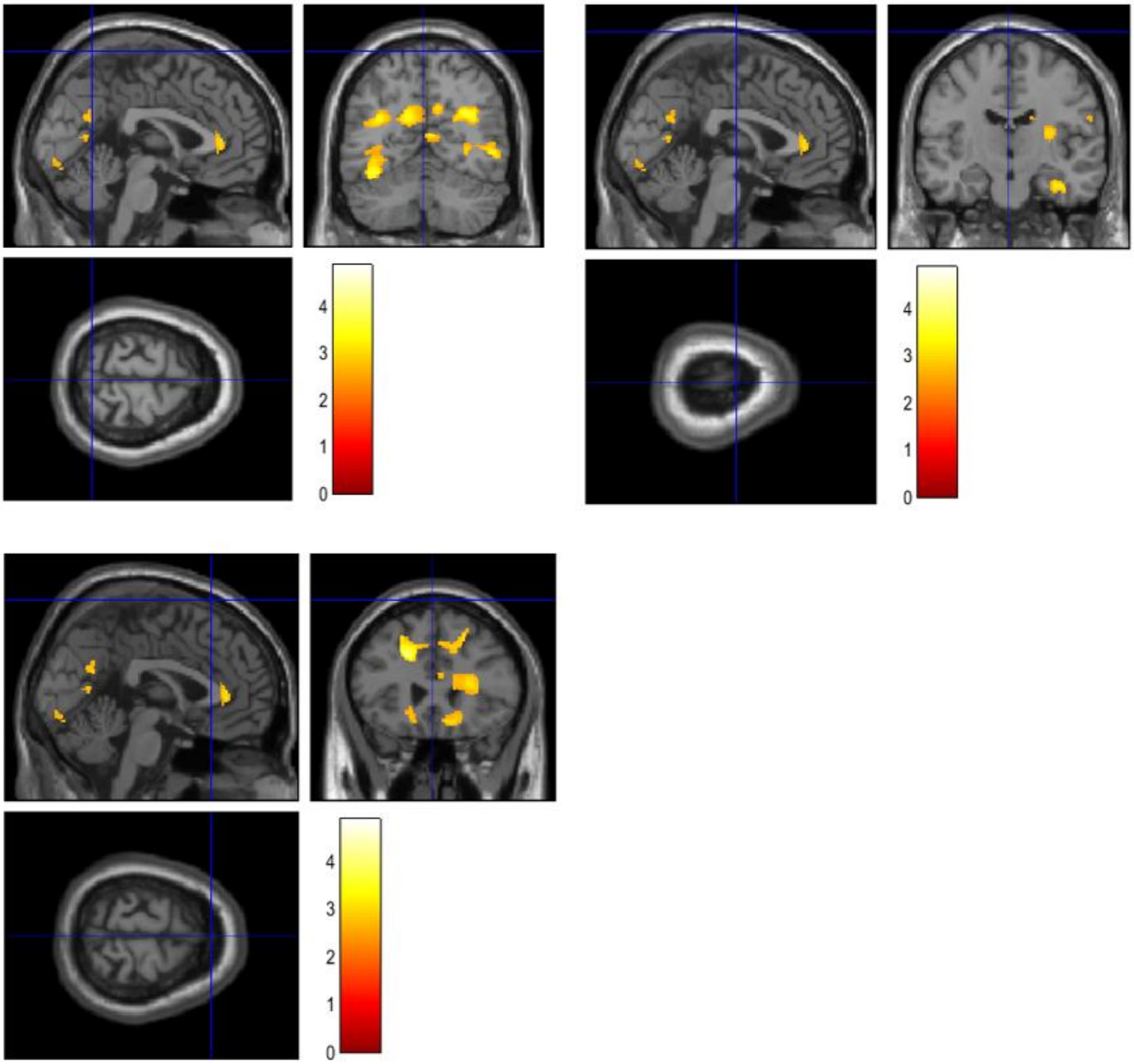

Figure 5.9: Brain regions (yellow-red clusters) exhibiting significantly ($P < 0.01$) lower white matter volume in the collapsed pre-frail and frail group versus the non-frail group. Brain regions and associated P values listed in Table 5.3.

Table 5.3: Regions of lower white matter volume in the collapsed pre-frail and frail group compared to the non-frail group. X, Y and Z coordinates refer to Harvard-Oxford Atlas. k denotes the number of voxels (i.e. the volume) exhibiting lower white matter volume in the collapsed pre-frail and frail group. L = left, R = right hemisphere.

Brain region	X (mm)	Y (mm)	Z (mm)	k	P value
L occipital fusiform gyrus	-40	-68	-12	253	P < 0.001
L superior frontal gyrus	-18	32	34	242	P < 0.001
R lateral occipital cortex	32	-64	27	187	P < 0.001
R frontal pole	36	44	24	165	P < 0.001
R postcentral gyrus	44	-28	46	267	P < 0.001
L angular gyrus	-33	-63	24	596	P = 0.001
R middle temporal gyrus, posterior division	68	-36	0	127	P = 0.001
L lingual gyrus	-3	-81	-14	248	P = 0.001
R middle temporal gyrus, temporooccipital part	50	-58	-2	594	P = 0.001
R intracalcarine cortex	6	-66	10	258	P = 0.001
L precuneus cortex	-12	-60	26	524	P = 0.001
L occipital pole	-14	-99	18	285	P = 0.001
R temporal fusiform cortex	36	-12	-26	327	P = 0.001
R superior frontal gyrus	21	22	45	446	P = 0.001
R subcallosal cortex	9	8	-16	179	P = 0.001
R temporal pole	39	21	-34	318	P = 0.002
L middle frontal gyrus	-33	15	28	72	P = 0.003
L temporal pole	-39	14	-21	50	P = 0.007

5.3.1.4 Surface based morphometry

5.3.1.4.1 Brain regional cortical thickness in non-frail versus the collapsed group of pre-frail and frail females

Mean maps of cortical thickness in the non-frail group and collapsed pre-frail and frail group are presented in **Figure 5.10 A** (left hemisphere) and **Figure 5.10 B** (right hemisphere). Maps represent cortical thickness measured in all regions of the cerebral cortex. In the collapsed pre-frail and frail group, significantly greater cortical thickness ($P = 0.002$) was observed in the left hemisphere paracingulate gyrus, compared to the non-frail group (**Table 5.4**). No differences were observed in cortical thickness of any brain region within the right hemisphere.

A) Left hemisphere

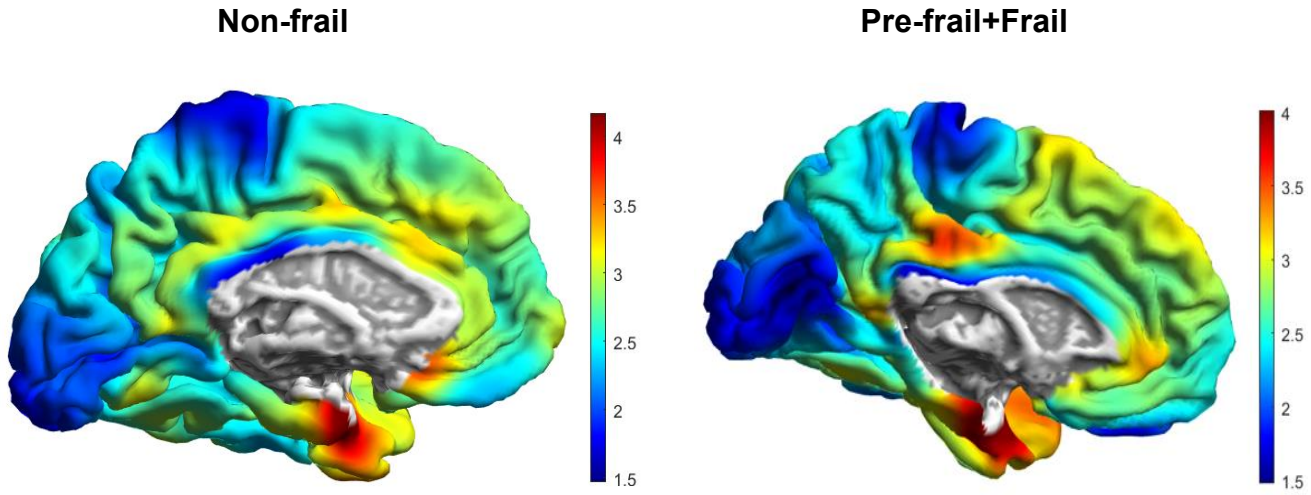

B) Right hemisphere

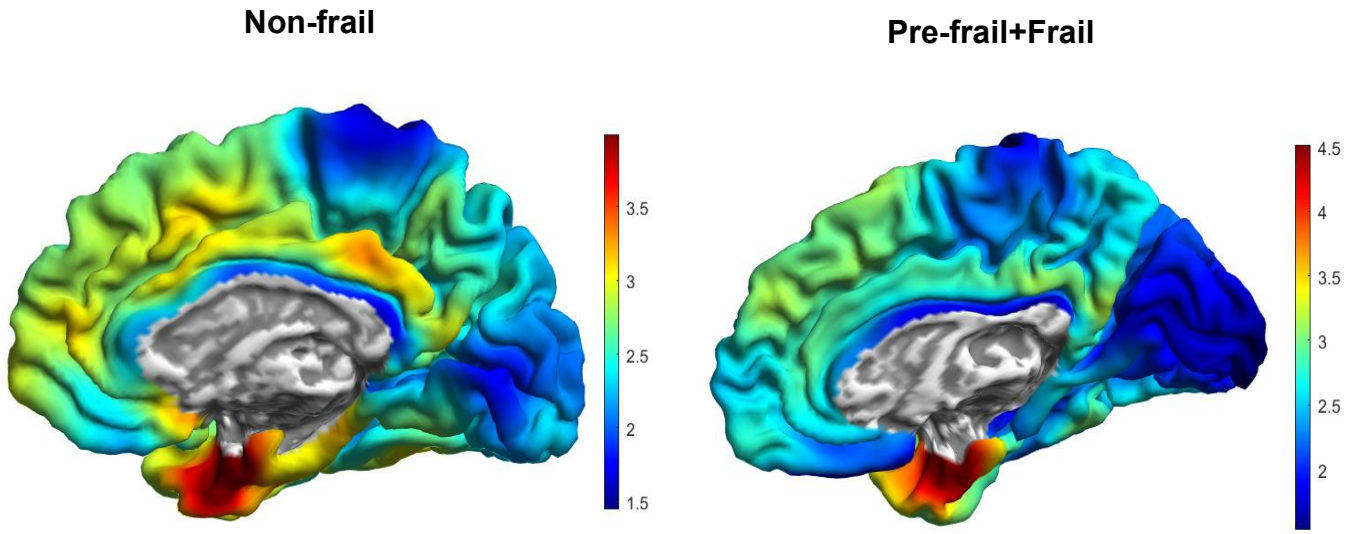

***Figure 5.10**: Mean maps of cortical thickness in the left (A) and right (B) hemispheres of the non-frail group and collapsed pre-frail and frail group. Scale bar denotes cortical thickness in mm.*

Table 5.4: Regions of greater cortical thickness in the collapsed pre-frail and frail group versus the non-frail group. k denotes the number of voxels (i.e. the volume) exhibiting greater cortical thickness in the collapsed pre-frail and frail group. X, Y and Z coordinates refer to Harvard-Oxford Atlas. L = left hemisphere.

Brain region	X (mm)	Y (mm)	Z (mm)	k	P value
L paracingulate gyrus	-11	42	-5	69	P = 0.002

5.3.1.4.2 Brain regional gyrification in non-frail versus the collapsed group of pre-frail and frail

Mean maps of gyrification (degree of folding of sulci and gyri on the cortical surface relative to the absolute mean curvature of the grey matter) in the non-frail group and collapsed pre-frail and frail group are presented in **Figure 5.11 A** (left hemisphere) and **Figure 5.11 B** (right hemisphere). Maps represent gyrification measured in all regions of the cerebral cortex. In the collapsed pre-frail and frail group, significantly greater gyrification was observed in the left angular gyrus (P = 0.001), superior parietal lobule (P = 0.002), middle temporal gyrus (P = 0.005) and right operculum cortex (P = 0.002) compared to the non-frail group (**Table 5.5**). In the non-frail group, significantly greater gyrification was observed in left parahippocampal gyrus (P = 0.002) and right frontal medial cortex (P = 0.002) compared to the collapsed pre-frail and frail group (**Table 5.6**).

A) Left hemisphere

Non-frail **Pre-frail+Frail**

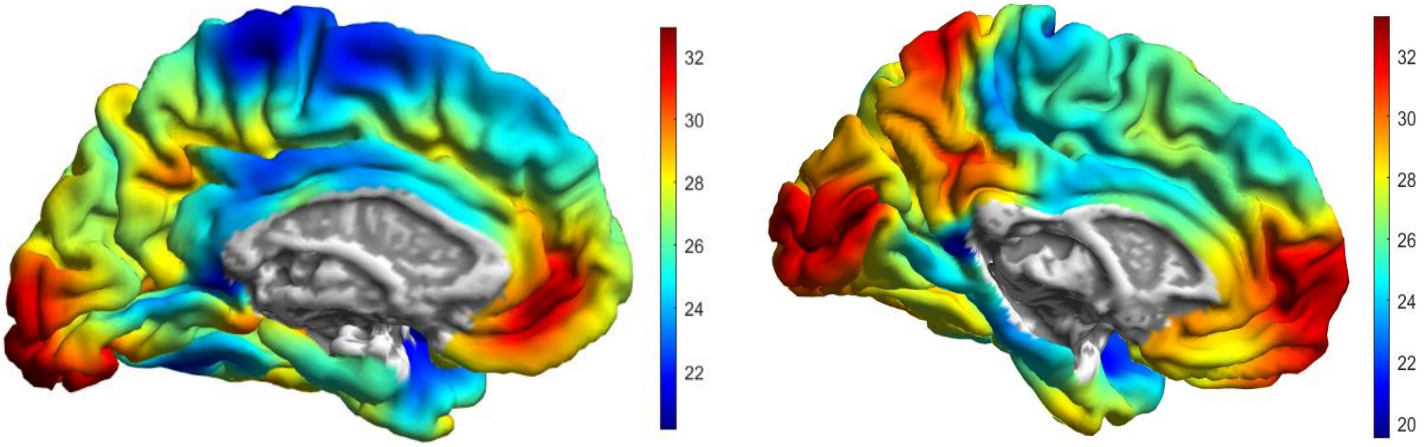

B) Right hemisphere

Non-frail **Pre-frail+Frail**

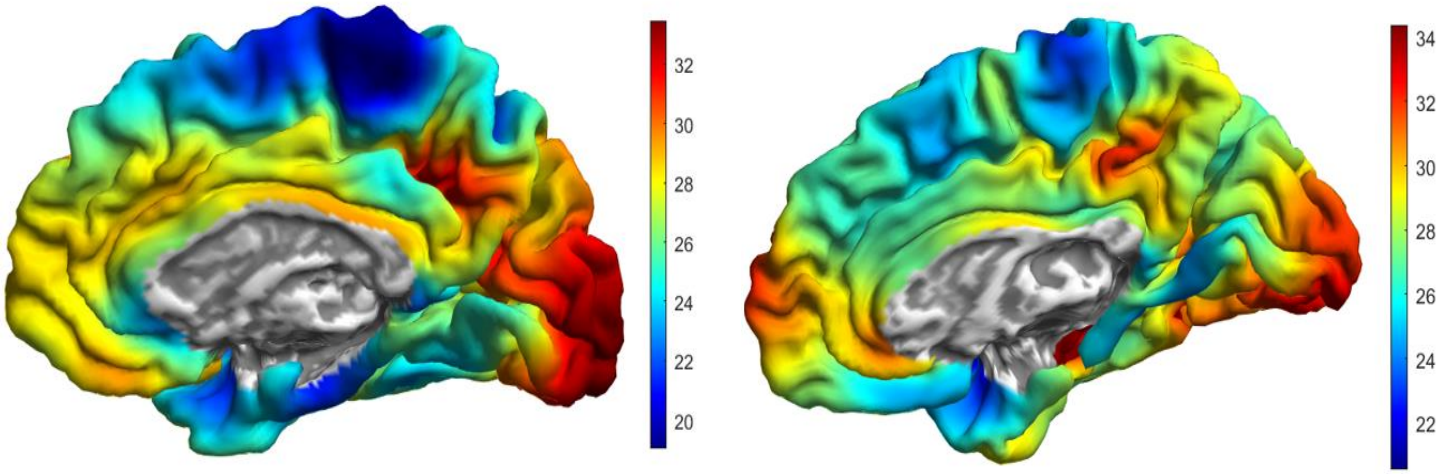

Figure 5.11: Mean maps of gyrification in the left (A) and right (B) hemispheres of the non-frail group and collapsed pre-frail and frail group. Scale bar represents the amount of cortical folding relative to the absolute mean curvature of the grey matter (measured in degrees).

Table 5.5: Regions of greater gyrification in the collapsed pre-frail and frail group versus the non-frail group. X, Y and Z coordinates refer to Harvard-Oxford Atlas. k denotes the number of voxels (i.e. the volume) exhibiting greater gyrification in the collapsed group of pre-frail and frail. L = left, R = right hemisphere.

Brain region	X (mm)	Y (mm)	Z (mm)	k	P value
L angular gyrus	-46	-58	42	162	P = 0.001
L superior parietal lobule	-28	-57	41	154	P = 0.002
L middle temporal gyrus	-50	-42	1	79	P = 0.005
R parietal operculum	49	-30	27	72	P = 0.002

Table 5.6: Regions of greater gyrification in the non-frail group versus collapsed pre-frail and frail group. X, Y and Z coordinates refer to Harvard-Oxford Atlas. k denotes the number of voxels (i.e. the volume) exhibiting greater gyrification in the non-frail group. L = left hemisphere, R = right hemisphere.

Brain region	X (mm)	Y (mm)	Z (mm)	k	P value
L parahippocampal gyrus	-19	-34	-17	165	P = 0.002
R frontal medial cortex	8	34	-12	58	P = 0.002

5.3.1.4.3 Brain regional sulcus depth in non-frail and the collapsed group of pre-frail and frail females

Mean maps of sulcus depth (distance between the cortical surface and the cerebral hull) in the non-frail group and collapsed pre-frail and frail group are presented in **Figure 5.12 A** (left hemisphere) and **Figure 5.12 B** (right hemisphere). Maps represent sulcus depth measured in all regions of the cerebral cortex. Scale bar denotes sulcus depth (measured in mm). In the collapsed pre-frail and frail group, significantly greater sulcus depth was observed in the left frontal operculum cortex (P = 0.001) and middle temporal gyrus (P = 0.002) compared to the non-frail group (**Table 5.7**). In the non-frail group, significantly greater sulcus depth was observed in the left supramarginal gyrus (P = 0.003), precuneus cortex (P = 0.004) and middle frontal gyrus (P = 0.004), and right precentral gyrus (P = 0.001), postcentral gyrus (P = 0.001), parietal operculum cortex (P = 0.003), central operculum cortex (P = 0.009) and cingulate gyrus (P = 0.009) compared to the collapsed group of pre-frail and frail females (**Table 5.8**).

A) Left hemisphere

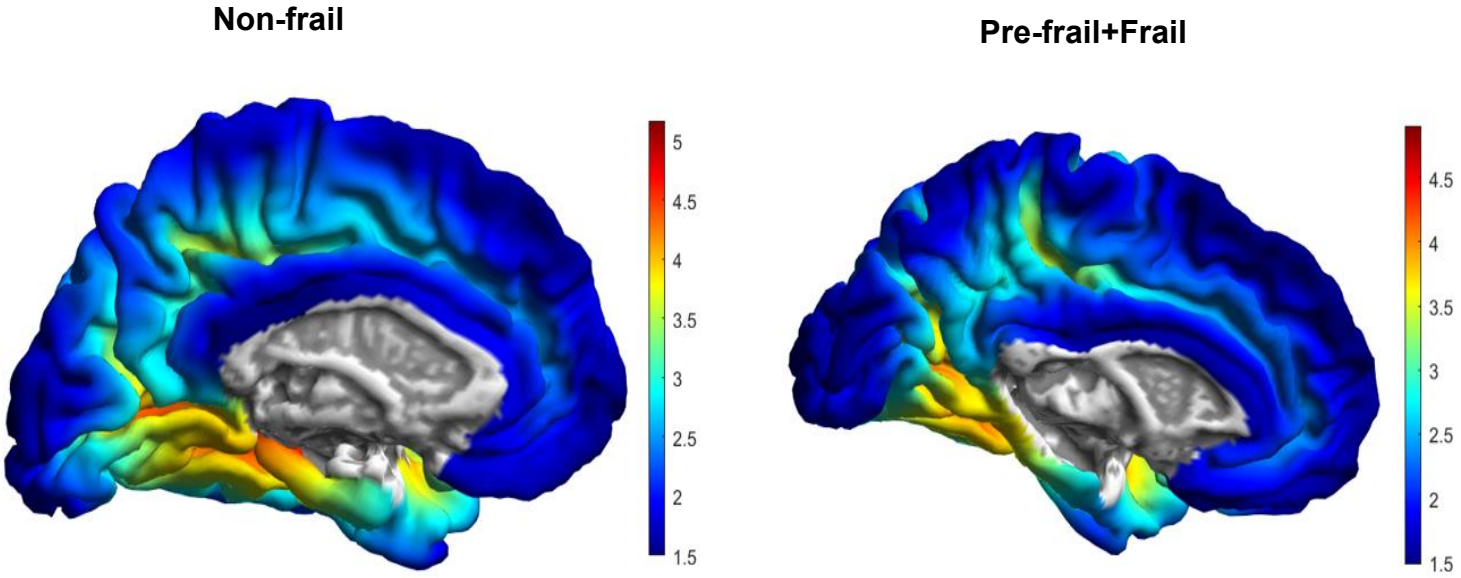

B) Right hemisphere

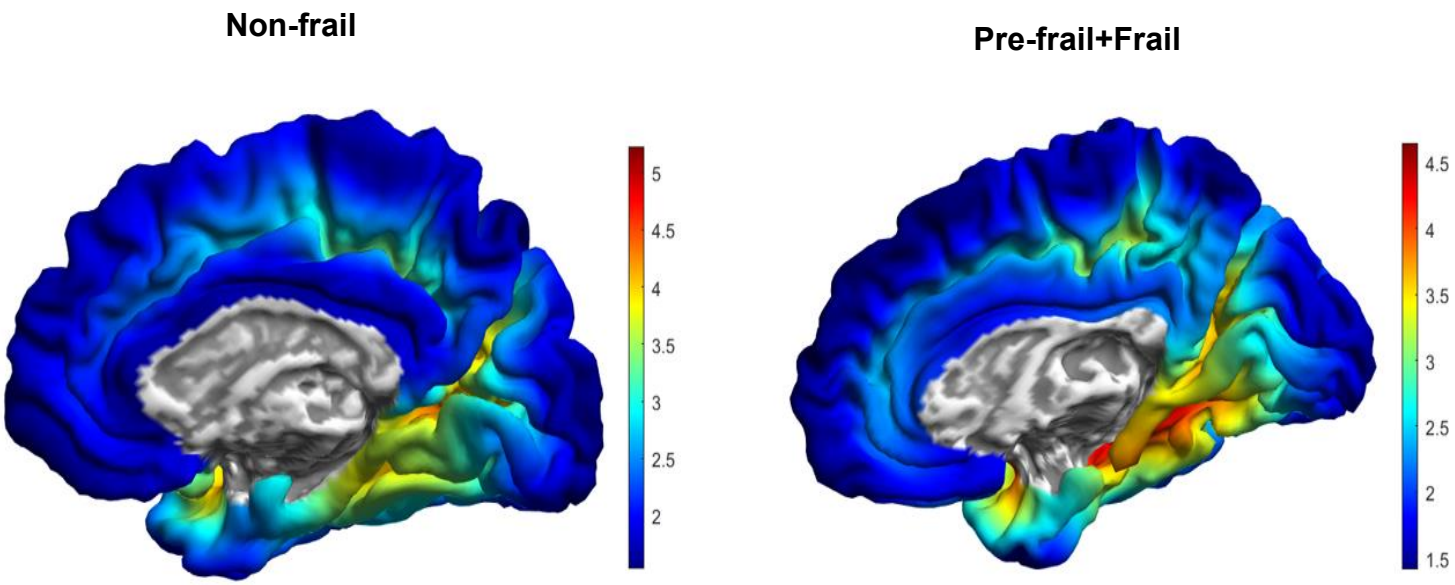

***Figure 5.12**: Mean maps of sulcus depth in the left (A) and right (B) hemispheres of the non-frail group and collapsed group of pre-frail and frail females. Scale bar represents the distance between the cortical surface and the cerebral hull in mm.*

Table 5.7: Regions of greater sulcus depth in the collapsed pre-frail and frail group versus the non-frail group. X, Y and Z coordinates refer to Harvard-Oxford Atlas. k denotes the number of voxels (i.e. the volume) exhibiting greater sulcus depth in the collapsed pre-frail and frail group. L = left hemisphere.

Brain region	X (mm)	Y (mm)	Z (mm)	k	P value
L frontal operculum cortex	-31	62	35	56	P = 0.001
L middle temporal gyrus	-43	12	-1	87	P = 0.002

Table 5.8: Regions of greater sulcus depth in the non-frail group versus collapsed pre-frail and frail group. X, Y and Z coordinates refer to Harvard-Oxford Atlas. k denotes the number of voxels (i.e. the volume) exhibiting greater sulcus depth in the non-frail group. L = left hemisphere, R = right hemisphere.

Brain region	X (mm)	Y (mm)	Z (mm)	k	P value
L supramarginal gyrus	-52	-46	38	137	P = 0.003
L precuneus cortex	-8	-53	15	175	P = 0.004
L middle frontal gyrus	-43	-4	62	138	P = 0.004
R precentral gyrus	45	-7	49	1114	P = 0.001
R postcentral gyrus	20	-42	71	188	P = 0.001
R parietal operculum	41	-35	26	122	P = 0.003
R central operculum cortex	49	-17	21	6	P = 0.009
R cingulate gyrus	9	-48	32	3	P = 0.009

5.3.1.5 Associations between regional brain volumes and physical function

The following section assesses the results of multiple linear regression analyses between regional brain morphometry and physical function measures. The Tables for GM volume, WM volume, cortical gyrification and sulcus depth associations with physical function along with atlas coordinates, T values, k and *P* values, are provided in **Appendix 5.2**. No significant associations were observed between regional cortical thickness and any physical function measures.

5.3.1.5.1 Associations between regional grey matter volumes and physical function

Brain regions exhibiting positive and negative associations between GM volume and each physical function measure are displayed on brain templates in **Figure 5.13**, with tables of significant associations provided in **Appendix 5.2.1**.

5.3.1.5.1.1 Associations between regional grey matter volumes and handgrip strength

Handgrip strength was significantly positively associated with GM volume in 12 brain regions (**Table 5.11**), with the strongest associations observed in the right superior frontal gyrus (T = 4.57, $P < 0.001$; **Table 5.11**), a brain region proposed to be responsible for control of skeletal muscle movement, such as hand motor control [382, 383]. There were no significant negative associations between regional GM volume and handgrip strength.

5.3.1.5.1.2 Associations between regional grey matter volumes and time taken to complete the 4.57m walk test

Time taken to complete the 4.57m walk test was significantly positively associated with GM volume in 5 brain regions (**Table 5.12**), with the strongest association evident in the right hemisphere angular gyrus (T = 3.58, *P* = 0.001; **Table 5.12**), a brain region responsible for number processing and reading comprehension [384]. Time taken to complete the 4.57m walk test was significantly negatively associated with GM volume in 19 brain regions (**Table 5.13**), with the strongest negative association observed in the left hemisphere lateral occipital cortex (T = 5.54, *P* < 0.001; **Table 5.13**), an area involved in object and face recognition [385, 386].

5.3.1.5.1.3 Associations between regional grey matter volumes and knee extensor isometric strength

Knee extensor isometric strength was significantly positively associated with GM volume in 12 brain regions (**Table 5.14**), with the strongest association apparent in the left hemisphere frontal pole (T = 4.51, *P* < 0.001; **Table 5.14**), a region activated during cognitive functions such as planning future actions and analogical reasoning [387, 388].

Knee extensor isometric strength was significantly and negatively associated with GM volume in 7 brain regions (**Table 5.15**), with the strongest negative association being in the left hemisphere inferior frontal gyrus (T = 3.66, *P* = 0.001; **Table 5.15**), an area implicated in inhibition of inappropriate motor responses to stimuli [389].

5.3.1.5.1.4 Associations between regional grey matter volumes and knee extensor work output (60°/s)

Knee extensor work output was significantly positively associated with GM volume in 11 brain regions (**Table 5.16**), the strongest positive association being in the right

hemisphere lateral occipital cortex (T = 4.74, *P* < 0.001; **Table 5.16**), which is known to be involved in object and face recognition [385, 386].

Knee extensor work output was significantly negatively associated with GM volume in 3 brain regions (**Table 5.17**), with the strongest negative association observed in the right hemisphere precentral gyrus (T = 3.88, *P* < 0.001; **Table 5.17**), which is involved in the control of voluntary movement, such as walking [390], knee extension [391] and finger abduction [392].

A) Handgrip strength(kg)

Positive associations

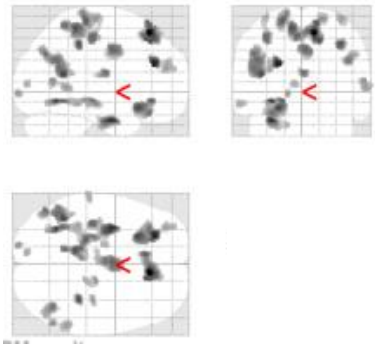

Negative associations

No significant associations

B) Time taken to complete the 4.57m walk (s)

Positive associations

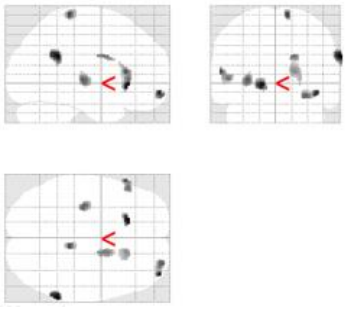

Negative associations

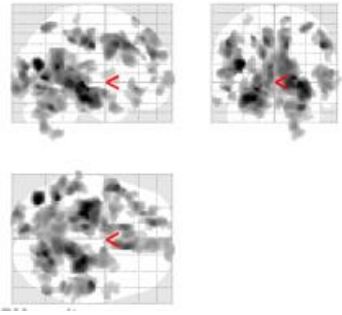

C Isometric strength (Nm)

Positive associations

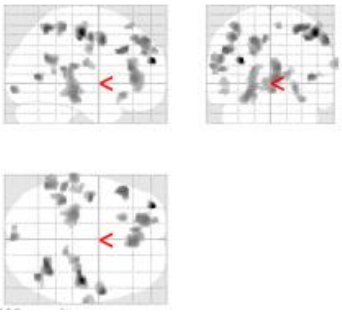

Negative associations

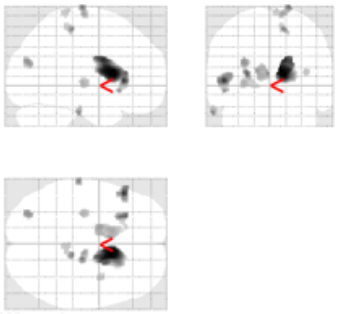

D) Work output (60°/s; J)

Positive associations

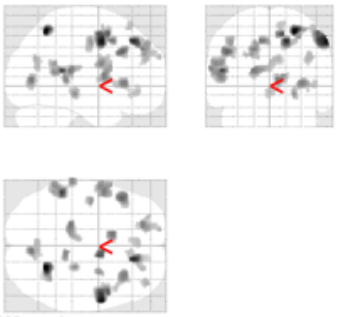

Negative associations

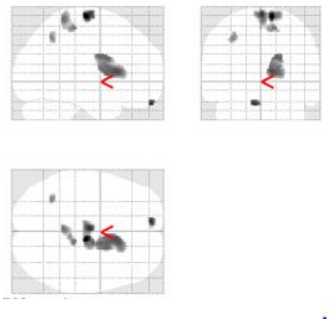

Figure 5.13: *Template brains (in the sagittal, coronal and axial views) highlighting the regions of brain grey matter volume exhibiting significant associations with physical function measures (regions shown with black clusters). Figure shows positive and negative associations between grey matter volume and* ***A)*** *handgrip strength,* ***B)*** *time taken to complete the 4.57m walk,* ***C)*** *knee extensor isometric strength and* ***D)*** *knee extensor work output. Kg = kilograms, s = seconds, Nm = Newton-metres, J = joules.*

5.3.1.5.2 Associations between regional white matter volumes and physical function parameters

The brain regions exhibiting positive and negative associations between WM volume and physical function measures are displayed on brain templates in **Figure 5.14**. and detailed in **Appendix 5.2.2**.

5.3.1.5.2.1 Associations between regional white matter volumes and handgrip strength

Handgrip strength was significantly positively associated with WM volume in 12 brain regions (**Table 5.18**), the strongest positive association observed in the left hemisphere inferior temporal gyrus (T = 5.72, $P < 0.001$; **Table 5.18**), an area proposed to be involved in visual perception [393]. Handgrip strength was significantly negatively associated with WM volume in the left hemisphere inferior temporal gyrus (T = 3.92, $P < 0.001$; **Table 5.19**).

5.3.1.5.2.2 Associations between regional white matter volumes and time taken to complete the 4.57m walk test

There were no significant positive associations between the time taken to complete the 4.57m walk test and regional WM volume, whilst significant negatively associations with WM volume were seen in 15 brain regions (**Table 5.20**). The strongest negative association was in right hemisphere middle temporal gyrus (T = 5.63, $P < 0.001$; **Table 5.20**), an area involved in language processing and object perception [394, 395].

5.3.1.5.2.3 Associations between regional white matter volumes and knee extensor isometric strength

Knee extensor isometric strength was significantly positively associated with WM volume in 13 brain regions (**Table 5.21**), with the strongest positive association apparent in the right hemisphere postcentral gyrus (T = 4.49, *P* < 0.001; **Table 5.21**), which is responsible for perception of somatosensory signals (i.e., proprioception) [396].

Knee extensor isometric strength was significantly negatively associated with WM volume in 6 brain regions (**Table 5.22**), with the strongest negative association observed in the left hemisphere inferior frontal gyrus (T = 3.66, *P* = 0.001; **Table 5.22**), which is implicated in inhibition of inappropriate motor responses to stimuli [389].

5.3.1.5.2.4 Associations between regional white matter volumes and knee extensor work output (60°/s)

Knee extensor work output was significantly positively associated with WM volume in 8 brain regions (**Table 5.23**), with the strongest association apparent in the right hemisphere cingulate gyrus (T = 4.05, *P* < 0.001; **Table 5.23**), an area associated with perception of risk [397] and attention [398]. Knee extensor work output was significantly negatively associated with WM volume in 3 brain regions (**Table 5.24**), with the strongest negative association observed in the left hemisphere cingulate gyrus (T = 4.84, *P* < 0.001; **Table 5.24**), an area involved in motor control and attention [398].

A) Handgrip strength (kg)

Positive associations

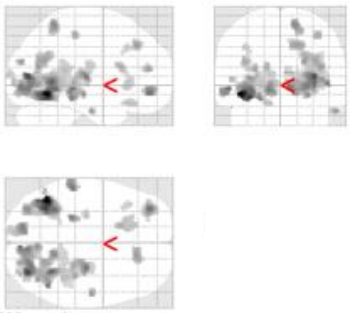

Negative associations

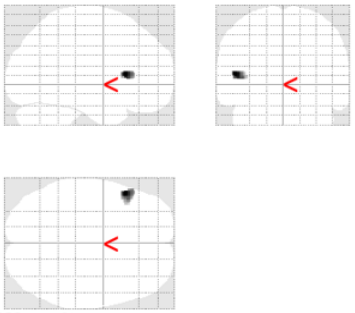

B) Time taken to complete the 4.57m walk (s)

Positive associations

No significant associations

Negative associations

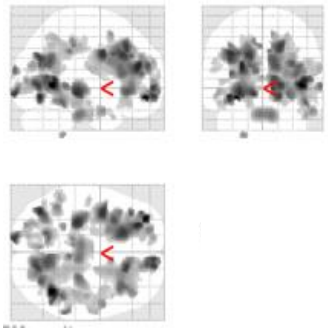

C) Isometric strength (Nm)

Positive associations

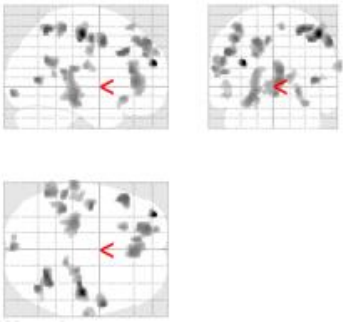

Negative associations

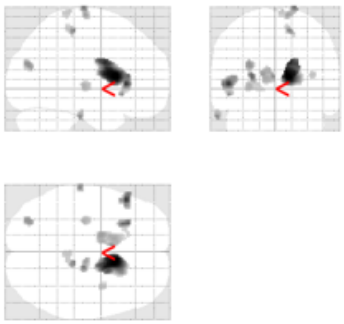

D) Work output (60°/s; J)

Positive associations

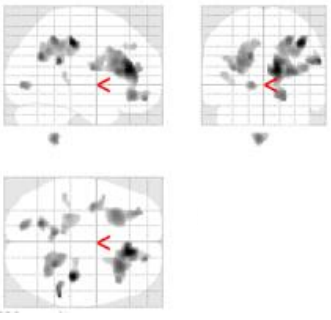

Negative associations

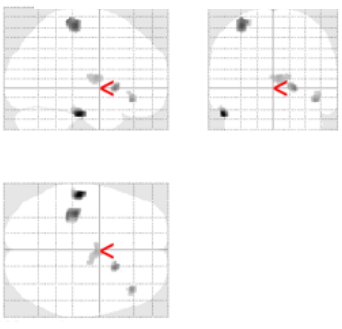

Figure 5.14: *Template brains (in the sagittal, coronal and axial views) highlighting the regions of brain white matter volume exhibiting significant associations with physical function measures (regions shown with black clusters). Figure shows positive and negative associations between white matter volume and* ***A)*** *handgrip strength,* ***B)*** *time taken to complete the 4.57m walk,* ***C)*** *knee extensor isometric strength and* ***D)*** *knee extensor work output. Kg = kilograms, s = seconds, Nm = Newton-metres, J = joules.*

5.3.1.5.3 Associations between regional gyrification and physical function parameters

The brain regions exhibiting positive and negative associations between gyrification and each physical function measure are displayed on brain templates in **Figure 5.15**. All brain regions exhibiting significant positive and negative associations are detailed in **Appendix 5.2.3**.

5.3.1.5.3.1 Associations between regional gyrification and handgrip strength

Handgrip strength was significantly positively associated with gyrification in 6 brain regions (**Table 5.25**), the strongest association observed in the right hemisphere postcentral gyrus (T = 3.67, $P < 0.001$; **Table 5.25**), an area responsible for perception of somatosensory signals (i.e., proprioception) [396]. Handgrip strength was significantly negatively associated with gyrification in 3 brain regions (**Table 5.26**), with the strongest association also observed in the right hemisphere postcentral gyrus (T = 5.37, $P < 0.001$; **Table 5.26**).

5.3.1.5.3.2 Associations between regional gyrification and time taken to complete the 4.57m walk test

Time taken to complete the 4.57m walk test was significantly and positively associated with gyrification in 2 brain regions (**Table 5.27**), with the strongest association evident in the left hemisphere inferior frontal gyrus (T = 3.19, $P = 0.002$; **Table 5.27**), a region implicated in inhibition of inappropriate motor responses to stimuli [389]. Time taken to complete the 4.57m walk test was significantly negatively associated with

gyrification in the right hemisphere cingulate gyrus only (T = 3.00, *P* = 0.003; **Table 5.28**), which is associated with perception of risk [397] and attention [398].

5.3.1.5.3.3 Associations between regional gyrification and knee extensor isometric strength

There were no significant positive associations between knee extensor isometric strength and regional gyrification. Knee extensor isometric strength was significantly negatively associated with gyrification in the right hemisphere postcentral gyrus only (T = 3.25, *P* = 0.002; **Table 5.29**), which is responsible for perception of somatosensory signals (i.e., proprioception) [396].

5.3.1.5.3.4 Associations between regional gyrification and knee extensor work output (60°/s)

There were no significant positive associations between regional gyrification and knee extensor work output. Knee extensor work output was significantly and negatively associated with gyrification in 7 brain regions (**Table 5.30**), with the strongest negative association evident in the right hemisphere precentral gyrus (T = 4.03, *P* < 0.001; **Table 5.30**), a region involved in voluntary movement, such as walking [390], knee extension [391] and finger abduction [392].

A) Handgrip strength (kg)

Positive associations

L hemisphere

R hemisphere

Negative associations

L hemisphere

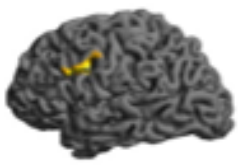

R hemisphere

B) Time taken to complete the 4.57m walk (s)

Positive associations

L hemisphere

R hemisphere

Negative associations

L hemisphere

No significant associations

R hemisphere

C) Isometric strength (Nm)

Positive associations

L hemisphere

No significant associations

R hemisphere

No significant associations

Negative associations

L hemisphere

No significant associations

R hemisphere

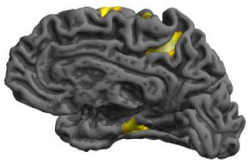

D) Work output (60°/s; J)

Positive associations

L hemisphere

No significant associations

R hemisphere

No significant associations

Negative associations

L hemisphere

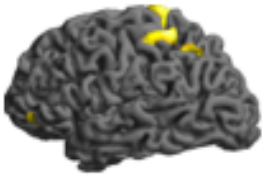

R hemisphere

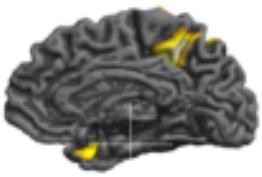

***Figure 5.15**: Template brains (in views of the left and right hemisphere) highlighting the regions of cortical gyrification exhibiting significant associations with physical function measures (regions shown with yellow clusters). Figure shows positive and negative associations between gyrification and **A)** handgrip strength, **B)** time taken to complete the 4.57m walk, **C)** knee extensor isometric strength and **D)** knee extensor work output. Kg = kilograms, s = seconds, Nm = Newton-metres, J = joules.*

5.3.1.5.4 Associations between regional sulcus depth and physical function parameters

The brain regions exhibiting positive and negative associations between sulcus depth and physical function measures are displayed on brain templates in **Figure 5.16** and detailed in **Appendix 5.2.4**.

5.3.1.5.4.1 Associations between regional sulcus depth and handgrip strength

Handgrip strength was significantly positively associated with sulcus depth in 3 brain regions (**Table 5.31**), with the strongest association being in left parietal operculum cortex (T = 3.30, *P* = 0.001; **Table 5.31**), a brain region involved in processing somatosensory information such as the perception of touch [399, 400]. There were no significant negative associations between handgrip strength and sulcus depth.

5.3.1.5.4.2 Associations between regional sulcus depth and time taken to complete the 4.57m walk test

There were no significant negative associations between the time taken to complete the 4.57m walk and sulcus depth. Time taken to complete the 4.57m walk test was significantly negatively associated with sulcus depth in 12 brain regions (**Table 5.32**), with the strongest association evident in the right hemisphere superior frontal gyrus (T = 4.48, *P* < 0.001; **Table 5.32**), which is involved in control of skeletal muscle movement, such as motor control of the hand [382, 383].

5.3.1.5.4.3 Associations between regional sulcus depth and knee extensor isometric strength

Knee extensor isometric strength was significantly positively associated with sulcus depth in 5 brain regions (**Table 5.33**), with the strongest observed in the right hemisphere lateral occipital cortex (T = 3.96, $P < 0.001$; **Table 5.33**), which is involved in object and face recognition [385, 386]. Knee extensor isometric strength was significantly negatively associated with gyrification in the left hemisphere angular gyrus only (T = 3.68, $P = 0.001$; **Table 5.34**), which is responsible for visual processing [384].

5.3.1.5.4.4 Associations between regional sulcus depth and knee extensor work output (60°/s)

Knee extensor work output was significantly positively associated with sulcus depth in 7 brain regions (**Table 5.35**), with the strongest association evident in the left hemisphere supramarginal gyrus (T = 4.06, $P < 0.001$; **Table 5.35**), which is involved in word processing [401]. There were no significant negative associations between knee extensor work output and regional sulcus depth.

A) Handgrip strength (kg)

Positive associations		Negative associations	
L hemisphere	R hemisphere	L hemisphere	R hemisphere
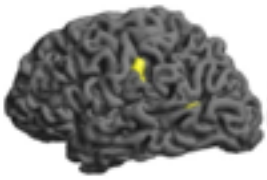		No significant associations	No significant associations

B) Time taken to complete the 4.57m walk (s)

Positive associations		Negative associations	
L hemisphere	R hemisphere	L hemisphere	R hemisphere
No significant associations	No significant associations	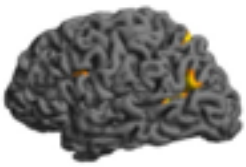	

C) Isometric strength (Nm)

Positive associations		Negative associations	
L hemisphere	R hemisphere	L hemisphere	R hemisphere
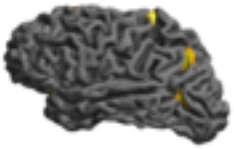	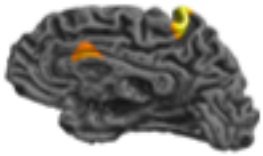	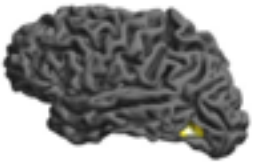	No significant associations

D) Work output (60°/s; J)

Positive associations		Negative associations	
L hemisphere	R hemisphere	L hemisphere	R hemisphere
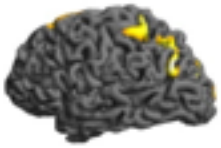		No significant associations	No significant associations

Figure 5.16: *Template brains (in views of the left and right hemisphere) highlighting the regions of sulcus depth exhibiting significant associations with physical function measures (regions shown with yellow clusters). Figure shows positive and negative associations between sulcus depth and* ***A)*** *handgrip strength,* ***B)*** *time taken to complete the 4.57m walk,* ***C)*** *knee extensor isometric strength and* ***D)*** *knee extensor work output. Kg = kilograms, s = seconds, Nm = Newton-metres, J = joules.*

5.3.1.6 White matter hyperintensity (WMH) volume in non-frail, pre-frail and frail females

Absolute WMH volume was significantly greater in the pre-frail (13.1 ± 15.8 cm^3) and frail (24.4 ± 19.2 cm^3) volunteers versus the non-frail volunteers (P = 0.024 and P = 0.017, respectively). No differences were apparent when comparing pre-frail and frail females (**Figure 5.17 A**). Relative WMH volume (normalised to TIV) was also significantly greater in the pre-frail (0.99 ± 1.21 %) and frail (1.84 ± 1.43 %) females in comparison to non-frail counterparts (P = 0.031 and P = 0.013, respectively). No differences were observed between the pre-frail and frail groups (**Figure 5.17 B**).

5.3.1.7 White matter hyperintensity volume in non-frail versus the collapsed group of pre-frail and frail females

The collapsed group of pre-frail and frail females also exhibited significantly greater absolute WMH volume compared to the non-frail group (16.0 ± 17.0 cm^3 vs 3.3 ± 2.1 cm^3; P < 0.001; **Figure 5.17 C**). Similarly, significantly greater relative WMH volume was also observed in the collapsed group of pre-frail and frail females versus the non-frail group (1.20 ± 1.29 % vs 0.25 ± 0.15 %; P < 0.001; **Figure 5.17 D**).

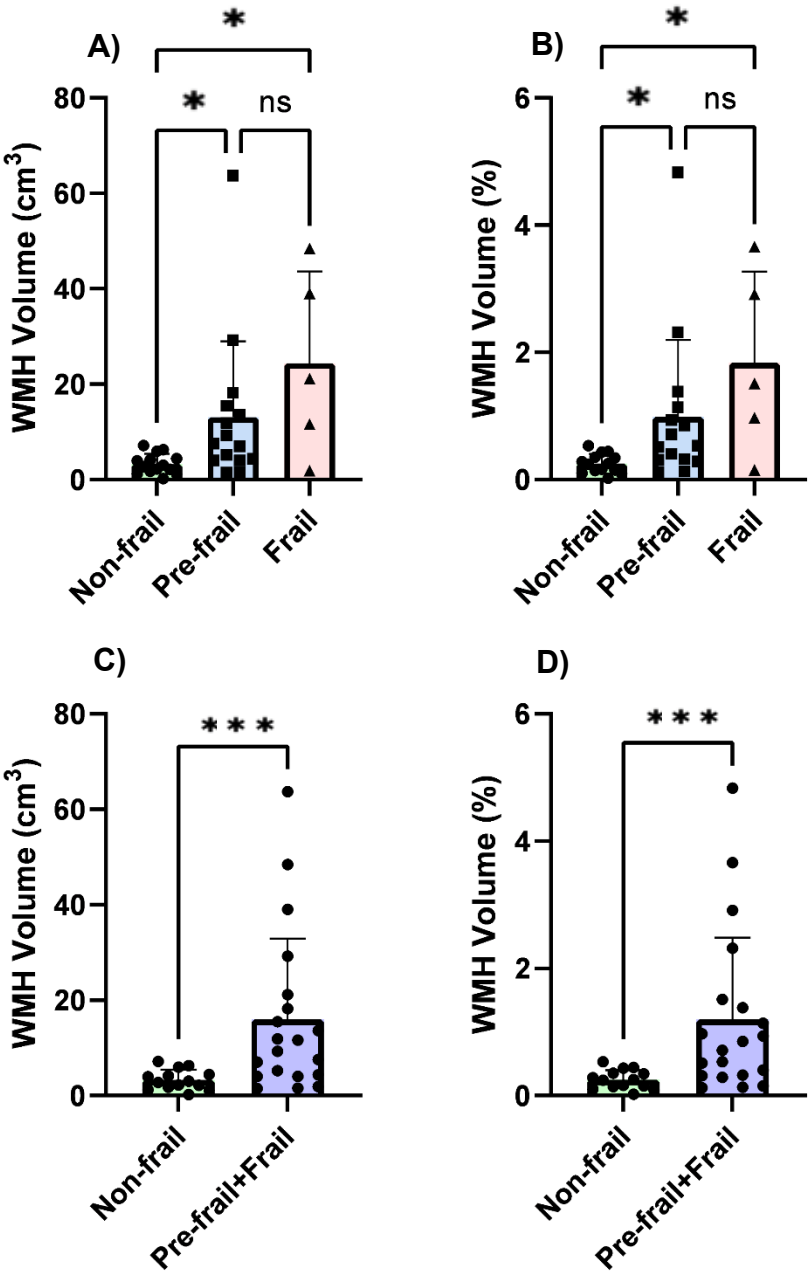

Figure 5.17: *Absolute (**A**) and relative (normalised to TIV; **B**) white matter hyperintensity (WMH) volume in non-frail versus the collapsed group of pre-frail and frail females. Absolute (**C**) and relative (**D**) WMH volume in non-frail versus the collapsed group of pre-frail and frail females. Values are mean ± standard deviation and individual values. * = P < 0.05; *** = P < 0.001.*

5.3.2 Resting state functional measures of brain vascular haemodynamics and fractional oxygen extraction

5.3.2.1 Cerebral artery cross-sectional area (CSA) in non-frail, pre-frail and frail females and in the non-frail versus the collapsed group of pre-frail and frail females

There were no significant differences in CSA of any cerebral artery when comparing non-frail, pre-frail and frail females, or when comparing non-frail to the collapsed group of pre-frail and frail females (**Table 5.9**).

Table 5.9: Cross-sectional area (CSA) of the left and right carotid and basilar arteries in non-frail, pre-frail, frail and collapsed group of pre-frail and frail females. No significant differences evident in cerebral artery CSA between groups.

Cerebral artery	Non-frail	Pre-frail	Frail	Pre-frail + Frail
Left carotid CSA (mm^2)	13.0 ± 3.5	11.1 ± 3.9	12.5 ± 2.1	11.5 ± 3.6
Right carotid CSA (mm^2)	12.1 ± 2.9	12.7 ± 4.8	14.1 ± 2.6	13.1 ± 4.3
Basilar CSA (mm^2)	5.9 ± 2.0	6.6 ± 2.6	6.9 ± 2.3	6.7 ± 2.5

5.3.2.2 Cerebral artery blood velocity and flow in non-frail, pre-frail and frail females

There were no significant differences in mean blood velocity between non-frail (22.3 ± 5.2 cm/s), pre-frail (19.6 ± 5.4 cm/s) and frail (18.0 ± 4.3 cm/s) volunteers (**Figure 5.18 A**). No differences were evident between non-frail (401 ± 115 ml/min), pre-frail (339 ± 96 ml/min) and frail (363 ± 80 ml/min) females in resting state cerebral blood flow (**Figure 5.18 B**). Similarly, the rate of gmCBF was no different between non-frail (42.4 ± 13.8 ml/100g/min), pre-frail (36.9 ± 10.2 ml/100g/min) and frail (42.5 ± 7.5 ml/100g/min) volunteers at rest (**Figure 5.18 C**)

5.3.2.3 Cerebral artery blood velocity and flow in non-frail versus the collapsed group of pre-frail and frail females

There was a trend for greater mean blood velocity in the non-frail group versus the collapsed group of pre-frail and frail volunteers (22.3 ± 5.2 cm/s vs 19.2 ± 5.1 cm/s; *P* = 0.053; **Figure 5.19 A**). However, there were no differences in resting state cerebral blood flow when comparing the non-frail group and collapsed group of pre-frail and frail females (**Figure 5.19 B**). The rate of gmCBF was also no different between the non-frail group and the collapsed group of pre-frail and frail females at rest (**Figure 5.19 C**).

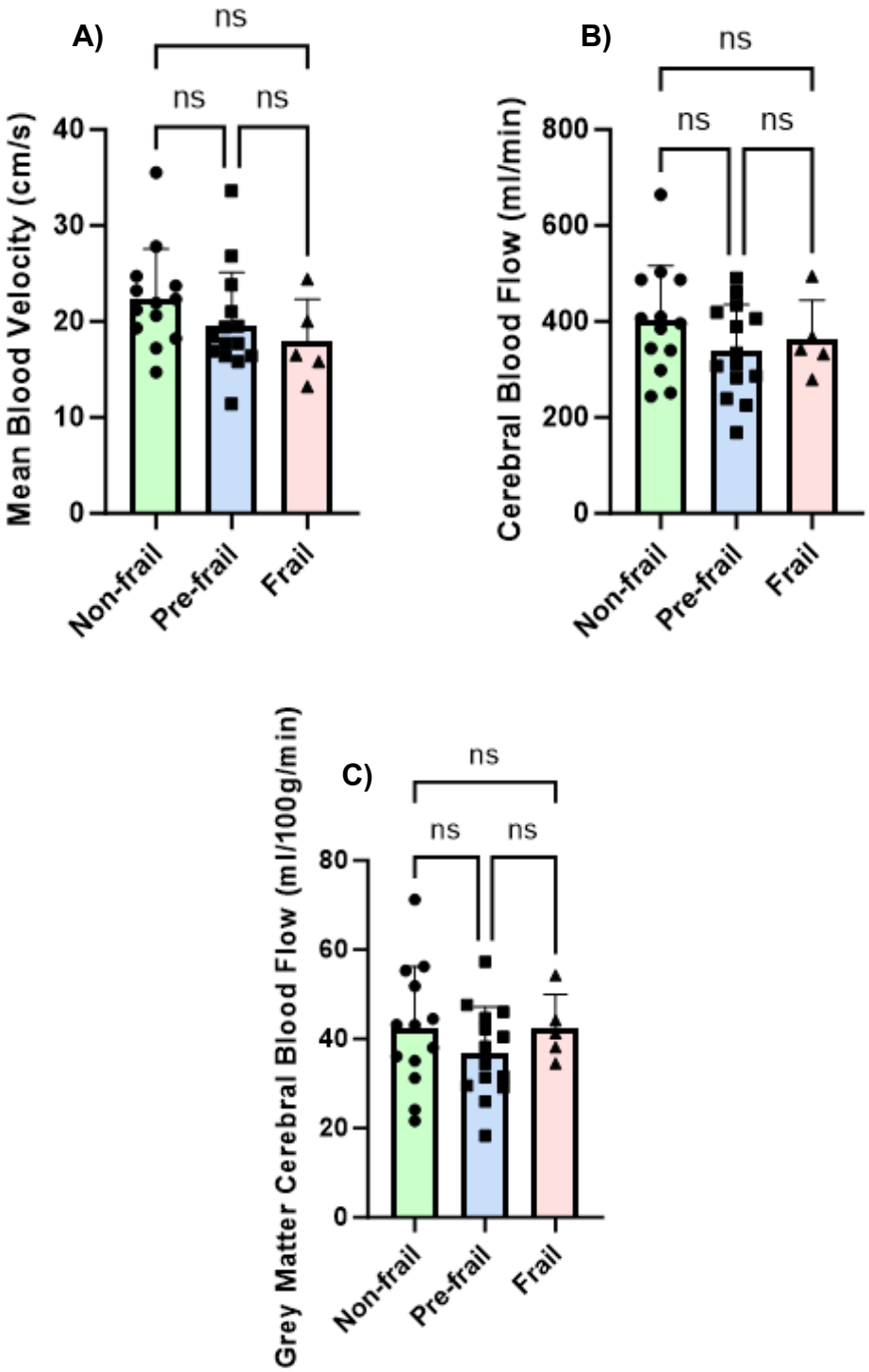

Figure 5.18: *Mean blood velocity (**A**), cerebral blood flow (**B**) and grey matter corrected cerebral blood flow (**C**) of cerebral arteries in non-frail, pre-frail and frail females. Values are mean ± standard deviation and individual values.*

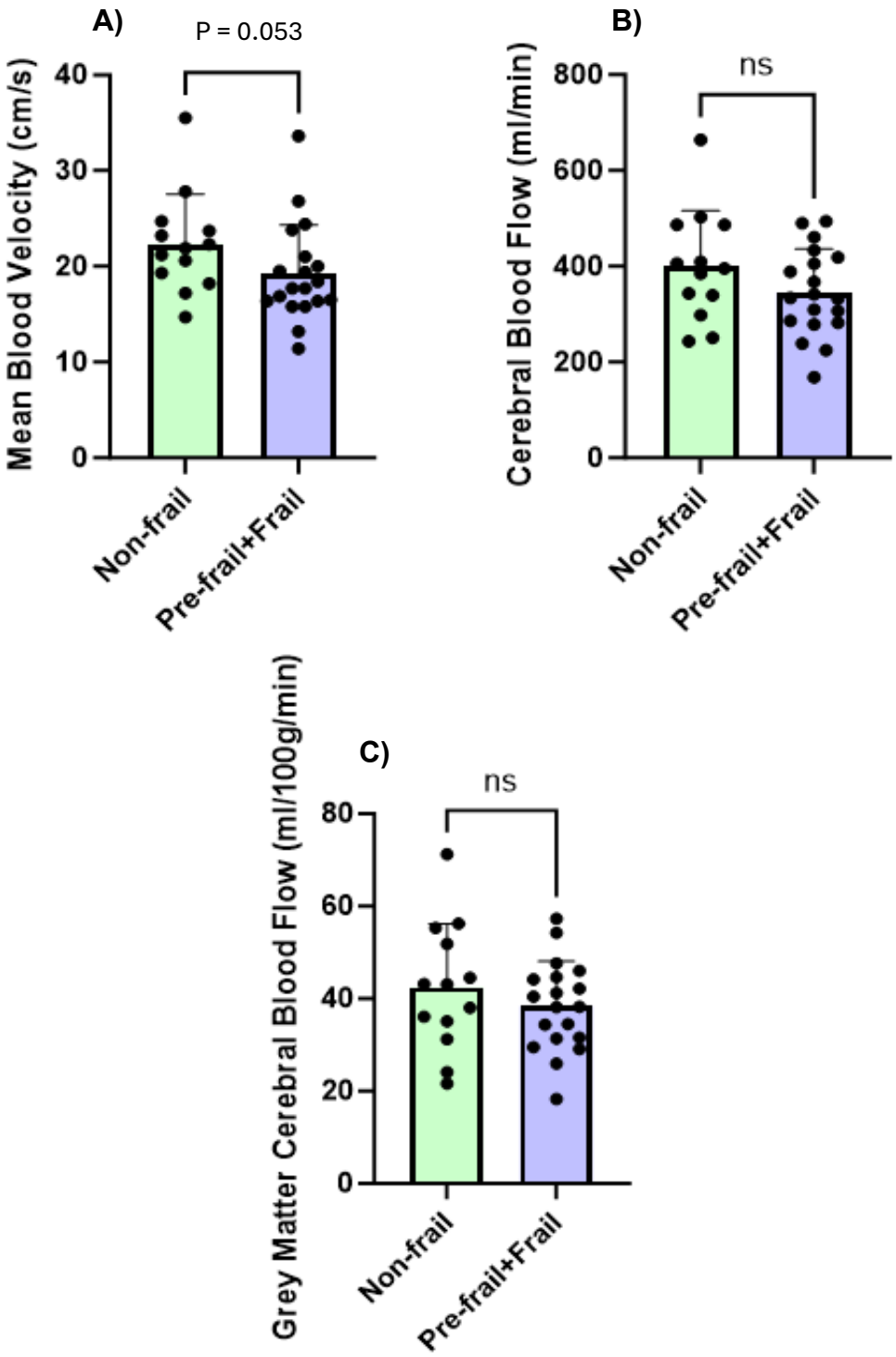

Figure 5.19: *Mean blood velocity (**A**), cerebral blood flow (**B**) and grey matter corrected cerebral blood flow (**C**) of cerebral arteries in non-frail versus the collapsed group of pre-frail and frail females. Values are mean ± standard deviation and individual values.*

5.3.2.4 Resting state venous oxygenation, cerebral oxygen extraction fraction and metabolic rate of oxygen in non-frail, pre-frail and frail females

Venous oxygenation was not different between non-frail (57.9 ± 5.4 %), pre-frail (54.9 ± 7.3 %) and frail (54.0 ± 2.5 %; **Figure 5.20 A**). Similarly, there were no differences in OEF between non-frail (39.3 ± 5.5 %), pre-frail (42.1 ± 7.3%) and frail (43.0 ± 2.6 %) volunteers (**Figure 5.20 B**). There were also no significant differences in gm$CMRO_2$ between non-frail (142 ± 39 μmol/g/min), pre-frail (129 ± 35 μmol/g/min) and frail (153 ± 35 μmol/g/min) volunteers (**Figure 5.20 C**).

5.3.2.5 Resting state venous oxygenation, cerebral oxygen extraction fraction and metabolic rate of oxygen in non-frail, pre-frail and frail females

No differences in venous oxygenation were evident between the non-frail group (57.9 ± 5.4 %) and the collapsed group of pre-frail and frail females (54.7 ± 6.4 %; **Figure 5.21 A**). OEF was also no different when comparing the non-frail group (39.3 ± 5.5 %) and the collapsed group of pre-frail and frail females (42.3 ± 6.4 %; **Figure 5.21 B**). Similarly, there were no significant differences in $CMRO_2$ between the non-frail group (142 ± 39 μmol/g/min) and the collapsed group of pre-frail and frail females (136 ± 35 μmol/g/min; **Figure 5.21 C**).

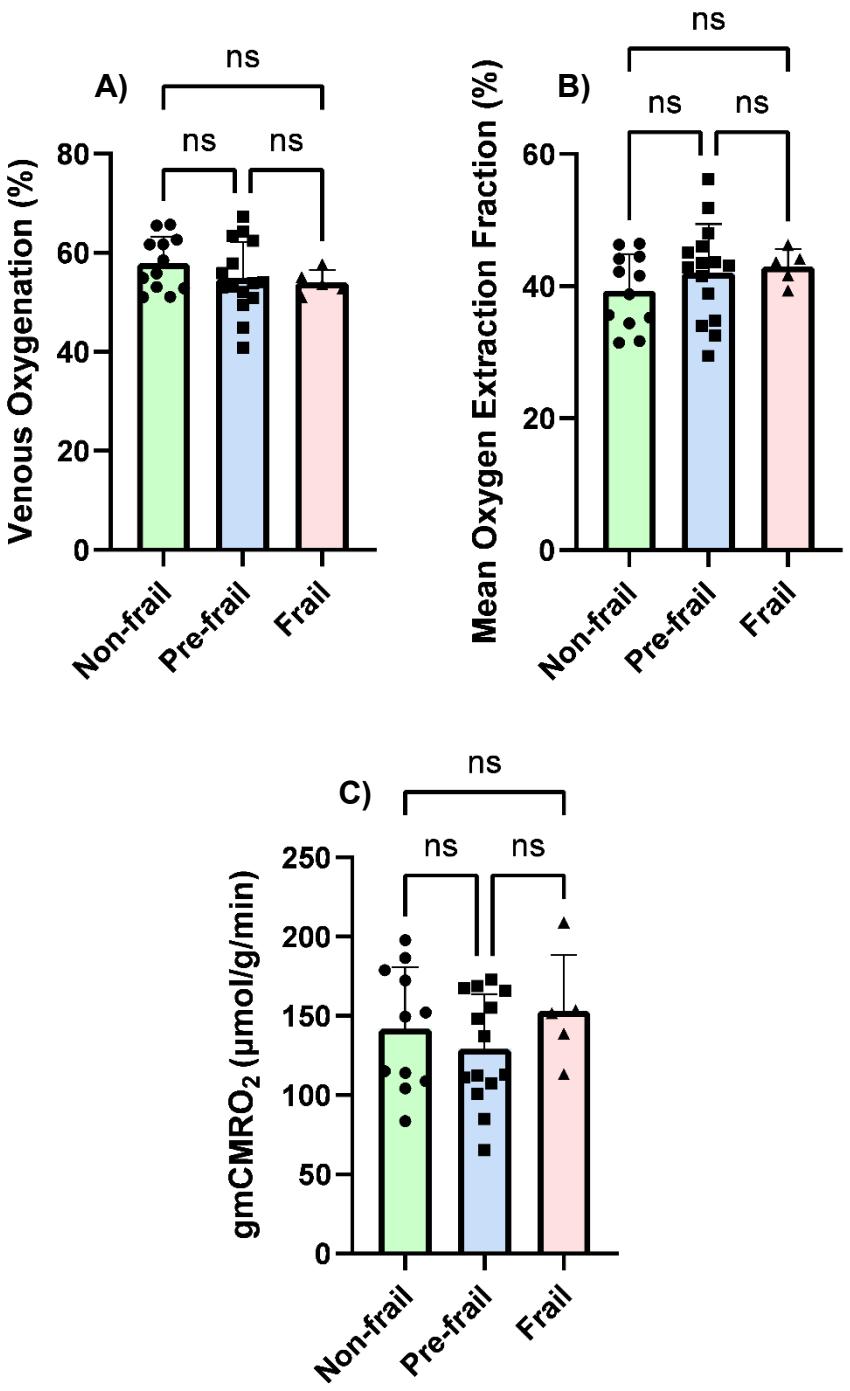

Figure 5.20: *Venous oxygenation (**A**), oxygen extraction fraction (OEF) (**B**) and grey matter corrected cerebral metabolic rate of oxygen (gmCMRO$_2$) (**C**) in non-frail, pre-frail and frail females. Values are mean ± standard deviation and individual values.*

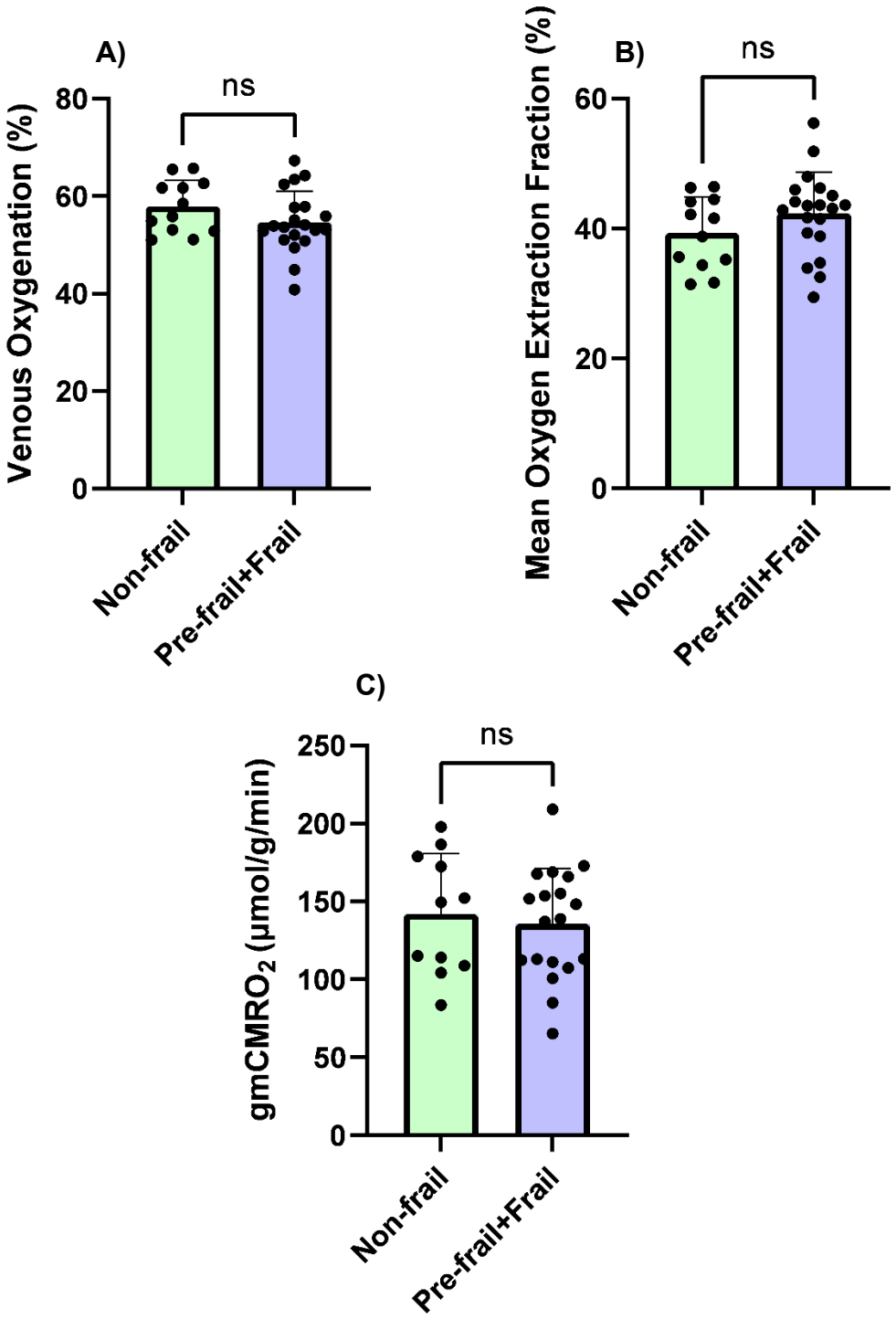

***Figure 5.21**: Venous oxygenation (**A**), oxygen extraction fraction (OEF) (**B**) and grey matter corrected cerebral metabolic rate of oxygen (gmCMRO$_2$) (**C**) in non-frail versus the collapsed group of pre-frail and frail females. Values are mean ± standard deviation and individual values.*

5.4 Discussion

This study shows that lower global and regional GM volumes and greater WMH volume is observed in frail compared to non-frail individuals [118, 123, 143]. However, this study also provides novel evidence of lower regional WM volumes and differences in regional gyrification and sulcus depth in pre-frail and frail versus non-frail females, indicating WM atrophy and changes in the cortical surface are features of the frailty phenotype. Furthermore, these differences in brain morphometry were significantly associated with handgrip strength, walking speed, and knee extensor strength and work output (fatigability), suggesting changes in brain morphometry during the trajectory to frailty are linked to the deficits in physical function that manifest. Finally, despite a trend for lower cerebral artery blood velocity in the collapsed pre-frail and frail group, CBF, OEF and $CMRO_2$ were found to be no different between non-frail, pre-frail, frail and the collapsed pre-frail and frail groups, indicating frailty is not associated with differences in cerebral haemodynamics.

5.4.1 Global brain volumes and WMH volume

The findings of lower global GM volume (**Figure 5.6 B**) and greater WMH volume (**Figure 5.17**) in frail compared to non-frail females are in agreement with previous literature [118, 123], reinforcing that GM atrophy and greater volume of WM lesions are features of the frailty phenotype. The present study observed lower global WM volume in the pre-frail and frail groups versus the non-frail group (**Figure 5.6 C**), whilst published research has reported no differences between non-frail, pre-frail and frail states [116, 118]. One reason for this discrepancy could be the mixed sex sample adopted in prior published studies, which may have increased data variance associated with sex-related differences in global brain volumes [122].

5.4.2 Regional grey matter and white matter volume

When considering the collapsed group of pre-frail and frail females versus the non-frail volunteers, lower GM volume was observed in 13 brain regions (**Table 5.2**) and lower WM volume was evident in 18 brain regions (**Table 5.3**). These findings point to regional atrophy of GM and WM as features of the frailty phenotype. The greatest differences in GM and WM volume between groups were observed in the postcentral gyrus, frontal pole, occipital fusiform gyrus and lateral occipital cortex ($P < 0.001$). In keeping with these observations, negative associations between frailty severity and GM volume were identified in 75 brain regions, including some of the same brain regions as the present study, such as the postcentral gyrus (Cohen's $d = -0.049$; $P < 0.001$) and occipital fusiform gyrus (Cohen's $d = -0.043$; $P < 0.001$), in a sample of over 40,000 individuals in the UK Biobank [123].

In the present study, the collapsed group of pre-frail and frail females exhibited lower GM and WM volume in several regions involved in cognition, such as the frontal pole and lateral occipital cortex, compared to the non-frail group (**Table 5.2, Table 5.3**). The frontal pole is an area important for cognitive functions such as attention and memory [402], and the lateral occipital cortex is important for face and object recognition, through the processing of visual information [403]. In a 3-year longitudinal study, older individuals who experienced cognitive decline in this period also exhibited greater GM atrophy of the frontal pole ($t = 3.99$; $P < 0.04$) compared to counterparts who experienced no cognitive decline [404]. Further, lower GM volume of the lateral occipital cortex has been shown to be associated with cognitive impairment ($t = 5.95$; $P < 0.05$) in Parkinson's Disease patients [405]. Interestingly, lower GM volume in the lateral occipital cortex was also associated with greater frailty severity ($t = 4.2$; $P < 0.05$) in this prior study [405]. Taken together, these findings suggest that GM atrophy

of the frontal pole and lateral occipital cortex may be related to cognitive impairment in frailty.

The findings of lower GM and WM volume of the postcentral gyrus in the collapsed pre-frail and frail group (**Table 5.2, Table 5.3**) are important as this region is responsible for the processing of somatosensory signals (i.e., proprioception) [406]. Previous work has reported a negative correlation between GM volume of the postcentral gyrus and time taken to complete the Four Square Step Test ($r = -0.40$; $P < 0.05$) in older individuals [407]. The Four-Square Step Test is a measure of balance and proprioception, with lower scores reflecting better performance, suggesting greater postcentral gyrus GM volume is associated with better proprioception and balance. Therefore, the atrophy of the postcentral gyrus in the collapsed pre-frail and frail group versus the non-frail group evidenced in the present study may be related to lower proprioceptive performance. In this way, lower performance on measures of proprioception has been demonstrated in frail versus non-frail adults in previous studies [408]. However, the associations between proprioceptive performance and GM/WM volume of the postcentral gyrus have not been explored [408], and this may be an interesting area for further research. A potential mechanism by which atrophy of the postcentral gyrus contributes to lower proprioception is through the loss of dopamine receptors and lower dopamine transmission. Dopamine is a key neurotransmitter involved in chemical signalling within the brain and studies have reported lower dopamine receptor availability of the postcentral gyrus in older versus young adults [409]. Furthermore, lower synaptic dopamine transmission in the ventral striatum has been associated with greater anterior-posterior body sway (indicating poorer balance and proprioception) ($R^2 = 0.25$; $P < 0.01$) in older adults [410].

This is the first study to assess WM regional volumes in the context of frailty. WM is primarily composed of myelinated axons which are fundamental for the transmission of electrical signals across different brain regions [120]. Therefore, lower regional WM volumes in the collapsed pre-frail and frail group (**Table 5.3**) may reflect important differences in structural and neurological function. WM atrophy has been linked to cognitive impairment, as individuals with lower WM volume have been shown to exhibit poorer performance in a processing speed task (a measure of cognitive ability quantifying how quickly an individual executes cognitive tasks) compared to individuals with greater WM volume [411]. Performance on processing speed tasks has also been shown to be worse in pre-frail and frail versus non-frail individuals [138], which may therefore be related to lower WM volume, particularly as the present study demonstrated differences in WM volume in brain regions responsible for cognitive processes, such as the frontal pole and lateral occipital cortex, in pre-frail and frail volunteers versus non-frail individuals (**Table 5.3**). Furthermore, WM volume has been correlated with measures of WM microstructure, such as fractional anisotropy ($F > 19.96$; $P < 0.05$), and the loss of WM microstructural integrity during ageing may (at least partially) be explained by loss of WM volume [367]. Therefore, the evidenced regional WM atrophy in the collapsed pre-frail and frail group versus the non-frail group in the present study may indicate a loss of WM microstructural integrity. Impaired WM microstructural integrity has been shown in frail versus non-frail individuals in previous studies using DTI measures [151, 366], however the influence of WM volume differences within these relationships has not been explored. As outlined in Chapter Two – Section 2.8.9, DTI measures were acquired in the present study to assess WM microstructure properties, but were not analysed in this thesis. Therefore, future

analysis of DTI WM microstructural integrity will provide insight into these relationships.

The causes of lower regional GM and WM volumes in frail versus non-frail individuals are poorly understood. However, some insight into mechanisms of regional brain atrophy can be inferred from studies of ageing. In previous work adopting assessments of regional brain blood flow, age has been negatively correlated with CBF in several brain regions, including the middle frontal gyrus ($r = -0.56$; $P < 0.01$) [412], which is a brain region that also exhibited lower GM and WM volumes in the collapsed pre-frail and frail group versus the non-frail group in the present study (**Table 5.3**). Lower regional CBF following bilateral occlusion of the cerebral arteries in rats has been associated with increased protein expression of encephalitogenic peptide, a demyelination marker [413]. Another mechanism may be related to lower elasticity of arteries within the brain. Using MRI and diffuse optical tomography, Chiarelli et al., [414] demonstrated lower regional cortical volume and arterial elasticity in older versus younger individuals, and the brain regions exhibiting lower cortical volume were positively correlated with regions of lower arterial elasticity ($r = 0.33$; $P = 0.017$). Whether regional differences in CBF and/or arterial elasticity contribute to regional brain atrophy in frailty is yet to be determined.

5.4.3 Regional cortical thickness, gyrification and sulcus depth

Greater cortical thickness in the paracingulate gyrus was found in the collapsed group of pre-frail and frail volunteers versus the non-frail participants in this study (**Table 5.4**). In contrast, a previous report has shown lower cortical thickness in the frontal lobe (the area of the brain in which the paracingulate gyrus is located) of pre-frail versus non-frail individuals [132]. However, this prior work did not perform analysis of sub-

structures within the frontal lobe to quantify cortical thickness of the paracingulate gyrus specifically [132]. This point aside, the paracingulate gyrus is part of the anterior cingulate cortex, which is considered to be responsible for cognitive processes such as decision making and motivation [415, 416], and regional cortical thinning has been linked with cognitive decline, in an 8 year longitudinal study [131]. These authors reported greater cortical thinning in cognitively impaired older adults in regions such as the parahippocampal gyrus ($t = 3.99$; $P < 0.0001$) and insula ($t = 4.31$; $P < 0.0001$) when compared to healthy controls [131], which differs from the greater cortical thickness in the paracingulate gyrus in the collapsed group of pre-frail and frail females of this study. However, the paracingulate gyrus has been shown to exhibit a high degree of morphological interindividual variability in size [417], with previous research reporting that the length of this region can vary between < 20 mm in some individuals and > 40 mm in others [418]. These interindividual differences may contribute to the divergence in findings reported here.

This study represents the first investigation of cortical gyrification and sulcus depth in the trajectory to frailty. Gyrification refers to the amount cortical surface folding, which is proposed to occur to increase the cortical surface area within the confines of the skull, thus increasing the number of neurons and neuronal connectivity [133]. As such, gyrification has been strongly correlated with cortical surface area ($r = 0.92$; $P < 0.001$) [134]. Studies have demonstrated an inverse association between age and regional gyrification in regions such as the pre-frontal cortex ($r = -0.13$; $P = 0.0004$) and negative associations between regional gyrification and cognitive function ($r = -0.13$; $P < 0.0003$) [135]. Lower gyrification was observed in the parahippocampal gyrus and frontal medial cortex in the collapsed pre-frail and frail volunteers versus the non-frail volunteers in the present study (**Table 5.6**), which are brain regions involved in

memory and cognition. Whilst these findings may reflect impaired cognitive ability in frail individuals [138], associations between cognitive function and gyrification have not been fully explored in the context of frailty. Interestingly, greater gyrification was observed in the angular and middle temporal gyrus of the collapsed pre-frail and frail volunteers versus the non-frail volunteers in the current study (**Table 5.5**), which may reflect greater cortical surface area in this region. Given global and regional gyrification has been reported to decline with age [419], these findings of greater regional gyrification may seem difficult to rationalise. However, greater gyrification in regions such as the prefrontal cortex, despite lower gyrification in other brain regions, has been reported in older versus young individuals [419] and may be related to the greater rate of WM versus GM atrophy in older adults [420]. In essence, given the majority of WM is evident in subcortical regions, greater atrophy of WM may cause the cortical surface (i.e., the GM) to buckle and thus increase gyrification.

Studies of ageing have highlighted lower sulcus depth (i.e., shallower sulci) in older versus middle aged individuals in cross-sectional studies [421], and a reduction in sulcus depth of the parieto-occipital region in a 5-year longitudinal study of older adults [136]. Similarly to gyrification, deeper sulci are postulated to improve neuronal connectivity through increased cortical surface area [133]. In the present study, lower sulcus depth was observed in several brain regions in the collapsed pre-frail and frail group versus the non-frail group, with the greatest differences in sulcal depth observed in the postcentral and precentral gyrus (**Table 5.8**). The postcentral gyrus contains the primary somatosensory cortex which is responsible for processing proprioceptive signals [396] and the precentral gyrus is the location of the primary motor cortex and the origin of several motor pathways such as the corticospinal tract [422]. Shallowing of sulci may therefore relate to lower proprioception [408] and motor function

performance [423] in frail individuals. However, there is scarce evidence in the literature investigating relationships between sulcus depth and motor function, particularly in longitudinal study designs. Studies have however shown that sulcus depth is related to cognitive impairment by demonstrating lower sulcus depth in cognitively impaired individuals versus healthy controls [137]. Therefore, the lower sulcus depth in brain regions associated with cognitive function, such as the supramarginal gyrus (**Table 5.8**), observed in the pre-frail and frail group in this study may be related to cognitive impairment in frail individuals.

The mechanisms underlying changes in gyrification and sulcus depth are poorly established. The “axon tension” theory is one proposed explanation of age-related changes in gyrification [424], which postulates that tension within axons of the WM pulls of the walls of the cortex to create folds (i.e., gyrification) and that damage to axons could lead to reduced tension and decreased gyrification. Evidence for this theory is provided by *in vivo* animal models demonstrating that neurons generate tension [425] and when tension is relaxed, neurons retract [426]. Consequently, damage of WM microstructure (which is made up of axons) during ageing [427] has been theorised contribute to reduced gyrification. As such, WM microstructure damage has been highlighted by greater mean diffusivity in frail versus non-frail individuals [119], which may contribute to lower gyrification through the loss of axonal tension.

Regarding mechanism of lower sulcus depth, a positive correlation between cortical thickness and sulcus depth ($r = 0.67$; $P < 0.01$) has been demonstrated in older adults [428], suggesting that cortical thinning may contribute to shallowing of sulci. This theory is plausible as sulcus depth is measured as the difference from the cortical surface and the cerebral hull, thus thinning of the cortex would logically lead to shallower sulci. As such, this study noted lower cortical thickness in the collapsed pre-

frail and frail volunteers versus the non-frail group (**Figure 5.7 E**), which may therefore underpin the lower sulcus depth in the pre-frail and frail volunteers.

5.4.4 Associations between brain structure and physical function measures

This study observed numerous positive and negative associations between physical function measures and GM volume, WM volume, gyrification and sulcus depth (**Table 5.11 - Table 5.35**). The positive associations between regional GM volume and handgrip strength (**Table 5.11**), and the negative associations between regional GM volume and time taken to complete the 4.57m walk test (i.e., slower walking speed) (**Table 5.13**), are in line with a previous study showcasing associations between lower GM and lower handgrip strength and walking speed [116]. This study demonstrates that regional WM volume and cortical surface measures (i.e., gyrification and sulcus depth) are also associated with functional performance across the progression to frailty. Furthermore, this study demonstrated knee extensor isometric strength and work output are related to brain structure parameters in the transition to frailty.

5.4.4.1 Handgrip strength

GM volume in the superior frontal gyrus (T = 4.57; $P < 0.001$; **Table 5.11**) and WM volume in the inferior temporal gyrus (T = 5.72; $P < 0.001$; **Table 5.18**) exhibited the strongest positive associations with handgrip strength. Interestingly, in a four-year longitudinal study, decline in knee extensor peak torque was positively correlated with decline in GM volume of the superior frontal gyrus (r = 0.49; $P = 0.01$) and the inferior temporal gyrus (r = 0.50; $P = 0.011$) in older adults [429]. These findings reinforce that atrophy of these brain regions may be associated with poorer physical function in frail individuals. Gyrification within the postcentral gyrus was also positively associated with handgrip strength in the present study (T = 3.67; $P < 0.001$; **Table 5.25**). Given the

postcentral gyrus is the location of the somatosensory cortex and is responsible for processing sensorimotor signals (i.e., proprioception) [406], this association is perhaps not unexpected, particularly as greater gyrification is postulated to increased neuronal connectivity through a greater amount of cortical surface area [134]. In keeping with this, individuals with greater functional connectivity between the motor cortex and postcentral gyrus have been shown to exhibit greater handgrip strength [430], suggesting greater processing of proprioceptive signals may underpin the positive association between gyrification and handgrip strength in the present study.

5.4.4.2 Time taken to complete the 4.57m walk test

GM volume in the lateral occipital cortex (T = 5.54; $P < 0.001$; **Table 5.13**) and WM volume in the middle temporal gyrus (T = 5.63; $P < 0.001$; **Table 5.20**) showed the strongest negative associations with time taken to complete the 4.57m walk test, suggesting atrophy in these regions is associated with slower walking speed. These brain regions are involved in cognitive processes such as object recognition and language processing [385, 386, 394, 395], which indicates that cognition may be related to slower walking speed in frail individuals. Similarly, gait variability has been negatively associated with GM volume in the middle temporal gyrus in older individuals with mild cognitive impairment [431] and a previous study in frailty has observed negative associations between GMV volume in several brain regions involved in cognitive processes, such as medial pre-frontal cortex, and walking speed [125]. Impaired cognition is thought to be related to walking performance due to declines in attention and awareness of surroundings [432]. For example, lower performance on cognitive measures of attention have been associated with disrupted gait and balance [433, 434]. Therefore, lower brain volumes in regions involved in cognitive processes

may contribute to slower walking speed in frail individuals through negative effects on attention and awareness during walking.

Assessments of cognitive function would have been useful to further investigate the potential relationships between physical function and brain volumes in regions responsible for cognition in frail individuals. For example, regression analysis could have been expanded to determine associations between GM and WM volumes and scores from cognitive tests, and subsequently to investigate if the brain volumes in regions exhibiting significant associations with physical function were also associated with cognitive function scores. This analysis would help elucidate the potential impact of cognition on physical function in frail individuals. Participants in this study underwent cognitive function testing with the Montreal Cognitive Assessment (MoCA) questionnaire. However, due to the significant allocation of time and resources to the analyses of the large body of physiological and physical function data gathered, the MoCA data were not analysed for inclusion in this thesis. These data have been archived and present an interesting area for further research to determine the associations between brain volumes, physical function and cognition in frail individuals.

5.4.4.3 Knee extensor isometric strength and work output

Several strong positive associations were observed between regional brain structure parameters and knee extensor measures. GM volume in the frontal pole (T = 4.51; *P* < 0.001; **Table 5.14**) and WM volume in the postcentral gyrus (T = 4.49; *P* < 0.001; **Table 5.21**) showed the strongest positive associations with knee extensor isometric strength, whilst GM volume in the lateral occipital cortex (T = 4.74; *P* < 0.001; **Table 5.16**) and precentral gyrus (T = 4.49; *P* < 0.001; **Table 5.16**) exhibited the strongest

positive associations with knee extensor work output. These findings suggest that greater brain volumes in several regions are associated with greater strength and lower fatigability of the knee extensors. The positive association between GM volume in the precentral gyrus and knee extensor work output is interesting as this brain region contains the primary motor cortex and is the origin of several motor pathways such as the corticospinal tract [422]. Therefore, the atrophy of this region may contribute to lower work output in frail individuals by disrupting neural connections in motor pathways. The mechanisms by which this may occur are poorly understood. However, previous studies of frailty have reported negative associations between GMV in motor related areas of the brain, such as the cerebellum ($T = 4.40$; $P < 0.05$) [116] and slower walking speed, and a previous longitudinal study has highlighted that atrophy of the primary motor cortex is associated with declines in walking speed (regression coefficient: 0.121; $P = 0.003$) in older adults [435]. These findings reinforce that atrophy within motor related areas of the brain may contribute to functional decline during frailty.

5.4.5 Cerebral blood flow

This study found no differences in resting CBF between non-frail, pre-frail and frail states (**Figure 5.18 B**) or between the collapsed pre-frail and frail group and non-frail group (**Figure 5.19 B**), indicating that frailty is not associated with changes in resting CBF measured in the supine state. Considering the lack of previous CBF measurements in the frailty literature, comparisons are difficult to make. A previous report demonstrated no differences in global grey matter perfusion in non-frail, pre-frail and frail individuals when assessed with ASL MRI [143]. ASL MRI measurements quantify whole brain blood perfusion by magnetically labelling and tracing arterial blood across the whole brain, which differs from the PC-MRI measurements of CBF

within the cerebral arteries adopted in the present study, but these measures are directly related. The lack of differences in cerebral perfusion between healthy and frail states reported by Kant et al., [143] reinforces that resting cerebral haemodynamics are not altered in frailty. CBF has been shown to be linearly related to cardiac output. For example, both CBF and cardiac output has been shown to decrease when standing up [436] and increase following albumin infusion [437]. Meng et al., [438] collated data from 5 studies and demonstrated that changes in cardiac output and CBF are linearly correlated (R^2 = 0.89). Cardiac index was no different between non-frail, pre-frail and frail females in the present study (Chapter Three – **Figure 3.6 E**), which may therefore underpin the lack of differences observed in CBF across these groups.

There was a trend for lower cerebral artery blood velocity in the collapsed group of pre-frail and frail females compared to the non-frail group in this study (**Figure 5.19 A**). This may be deemed consistent with a prior study highlighting lower mean blood flow velocity of the cerebral arteries in frail versus non-frail individuals when assessed by transcranial Doppler ultrasound [156]. A meta-analysis of 28 studies revealed that patients with mild cognitive impairment exhibited lower cerebral artery blood velocity compared to healthy controls (mean difference: -3.79 cm/s; P < 0.001) [439]. Therefore, lower cerebral artery blood velocity may be related to cognitive impairment in frail individuals [440]. One mechanism potentially contributing to lower cerebral artery blood velocity in frail individuals is greater amounts of sedentary time. In a study measuring sedentary behaviour with accelerometry over 7 days in older adults, daily sedentary time was negatively correlated with CBF in medial frontal regions of the brain, including the middle frontal gyrus (regression coefficient: -0.63; *P* < 0.01) [441]. Over a more acute timeframe, middle aged adults subjected to 4 hours of

uninterrupted sitting exhibited a decline in cerebral artery blood velocity relative to baseline, whereas counterparts performing 2 minutes of physical activity at 30-minute intervals over 4 hours did not exhibit any changes in cerebral artery blood velocity [163]. The greater amount of sedentary behaviour exhibited by frail versus non-frail individuals [69] may contribute to lower velocity of blood in the cerebral arteries.

5.4.6 Cerebral venous oxygenation, oxygen extraction fraction and metabolic rate of oxygen

Following the novel application of TRUST MRI, cerebral venous oxygenation, oxygen extraction fraction and metabolic rate of oxygen was found to be no different between the non-frail, pre-frail, frail and collapsed pre-frail and frail groups in the current work (**Figure 5.22**, **Figure 5.23**). This is in line with a previous study demonstrating no differences in cerebral oxygen saturation between non-frail, pre-frail and frail individuals [157]. In this previous study, cerebral oxygenation was determined with NIRS measurements which were limited to the left frontal lobe of the brain [157] and therefore may be deemed regional assessments of oxygenation. Therefore, the assessments of global cerebral oxygenation, permitted with the TRUST MRI method adopted herein, furthers insight by indicating that whole brain cerebral oxygenation is not altered in pre-frail and frail individuals at rest. Given the lack of differences between healthy and frail states in CBF (**Figure 5.18**) and cardiac output (Chapter Three – **Figure 3.6 E**), in the present study, the lack of differences in cerebral haemodynamic parameters such as OEF and $CMRO_2$ seems logical. Furthermore, lower cerebral oxygenation [442] and $CMRO_2$ [443] has been shown in Alzheimer's Disease patients compared to healthy controls, suggesting neurodegenerative disease may contribute to haemodynamic changes in the brain. The volunteers in this study did not present any neurodegenerative diseases (Chapter Two – **Table 2.1**), thus were not susceptible

to the potential influence of neurodegenerative disease on haemodynamic parameters. Taken together, these findings provide strong evidence that resting cerebral oxygenation, OEF and $CMRO_2$ are not associated with frailty.

It is important to note that volunteers in the current study were assessed at rest and in a supine position. An interesting area for further research may be performing similar cerebral haemodynamic measurements during conditions of physiological stress, such as exercise. A physiological stress stimulus may induce physiological changes differently in healthy versus frail individuals, particularly as frailty is defined by a disruption in homeostasis [252]. In this way, similar CBF velocity between young and older individuals has been observed at rest, but during exercise a blunted elevation in the older versus young participants was seen [444]. Furthermore, cerebral oxygen saturation has been found to be similar at rest in non-frail, pre-frail and frail individuals, however following orthostasis a negative association between frailty severity and cerebral oxygen saturation was observed ($t = -2.77$; $P < 0.05$) [157]. Therefore, differences in cerebral haemodynamics between healthy and frail individuals may be manifested better under conditions of physiological stress.

5.4.7 Conclusion

This study evidenced multiple morphological differences within the brain across the frailty trajectory, including lower global GM and WM volumes, and greater global WMH volume. In regional analyses, lower GM and WM volume was observed in multiple regions of the brain in a collapsed group of pre-frail and frail volunteers compared to non-frail volunteers. The greatest differences in GM and WM volume were evident in the postcentral gyrus, frontal pole and lateral occipital cortex, which are brain regions responsible for proprioception and cognitive functions, therefore atrophy of these

regions may be related to proprioceptive and cognitive performance in frail individuals. In regression analyses, GM and WM volumes in numerous brain regions related to motor function and cognition were strongly associated with physical function measures, including knee extensor isometric strength and work output, which may present as physiological underpinnings of functional deterioration during frailty. This study is the first to quantify CBF, OEF and $CMRO_2$ in pre-frail and frail individuals with MRI, and revealed no differences in these haemodynamic parameters across healthy and frail states, suggesting differences in cerebral haemodynamics do not differentiate healthy and frail phenotypes, at least when measured in a resting supine state.

Chapter Five Appendices

Appendix 5.1 - Calculations of coefficient of variation of cerebral artery 2D-QFLOW parameters

Table 5.10: Data used to generate coefficient of variation for repeated analysis of 2D-QFLOW data.

Parameter	Measurement #1	Measurement #2	Measurement #3
Left carotid CSA (mm^2)	7.1	7.1	6.9
Right carotid CSA (mm^2)	8.8	9.1	8.8
Basilar CSA (mm^2)	2.5	2.5	2.4
Mean blood velocity (cm/s)	20.6	20.6	20.5
Cerebral blood flow (ml/min)	251	252	247
Grey matter cerebral blood flow (ml/min/g)	24.1	24.2	23.7

Appendix 5.2 – Regression analyses of VBM and SBM measures against physical function measures

Appendix 5.2.1 Grey matter

Positive associations between regional grey matter volumes and handgrip strength

Table 5.11: Regions of grey matter volume exhibiting positive associations with handgrip strength. X, Y and Z coordinates refer to Harvard-Oxford Atlas. The T value denotes the magnitude of association, with greater values reflecting stronger associations. k denotes the number of voxels (i.e., the volume) of grey matter exhibiting the association. L = left hemisphere, R = right hemisphere.

Brain region	X (mm)	Y (mm)	Z (mm)	T	k	P value
R superior frontal gyrus	9	32	54	4.57	1056	P < 0.001
L middle frontal gyrus	-26	34	24	4.17	321	P < 0.001
L parahippocampal gyrus	-33	-4	-28	4.03	559	P < 0.001
L frontal orbital gyrus	-26	21	-16	3.80	822	P < 0.001
L occipital fusiform	-32	-58	-10	3.88	525	P < 0.001
L supramarginal gyrus	-40	-52	15	3.44	995	P < 0.001
R parietal lobe	34	-38	44	3.72	126	P < 0.001
R postcentral gyrus	-12	-40	58	3.72	618	P < 0.001
L postcentral gyrus	-21	-30	66	3.59	308	P = 0.001
L precentral gyrus	-36	-22	50	3.56	244	P = 0.001
R Posterior cingulate	0	-3	39	3.54	521	P = 0.001
R lateral occipital cortex	42	-63	27	3.38	270	P = 0.001

Negative associations between regional grey matter volumes and handgrip strength

No significant negative associations between regional grey matter volumes and handgrip strength were observed.

Positive associations between regional grey matter volumes and the time taken to complete the 4.57m walk test

Table 5.12: Regions of grey matter volume exhibiting positive associations with the time taken to complete the 4.57m walk. X, Y and Z coordinates refer to Harvard-Oxford Atlas. The T value denotes the magnitude of association, with greater values reflecting stronger associations. k denotes the number of voxels (i.e., the volume) of grey matter exhibiting the association. L = left hemisphere, R = right hemisphere.

Brain region	X (mm)	Y (mm)	Z (mm)	T	k	P value
R angular gyrus	66	-46	26	3.58	179	P = 0.001
R frontal pole	40	58	-12	3.40	118	P = 0.001
R postcentral gyrus	10	-34	70	3.22	99	P = 0.002
L inferior frontal gyrus	-58	22	10	3.17	163	P = 0.002
L insular cortex	-32	-21	2	3.07	176	P = 0.002

Negative associations between regional grey matter volumes and the time taken to complete the 4.57m walk test

Table 5.13: Regions of grey matter volume exhibiting negative associations with the time taken to complete the 4.57m walk. X, Y and Z coordinates refer to Harvard-Oxford Atlas. The T value denotes the magnitude of association, with greater values reflecting stronger associations. k denotes the number of voxels (i.e., the volume) of grey matter exhibiting the association. L = left hemisphere, R = right hemisphere.

Brain region	X (mm)	Y (mm)	Z (mm)	T	k	P value
L lateral occipital cortex	-39	-75	18	5.54	541	P < 0.001
L parahippocampal gyrus	-24	-24	-20	5.52	21180	P < 0.001
L middle temporal gyrus	-40	-52	14	5.27	2337	P < 0.001
R postcentral gyrus	50	-16	36	4.80	713	P < 0.001
L middle frontal gyrus	-51	10	38	4.65	1542	P < 0.001
L cingulate gyrus	-10	-22	40	4.59	2797	P < 0.001
L frontal pole	-14	50	27	4.33	618	P < 0.001
R lateral occipital cortex	30	-66	54	3.98	337	P < 0.001
R occipital fusiform gyrus	18	-74	-8	4.42	183	P < 0.001
L cuneal cortex	-8	-87	14	4.38	188	P < 0.001
L occipital pole	-24	-96	-8	4.05	109	P < 0.001
L supramarginal gyrus	-57	-48	9	3.83	52	P < 0.001
L precuneus cortex	-9	-54	9	3.75	131	P < 0.001
L juxtapositional lobule cortex	-9	-2	45	3.30	66	P < 0.001
R superior frontal gyrus	6	50	42	3.54	840	P = 0.001
R frontal medial cortex	4	32	-22	3.40	391	P = 0.001
L inferior temporal gyrus	-50	-45	-16	3.17	79	P = 0.002
R precentral gyrus	54	2	33	2.87	223	P = 0.004

R central opercular cortex	63	0	6	2.83	268	P = 0.004

Positive associations between regional grey matter volumes and knee extensor isometric strength

Table 5.14: Regions of grey matter volume exhibiting positive associations with knee extensor isometric strength. X, Y and Z coordinates refer to Harvard-Oxford Atlas. The T value denotes the magnitude of association, with greater values reflecting stronger associations. k denotes the number of voxels (i.e., the volume) of grey matter exhibiting the association. L = left hemisphere, R = right hemisphere.

Brain region	X (mm)	Y (mm)	Z (mm)	T	k	P value
L frontal pole	-33	56	22	4.51	66	P < 0.001
R postcentral gyrus	45	-20	51	4.49	457	P < 0.001
R occipital cortex	28	-57	56	3.83	340	P < 0.001
R precentral gyrus	57	2	44	3.67	231	P = 0.001
L middle frontal gyrus	-48	22	32	3.61	207	P = 0.001
L precentral gyrus	-42	-10	46	3.52	267	P = 0.001
L frontal pole	-20	48	44	3.49	599	P = 0.001
R occipital gyrus	42	-66	4	3.45	99	P = 0.001
R anterior cingulate	6	32	15	3.41	985	P = 0.001
L superior parietal lobe	-38	-39	57	3.39	216	P = 0.001
L angular gyrus	-54	-57	24	3.37	363	P = 0.001
L parahippocampal gyrus	-26	-28	-15	3.36	812	P = 0.001

Negative associations between regional grey matter volumes and knee extensor isometric strength

Table 5.15: Regions of grey matter volume exhibiting negative associations with knee extensor isometric strength. X, Y and Z coordinates refer to Harvard-Oxford Atlas. The T value denotes the magnitude of association, with greater values reflecting stronger associations. k denotes the number of voxels (i.e., the volume) of grey matter exhibiting the association. L = left hemisphere, R = right hemisphere.

Brain region	X (mm)	Y (mm)	Z (mm)	T	k	P value
L inferior frontal gyrus	-51	24	3	3.66	270	P = 0.001
L insular cortex	-27	26	10	3.36	129	P = 0.001
R precentral gyrus	16	-20	80	3.25	115	P = 0.002
L inferior temporal gyrus	-63	-24	-30	3.10	55	P = 0.002
L lateral occipital cortex	-30	-78	22	3.01	91	P = 0.003
R insular cortex	36	-2	12	2.71	50	P = 0.006
R postcentral gyrus	4	-38	74	2.68	53	P = 0.006

Positive associations between regional grey matter volumes and knee extensor work output (60°/s)

Table 5.16: Regions of grey matter volume exhibiting positive associations with knee extensor work output at 60 °/s. X, Y and Z coordinates refer to Harvard-Oxford Atlas. The T value denotes the magnitude of association, with greater values reflecting stronger associations. k denotes the number of voxels (i.e., the volume) of grey matter exhibiting the association. L = left hemisphere, R = right hemisphere.

Brain region	X (mm)	Y (mm)	Z (mm)	T	k	P value
R lateral occipital cortex	24	-58	54	4.74	326	P < 0.001
R precentral gyrus	57	0	44	4.49	658	P < 0.001
R superior frontal gyrus	15	34	44	4.25	303	P < 0.001
L planum temporale	-52	-40	14	4.02	500	P < 0.001
R juxtapositional lobule cortex	12	-2	51	3.85	113	P < 0.001
L middle frontal gyrus	-46	22	33	3.70	321	P = 0.001
L paracingulate gyrus	-9	12	44	3.48	154	P = 0.001
R lingual gyrus	8	-74	3	3.46	201	P = 0.001
L precentral gyrus	-54	3	8	3.44	925	P = 0.001
R insular cortex	33	24	2	3.40	290	P = 0.001
L frontal pole	-18	45	36	3.40	403	P = 0.001

Negative associations between regional grey matter volumes and knee extensor work output (60°/s)

Table 5.17: Regions of grey matter volume exhibiting negative associations with knee extensor work output at 60 °/s. X, Y and Z coordinates refer to Harvard-Oxford Atlas. The T value denotes the magnitude of association, with greater values reflecting stronger associations. k denotes the number of voxels (i.e., the volume) of grey matter exhibiting the association. L = left hemisphere, R = right hemisphere.

Brain region	X (mm)	Y (mm)	Z (mm)	T	k	P value
R precentral gyrus	9	-16	69	3.88	583	P < 0.001
L frontal pole	-9	56	-26	3.52	63	P = 0.001
L superior parietal lobe	-33	-56	45	3.01	68	P = 0.003

Appendix 5.2.2 White matter

Positive associations between regional white matter volumes and handgrip strength

Table 5.18: Regions of white matter volume exhibiting positive associations with handgrip strength. X, Y and Z coordinates refer to Harvard-Oxford Atlas. The T value denotes the magnitude of association, with greater values reflecting stronger associations. k denotes the number of voxels (i.e., the volume) of white matter exhibiting the association. L = left hemisphere, R = right hemisphere.

Brain region	X (mm)	Y (mm)	Z (mm)	T	k	P value
L inferior temporal gyrus	-44	-58	-12	5.72	560	P < 0.001
R lateral occipital cortex	33	-78	6	4.58	192	P < 0.001
R lingual gyrus	32`	-54	2	4.12	68	P < 0.001
L middle temporal gyrus	-56	-33	-4	3.98	57	P < 0.001
L frontal pole	-33	46	-9	3.96	58	P < 0.001
L parahippocampal gyrus	-24	-34	-15	3.75	75	P < 0.001
R superior parietal lobule	14	-51	60	3.65	228	P < 0.001
R postcentral gyrus	36	-30	50	3.22	75	P = 0.002
R intracalcarine cortex	4	-69	10	3.15	54	P = 0.002
L frontal orbital cortex	-12	22	-21	2.91	111	P = 0.003
L middle frontal gyrus	-36	22	36	2.72	68	P = 0.005
R cingulate gyrus	14	-40	3	2.70	260	P = 0.006

Negative associations between regional white matter volumes and handgrip strength

Table 5.19: Regions of white matter volume exhibiting negative associations with handgrip strength. X, Y and Z coordinates refer to Harvard-Oxford Atlas. The T value denotes the magnitude of association, with greater values reflecting stronger associations. k denotes the number of voxels (i.e., the volume) of white matter exhibiting the association. L = left hemisphere.

Brain region	X (mm)	Y (mm)	Z (mm)	T	k	P value
L inferior temporal gyrus	-50	20	8	3.92	173	P < 0.001

Positive associations between regional white matter volumes and the time taken to complete the 4.57m walk test

No significant positive associations between regional white matter volumes and the time taken to complete the 4.57m walk were observed.

Negative associations between regional white matter volumes and the time taken to complete the 4.57m walk test

Table 5.20: Regions of white matter volume exhibiting negative associations with the time taken to complete the 4.57m walk. X, Y and Z coordinates refer to Harvard-Oxford Atlas. The T value denotes the magnitude of association, with greater values reflecting stronger associations. k denotes the number of voxels (i.e., the volume) of white matter exhibiting the association. L = left hemisphere, R = right hemisphere.

Brain region	X (mm)	Y (mm)	Z (mm)	T	k	P value
R middle temporal gyrus	40	-56	2	5.63	396	P < 0.001
L frontal pole	-26	40	21	5.04	2751	P < 0.001
L occipital fusiform gyrus	-38	-69	10	4.97	102	P < 0.001
L occipital pole	-12	-98	-8	4.69	89	P < 0.001
L lateral occipital cortex	-39	-70	28	4.67	168	P < 0.001
R lingual gyrus	16	-70	0	4.64	760	P < 0.001
R superior frontal gyrus	12	51	20	4.39	172	P < 0.001
R precuneus cortex	10	-58	22	4.38	287	P < 0.001
R frontal operculum cortex	34	22	12	4.17	392	P < 0.001
R temporal occipital fusiform cortex	45	-44	-16	4.12	50	P < 0.001
R parahippocampal gyrus	27	-26	-8	4.11	127	P < 0.001
L cingulate gyrus	-4	-32	40	3.79	712	P < 0.001
L inferior temporal gyrus	-44	-51	-15	3.73	681	P < 0.001
L supramarginal gyrus	-46	-48	30	2.91	205	P = 0.003
R temporal pole	45	12	-32	2.91	52	P = 0.003

Positive associations between regional white matter volumes and knee extensor isometric strength

Table 5.21: Regions of white matter volume exhibiting positive associations with knee extensor isometric strength. X, Y and Z coordinates refer to Harvard-Oxford Atlas. The T value denotes the magnitude of association, with greater values reflecting stronger associations. k denotes the number of voxels (i.e., the volume) of white matter exhibiting the association. L = left hemisphere, R = right hemisphere.

Brain region	X (mm)	Y (mm)	Z (mm)	T	k	P value
R postcentral gyrus	45	-20	51	4.49	61	P < 0.001
L frontal pole	-33	56	22	4.51	66	P < 0.001
R lateral occipital cortex	28	-57	56	3.83	340	P < 0.001
R precentral gyrus	57	2	44	3.67	231	P = 0.001
L middle frontal gyrus	-48	22	32	3.61	207	P = 0.001
R cingulate gyrus	6	32	15	3.41	985	P = 0.001
L superior parietal lobe	-38	-39	57	3.39	216	P = 0.001
L angular gyrus	-54	-57	24	3.37	363	P = 0.001
L parahippocampal gyrus	-26	-28	-15	3.36	812	P = 0.001
R occipital pole	0	-92	-9	3.27	120	P = 0.002
L planum temporale	-64	-28	16	3.24	108	P = 0.002
L superior temporal gyrus	-54	-39	12	3.23	73	P = 0.002
L frontal orbital cortex	-20	24	-14	3.14	99	P = 0.002

Negative associations between regional white matter volumes and knee extensor isometric strength

Table 5.22: Regions of white matter volume exhibiting negative associations with knee extensor isometric strength. X, Y and Z coordinates refer to Harvard-Oxford Atlas. The T value denotes the magnitude of association, with greater values reflecting stronger associations. k denotes the number of voxels (i.e., the volume) of white matter exhibiting the association. L = left hemisphere, R = right hemisphere.

Brain region	X (mm)	Y (mm)	Z (mm)	T	k	P value
L inferior frontal gyrus	-51	24	3	3.66	270	P = 0.001
L insular cortex	-27	26	10	3.36	129	P = 0.001
L inferior temporal gyrus	-63	-24	-30	3.10	55	P = 0.002
R precentral gyrus	16	-20	80	3.25	115	P = 0.002
L lateral occipital cortex	-30	-78	22	3.01	91	P = 0.003
R postcentral gyrus	4	-38	74	2.68	53	P = 0.006

Positive associations between regional white matter volumes and knee extensor work output (60°/s)

Table 5.23: Regions of white matter volume exhibiting positive associations with knee extensor work output (60 °/s). X, Y and Z coordinates refer to Harvard-Oxford Atlas. The T value denotes the magnitude of association, with greater values reflecting stronger associations. k denotes the number of voxels (i.e., the volume) of white matter exhibiting the association. L = left hemisphere, R = right hemisphere.

Brain region	X (mm)	Y (mm)	Z (mm)	T	k	P value
R cingulate gyrus	12	33	14	4.05	167	P < 0.001
R postcentral gyrus	38	-27	40	3.95	295	P < 0.001
R supramarginal gyrus	58	-42	22	3.57	131	P = 0.001
L preceuneus cortex	-16	-62	27	3.38	302	P = 0.001
R superior parietal lobe	26	-48	45	3.36	1264	P = 0.001`
L lingual gyrus	-15	-81	-2	3.13	130	P = 0.002
R frontal pole	20	38	38	2.75	50	P = 0.005
L planum temporale	-45	-36	8	2.68	82	P = 0.006

Negative associations between regional white matter volumes and knee extensor work output (60°/s)

Table 5.24: Regions of white matter volume exhibiting negative associations with knee extensor work output (60 °/s). X, Y and Z coordinates refer to Harvard-Oxford Atlas. The T value denotes the magnitude of association, with greater values reflecting stronger associations. k denotes the number of voxels (i.e., the volume) of white matter exhibiting the association. L = left hemisphere, R = right hemisphere.

Brain region	X (mm)	Y (mm)	Z (mm)	T	k	P value
L cingulate gyrus	-54	-24	-28	4.84	133	P < 0.001
L inferior temporal gyrus	-34	-27	62	3.97	57	P < 0.001
R frontal orbital cortex	42	32	-15	3.26	82	P = 0.002

Appendix 5.2.3 Gyrification

Positive associations between regional gyrification and handgrip strength

Table 5.25: Regions of gyrification exhibiting positive associations with handgrip strength. X, Y and Z coordinates refer to Harvard-Oxford Atlas. The T value denotes the magnitude of association, with greater values reflecting stronger associations. k denotes the number of voxels (i.e., the volume) of gyrification exhibiting the association. L = left hemisphere, R = right hemisphere.

Brain region	X (mm)	Y (mm)	Z (mm)	T	k	P value
R postcentral gyrus	32	-25	47	3.67	109	P < 0.001
R superior frontal gyrus	10	21	71	3.39	236	P = 0.001
L postcentral gyrus	-55	-20	26	3.28	118	P = 0.001
R preceneus cortex	10	-58	21	3.15	173	P = 0.002
R supramarginal gyrus	48	-42	32	2.98	66	P = 0.003
L superior parietal lobule	-15	-57	66	2.96	63	P = 0.003

Negative associations between regional gyrification and handgrip strength

Table 5.26: Regions of gyrification exhibiting negative associations with handgrip strength. X, Y and Z coordinates refer to Harvard-Oxford Atlas. The T value denotes the magnitude of association, with greater values reflecting stronger associations. k denotes the number of voxels (i.e., the volume) of gyrification exhibiting the association. L = left hemisphere, R = right hemisphere.

Brain region	X (mm)	Y (mm)	Z (mm)	T	k	P value
R postcentral gyrus	55	-19	40	5.37	373	P < 0.001
L middle frontal gyrus	-44	26	44	3.91	201	P < 0.001
R middle temporal gyrus	46	-41	5	2.84	89	P = 0.004

Positive associations between regional gyrification and the time taken to complete the 4.57m walk test

Table 5.27: Regions of gyrification exhibiting positive associations with the time taken to complete the 4.57m walk. X, Y and Z coordinates refer to Harvard-Oxford Atlas. The T value denotes the magnitude of association, with greater values reflecting stronger associations. k denotes the number of voxels (i.e., the volume) of gyrification exhibiting the association. L = left hemisphere, R = right hemisphere.

Brain region	X (mm)	Y (mm)	Z (mm)	T	k	P value
L inferior frontal gyrus	-38	14	23	3.19	59	P = 0.002
R superior parietal lobule	22	-46	65	3.08	115	P = 0.002

Negative associations between regional gyrification and the time taken to complete the 4.57m walk test

Table 5.28: Regions of gyrification exhibiting negative associations with the time taken to complete the 4.57m walk. X, Y and Z coordinates refer to Harvard-Oxford Atlas. The T value denotes the magnitude of association, with greater values reflecting stronger associations. k denotes the number of voxels (i.e., the volume) of gyrification exhibiting the association. L = left hemisphere, R = right hemisphere.

Brain region	X (mm)	Y (mm)	Z (mm)	T	k	P value
R cingulate gyrus	3	-36	37	3.0	258	P = 0.003

Positive associations between regional gyrification and knee extensor isometric strength

No significant positive associations between regional gyrification index and knee extensor isometric strength were observed.

Negative associations between regional gyrification and knee extensor isometric strength

Table 5.29: Regions of gyrification exhibiting negative associations with knee extensor isometric strength. X, Y and Z coordinates refer to Harvard-Oxford Atlas. The T value denotes the magnitude of association, with greater values reflecting stronger associations. k denotes the number of voxels (i.e., the volume) of gyrification exhibiting the association. L = left hemisphere, R = right hemisphere.

Brain region	X (mm)	Y (mm)	Z (mm)	T	k	P value
R postcentral gyrus	32	-26	48	3.25	220	P = 0.002

Positive associations between regional gyrification and knee extensor work output (60 °/s)

No significant positive associations between regional gyrification index and knee extensor work output were observed.

Negative associations between regional gyrification and knee extensor work output (60 °/s)

Table 5.30: Regions of gyrification exhibiting negative associations with knee extensor work output (60°/s). X, Y and Z coordinates refer to Harvard-Oxford Atlas. The T value denotes the magnitude of association, with greater values reflecting stronger associations. k denotes the number of voxels (i.e., the volume) of gyrification exhibiting the association. L = left hemisphere, R = right hemisphere.

Brain region	X (mm)	Y (mm)	Z (mm)	T	k	P value
R precentral gyrus	13	-30	62	4.03	166	P < 0.001
R superior parietal lobe	24	-50	66	3.93	182	P < 0.001
L precentral gyrus	-7	-27	74	3.80	56	P < 0.001
R superior frontal gyrus	18	-12	83	3.64	175	P = 0.001
L postcentral gyrus	-41	-24	69	3.40	184	P = 0.001
R frontal orbital cortex	30	27	-2	3.19	102	P = 0.002
L frontal pole	-28	61	12	3.04	56	P = 0.003

Appendix 5.2.4 Sulcus depth

Positive associations between regional sulcus depth and handgrip strength

Table 5.31: Regions of sulcus depth exhibiting positive associations with handgrip strength. X, Y and Z coordinates refer to Harvard-Oxford Atlas. The T value denotes the magnitude of association, with greater values reflecting stronger associations. k denotes the number of voxels (i.e., the volume) of sulcus depth exhibiting the association. L = left hemisphere, R = right hemisphere.

Brain region	X (mm)	Y (mm)	Z (mm)	T	k	P value
L parietal operculum cortex	-43	-39	26	3.30	122	P = 0.001
R postcentral gyrus	36	-30	48	3.15	169	P = 0.002
L precentral gyrus	-59	-5	48	2.81	71	P = 0.004

Negative associations between regional sulcus depth and handgrip strength

No significant negative associations between regional sulcus depth and handgrip strength were observed.

Positive associations between regional sulcus depth and the time taken to complete the 4.57m walk test

No significant positive associations between regional sulcus depth and the time taken to complete the 4.57m walk were observed.

Negative associations between regional sulcus depth and the time taken to complete the 4.57m walk test

Table 5.32: Regions of sulcus depth exhibiting negative associations with the time taken to complete the 4.57m walk. X, Y and Z coordinates refer to Harvard-Oxford Atlas. The T value denotes the magnitude of association, with greater values reflecting stronger associations. k denotes the number of voxels (i.e., the volume) of sulcus depth exhibiting the association. L = left hemisphere, R = right hemisphere.

Brain region	X (mm)	Y (mm)	Z (mm)	T	k	P value
R superior frontal gyrus	11	27	52	4.48	238	P < 0.001
R central operculum cortex	47	-15	23	4.36	174	P < 0.001
R middle frontal gyrus	37	32	32	4.28	323	P < 0.001
R superior parietal lobule	27	-45	65	4.09	418	P < 0.001
L cingulate gyrus	-10	-33	41	3.91	94	P < 0.001
L precentral gyrus	-6	-21	64	3.83	208	P < 0.001
L superior frontal gyrus	-8	5	64	3.75	121	P < 0.001
R precuneus cortex	18	-50	37	3.73	136	P < 0.001
L postcentral gyrus	-11	-45	65	3.24	158	P = 0.001
R precentral gyrus	11	-21	52	3.20	375	P =0.002
L middle frontal gyrus	-36	31	44	3.07	52	P = 0.002
R inferior frontal gyrus	32	30	9	2.82	72	P = 0.004

Positive associations between regional sulcus depth and knee extensor isometric strength

Table 5.33: Regions of sulcus depth exhibiting positive associations with knee extensor isometric strength. X, Y and Z coordinates refer to Harvard-Oxford Atlas. The T value denotes the magnitude of association, with greater values reflecting stronger associations. k denotes the number of voxels (i.e., the volume) of sulcus depth exhibiting the association. L = left hemisphere, R = right hemisphere.

Brain region	X (mm)	Y (mm)	Z (mm)	T	k	P value
R lateral occipital cortex	31	-58	71	3.96	153	P < 0.001
L superior parietal lobule	-21	-44	-42	3.68	59	P < 0.001
L lateral occipital cortex	-44	-62	49	3.39	73	P = 0.001
R postcentral gyrus	49	-29	65	3.00	316	P = 0.003
L superior frontal gyrus	-20	30	56	2.89	89	P = 0.004

Negative associations between regional sulcus depth and knee extensor isometric strength

Table 5.34: Regions of sulcus depth exhibiting negative associations with knee extensor isometric strength. X, Y and Z coordinates refer to Harvard-Oxford Atlas. The T value denotes the magnitude of association, with greater values reflecting stronger associations. k denotes the number of voxels (i.e., the volume) of sulcus depth exhibiting the association. L = left hemisphere, R = right hemisphere.

Brain region	X (mm)	Y (mm)	Z (mm)	T	k	P value
L angular gyrus	-49	-56	36	3.68	113	P = 0.001

Positive associations between regional sulcus depth and knee extensor work output (60°/s)

Table 5.35: Regions of sulcus depth exhibiting positive associations with knee extensor work output (60°/s). X, Y and Z coordinates refer to Harvard-Oxford Atlas. The T value denotes the magnitude of association, with greater values reflecting stronger associations. k denotes the number of voxels (i.e., the volume) of sulcus depth exhibiting the association. L = left hemisphere, R = right hemisphere.

Brain region	X (mm)	Y (mm)	Z (mm)	T	k	P value
L supramarginal gyrus	-50	-49	41	4.06	103	P < 0.001
L lateral occipital cortex	-27	-69	36	3.95	77	P < 0.001
L postcentral gyrus	-28	-29	71	3.70	364	P = 0.001
L superior parietal lobule	-32	-45	53	3.63	228	P = 0.001
L cuneal cortex	-5	-80	23	2.86	55	P = 0.004
R postcentral gyrus	4	-32	79	5.05	566	P < 0.001
R parietal operculum cortex	54	-30	29	4.74	70	P < 0.001

Negative associations between regional sulcus depth and knee extensor work output (60°/s)

No significant negative associations between regional sulcus depth and knee extensor work output were observed.

Chapter Six: Data integration to further insight of the physiological phenotype of frailty

6.1 Introduction

The experimental Chapters of this thesis have primarily focused on characteristics of physiological systems in isolation within the context of human frailty (e.g., the heart, skeletal muscle, adipose tissue or brain). Differences in physiological traits, such as skeletal muscle volume (Chapter Four) and brain volumes (Chapter Five), between non-frail and frail individuals have been identified, some of which are novel and others directly in line with previous studies assessing similar characteristics of individual organs in frail individuals. However, as outlined in Chapter One – Section 1.5.6, focus on individual organs does not seem optimal for characterising the physiological phenotype of frailty which manifests at the whole-body level. Indeed, the syndrome is likely driven by the simultaneous dysregulation within, and interactions between, multiple physiological systems. For example, Fried et al., [245] assessed blood biomarker and functional measures in six physiological systems (anaemia, inflammation, endocrine, micronutrients, adiposity, and fine motor speed) and highlighted that abnormal values in five systems increased frailty risk by 26-fold (compared to zero abnormal systems). Adopting alternate measures of physiological systems to those assessed by Fried et al., [245], other research groups have also demonstrated multisystem dysregulation as a feature of frailty [180, 249]. Despite the improved insight provided by these investigations into multisystem dysregulation, studies in this area have adopted indirect measures to investigate organ structure and function, such as blood biomarkers. Therefore, there is large potential for improving insight into the frailty phenotype with direct measures of organ structure and function.

In addition to the imprecise measurements adopted in previous studies, the small number of outcome measures assessed may be deemed a superficial characterisation of the whole body frailty phenotype. For example, most studies have assessed multisystem dysregulation in frail individuals on the basis of abnormal values within six systems (systems being defined differently each time) [180, 245, 249]. As outlined in Chapter One – Section 1.4, the term "phenotype" has been defined as "the observable traits of the organism," which encompasses a wide range of characteristics such as morphology, physiology, and behaviour [26]. Therefore the small number of systems investigated in previous studies should be expanded to include more measures of physiological traits and thus further insight into the frailty phenotype. Moreover, further investigation into how different organs and physiological processes interact and affect each other is needed to provide greater granularity and thus identify physiological targets for longitudinal studies aiming to uncover mechanisms of frailty progression.

Together, the caveats outlined above provided the rationale for this thesis, and the overarching aim was to provide novel insight into the physiological phenotype of frailty with the application of robust multi-organ assessment techniques. Therefore, the aim of this Chapter was to integrate the structural and functional data gathered in a number of organ systems in this thesis to bring further novel insight into the physiological phenotype of frailty.

6.2 Methods

Correlation analysis was used to determine associations between organ structural and functional data and physical function end-point measurements performed in this thesis (analysis method detailed in Chapter Two – Section 2.9). Pearson's linear correlation was performed on 25 variables using GraphPad Prism V.9 (GraphPad Software, Boston, Massachusetts, USA). Generated *r* and *P* values between all variables were

then ran through a custom in-house MATLAB code to identify significant positive and negative associations between (and within) physiological systems and physical function characteristics within matrices. One matrix was created to present *P* values of associations and another matrix was created to present *r* values, which were grouped into: $r = >0.35$, $r = <-0.35$ and $0.35< r <-0.35$. Variables were grouped into physical function characteristics and metrics within four physiological systems: body composition, cardiac, brain morphometry, and brain haemodynamics and oxygenation. Group comparisons (i.e., non-frail, pre-frail, frail) of all metrics presented in this Chapter were outlined in Chapters Three, Four and Five.

6.3 Results and Discussion

Results are presented in correlation matrices in **Figure 6.1** (showing correlation *P* values) and **Figure 6.2** (showing correlation *r* values).

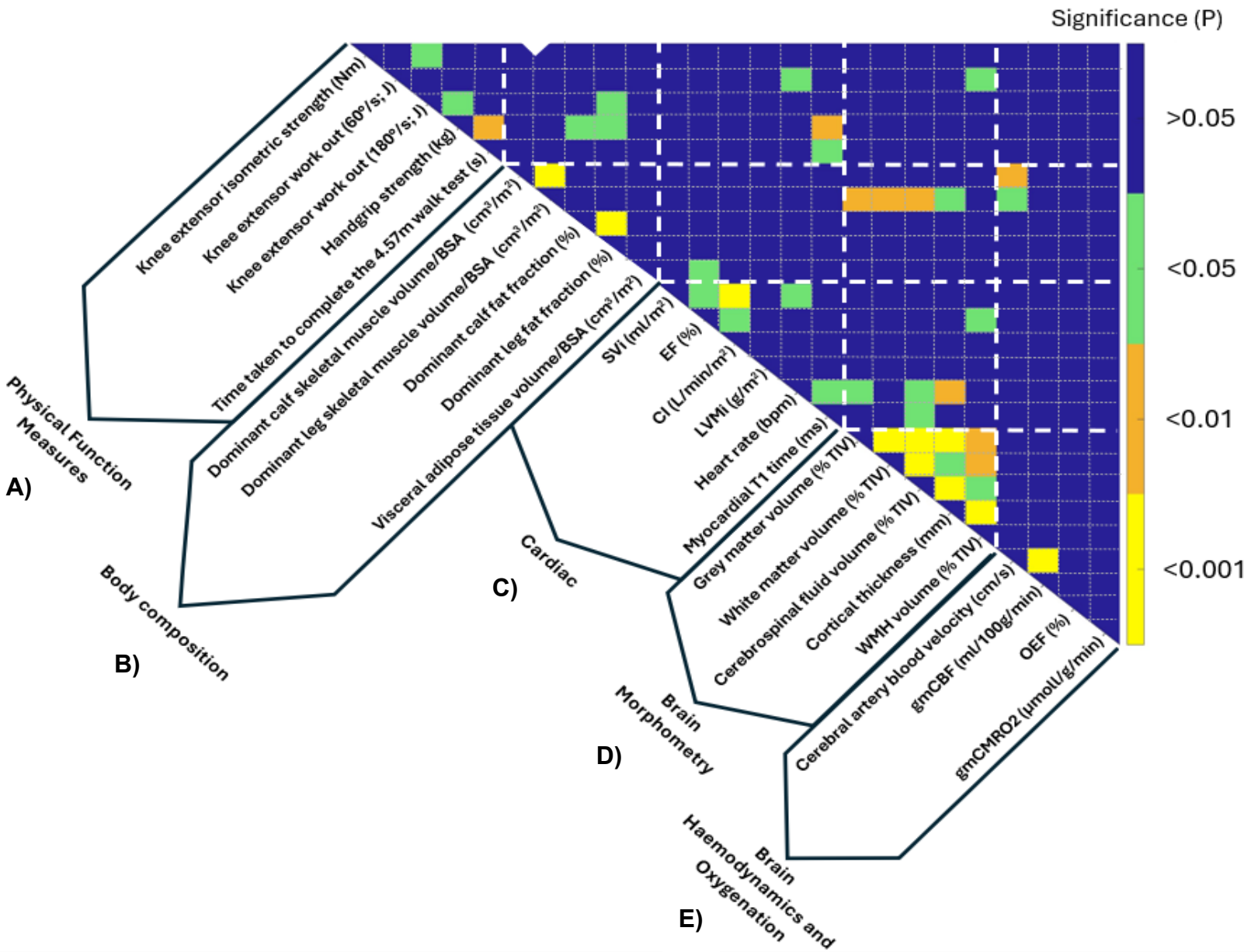
Significance (P)
>0.05
<0.05
<0.01
<0.001
Knee extensor isometric strength (Nm)
Knee extensor work out (60°/s; J)
Knee extensor work out (180°/s; J)
Handgrip strength (kg)
Time taken to complete the 4.57m walk test (s)
Dominant calf skeletal muscle volume/BSA (cm³/m²)
Dominant leg skeletal muscle volume/BSA (cm³/m²)
Dominant calf fat fraction (%)
Dominant leg fat fraction (%)
Visceral adipose tissue volume/BSA (cm³/m²)
SVi (ml/m²)
EF (%)
CI (L/min/m²)
LVMi (g/m²)
Heart rate (bpm)
Myocardial T1 time (ms)
Grey matter volume (% TIV)
White matter volume (% TIV)
Cerebrospinal fluid volume (% TIV)
Cortical thickness (mm)
WMH volume (% TIV)
Cerebral artery blood velocity (cm/s)
gmCBF (ml/100g/min)
OEF (%)
gmCMRO2 (µmolI/g/min)
Physical Function Measures
A)
Body composition
B)
Cardiac
C)
Brain Morphometry
D)
Brain Haemodynamics and Oxygenation
E)

***Figure 6.1**: Matrix showing P values of correlations between physical function and physiological measures collected in this thesis. Colours within small white dashed boxes denote P values of correlations between individual parameters. Large white dashed boxes are used to guide the comparison of correlation P values between the grouped physical function measures (**A**) and physiological measures grouped by specific organs: (**B**) body composition, (**C**) cardiac, (**D**) brain morphometry and (**E**) brain haemodynamics and oxygenation. BSA; body surface area, CI; cardiac index, EF; ejection fraction, gmCBF; grey matter corrected cerebral blood flow, gmCMRO$_2$; grey matter cerebral metabolic rate of oxygen, LVMi; left ventricular mass index, OEF; oxygen extraction fraction, SVi; stroke volume index.*

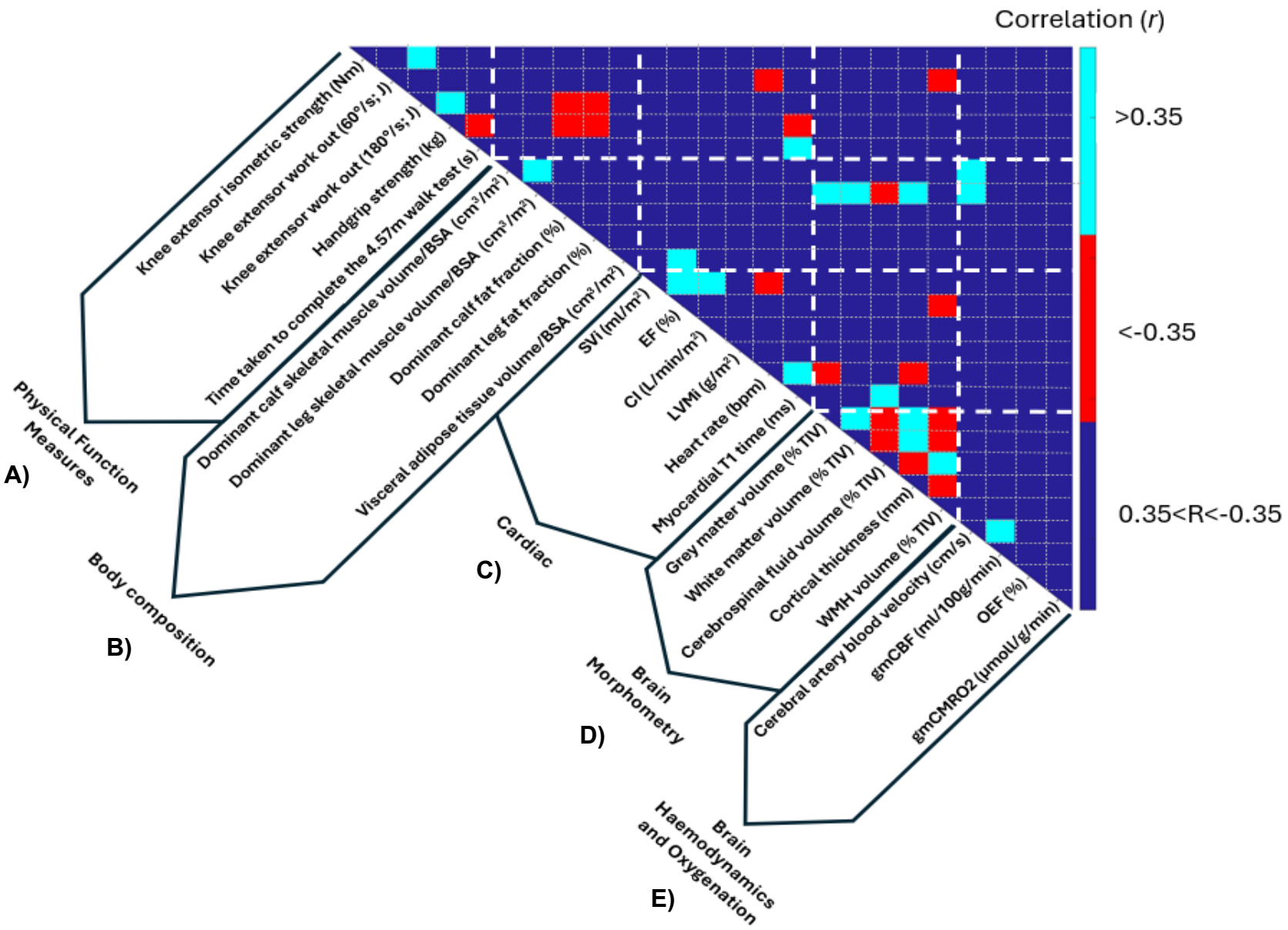
Correlation (r)
>0.35
<-0.35
0.35<R<-0.35
Knee extensor isometric strength (Nm)
Knee extensor work out (60°/s; J)
Knee extensor work out (180°/s; J)
Handgrip strength (kg)
Time taken to complete the 4.57m walk test (s)
Dominant calf skeletal muscle volume/BSA (cm³/m²)
Dominant leg skeletal muscle volume/BSA (cm³/m²)
Dominant calf fat fraction (%)
Dominant leg fat fraction (%)
Visceral adipose tissue volume/BSA (cm³/m²)
SVi (ml/m²)
EF (%)
CI (L/min/m²)
LVMi (g/m²)
Heart rate (bpm)
Myocardial T1 time (ms)
Grey matter volume (% TIV)
White matter volume (% TIV)
Cerebrospinal fluid volume (% TIV)
Cortical thickness (mm)
WMH volume (% TIV)
Cerebral artery blood velocity (cm/s)
gmCBF (ml/100g/min)
OEF (%)
gmCMRO2 (umolU/g/min)
A)
Physical Function Measures
B)
Body composition
C)
Cardiac
D)
Brain Morphometry
E)
Brain Haemodynamics and Oxygenation

Figure 6.2: *Correlation matrix showing r values of correlations between physical function and physiological measures collected in this thesis. Colours within small white dashed boxes denote r values of correlations between individual parameters. Large white dashed boxes are used to guide the comparison of correlation r values between the grouped physical function measures (**A**) and physiological measures grouped by specific organs: (**B**) body composition, (**C**) cardiac, (**D**) brain morphometry and (**E**) brain haemodynamics and oxygenation. BSA; body surface area, CI; cardiac index, EF; ejection fraction, gmCBF; grey matter corrected cerebral blood flow, gmCMRO$_2$; grey matter cerebral metabolic rate of oxygen, LVMi; left ventricular mass index, OEF; oxygen extraction fraction, SVi; stroke volume index.*

6.3.1 Associations between physical function and physiological systems characteristics

Considering measures of physical function are currently the most robust end-point measures associated with frailty, particular attention should be given to the associations between physical function and physiological metrics highlighted in **Figure 6.1** and **Figure 6.2**. Interestingly, physical function measures (**A**) were significantly related to several body composition (**B**), cardiac (**C**) and brain morphometry parameters (**D**). For example, dominant leg fat fraction showed a significant negative correlation with knee extensor work output at 180°/s (r < -0.35; P < 0.05), pointing to an association between muscle work capability during repeated contractions and muscle fat infiltration. A previous study of frail individuals has similarly reported significant negative correlations between calf muscle fat fraction and plantar flexion exercise duration (r = -0.36; P < 0.05) and maximal oxidative capacity (r = -0.63; P < 0.001), suggesting greater intramuscular fat may be related to exercise intolerance in frail individuals [53]. These findings also support the notions outlined in Chapter Four, in that changes in body composition may contribute to functional decline during frailty. Whether these association are attributable to reduced physical activity levels or positive energy balance is unclear, but given visceral adiposity (the primary site of lipid

deposition) was no different between groups it points to a larger role for physical inactivity.

A significant negative association was also observed between global brain WMH volume and knee extensor work output at 60°/s (r < -0.35; P < 0.05), highlighting potential interactions between brain morphometry and functional decline during frailty. Previous studies have demonstrated significant associations between regional brain morphometry parameters (e.g., grey matter volume) and physical function measures of handgrip strength and walking speed in frail individuals [116, 125]. Similar findings were reported in Chapter Five, which outlined strong associations between several physical function and regional brain morphometry measures, such as positive associations between handgrip strength and GM volume in the superior frontal gyrus (T = 4.57; P < 0.001; Chapter Five Appendices, **Table 5.11**) and WM volume in the inferior temporal gyrus (T = 5.72; P < 0.001, Chapter Five Appendices, **Table 5.18**). However, when combining the associations between global brain morphometry and physical function outlined in **Figure 6.1** and **Figure 6.2** with the multiple associations between regional GM and WM volume and physical function parameters outlined in Chapter Five, this thesis provided evidence that both global and regional alterations in brain morphometry may be associated with functional decline in frail individuals. Such granularity at a global and regional level of the brain has not been achieved in previous studies of frailty, which reinforces the deep phenotyping approach adopted in this thesis to provide powerful physiological insight into frailty. Whether or not these are causal associations should be a focus of future research. Providing some insight were the findings presented in Chapter Five, which demonstrated significant positive associations between WM volume in the postcentral and precentral gyri and knee extensor isometric strength (Chapter Five appendices, **Table 5.21**). These brain

regions contain the primary motor cortex and are the origin of several motor pathways, such as the corticospinal tract [422]. Therefore, atrophy of these regions may contribute to lower work output in frail individuals by affecting neural connections in motor pathways.

From a broader perspective, the significant associations depicted in **Figure 6.1** and **Figure 6.2** highlight that physiological traits across several organs are associated with functional decline in frailty. For example, in addition to the significant associations between physiological system and physical function characteristics outlined above, handgrip strength was significantly and negatively associated with myocardial T1 time ($r < -0.35$; $P < 0.01$) and calf muscle fat fraction ($r < -0.35$; $P < 0.05$). These findings stress the need for whole body phenotyping investigations when exploring the physiological underpinnings and aetiology of human frailty, and that single organ assessments represent a reductionist approach to characterising a multifactorial syndrome. Future research should investigate physiological traits across multiple organs alongside physical function measures in longitudinal study designs. If functional decline occurs in tandem with deterioration in physiological characteristics (e.g., loss of muscle mass and brain atrophy) over time then these physiological traits may be viewed as targets for interventions aiming to improve functional capacity and mitigate frailty development in older individuals.

6.3.2 Brain-Muscle axis

The correlation matrices highlight significant associations between global brain morphometry parameters and body composition measures (groupings **B** and **D** in **Figure 6.1** and **Figure 6.2**). For example, global GM and WM volume exhibited significant positive correlations ($r > 0.35$; $P < 0.01$), and global CSF volume showed

significant negative correlations (r < -0.35; P < 0.01), with leg skeletal muscle volume. This suggests atrophy of skeletal muscle and the brain occurs in tandem in the decline into frailty. Previous ageing research has similarly reported positive associations between global brain volumes and muscle mass [445], reinforcing that phenotypic traits of ageing and frailty may include interactions between the skeletal muscle and the brain. Of course, mechanistic insight into these relationships is lacking and whether such association is mediated by interactions between these organs requires closer scrutiny.

6.3.3 Cardiovascular and brain haemodynamic traits

Interestingly, there were no significant associations between cardiac and brain haemodynamic metrics (groupings **C** and **E** in **Figure 6.1** and **Figure 6.2**). This may be surprising as cardiovascular and brain haemodynamic measures, such as CBF, are closely correlated. For example, using collated data from 5 studies, Meng et al., [438] demonstrated that changes in cardiac output and CBF during exercise are strongly correlated (R^2 = 0.89). However, the lack of associations between cardiac and brain haemodynamic measurements in the current study may be attributed to assessments being performed at rest and in a volunteer cohort free from overt disease, thus these phenotypic traits may not have been manifested due to the absence of physiological perturbation. A limited number of studies have utilised a physiological stressor to study cardiovascular and brain haemodynamic responses in frail individuals. NIRS assessments have revealed similar cerebral oxygen saturation values at rest in non-frail, pre-frail and frail individuals, however following orthostasis a negative association between frailty severity and cerebral oxygen saturation was observed (t = -2.77; P < 0.05) [157]. Furthermore, a previous study demonstrated that heart rate

measurements performed during walking exercise exhibited stronger associations with frailty status compared to resting-state measures [318]. Whilst these studies indicate a physiological stress stimulus may better manifest phenotypic traits than resting state measures, NIRS does not permit whole brain oxygenation measurements and measurements of heart rate could be expanded to other cardiovascular metrics (e.g., SV, EF) to improve insight. These considerations provide a strong rationale for further research in frail individuals adopting protocols of exercise within an MRI scanner with MR compatible ergometers, during which a comprehensive battery of MRI scans quantifying dynamic parameters of the heart and whole brain haemodynamics would provide powerful insight into the phenotypic traits of frailty.

6.3.4 Visceral adiposity

It is perhaps surprising to note that, with the exception of a significant positive correlation between EF and visceral adipose tissue volume ($r > 0.35$; $P < 0.05$; **Figure 6.1**, **Figure 6.2**), there were no significant associations observed between visceral adiposity and any other physiological system measure (grouping **B**, **Figure 6.1**, **Figure 6.2**). Greater visceral adiposity is a robust marker of poor metabolic health, associated with comorbidities across several organs (e.g., type 2 diabetes [360], coronary heart disease [361]), which may contribute to the to the multi-morbidity aspect of frailty [362]. However, the lack of associations between visceral adiposity and other endpoint measures outlined herein (**Figure 6.1**, **Figure 6.2**) do not support this theory. Perhaps underpinning the lack of associations between adiposity and other endpoint measures may have been the low incidence of obesity and diabetes that were observed in the participant cohort of this study (Chapter Two, **Table 2.1**). Of course, the small sample size of frail individuals recruited (n = 6) may have contributed to the low incidence of

these comorbidities, and larger sample sizes in future studies may provide greater insight into relationships between adiposity and other physiological and physical function endpoints.

6.3.5 Novel insight into the frailty phenotype gained by integrating data within this thesis

Perhaps the greatest novel insight into the frailty phenotype shown in this thesis comes from the direct measurements of organ structural and functional characteristics. Previous studies have mostly adopted imprecise metrics to characterise organs/physiological systems. For example, adiposity has been assessed with crude BMI and skinfold thickness measures previously [180, 245], whereas the present study directly quantified visceral adipose tissue volume with MRI. This improved accuracy in measurement techniques provides greater validity to the findings of altered phenotypic traits in frail versus non-frail individuals. Another strength of the present study was the number of physiological metrics assessed within the whole body phenotype. Previous studies have typically adopted metrics to define six physiological systems to determine multisystem dysregulation in frailty studies [180, 245, 249] whereas the present study assessed 25 variables (**Figure 6.1, Figure 6.2**). Despite these measures being grouped into five systems (i.e., physical function, body composition, cardiac, brain morphometry, brain haemodynamics and oxygenation) for some comparisons, associations between individual variables were quantified, which produced greater granularity regarding how specific measures of organ structure and function are interrelated within the frailty phenotype. Of course, a comprehensive characterisation of the frailty phenotype would require further expanding of physiological measurements across organs and physiological systems. Furthermore, the smaller

sample size of the present study (n = 35) versus previous studies (e.g., n = 1754 [249], n = 704 [245]) should be considered when interpreting the findings. Nonetheless, the insight gained by the current study could be used in future phenotyping studies adopting similar multi-organ measurement techniques to more comprehensively characterise the phenotype of frailty.

6.3.6 Conclusion

The findings of this Chapter demonstrate that the physiological phenotype of frailty is primarily characterised by alterations and interactions within the skeletal muscle and brain, which may contribute to physical function decline in frail individuals. Alterations within the cardiovascular and brain haemodynamic systems do not appear to be phenotypic traits of frailty, although this may be due to measurement being made in the resting state. In-bore exercise protocols within the MRI scanner may provide greater insight into if these metrics present within the phenotype following a stress stimulus. By adopting robust assessments of organ structure and function, alongside a greater number of associations between physiological variables than previous studies, this Chapter has provided novel insight into the multi-organ phenotype of frailty and identified several physiological targets for future studies aiming to explore interactions between physiological traits of several organs and physical function in frail individuals.

Chapter Seven: General Discussion

7.1 Thesis rationale and aims

Frailty is an age-related syndrome characterised by an increased vulnerability to adverse health outcomes and death when compared to the non-frail state [3]. Despite considerable knowledge of the negative outcomes associated with this syndrome, the physiological characteristics and mechanistic drivers (i.e., the physiological phenotype) of frailty are poorly understood. As such, frailty is at present entirely operationally defined by way of clinical symptoms and physical functional assessments (e.g., handgrip strength), which restricts the identification of physiological traits that can be targeted with treatments and interventions to mitigate frailty progression. Research studies aiming to improve understanding by investigating the phenotypic traits of frail versus non-frail individuals have largely focussed investigations on single organs in the human body with imprecise physiological measurement techniques, and results have reported conflicting findings. Furthermore, some authors have purported that investigations of single organs represent a reductionist approach to a syndrome that likely has a complex and multifactorial aetiology, and that a multi-organ perspective is more appropriate to illuminate the physiological phenotype of frailty [180, 245]. Empirical evidence reinforcing these notions has highlighted that frailty is likely concomitant with simultaneous decline in numerous physiological systems [249]. For example, in a seminal study of older women, Fried et al., [245] assessed blood biomarker and functional measures in six physiological systems (anaemia, inflammation, endocrine, micronutrients, adiposity, and fine motor speed) and highlighted that abnormal values in five systems increased frailty risk by 26-fold (compared to zero abnormal systems). However, current findings

from these studies assessing multisystem dysregulation may be compromised by imprecise measurements of organ structure and function (e.g., blood biomarkers). Therefore, there is large potential for improving insight into the phenotype of frailty with the application of robust multi-organ physiological techniques in studies of frail individuals.

The aim of this thesis was to provide novel insight into the physiological phenotype of frailty by employing multi-organ assessment techniques and measures of physical function in older human volunteers. Particular focus was applied to investigations of the heart, skeletal muscle, adipose tissue, neuromuscular system and brain, as these systems have been shown to be key mediators of age-related physiological change and have been implicated within the frailty phenotype. This multi-organ approach aimed to highlight distinct physiological characteristics of frailty, which may be viewed as areas for further research into mechanisms of frailty development and targets for future interventions aiming to mitigate the syndrome's development.

7.2 Summary of main findings

7.2.1 Cardiac structure and function in pre-frailty and frailty

In Chapter Three, resting cardiac MRI revealed no differences in structural (e.g., left ventricular mass, aortic CSA) or functional (e.g., stroke volume, cardiac output) cardiac parameters between non-frail, pre-frail and frail females, indicating structural and functional differences within the cardiovascular system do not differentiate the frail versus non-frail phenotypes when measured in a supine state at rest. Novelty in this Chapter was presented through the first study of MRI techniques to quantify cardiac metrics in pre-frail and frail individuals, which improves the validity of findings compared to previous studies adopting echocardiography protocols, given MRI is less

prone to patient- and operator-related variance [183-185]. Furthermore, the majority of previous studies have adopted mixed sex participant samples, which likely introduced variance to the data due to sex differences in cardiac morphology and function [299]. As such, with the application of MRI within an all-female group, the present study provides greater insight into cardiac characteristics in pre-frail and frail individuals.

7.2.2 Body composition, neuromuscular characteristics and muscle function in pre-frailty and frailty

Chapter Four detailed investigations into body composition, neuromuscular, and physical function characteristics in non-frail, pre-frail and frail females. The main findings included lower skeletal muscle volume of the dominant leg and lower functional quality, isometric strength, work output and neuromuscular control of the knee extensors in pre-frail and frail versus non-frail females, but no differences in intramuscular or visceral adipose tissue volume between groups. The lower skeletal muscle volume observed in the pre-frail and frail groups likely underpinned the lower isometric strength exhibited by these groups, as these functional measures are dictated by muscle mass. Interestingly though, the lack of differences in intramuscular and visceral adipose tissue volume between groups suggests greater adiposity is not underpinning the lower muscle metabolic quality observed (i.e., lower knee extensor functional quality and work output capacity) in pre-frailty and frailty, and points to deconditioning of the muscle as an alternate driver of reduced muscle quality in frailty. A loss of mitochondrial content and/or function may underpin this deconditioning of the muscle, which should be explored in future research. The finding of poorer neuromuscular control of the knee extensors in the pre-frail and frail groups also

provides insight into functional impairments during frailty, as poorer neuromuscular control has been linked to slower walking speed [286] and greater risk of falls [353]. By combining robust MRI-derived body composition measurements with multiple functional assessments indicative of skeletal muscle strength, neuromuscular control and metabolic quality, this study provides insight into the physiological underpinnings of diminished functional capacity during frailty.

7.2.3 Brain morphometry, haemodynamics and oxygenation in pre-frailty and frailty

In Chapter Five structural and resting haemodynamic measures of the brain were investigated in non-frail, pre-frail and frail using MRI, with several novel findings reported. Lower regional grey and white matter volumes and differences in cortical folding were observed in frail compared to non-frail volunteers. The greatest differences in regional grey and white matter volume were evident in the postcentral gyrus, frontal pole and lateral occipital cortex, and atrophy of these regions may be related to reduced proprioceptive and cognitive performance in frail individuals. In regression analyses, grey and white matter volumes in numerous brain regions related to motor function and cognition were strongly associated with physical function measures, including knee extensor isometric strength and work output. Interestingly, this indicates that, in conjunction with motor processes, cognitive processes may also be related to functional decline in frailty. Finally, the MRI measures of functional and haemodynamic measures of the brain including CBF, OEF and $CMRO_2$, revealed a lack of differences between groups, suggesting frailty is not characterised by differences in resting cerebral blood flow and oxygen utilisation compared to the non-frail state in the supine resting state. By combining assessments of multiple global and

regional structural and functional parameters of the brain, this Chapter provided more comprehensive insight into the physiological characteristics of the brain in frailty compared to previous studies focusing on individual structural parameters (e.g., grey matter volume).

7.2.4 Data integration to further insight of the physiological phenotype of frailty

By integrating the physiological and physical function data presented in the experimental Chapters of this thesis, Chapter Six revealed numerous significant associations between measures of physical function and organ structure and function traits. Physical function characteristics were significantly associated with several body composition, cardiac and brain morphometry parameters. These findings indicate that functional decline, the hallmark characteristic of frailty, may be underpinned by deterioration in physiological characteristics across multiple organs. Significant associations were also observed between skeletal muscle volume and brain morphometry parameters, indicating interactions between these organs may be key contributors to the physiological phenotype of frailty. Given the direct assessments of organ structure and function with MRI, alongside a greater number of associations between physiological variables than previous studies, this Chapter provided novel insight into the multi-organ phenotype of frailty, thus identifying several targets for future studies aiming to further explore interactions between physiological traits as features of the frailty phenotype.

7.3 Strengths of this research

The main strength of this thesis was the multi-organ approach adopted to investigate the phenotype of frailty, this involved MRI-derived physiological assessments of multiple organs alongside measurements of neuromuscular and physical function.

This approach has provided greater insight compared to the majority of previous frailty studies focusing investigations on single organs (e.g., the heart or skeletal muscle). For example, lower skeletal muscle volume was observed alongside lower isometric strength of the knee extensors in pre-frail and frail versus non-frail females (evidenced in Chapter Four), indicating that skeletal muscle atrophy may underpin functional impairments during frailty. Similarly, in Chapter Five, grey and white matter volumes were strongly associated with physical function measures, which suggests that atrophy of the brain may also contribute to functional impairments in frail individuals. Furthermore, the direct measurements of organ structure and function utilised herein provide greater validity to findings from previous studies that have adopted imprecise measurements of organ characteristics (e.g., blood biomarkers) to investigate multisystem dysregulation during frailty [245]. The present study therefore provides novel and valid evidence that frailty is associated with physiological differences in the skeletal muscle and brain compared to the non-frail state.

The use of MRI in this study provides greater validity compared to previous studies of frailty assessing cardiac and skeletal muscle characteristics. MRI is considered the gold standard modality for assessment of cardiac structure and function, and Chapter Three provides greater validity of findings compared to the majority of previous studies of frailty that have assessed cardiac parameters with echocardiography [179, 181]. Measurements of skeletal muscle volume with MRI are also considered the gold standard, due to the method's excellent accuracy compared with cadaver analysis (r = 0.99) [46]. The use of MRI to quantify whole muscle and IMAT volume of the lower limbs in Chapter Four improves insight compared to previous frailty studies performing body composition assessments with less precise DEXA and BIA measurements of

lean mass [42, 43], and estimations of skeletal muscle and IMAT CSA with imaging techniques [49, 53].

The all-female sample of participants adopted in the present study is a strength considering many of the physiological parameters are reportedly influenced by sex, such as skeletal muscle volume [28], cardiac structure and function measures [299] and brain volume [122]. This reinforces that sex stratification of participants prior to analyses is a key consideration when designing physiological research studies with frail participants. The all-female sample adopted herein is an improvement in study design compared to the majority of previous studies, for example two previous studies assessing similar cardiac parameters as the present study used a mixed sex sample with the proportion of males with frailty of 51% [179] and 30% [180]. The combination of sexes potentially imparts variation into these data, and limits comparisons between studies due to potential differences in the magnitude of sex-related variance.

7.4 Reflective considerations

The low number of frail individuals recruited in the present study (n = 6) should be considered. The low statistical power in the frail group may have contributed to the larger variance observed in some of the physiological parameters assessed (e.g., aortic blood flow; **Figure 3.9**). It is possible that a greater sample size would have reduced this variance and therefore different outcomes for these metrics. Recruitment of frail individuals in this study proved difficult, perhaps due to the recruitment setting of outpatient clinics. It became clear during recruitment that frail older people do not often present to in-person clinics, with many consultations occurring over the phone due to difficulties in patient mobility and feasibility of transportation to the hospital. Recruitment from a community setting (e.g., local general practitioners and care

homes) may have been more appropriate to access individuals living with frailty that were not able to attend hospital clinics. Although transport to the laboratory and performance of physiological testing may be difficult in care home residents with very low functional capacity, which makes physiological research using specialist equipment (e.g., MRI scanners) difficult. Of course, recruitment of frail individuals remains a difficulty for many other research studies, with reports of low enrolment and high drop-out rates of frail older individuals in research studies [446, 447]. Further, previous physiological research studies note a much lower number of frail versus non-frail individuals in participant samples. For example, in a study of 484 older individuals, only 12 were identified as frail [132], and in a study assessing frailty within the UK Biobank data, 4% of individuals were classified as frail [123], which reinforces the difficulty of recruiting large sample sizes of frail individuals, despite the increasing prevalence of frailty in the UK ageing population [448]. Considering frailty is associated with a wide and varying array of presentations, many factors could potentially act as barriers to participation. In studies exploring these barriers, a lack of perceived benefit, poor health and mobility problems have all been identified as reasons for lower recruitment of frail individual to research studies [449]. Indeed, during recruitment for the present study, mobility limitations and poor health were acknowledged by many potential participants as reasons not to participate, with individuals expressing an inability to perform the functional assessments (e.g., knee extension strength and iEMG testing), apprehension in transportation to the laboratory setting, and manoeuvring into the MRI scanner, as reasons for refusal to participate. The current study was also observational in nature, which may have been viewed as little benefit to potential participants. From the perspective of physiological research, recruitment of frail individuals into studies employing multi-organ assessments may also be

hindered by the high prevalence of comorbidities in this demographic [362]. Individuals with certain comorbidities are likely to be excluded due to the potential effects of these existing conditions influencing physiological parameters separately to frailty. Nonetheless, this study showed that in-depth multi-organ physiological assessments are feasible within the frailty demographic, and the fact that significant differences were observed between non-frail and frail groups for several metrics suggests adequate power was achieved. Previous studies have also highlighted strategies to improve recruitment and retention of frail individuals in research studies, which include establishing a partnership with staff that participants know and trust [449]. This calls for greater collaboration between clinical staff, that are known to potential participants, and research staff to make the patient feel at ease with participation.

The demographic characteristics of the sample adopted in this study may be deemed somewhat atypical of the wider ageing population in the UK. For example, in the ELSA cohort of 5,087 older females (mean age: 66 years), 46% presented with hypertension and 44% with arthritis [359]. In the current study, hypertension was reported in 29-33% and arthritis in 20-21% of non-frail and pre-frail females (Chapter Two – Table 2.1). The lower rates of hypertension in females in the current study versus the ELSA cohort suggest the current sample were relatively robust regarding cardiovascular function, which may have contributed to the lack of differences in cardiovascular characteristics between non-frail and frail states detailed in Chapter Three. Furthermore, BMI values in the non-frail and frail females in the present study (mean: 23.3 kg/m^2; Chapter Two – Table 2.1) were lower than those observed in a sample of 265,988 older females in the UK Biobank (27.0 kg/m^2) [450], which may have underpinned the similar IMAT and visceral adipose volume values observed between groups in Chapter Five. Of course, the lower sample size (n = 35) of the current study versus these previous population-

based cohorts likely contributed to these discrepancies in demographic characteristics, and greater recruitment would have likely reduced this variance.

Whilst the all-female sample in the present study was a strength in terms of variance, male individuals and the physiological phenotype of frailty in males was not studied. Frailty is more prevalent in females than males [251], and this may be underpinned by differences in physiological presentations and mechanisms causing frailty progression. Ideally, future studies should assess male and female participants separately in analyses to overcome potential sex-related variance in the data. Whilst accounting for both males and females may make the already difficult task of recruiting adequate numbers of frail individuals into research studies more difficult, it is a fundamental consideration to ensure validity of findings by reducing variance external to frailty.

One consideration of the present study concerns the cross-sectional study design. Functional and physiological phenotyping assessments were performed only once, providing associational evidence with little insight into whether the physiological differences observed between healthy and frail states are indeed related to frailty progression over time. A longitudinal study design would have been required to provide this insight. It should be noted that a longitudinal study was outside the scope of this thesis, and studies gathering physiological data within longitudinal study designs are rare within the context of frailty research. This is perhaps due to the vulnerable nature of frail individuals and the fact that this demographic may be approaching the end of life. Promisingly, large scale research databases such as the UK Biobank [451] contain longitudinal data regarding frailty status, which has been used to investigate associations between frailty severity and structural brain parameters (e.g., grey matter

volume) derived from MRI [123]. Furthermore, prospective studies using baseline physiological measurements have been used to provide associations between differences in structural brain measures (e.g., greater WMH volume and lower cortical thickness) and incidence of frailty when assessed at follow up [132, 146]. Whilst these studies are limited by prospective designs (i.e., physiological assessments performed only at baseline), they indicate that longitudinal investigations are possible with frail volunteers.

Importantly, the present study provides several physiological end-point measures that should be investigated in future longitudinal studies of frailty. For example, given the observations of lower skeletal muscle volume in the pre-frail and frail versus non-frail volunteers in this study, future studies should determine if skeletal muscle volume declines in tandem with frailty progression over time. If so, loss of skeletal muscle volume may be deemed a contributing factor towards frailty progression and subsequent interventions could be designed to increase muscle volume and potentially mitigate frailty development. The temporal relationship between frailty and changes in brain structure parameters should also be investigated further in longitudinal studies, considering the findings of lower grey and white matter volumes and greater WMH volume in pre-frail and frail versus non-frail volunteers in the present study. Ideally, future longitudinal investigations should perform multi-organ phenotyping assessments in frail individuals, similarly to the present study, to provide insight into which tissues are key mediators of physiological decline and therefore important targets for interventions.

In Chapter Five, regression analyses were performed to determine associations between regional brain volumes and handgrip strength and walking speed, which

revealed strong associations between these physical function measures and GM and WM volumes in several brain regions. It should be noted that low handgrip strength and walking speed were used to define frailty status, as proposed by the Fried Physical Frailty Phenotype [17]. Therefore, the likelihood of handgrip strength and walking speed being associated with brain volumes in frail individuals may have been increased as the groups were primarily defined using these physical function measures. Nonetheless, strong associations were also observed between regional GM and WM volumes and other physical function measures that were not utilised to define frailty (i.e., knee extensor isometric strength and work output), reinforcing the conclusion that lower brain volumes may be related to diminished physical function in frail individuals.

7.5 Future directions

7.5.1 Additional measures for multi-organ phenotyping

A logical next step for research is the inclusion of other physiological systems into multi-organ investigations of the frailty phenotype. As outlined in Chapter Two, Section 2.8.9, this study collected data from several MRI sequences to quantify metrics such as cerebral perfusion and white matter microstructural integrity from DTI, but these were not analysed for inclusion in this thesis. Therefore, in future adding these measures will provide a more comprehensive characterisation of the physiological characteristics of the brain in frail individuals. Furthermore, whilst this study purposefully focussed on major organs associated with physiological changes during ageing, alterations within other organs may also contribute to the frailty phenotype. Whole body MRI scanners allow multiple organs to be studied in a single ~1 hour scan session and the choice of organs could be expanded. Other research groups have

also started to explore the physiological characteristics of frailty using multi-organ MRI, with preliminary data highlighting interstitial fibrosis within the liver and skeletal muscle in frailty [303]. Similar metrics of organ size and volume can in future be analysed using the data gathered in this study, as well as measures of liver T1 mapping to similarly investigate fibrosis. This reinforces that MRI is well suited to investigate multi-organ physiology in studies of frailty, given the wide range of measures available to this modality, and can be adopted to investigate other organs that may contribute to the frailty phenotype.

7.5.2 Physiological modelling

In tandem with this expansion of MRI measures, physiological modelling approaches are likely to provide greater insight into the physiological phenotype of frailty. These approaches utilise physiological data gathered from several organs to create a statistical model by which interactions between organ characteristics can be quantified. This modelling approach would provide greater insight than investigations of single organs and tissues, which have been adopted in the majority of frailty studies to date, in conjunction with providing much greater physiological insight than studies assessing multisystem dysregulation by inferring complex organ physiology from imprecise blood biomarkers.

7.5.3 Investigations performed during conditions of physiological stress

The lack of differences in cardiac (Chapter Three) and cerebral (Chapter Five) haemodynamic parameters between non-frail and frail states may be attributed to measurements being made in the resting supine state. As outlined in Chapter One, Section 1.6, dynamic measurements made during conditions of physiological stress have been identified as potentially more insightful methods of characterising the

physiological phenotype of frailty, compared to resting state assessments, on the basis that the syndrome is defined as a dysregulation of homeostasis [252]. Furthermore, changes in haemodynamic parameters are known to occur across several organs during exercise, such as an elevation in cardiac output and cerebral blood flow [255], indicating that a stress stimulus induces a different physiological state to the resting condition at a multi-organ level, which is appropriate given the evidence of multi-organ dysregulation as concomitant with frailty. Future work should therefore perform physiological assessments during conditions of physiological stress, such as exercise, to investigate dynamic characteristics of the frailty phenotype. MR compatible ergometers are now available for the measurement of dynamic physiological parameters within multiple organs during in-bore exercise, which could be utilised within the context of frailty. A small number of studies have performed investigations of skeletal muscle PCr hydrolysis during and following plantar flexion exercise using ^{31}P MRS in frail individuals, and have highlighted greater rates of PCr hydrolysis during exercise and longer PCr recovery times following exercise in pre-frail and frail versus non-frail individuals [53, 262]. Although dynamic measurements of other key organs, such as the heart and brain, are yet to be explored during conditions of physiological stress within the context of frailty. Nonetheless, these studies demonstrate that dynamic physiological measurements performed during a stress stimulus are feasible in studies of frailty, which may be a consideration given the older and functionally impaired demographic of frail individuals, and should be expanded to investigations of other organs.

7.5.4 Adherence to frailty assessment criteria

Frailty assessment tools are fundamental for identifying individuals at greater risk of negative outcomes and are extremely valuable in a clinical setting. However, from a research perspective, there is a profound requirement for the adoption of standardised frailty assessment criteria in studies of frailty. One issue concerns the large number of instruments available for the identification of frailty, with a systematic review evidencing that 67 different frailty assessment methods have been cited in the literature [21]. In the present study, the Physical Frailty Phenotype assessment [17] was adopted as this has been identified as the gold standard criteria [10], and it has been demonstrated that this method is the most frequently adopted assessment within the frailty literature [21]. Despite this supposed adoption of the same method across studies, authors frequently exclude and modify several components of the assessment criteria. For example, some authors have substituted walking speed assessments with the timed up and go test to assess the ‘slowness’ criterion [118, 143]. A systematic review of 264 studies implementing the Physical Frailty Phenotype method revealed that 224 studies performed at least one modification to the assessment criteria, such as excluding certain criteria or assessing the ‘weakness’ criterion by questions (e.g., ability to lift groceries) rather than handgrip strength tests [250]. In secondary analyses, Theou et al., [250] used frailty assessment data available from 2539 older individuals and excluded specific criteria from the assessment to determine the effects of these exclusions on frailty identification. These exclusions resulted in large variations in the prevalence of frailty, for example, when the ‘weight loss’ criterion was excluded frailty prevalence was 24% and when the ‘weakness’ criterion was excluded frailty prevalence was 13.9% [250]. These findings suggest that modifications to frailty criteria are common and may result in the differential identification of frail individuals

across studies, thus impacting the validity of comparisons between studies. In conjunction with frequent modifications to frailty assessment criteria, some authors have also proposed that the Physical Frailty Phenotype [17] and Frailty Index [19] methods cannot be used synonymously when identifying frailty, due to differing designs and rationales between methods [452]. Accordingly, when the Physical Frailty Phenotype and Frailty Index methods were both used to assess frailty status in a cohort of 4096 older adults, the prevalence of frailty was demonstrated to be 3.6% and 34%, respectively [453]. These findings indicate that comparisons of findings from studies utilising the Physical Frailty Phenotype versus Frailty Index criteria may not be valid as the methods identify frail individuals differently, which is particularly alarming considering these methods are the two most cited assessments within studies of frailty [21]. Together these findings highlight profound issues in the assessment of frailty in research studies at present, which have negative effects on data comparison across studies. Adherence to a single assessment method is therefore fundamental to achieve valid comparisons and consensus of findings between studies.

7.6 Conclusion

Findings of this thesis improved understanding of the physiological phenotype of frailty. The robust measurement techniques employed to investigate several organs provided greater validity to previous findings demonstrating dysregulation in multiple physiological systems during frailty. Novel assessments of several organ parameters were performed, such as cardiac T1 mapping and oxygen utilisation of the brain, which improved understanding of the physiological characteristics of these organs in frail individuals. Furthermore, by integrating physiological and physical function data, characteristics of body composition, the heart and the brain were shown to be associated with physical function in frail individuals. This integration of physical

function data with intricate physiological variables across multiple organs has not been achieved previously, which provided much needed insight into the potential underpinnings of functional decline during frailty. In particular, the phenotype of frailty seems to be primarily characterised by alterations and interactions within the skeletal muscle and brain, which may contribute to physical function decline in frail individuals. Several physiological targets have been identified for further assessment in studies employing a stress stimulus (e.g., exercise) to manifest differences in dynamic parameters between non-frail and frail states, which is key in understanding the dysregulation in homeostasis that is central to frailty. Furthermore, this thesis has identified a research pathway to inform on the design of longitudinal studies to determine the physiological changes underlying frailty progression.

References

1. Office for National, S., https://www.ons.gov.uk/peoplepopulationandcommunity/birthsdeathsandmarriages/lifeexpectancies/bulletins/pastandprojecteddatafromtheperiodandcohortlifetables/1981to2018.
2. House of Lords, S. and C. Technology, Ageing: Science, Technology and Healthy Living. https://committees.parliament.uk/work/1/ageing-science-technology-and-healthy-living/publications/, 2021.
3. Morley, J.E., B. Vellas, G.A. Van Kan, et al., Frailty consensus: a call to action. Journal of the American Medical Directors Association, 2013. 14(6): p. 392-397.
4. O'Caoimh, R., L. Galluzzo, Á. Rodríguez-Laso, et al., Prevalence of frailty at population level in European ADVANTAGE Joint Action Member States: a systematic review and meta-analysis. Annali dell'Istituto superiore di sanita, 2018. 54(3): p. 226-239.
5. Fried, L.P., L. Ferrucci, J. Darer, et al., Untangling the concepts of disability, frailty, and comorbidity: implications for improved targeting and care. The Journals of Gerontology Series A: Biological Sciences and Medical Sciences, 2004. 59(3): p. M255-M263.
6. Wong, C.H., D. Weiss, N. Sourial, et al., Frailty and its association with disability and comorbidity in a community-dwelling sample of seniors in Montreal: a cross-sectional study. Aging clinical and experimental research, 2010. 22(1): p. 54-62.
7. Fang, X., J. Shi, X. Song, et al., And mortality in older Chinese adults: Results from the Beijing longitudinal study of aging. The journal of nutrition, health & aging, 2012. 16(10): p. 903-907.
8. Gill, T.M., E.A. Gahbauer, L. Han, et al., The relationship between intervening hospitalizations and transitions between frailty states. Journals of Gerontology Series A: Biomedical Sciences and Medical Sciences, 2011. 66(11): p. 1238-1243.
9. Lee, L., T. Patel, A. Costa, et al., Screening for frailty in primary care: Accuracy of gait speed and hand-grip strength. Canadian Family Physician, 2017. 63(1): p. e51-e57.
10. Dent, E., J.E. Morley, A.J. Cruz-Jentoft, et al., Physical Frailty: ICFSR International Clinical Practice Guidelines for Identification and Management. J Nutr Health Aging, 2019. 23(9): p. 771-787.
11. Dapp, U., C.E. Minder, J. Anders, et al., Long-term prediction of changes in health status, frailty, nursing care and mortality in community-dwelling senior citizens-results from the longitudinal urban cohort ageing study (LUCAS). BMC geriatrics, 2014. 14(1): p. 141.
12. Hoogendijk, E.O., L. Romero, P.M. Sánchez-Jurado, et al., A new functional classification based on frailty and disability stratifies the risk for mortality among older adults: The FRADEA Study. Journal of the American Medical Directors Association, 2019. 20(9): p. 1105-1110.
13. Organization, W.H., World Report on Ageing and Health. 2015.
14. Organization, W.H., WHO clinical consortium on healthy ageing: topic focus: frailty and intrinsic capacity: report of consortium meeting, 1–2 December 2016 in Geneva, Switzerland. 2017, World Health Organization.

15. Belloni, G. and M. Cesari, Frailty and intrinsic capacity: two distinct but related constructs. Frontiers in medicine, 2019. 6: p. 133.
16. Liu, S., X. Yu, X. Wang, et al., Intrinsic Capacity predicts adverse outcomes using Integrated Care for Older People screening tool in a senior community in Beijing. Arch Gerontol Geriatr, 2021. 94: p. 104358.
17. Fried, L.P., C.M. Tangen, J. Walston, et al., Frailty in older adults: evidence for a phenotype. The Journals of Gerontology Series A: Biological Sciences and Medical Sciences, 2001. 56(3): p. M146-M157.
18. Liu, S., L. Kang, X. Liu, et al., Trajectory and correlation of intrinsic capacity and frailty in a Beijing elderly community. Frontiers in medicine, 2021. 8: p. 751586.
19. Mitnitski, A.B., A.J. Mogilner, and K. Rockwood, Accumulation of deficits as a proxy measure of aging. Sci World J, 2001. 1: p. 323-336.
20. Boreskie, K.F., J.L. Hay, P.E. Boreskie, et al., Frailty-aware care: giving value to frailty assessment across different healthcare settings. BMC geriatrics, 2022. 22: p. 1-12.
21. Buta, B.J., J.D. Walston, J.G. Godino, et al., Frailty assessment instruments: systematic characterization of the uses and contexts of highly-cited instruments. Ageing research reviews, 2016. 26: p. 53-61.
22. Bouillon, K., M. Kivimaki, M. Hamer, et al., Measures of frailty in population-based studies: an overview. BMC geriatrics, 2013. 13(1): p. 64.
23. Rockwood, K. and A. Mitnitski, Frailty in relation to the accumulation of deficits. The Journals of Gerontology Series A: Biological Sciences and Medical Sciences, 2007. 62(7): p. 722-727.
24. Gill, T.M., E.A. Gahbauer, H.G. Allore, et al., Transitions between frailty states among community-living older persons. Archives of internal medicine, 2006. 166(4): p. 418-423.
25. Lang, P.O., J.P. Michel, and D. Zekry, Frailty syndrome: a transitional state in a dynamic process. Gerontology, 2009. 55(5): p. 539-49.
26. Nachtomy, O., A. Shavit, and Z. Yakhini, Gene expression and the concept of the phenotype. Studies in History and Philosophy of Science Part C: Studies in History and Philosophy of Biological and Biomedical Sciences, 2007. 38(1): p. 238-254.
27. Fielding, R.A., B. Vellas, W.J. Evans, et al., Sarcopenia: an undiagnosed condition in older adults. Current consensus definition: prevalence, etiology, and consequences. International working group on sarcopenia. Journal of the American Medical Directors Association, 2011. 12(4): p. 249-256.
28. Janssen, I., S.B. Heymsfield, Z. Wang, et al., Skeletal muscle mass and distribution in 468 men and women aged 18–88 yr. Journal of applied physiology, 2000.
29. Berger, M.J. and T.J. Doherty, Sarcopenia: prevalence, mechanisms, and functional consequences. Body composition and aging, 2010. 37: p. 94-114.
30. Shou, J., P.-J. Chen, and W.-H. Xiao, Mechanism of increased risk of insulin resistance in aging skeletal muscle. Diabetology & Metabolic Syndrome, 2020. 12(1): p. 1-10.
31. Marzetti, E., R. Calvani, M. Cesari, et al., Mitochondrial dysfunction and sarcopenia of aging: from signaling pathways to clinical trials. The international journal of biochemistry & cell biology, 2013. 45(10): p. 2288-2301.

32. Fiatarone, M.A., E.F. O'Neill, N.D. Ryan, et al., Exercise training and nutritional supplementation for physical frailty in very elderly people. New England Journal of Medicine, 1994. 330(25): p. 1769-1775.
33. Broskey, N.T., C. Greggio, A. Boss, et al., Skeletal muscle mitochondria in the elderly: effects of physical fitness and exercise training. The Journal of Clinical Endocrinology & Metabolism, 2014. 99(5): p. 1852-1861.
34. Fiatarone, M.A., E.C. Marks, N.D. Ryan, et al., High-intensity strength training in nonagenarians: effects on skeletal muscle. Jama, 1990. 263(22): p. 3029-3034.
35. McGregor, R.A., D. Cameron-Smith, and S.D. Poppitt, It is not just muscle mass: a review of muscle quality, composition and metabolism during ageing as determinants of muscle function and mobility in later life. Longevity & healthspan, 2014. 3(1): p. 9.
36. Newman, A.B., C.L. Haggerty, B. Goodpaster, et al., Strength and muscle quality in a well-functioning cohort of older adults: the Health, Aging and Body Composition Study. Journal of the American Geriatrics Society, 2003. 51(3): p. 323-330.
37. Gingrich, A., D. Volkert, E. Kiesswetter, et al., Prevalence and overlap of sarcopenia, frailty, cachexia and malnutrition in older medical inpatients. BMC geriatrics, 2019. 19(1): p. 1-10.
38. Kim, S.-K., Y.-H. Kwon, J.H. Cho, et al., Changes in body composition according to age and sex among young non-diabetic Korean adults: the Kangbuk Samsung Health Study. Endocrinology and Metabolism, 2017. 32(4): p. 442-450.
39. Koster, A., J. Ding, S. Stenholm, et al., Does the amount of fat mass predict age-related loss of lean mass, muscle strength, and muscle quality in older adults? Journals of Gerontology Series A: Biomedical Sciences and Medical Sciences, 2011. 66(8): p. 888-895.
40. Rizzoli, R., J.Y. Reginster, J.F. Arnal, et al., Quality of life in sarcopenia and frailty. Calcif Tissue Int, 2013. 93(2): p. 101-20.
41. Han, S.S., K.W. Kim, K.I. Kim, et al., Lean mass index: a better predictor of mortality than body mass index in elderly Asians. Journal of the American Geriatrics Society, 2010. 58(2): p. 312-317.
42. Falsarella, G.R., L.P.R. Gasparotto, C.C. Barcelos, et al., Body composition as a frailty marker for the elderly community. Clinical interventions in aging, 2015. 10: p. 1661.
43. Liu, L.K., W.J. Lee, L.Y. Chen, et al., Association between Frailty, Osteoporosis, Falls and Hip Fractures among Community-Dwelling People Aged 50 Years and Older in Taiwan: Results from I-Lan Longitudinal Aging Study. PLoS One, 2015. 10(9): p. e0136968.
44. Sao Romao Preto, L., M.D.C. Dias Conceicao, T.M. Figueiredo, et al., Frailty, body composition and nutritional status in non-institutionalised elderly. Enferm Clin, 2017. 27(6): p. 339-345.
45. Frisoli Jr, A., P.H. Chaves, S.J.M. Ingham, et al., Severe osteopenia and osteoporosis, sarcopenia, and frailty status in community-dwelling older women: results from the Women's Health and Aging Study (WHAS) II. Bone, 2011. 48(4): p. 952-957.
46. Mitsiopoulos, N., R. Baumgartner, S. Heymsfield, et al., Cadaver validation of skeletal muscle measurement by magnetic resonance imaging and

computerized tomography. Journal of applied physiology, 1998. 85(1): p. 115-122.
47. Farrow, M., J. Biglands, S.F. Tanner, et al., The effect of ageing on skeletal muscle as assessed by quantitative MR imaging: an association with frailty and muscle strength. Aging Clin Exp Res, 2020. 33(2): p. 291-301.
48. Ogawa, M., T. Yasuda, and T. Abe, Component characteristics of thigh muscle volume in young and older healthy men. Clinical physiology and functional imaging, 2012. 32(2): p. 89-93.
49. Addison, O., M. Drummond, P. LaStayo, et al., Intramuscular fat and inflammation differ in older adults: the impact of frailty and inactivity. The journal of nutrition, health & aging, 2014. 18(5): p. 532-538.
50. Delgado, C., J.W. Doyle, and K.L. Johansen, Association of frailty with body composition among patients on hemodialysis. Journal of Renal Nutrition, 2013. 23(5): p. 356-362.
51. Cesari, M., C. Leeuwenburgh, F. Lauretani, et al., Frailty syndrome and skeletal muscle: results from the Invecchiare in Chianti study. The American journal of clinical nutrition, 2006. 83(5): p. 1142-1148.
52. Idoate, F., E.L. Cadore, A. Casas-Herrero, et al., Adipose tissue compartments, muscle mass, muscle fat infiltration, and coronary calcium in institutionalized frail nonagenarians. European radiology, 2015. 25(7): p. 2163-2175.
53. Lewsey, S.C., K. Weiss, M. Schär, et al., Exercise intolerance and rapid skeletal muscle energetic decline in human age-associated frailty. JCI insight, 2020. 5(20).
54. Buckinx, F., J.-Y. Reginster, J. Petermans, et al., Relationship between frailty, physical performance and quality of life among nursing home residents: the SENIOR cohort. Aging clinical and experimental research, 2016. 28(6): p. 1149-1157.
55. Skoglund, E., T.R. Lundberg, E. Rullman, et al., Functional improvements to 6 months of physical activity are not related to changes in size or density of multiple lower-extremity muscles in mobility-limited older individuals. Experimental gerontology, 2022. 157: p. 111631.
56. Latimer, L.E., D. Constantin-Teodosiu, B. Popat, et al., Whole-body & muscle responses to aerobic exercise training and withdrawal in ageing & COPD. European Respiratory Journal, 2021.
57. Melville, D.M., J. Mohler, M. Fain, et al., Multi-parametric MR imaging of quadriceps musculature in the setting of clinical frailty syndrome. Skeletal radiology, 2016. 45(5): p. 583-589.
58. Beasley, L.E., A. Koster, A.B. Newman, et al., Inflammation and race and gender differences in computerized tomography-measured adipose depots. Obesity, 2009. 17(5): p. 1062-1069.
59. Villareal, D.T., M. Banks, C. Siener, et al., Physical frailty and body composition in obese elderly men and women. Obes Res, 2004. 12(6): p. 913-20.
60. Morley, J.E., S.D. Anker, and S. Von Haehling, Prevalence, incidence, and clinical impact of sarcopenia: facts, numbers, and epidemiology—update 2014. J Cachexia Sarcopenia Muscle, 2014. 5: p. 253-259.

61. Cuthbertson, D., K. Smith, J. Babraj, et al., Anabolic signaling deficits underlie amino acid resistance of wasting, aging muscle. The FASEB Journal, 2005. 19(3): p. 1-22.
62. Kumar, V., A. Selby, D. Rankin, et al., Age-related differences in the dose–response relationship of muscle protein synthesis to resistance exercise in young and old men. The Journal of physiology, 2009. 587(1): p. 211-217.
63. Brook, M.S., D.J. Wilkinson, W.K. Mitchell, et al., Synchronous deficits in cumulative muscle protein synthesis and ribosomal biogenesis underlie age-related anabolic resistance to exercise in humans. The Journal of physiology, 2016. 594(24): p. 7399-7417.
64. Rennie, M., A. Selby, P. Atherton, et al., Facts, noise and wishful thinking: muscle protein turnover in aging and human disuse atrophy. Scandinavian journal of medicine & science in sports, 2010. 20(1): p. 5-9.
65. Haddad, F., F. Zaldivar, D.M. Cooper, et al., IL-6-induced skeletal muscle atrophy. J Appl Physiol, 2005. 98(3): p. 911-917.
66. De Benedetti, F., C. Meazza, M. Oliveri, et al., Effect of IL-6 on IGF binding protein-3: a study in IL-6 transgenic mice and in patients with systemic juvenile idiopathic arthritis. Endocrinology, 2001. 142(11): p. 4818-4826.
67. Chew, J., L. Tay, J.P. Lim, et al., Serum Myostatin and IGF-1 as Gender-Specific Biomarkers of Frailty and Low Muscle Mass in Community-Dwelling Older Adults. J Nutr Health Aging, 2019. 23(10): p. 979-986.
68. Hassan-Smith, Z.K., S.A. Morgan, M. Sherlock, et al., Gender-specific differences in skeletal muscle 11β-HSD1 expression across healthy aging. The Journal of Clinical Endocrinology & Metabolism, 2015. 100(7): p. 2673-2681.
69. Blodgett, J., O. Theou, S. Kirkland, et al., The association between sedentary behaviour, moderate–vigorous physical activity and frailty in NHANES cohorts. Maturitas, 2015. 80(2): p. 187-191.
70. Rice, H., K. Hill, R. Fowler, et al., Reduced Step Count and Clinical Frailty in Hospitalized Adults With Community-Acquired Pneumonia. Respir Care, 2020. 65(4): p. 455-463.
71. Theou, O., J.M. Jakobi, A.A. Vandervoort, et al., A comparison of physical activity (PA) assessment tools across levels of frailty. Arch Gerontol Geriatr, 2012. 54(3): p. e307-14.
72. Breen, L., K.A. Stokes, T.A. Churchward-Venne, et al., Two weeks of reduced activity decreases leg lean mass and induces “anabolic resistance” of myofibrillar protein synthesis in healthy elderly. The Journal of Clinical Endocrinology & Metabolism, 2013. 98(6): p. 2604-2612.
73. Milanović, Z., S. Pantelić, N. Trajković, et al., Age-related decrease in physical activity and functional fitness among elderly men and women. Clin Interv Aging, 2013. 8: p. 549-56.
74. Crossland, H., S. Skirrow, Z.A. Puthucheary, et al., The impact of immobilisation and inflammation on the regulation of muscle mass and insulin resistance: different routes to similar end-points. The Journal of physiology, 2019. 597(5): p. 1259-1270.
75. Kortebein, P., A. Ferrando, J. Lombeida, et al., Effect of 10 days of bed rest on skeletal muscle in healthy older adults. Jama, 2007. 297(16): p. 1769-1774.
76. Deane, C.S., C.R.G. Willis, B.E. Phillips, et al., Transcriptomic meta-analysis of disuse muscle atrophy vs. resistance exercise-induced hypertrophy in

young and older humans. J Cachexia Sarcopenia Muscle, 2021. 12(3): p. 629-645.
77. Zhang, Y., I. Chatzistamou, and H. Kiaris, Identification of frailty-associated genes by coordination analysis of gene expression. Aging (Albany NY), 2020. 12(5): p. 4222-4229.
78. Ferrando, A.A., H.W. Lane, C.A. Stuart, et al., Prolonged bed rest decreases skeletal muscle and whole body protein synthesis. American Journal of Physiology-Endocrinology And Metabolism, 1996. 270(4): p. E627-E633.
79. Shur, N.F., L. Creedon, S. Skirrow, et al., Age-related changes in muscle architecture and metabolism in humans: The likely contribution of physical inactivity to age-related functional decline. Ageing Res Rev, 2021. 68: p. 101344.
80. Lee, J.S., T.-W. Auyeung, J. Leung, et al., Transitions in frailty states among community-living older adults and their associated factors. Journal of the American Medical Directors Association, 2014. 15(4): p. 281-286.
81. Piasecki, M., A. Ireland, J. Piasecki, et al., Failure to expand the motor unit size to compensate for declining motor unit numbers distinguishes sarcopenic from non-sarcopenic older men. The Journal of physiology, 2018. 596(9): p. 1627-1637.
82. Nandedkar, S.D., D.B. Sanders, E.V. Stälberg, et al., Simulation of concentric needle EMG motor unit action potentials. Muscle & Nerve: Official Journal of the American Association of Electrodiagnostic Medicine, 1988. 11(2): p. 151-159.
83. Larsson, L., H. Degens, M. Li, et al., Sarcopenia: Aging-Related Loss of Muscle Mass and Function. Physiol Rev, 2019. 99(1): p. 427-511.
84. Ansved, T. and L. Larsson, Quantitative and qualitative morphological properties of the soleus motor nerve and the L5 ventral root in young and old rats: relation to the number of soleus muscle fibres. Journal of the neurological sciences, 1990. 96(2-3): p. 269-282.
85. Ansved, T., P. Wallner, and L. Larsson, Spatial distribution of motor unit fibres in fast-and slow-twitch rat muscles with special reference to age. Acta physiologica scandinavica, 1991. 143(3): p. 345-354.
86. Edström, L. and L. Larsson, Effects of age on contractile and enzyme-histochemical properties of fast-and slow-twitch single motor units in the rat. The Journal of physiology, 1987. 392(1): p. 129-145.
87. Power, G.A., B.H. Dalton, D.G. Behm, et al., Motor unit survival in lifelong runners is muscle dependent. Med Sci Sports Exerc, 2012. 44(7): p. 1235-1242.
88. Piasecki, M., A. Ireland, D. Stashuk, et al., Age-related neuromuscular changes affecting human vastus lateralis. J Physiol, 2016. 594(16): p. 4525-36.
89. R Deschenes, M., Motor unit and neuromuscular junction remodeling with aging. Current aging science, 2011. 4(3): p. 209-220.
90. Hepple, R.T. and C.L. Rice, Innervation and neuromuscular control in ageing skeletal muscle. The Journal of physiology, 2016. 594(8): p. 1965-1978.
91. Banker, B.Q., S. Kelly, and N. Robbins, Neuromuscular transmission and correlative morphology in young and old mice. The Journal of physiology, 1983. 339(1): p. 355-377.

92. Fahim, M., J. Holley, and N. Robbins, Scanning and light microscopic study of age changes at a neuromuscular junction in the mouse. Journal of neurocytology, 1983. 12(1): p. 13-25.
93. Tohgi, H., H. Tsukagoshi, and Y. Toyokura, Quantitative changes with age in normal sural nerves. Acta Neuropathologica, 1977. 38(3): p. 213-220.
94. Jacobs, J. and S. Love, Qualitative and quantitative morphology of human sural nerve at different ages. Brain, 1985. 108(4): p. 897-924.
95. Swiecicka, A., M. Piasecki, D.W. Stashuk, et al., Frailty phenotype and frailty index are associated with distinct neuromuscular electrophysiological characteristics in men. Experimental physiology, 2019. 104(8): p. 1154-1161.
96. Guo, Y., E.J. Jones, T. Smart, et al., Sex disparities in age-related neuromuscular decline: unveiling female susceptibility from early to late elderly. bioRxiv, 2023: p. 2023.06. 13.544761.
97. Hunter, S.K., H.M. Pereira, and K.G. Keenan, The aging neuromuscular system and motor performance. J Appl Physiol, 2016. 121(4): p. 982-995.
98. Sonjak, V., K. Jacob, J.A. Morais, et al., Fidelity of muscle fibre reinnervation modulates ageing muscle impact in elderly women. J Physiol, 2019. 597(19): p. 5009-5023.
99. de Waard, M.C., I. van der Pluijm, N. Zuiderveen Borgesius, et al., Age-related motor neuron degeneration in DNA repair-deficient Ercc1 mice. Acta neuropathologica, 2010. 120(4): p. 461-475.
100. Shinpo, K., S. Kikuchi, H. Sasaki, et al., Selective vulnerability of spinal motor neurons to reactive dicarbonyl compounds, intermediate products of glycation, in vitro: implication of inefficient glutathione system in spinal motor neurons. Brain research, 2000. 861(1): p. 151-159.
101. Brown, M., W. Hopkins, and R. Keynes, Comparison of effects of denervation and botulinum toxin paralysis on muscle properties in mice. The Journal of Physiology, 1982. 327: p. 29.
102. Samuel, M.A., G. Valdez, J.C. Tapia, et al., Agrin and synaptic laminin are required to maintain adult neuromuscular junctions. 2012.
103. Balice-Gordon, R.J. and J.W. Lichtman, Long-term synapse loss induced by focal blockade of postsynaptlc receptors. Nature, 1994. 372(6506): p. 519-524.
104. Barik, A., Y. Lu, A. Sathyamurthy, et al., LRP4 is critical for neuromuscular junction maintenance. Journal of Neuroscience, 2014. 34(42): p. 13892-13905.
105. Swiecicka, A., M. Piasecki, D. Stashuk, et al., Relationship of Anabolic Hormones With Motor Unit Characteristics in Quadriceps Muscle in Healthy and Frail Aging Men. The Journal of Clinical Endocrinology & Metabolism, 2020. 105(7): p. dgaa100.
106. Byers, J.S., A.L. Huguenard, D. Kuruppu, et al., Neuroprotective effects of testosterone on motoneuron and muscle morphology following spinal cord injury. Journal of Comparative Neurology, 2012. 520(12): p. 2683-2696.
107. Kurz, E., R. Brewer, and D. Sengelaub, Hormonally mediated plasticity of motoneuron morphology in the adult rat spinal cord: a cholera toxin-HRP study. Journal of neurobiology, 1991. 22(9): p. 976-988.
108. Kurz, E.M., D.R. Sengelaub, and A.P. Arnold, Androgens regulate the dendritic length of mammalian motoneurons in adulthood. Science, 1986. 232(4748): p. 395-398.

109. Blinkouskaya, Y., A. Caçoilo, T. Gollamudi, et al., Brain aging mechanisms with mechanical manifestations. Mechanisms of ageing and development, 2021. 200: p. 111575.
110. Leenders, K., D. Perani, A. Lammertsma, et al., Cerebral blood flow, blood volume and oxygen utilization: normal values and effect of age. Brain, 1990. 113(1): p. 27-47.
111. Newman, L., H. Nolan, D. Carey, et al., Age and sex differences in frontal lobe cerebral oxygenation in older adults—normative values using novel, scalable technology: findings from the Irish Longitudinal Study on Ageing (TILDA). Archives of gerontology and geriatrics, 2020. 87: p. 103988.
112. Lobo, A., L.J. Launer, L. Fratiglioni, et al., Prevalence of dementia and major subtypes in Europe: A collaborative study of population-based cohorts. Neurologic Diseases in the Elderly Research Group. Neurology, 2000. 54(11 Suppl 5): p. S4-9.
113. Avila-Funes, J.A., L. Carcaillon, C. Helmer, et al., Is Frailty a Prodromal Stage of Vascular Dementia? Results From the Three-City Study. Journal of the American Geriatrics Society, 2012. 60(9): p. 1708-1712.
114. Buchman, A.S., L. Yu, R.S. Wilson, et al., Brain pathology contributes to simultaneous change in physical frailty and cognition in old age. Journals of Gerontology Series A: Biomedical Sciences and Medical Sciences, 2014. 69(12): p. 1536-1544.
115. Solfrizzi, V., E. Scafato, V. Frisardi, et al., Frailty syndrome and the risk of vascular dementia: the Italian Longitudinal Study on Aging. Alzheimer's & Dementia, 2013. 9(2): p. 113-122.
116. Chen, W.T., K.H. Chou, L.K. Liu, et al., Reduced cerebellar gray matter is a neural signature of physical frailty. Human brain mapping, 2015. 36(9): p. 3666-3676.
117. Del Brutto, O.H., R.M. Mera, K. Cagino, et al., Neuroimaging signatures of frailty: A population-based study in community-dwelling older adults (the A tahualpa P roject). Geriatrics & gerontology international, 2017. 17(2): p. 270-276.
118. Kant, I.M.J., J. de Bresser, S.J.T. van Montfort, et al., The association between brain volume, cortical brain infarcts, and physical frailty. Neurobiol Aging, 2018. 70: p. 247-253.
119. Tian, Q., O.A. Williams, B.A. Landman, et al., Microstructural Neuroimaging of Frailty in Cognitively Normal Older Adults. Frontiers in Medicine, 2020. 7: p. 546344.
120. Wang, S.S.-H., J.R. Shultz, M.J. Burish, et al., Functional trade-offs in white matter axonal scaling. Journal of neuroscience, 2008. 28(15): p. 4047-4056.
121. Pelvig, D.P., H. Pakkenberg, A.K. Stark, et al., Neocortical glial cell numbers in human brains. Neurobiology of aging, 2008. 29(11): p. 1754-1762.
122. Ruigrok, A.N., G. Salimi-Khorshidi, M.-C. Lai, et al., A meta-analysis of sex differences in human brain structure. Neuroscience & Biobehavioral Reviews, 2014. 39: p. 34-50.
123. Jiang, R., S. Noble, J. Sui, et al., Associations of physical frailty with health outcomes and brain structure in 483 033 middle-aged and older adults: a population-based study from the UK Biobank. The Lancet Digital Health, 2023. 5(6): p. e350-e359.

124. Salat, D.H., D.N. Greve, J.L. Pacheco, et al., Regional white matter volume differences in nondemented aging and Alzheimer's disease. Neuroimage, 2009. 44(4): p. 1247-1258.
125. Nishita, Y., A. Nakamura, T. Kato, et al., Links Between Physical Frailty and Regional Gray Matter Volumes in Older Adults: A Voxel-Based Morphometry Study. J Am Med Dir Assoc, 2019. 20(12): p. 1587-1592.e7.
126. Callisaya, M.L., R. Beare, T.G. Phan, et al., Brain structural change and gait decline: a longitudinal population-based study. Journal of the American Geriatrics Society, 2013. 61(7): p. 1074-1079.
127. Salat, D.H., R.L. Buckner, A.Z. Snyder, et al., Thinning of the cerebral cortex in aging. Cerebral cortex, 2004. 14(7): p. 721-730.
128. Lemaitre, H., A.L. Goldman, F. Sambataro, et al., Normal age-related brain morphometric changes: nonuniformity across cortical thickness, surface area and gray matter volume? Neurobiology of aging, 2012. 33(3): p. 617. e1-617. e9.
129. Ziegler, D.A., O. Piguet, D.H. Salat, et al., Cognition in healthy aging is related to regional white matter integrity, but not cortical thickness. Neurobiology of aging, 2010. 31(11): p. 1912-1926.
130. Dickerson, B.C., A. Bakkour, D.H. Salat, et al., The cortical signature of Alzheimer's disease: regionally specific cortical thinning relates to symptom severity in very mild to mild AD dementia and is detectable in asymptomatic amyloid-positive individuals. Cerebral cortex, 2009. 19(3): p. 497-510.
131. Pacheco, J., J.O. Goh, M.A. Kraut, et al., Greater cortical thinning in normal older adults predicts later cognitive impairment. Neurobiology of aging, 2015. 36(2): p. 903-908.
132. Lu, W.-H., P. de Souto Barreto, Y. Rolland, et al., Cross-sectional and prospective associations between cerebral cortical thickness and frailty in older adults. Experimental Gerontology, 2020. 139: p. 111018.
133. Essen, D.C.v., A tension-based theory of morphogenesis and compact wiring in the central nervous system. Nature, 1997. 385(6614): p. 313-318.
134. Luders, E., P.M. Thompson, K. Narr, et al., A curvature-based approach to estimate local gyrification on the cortical surface. Neuroimage, 2006. 29(4): p. 1224-1230.
135. Jockwitz, C., S. Caspers, S. Lux, et al., Age-and function-related regional changes in cortical folding of the default mode network in older adults. Brain Structure and Function, 2017. 222: p. 83-99.
136. Rettmann, M.E., M.A. Kraut, J.L. Prince, et al., Cross-sectional and longitudinal analyses of anatomical sulcal changes associated with aging. Cerebral Cortex, 2006. 16(11): p. 1584-1594.
137. Im, K., J.-M. Lee, S.W. Seo, et al., Sulcal morphology changes and their relationship with cortical thickness and gyral white matter volume in mild cognitive impairment and Alzheimer's disease. Neuroimage, 2008. 43(1): p. 103-113.
138. Robertson, D.A., G.M. Savva, R.F. Coen, et al., Cognitive function in the prefrailty and frailty syndrome. J Am Geriatr Soc, 2014. 62(11): p. 2118-2124.
139. Huang, C.-C., A.C. Yang, K.-H. Chou, et al., Nonlinear pattern of the emergence of white matter hyperintensity in healthy Han Chinese: an adult lifespan study. Neurobiology of aging, 2018. 67: p. 99-107.

140. Kynast, J., L. Lampe, T. Luck, et al., White matter hyperintensities associated with small vessel disease impair social cognition beside attention and memory. Journal of Cerebral Blood Flow & Metabolism, 2018. 38(6): p. 996-1009.
141. Srikanth, V., R. Beare, L. Blizzard, et al., Cerebral white matter lesions, gait, and the risk of incident falls: a prospective population-based study. Stroke, 2009. 40(1): p. 175-180.
142. Dhamoon, M.S., Y.-K. Cheung, Y. Moon, et al., Cerebral white matter disease and functional decline in older adults from the Northern Manhattan Study: A longitudinal cohort study. PLoS medicine, 2018. 15(3): p. e1002529.
143. Kant, I.M., H.J. Mutsaerts, S.J. van Montfort, et al., The association between frailty and MRI features of cerebral small vessel disease. Scientific reports, 2019. 9(1): p. 1-9.
144. Siejka, T.P., V.K. Srikanth, R.E. Hubbard, et al., Frailty and Cerebral Small Vessel Disease: A Cross-Sectional Analysis of the Tasmanian Study of Cognition and Gait (TASCOG). J Gerontol A Biol Sci Med Sci, 2018. 73(2): p. 255-260.
145. Siejka, T.P., V.K. Srikanth, R.E. Hubbard, et al., White Matter Hyperintensities and the Progression of Frailty—The Tasmanian Study of Cognition and Gait. The Journals of Gerontology: Series A, 2020. 75(8): p. 1545-1550.
146. Ducca, E.L., G.T. Gomez, P. Palta, et al., Physical Frailty and Brain White Matter Abnormalities: The ARIC Study. The Journals of Gerontology: Series A, 2022.
147. Moseley, M., Diffusion tensor imaging and aging–a review. NMR in Biomedicine: An International Journal Devoted to the Development and Application of Magnetic Resonance In Vivo, 2002. 15(7-8): p. 553-560.
148. Yassa, M.A., L.T. Muftuler, and C.E. Stark, Ultrahigh-resolution microstructural diffusion tensor imaging reveals perforant path degradation in aged humans in vivo. Proceedings of the national academy of sciences, 2010. 107(28): p. 12687-12691.
149. Beaudet, G., A. Tsuchida, L. Petit, et al., Age-related changes of peak width skeletonized mean diffusivity (PSMD) across the adult lifespan: a multi-cohort study. Frontiers in psychiatry, 2020. 11: p. 342.
150. Avila-Funes, J.A., A. Pelletier, C. Meillon, et al., Vascular Cerebral Damage in Frail Older Adults: The AMImage Study. J Gerontol A Biol Sci Med Sci, 2017. 72(7): p. 971-977.
151. Tamura, Y., K. Shimoji, J. Ishikawa, et al., Association between white matter alterations on diffusion tensor imaging and incidence of frailty in older adults with cardiometabolic diseases. Frontiers in Aging Neuroscience, 2022. 14: p. 912972.
152. Catchlove, S.J., H. Macpherson, M.E. Hughes, et al., An investigation of cerebral oxygen utilization, blood flow and cognition in healthy aging. PLoS One, 2018. 13(5): p. e0197055.
153. Fallgatter, A., M. Roesler, a. Sitzmann, et al., Loss of functional hemispheric asymmetry in Alzheimer's dementia assessed with near-infrared spectroscopy. Cognitive Brain Research, 1997. 6(1): p. 67-72.
154. Rockwood, K., M. Andrew, and A. Mitnitski, A comparison of two approaches to measuring frailty in elderly people. The Journals of Gerontology Series A: Biological Sciences and Medical Sciences, 2007. 62(7): p. 738-743.

155. Armstrong, J.J., P. Stolee, J.P. Hirdes, et al., Examining three frailty conceptualizations in their ability to predict negative outcomes for home-care clients. Age Ageing, 2010. 39(6): p. 755-8.
156. Aguilar-Navarro, S.G., A.J. Mimenza-Alvarado, I. Corona-Sevilla, et al., Cerebral Vascular Reactivity in Frail Older Adults with Vascular Cognitive Impairment. Brain sciences, 2019. 9(9): p. 214.
157. Maguire, F., R. Romero-Ortuno, J.D. O'Connor, et al., One-dimensional statistical parametric mapping identifies impaired orthostatic cerebrovascular and cardiovascular response in frailty index. The Journals of Gerontology: Series A, 2021. 76(5): p. 885-892.
158. Skhirtladze-Dworschak, K. and M. Dworschak. *Cerebral oximetry and cardiac arrest*. in *Seminars in cardiothoracic and vascular anesthesia*. 2013. SAGE Publications Sage CA: Los Angeles, CA.
159. Lu, H., F. Xu, K.M. Rodrigue, et al., Alterations in cerebral metabolic rate and blood supply across the adult lifespan. Cerebral cortex, 2011. 21(6): p. 1426-1434.
160. Peng, S.-L., J.A. Dumas, D.C. Park, et al., Age-related increase of resting metabolic rate in the human brain. Neuroimage, 2014. 98: p. 176-183.
161. Arnardottir, N.Y., A. Koster, D.R. Van Domelen, et al., Association of change in brain structure to objectively measured physical activity and sedentary behavior in older adults: Age, Gene/Environment Susceptibility-Reykjavik Study. Behavioural brain research, 2016. 296: p. 118-124.
162. Bronas, U.G., A. Steffen, C. Dion, et al., Sedentary time and white matter hyperintensity volume in older adults. Medicine and science in sports and exercise, 2019. 51(8): p. 1613.
163. Carter, S.E., R. Draijer, S.M. Holder, et al., Regular walking breaks prevent the decline in cerebral blood flow associated with prolonged sitting. Journal of applied physiology, 2018.
164. Kudo, T., M. Takeda, S. Tanimukai, et al., Neuropathologic changes in the gerbil brain after chronic hypoperfusion. Stroke, 1993. 24(2): p. 259-264.
165. Yamauchi, H., H. Fukuyama, Y. Nagahama, et al., Brain arteriolosclerosis and hemodynamic disturbance may induce leukoaraiosis. Neurology, 1999. 53(8): p. 1833-1833.
166. Chuang, Y.-M., K.-L. Huang, Y.-J. Chang, et al., Immediate regression of leukoaraiosis after carotid artery revascularization. Cerebrovascular Diseases, 2011. 32(5): p. 439-446.
167. Kempuraj, D., R. Thangavel, P. Natteru, et al., Neuroinflammation induces neurodegeneration. Journal of neurology, neurosurgery and spine, 2016. 1(1).
168. Lu, T., Y. Pan, S.-Y. Kao, et al., Gene regulation and DNA damage in the ageing human brain. Nature, 2004. 429(6994): p. 883-891.
169. Chen, W.W., X. Zhang, and W.J. Huang, Role of neuroinflammation in neurodegenerative diseases (Review). Mol Med Rep, 2016. 13(4): p. 3391-6.
170. Buchman, A.S., J.A. Schneider, S. Leurgans, et al., Physical frailty in older persons is associated with Alzheimer disease pathology. Neurology, 2008. 71(7): p. 499-504.
171. Sala-Llonch, R., A.-V. Idland, T. Borza, et al., Inflammation, amyloid, and atrophy in the aging brain: relationships with longitudinal changes in cognition. J Alzheimer's Dis, 2017. 58(3): p. 829-840.

172. Falcon, C., G.C. Monté-Rubio, O. Grau-Rivera, et al., CSF glial biomarkers YKL40 and sTREM2 are associated with longitudinal volume and diffusivity changes in cognitively unimpaired individuals. NeuroImage: Clinical, 2019. 23: p. 101801.
173. Veronese, N., E. Cereda, B. Stubbs, et al., Risk of cardiovascular disease morbidity and mortality in frail and pre-frail older adults: Results from a meta-analysis and exploratory meta-regression analysis. Ageing research reviews, 2017. 35: p. 63-73.
174. Lakatta, E.G. and D. Levy, Arterial and cardiac aging: major shareholders in cardiovascular disease enterprises: Part II: the aging heart in health: links to heart disease. Circulation, 2003. 107(2): p. 346-354.
175. Alshawabkeh, L.I., L.M. Yee, J.M. Gardin, et al., Years of able life in older persons—the role of cardiovascular imaging and biomarkers: the Cardiovascular Health Study. Journal of the American Heart Association, 2015. 4(4): p. e001745.
176. Leibowitz, D., J.M. Jacobs, I. Lande-Stessman, et al., Cardiac structure and function predicts functional decline in the oldest old. Eur J Prev Cardiol, 2018. 25(3): p. 263-269.
177. Newman, A.B., J.S. Gottdiener, M.A. McBurnie, et al., Associations of subclinical cardiovascular disease with frailty. J Gerontol A Biol Sci Med Sci, 2001. 56(3): p. M158-66.
178. Kusunose, K., Y. Okushi, H. Yamada, et al., Prognostic value of frailty and diastolic dysfunction in elderly patients. Circulation Journal, 2018. 82(8): p. 2103-2110.
179. Leibowitz, D., J.M. Jacobs, D. Gilon, et al., Cardiac structure and function and frailty in subjects aged 85 and 86 years. The American journal of cardiology, 2016. 118(5): p. 760-764.
180. Nadruz Jr, W., D. Kitzman, B.G. Windham, et al., Cardiovascular dysfunction and frailty among older adults in the community: the ARIC study. Journals of Gerontology Series A: Biomedical Sciences and Medical Sciences, 2016. 72(7): p. 958-964.
181. Gharacholou, S.M., T. Tashiro, S.S. Cha, et al., Echocardiographic indices associated with frailty in adults >/=65 years. Am J Cardiol, 2015. 116(10): p. 1591-5.
182. Sanchis, J., E. Núñez, V. Ruiz, et al., Usefulness of clinical data and biomarkers for the identification of frailty after acute coronary syndromes. Canadian Journal of Cardiology, 2015. 31(12): p. 1462-1468.
183. Bellenger, N.G., M.I. Burgess, S.G. Ray, et al., Comparison of left ventricular ejection fraction and volumes in heart failure by echocardiography, radionuclide ventriculography and cardiovascular magnetic resonance. Are they interchangeable? European heart journal, 2000. 21(16): p. 1387-1396.
184. Grothues, F., G.C. Smith, J.C. Moon, et al., Comparison of interstudy reproducibility of cardiovascular magnetic resonance with two-dimensional echocardiography in normal subjects and in patients with heart failure or left ventricular hypertrophy. The American journal of cardiology, 2002. 90(1): p. 29-34.
185. Malik, S.B., N. Chen, R.A. Parker III, et al., Transthoracic Echocardiography: Pitfalls and Limitations as Delineated at Cardiac CT and MR Imaging—Erratum. Radiographics, 2017. 37(3): p. 1004-1004.

186. Saeed, M., H. Liu, C.-H. Liang, et al., Magnetic resonance imaging for characterizing myocardial diseases. The international journal of cardiovascular imaging, 2017. 33(9): p. 1395-1414.
187. AlGhatrif, M., J.B. Strait, C.H. Morrell, et al., Longitudinal trajectories of arterial stiffness and the role of blood pressure: the Baltimore Longitudinal Study of Aging. Hypertension, 2013. 62(5): p. 934-941.
188. Van den Munckhof, I., R. Scholten, N.T. Cable, et al., Impact of age and sex on carotid and peripheral arterial wall thickness in humans. Acta physiologica, 2012. 206(4): p. 220-228.
189. Celermajer, D.S., K.E. Sorensen, D.J. Spiegelhalter, et al., Aging is associated with endothelial dysfunction in healthy men years before the age-related decline in women. Journal of the American College of Cardiology, 1994. 24(2): p. 471-476.
190. Singh, N., S. Prasad, D.R. Singer, et al., Ageing is associated with impairment of nitric oxide and prostanoid dilator pathways in the human forearm. Clinical science, 2002. 102(5): p. 595-600.
191. Jeon, Y.K., M.J. Shin, S.K. Saini, et al., Vascular dysfunction as a potential culprit of sarcopenia. Experimental Gerontology, 2021. 145: p. 111220.
192. Brunner, E.J., M.J. Shipley, D.R. Witte, et al., Arterial stiffness, physical function, and functional limitation: the Whitehall II Study. Hypertension, 2011. 57(5): p. 1003-1009.
193. Orkaby, A.R., K.L. Lunetta, F.J. Sun, et al., Cross-sectional association of frailty and arterial stiffness in community-dwelling older adults: the Framingham heart study. The Journals of Gerontology: Series A, 2019. 74(3): p. 373-379.
194. Amarasekera, A.T., D. Chang, P. Schwarz, et al., Does vascular endothelial dysfunction play a role in physical frailty and sarcopenia? A systematic review. Age and Ageing, 2020.
195. Alonso-Bouzón, C., L. Carcaillon, F.J. García-García, et al., Association between endothelial dysfunction and frailty: the Toledo Study for Healthy Aging. Age (Dordr), 2014. 36(1): p. 495-505.
196. Santillo, E., M. Migale, and F. Balestrini, Frailty and flow-mediated dilation: A pilot study in hospitalized elderly. Journal of Current Research in Scientific Medicine, 2016. 2(2): p. 92.
197. Mansur, H.N., J.C.M. Lovisi, F.A.B. Colugnati, et al., Association of frailty with endothelial dysfunction and its possible impact on negative outcomes in Brazilian predialysis patients with chronic kidney disease. BMC nephrology, 2015. 16(1): p. 1-9.
198. Masiha, S., J. Sundström, and L. Lind, Inflammatory markers are associated with left ventricular hypertrophy and diastolic dysfunction in a population-based sample of elderly men and women. Journal of human hypertension, 2013. 27(1): p. 13-17.
199. Hartupee, J., G.D. Szalai, W. Wang, et al., Impaired protein quality control during left ventricular remodeling in mice with cardiac restricted overexpression of tumor necrosis factor. Circulation: Heart Failure, 2017. 10(12): p. e004252.
200. Sivasubramanian, N., M.L. Coker, K.M. Kurrelmeyer, et al., Left ventricular remodeling in transgenic mice with cardiac restricted overexpression of tumor necrosis factor. Circulation, 2001. 104(7): p. 826-831.

201. Schafnitzel, A., R. Lorbeer, C. Bayerl, et al., Association of smoking and physical inactivity with MRI derived changes in cardiac function and structure in cardiovascular healthy subjects. Scientific reports, 2019. 9(1): p. 1-10.
202. Dorfman, T.A., B.D. Levine, T. Tillery, et al., Cardiac atrophy in women following bed rest. J Appl Physiol, 2007. 103(1): p. 8-16.
203. Bederman, I.R., N. Lai, J. Shuster, et al., Chronic hindlimb suspension unloading markedly decreases turnover rates of skeletal and cardiac muscle proteins and adipose tissue triglycerides. J Appl Physiol, 2015. 119(1): p. 16-26.
204. Park, W., H.-Y. Park, K. Lim, et al., The role of habitual physical activity on arterial stiffness in elderly individuals: a systematic review and meta-analysis. Journal of exercise nutrition & biochemistry, 2017. 21(4): p. 16.
205. Gnasso, A., C. Carallo, C. Irace, et al., Association between wall shear stress and flow-mediated vasodilation in healthy men. Atherosclerosis, 2001. 156(1): p. 171-176.
206. Cheng, C., R. van Haperen, M. de Waard, et al., Shear stress affects the intracellular distribution of eNOS: direct demonstration by a novel in vivo technique. Blood, 2005. 106(12): p. 3691-3698.
207. Wilkinson, I.B., A. Qasem, C.M. McEniery, et al., Nitric oxide regulates local arterial distensibility in vivo. Circulation, 2002. 105(2): p. 213-217.
208. Goodpaster, B.H., S.W. Park, T.B. Harris, et al., The loss of skeletal muscle strength, mass, and quality in older adults: the health, aging and body composition study. The Journals of Gerontology Series A: Biological Sciences and Medical Sciences, 2006. 61(10): p. 1059-1064.
209. Machann, J., C. Thamer, B. Schnoedt, et al., Age and gender related effects on adipose tissue compartments of subjects with increased risk for type 2 diabetes: a whole body MRI/MRS study. Magnetic Resonance Materials in Physics, Biology and Medicine, 2005. 18(3): p. 128-137.
210. Fuke, Y., S. Okabe, N. Kajiwara, et al., Increase of visceral fat area in Indonesians and Japanese with normal BMI. Diabetes research and clinical practice, 2007. 77(3): p. S224-S227.
211. Schwenzer, N.F., P. Martirosian, J. Machann, et al., Aging effects on human calf muscle properties assessed by MRI at 3 Tesla. Journal of Magnetic Resonance Imaging: An Official Journal of the International Society for Magnetic Resonance in Medicine, 2009. 29(6): p. 1346-1354.
212. Monteverde, M., K. Noronha, A. Palloni, et al., Obesity and excess mortality among the elderly in the United States and Mexico. Demography, 2010. 47(1): p. 79-96.
213. Freedman, D., E. Ron, R. Ballard-Barbash, et al., Body mass index and all-cause mortality in a nationwide US cohort. International journal of obesity, 2006. 30(5): p. 822-829.
214. Chapman, I.M., Obesity paradox during aging. Body composition and aging, 2010. 37: p. 20-36.
215. Wang, L., W. Liu, X. He, et al., Association of overweight and obesity with patient mortality after acute myocardial infarction: a meta-analysis of prospective studies. International journal of obesity, 2016. 40(2): p. 220-228.
216. Greenlee, H., J.M. Unger, M. LeBlanc, et al., Association between body mass index and cancer survival in a pooled analysis of 22 clinical trials. Cancer Epidemiology and Prevention Biomarkers, 2017. 26(1): p. 21-29.

217. Boutin, E., P.-A. Natella, A.-M. Schott, et al., Interrelations between body mass index, frailty, and clinical adverse events in older community-dwelling women: The EPIDOS cohort study. Clinical Nutrition, 2018. 37(5): p. 1638-1644.
218. Schaap, L.A., A. Koster, and M. Visser, Adiposity, muscle mass, and muscle strength in relation to functional decline in older persons. Epidemiologic reviews, 2013. 35(1): p. 51-65.
219. Cawthon, P.M., K.M. Fox, S.R. Gandra, et al., Clustering of strength, physical function, muscle, and adiposity characteristics and risk of disability in older adults. Journal of the American Geriatrics Society, 2011. 59(5): p. 781-787.
220. Feng, Z., M. Lugtenberg, C. Franse, et al., Risk factors and protective factors associated with incident or increase of frailty among community-dwelling older adults: A systematic review of longitudinal studies. PloS one, 2017. 12(6): p. e0178383.
221. Woods, N.F., A.Z. LaCroix, S.L. Gray, et al., Frailty: emergence and consequences in women aged 65 and older in the Women's Health Initiative Observational Study. Journal of the American Geriatrics Society, 2005. 53(8): p. 1321-1330.
222. Landré, B., S. Czernichow, M. Goldberg, et al., Association Between Life-Course Obesity and Frailty in Older Adults: Findings in the GAZEL Cohort. Obesity, 2020. 28(2): p. 388-396.
223. Blaum, C.S., Q.L. Xue, E. Michelon, et al., The association between obesity and the frailty syndrome in older women: the Women's Health and Aging Studies. Journal of the American Geriatrics Society, 2005. 53(6): p. 927-934.
224. Sewo Sampaio, P.Y., R.A.C. Sampaio, H.J. Coelho Júnior, et al., Differences in lifestyle, physical performance and quality of life between frail and robust Brazilian community-dwelling elderly women. Geriatrics & gerontology international, 2016. 16(7): p. 829-835.
225. Bowden Davies, K.A., V.S. Sprung, J.A. Norman, et al., Short-term decreased physical activity with increased sedentary behaviour causes metabolic derangements and altered body composition: effects in individuals with and without a first-degree relative with type 2 diabetes. Diabetologia, 2018. 61(6): p. 1282-1294.
226. Olsen, R.H., R. Krogh-Madsen, C. Thomsen, et al., Metabolic responses to reduced daily steps in healthy nonexercising men. Jama, 2008. 299(11): p. 1261-3.
227. del Pozo-Cruz, B., A. Mañas, M. Martín-García, et al., Frailty is associated with objectively assessed sedentary behaviour patterns in older adults: Evidence from the Toledo Study for Healthy Aging (TSHA). PloS one, 2017. 12(9): p. e0183911.
228. Petersen, K.F., S. Dufour, D.B. Savage, et al., The role of skeletal muscle insulin resistance in the pathogenesis of the metabolic syndrome. Proceedings of the National Academy of Sciences, 2007. 104(31): p. 12587-12594.
229. Rector, R.S. and J.P. Thyfault, Does physical inactivity cause nonalcoholic fatty liver disease? Journal of applied physiology, 2011. 111(6): p. 1828-1835.
230. Blanc, S.p., S. Normand, C. Pachiaudi, et al., Fuel homeostasis during physical inactivity induced by bed rest. The journal of clinical endocrinology & metabolism, 2000. 85(6): p. 2223-2233.

231. Manini, T.M., B.C. Clark, M.A. Nalls, et al., Reduced physical activity increases intermuscular adipose tissue in healthy young adults. The American journal of clinical nutrition, 2007. 85(2): p. 377-384.
232. Gemmink, A., B.H. Goodpaster, P. Schrauwen, et al., Intramyocellular lipid droplets and insulin sensitivity, the human perspective. Biochimica et Biophysica Acta (BBA)-Molecular and Cell Biology of Lipids, 2017. 1862(10): p. 1242-1249.
233. Hannukainen, J.C., P. Nuutila, B. Ronald, et al., Increased physical activity decreases hepatic free fatty acid uptake: a study in human monozygotic twins. The Journal of physiology, 2007. 578(1): p. 347-358.
234. Iozzo, P., T. Takala, V. Oikonen, et al., Effect of training status on regional disposal of circulating free fatty acids in the liver and skeletal muscle during physiological hyperinsulinemia. Diabetes Care, 2004. 27(9): p. 2172-2177.
235. Leng, S.X., H. Yang, and J.D. Walston, Decreased cell proliferation and altered cytokine production in frail older adults. Aging clinical and experimental research, 2004. 16(3): p. 249-252.
236. Walston, J., M.A. McBurnie, A. Newman, et al., Frailty and activation of the inflammation and coagulation systems with and without clinical comorbidities: results from the Cardiovascular Health Study. Archives of internal medicine, 2002. 162(20): p. 2333-2341.
237. Cesari, M., S.B. Kritchevsky, R.N. Baumgartner, et al., Sarcopenia, obesity, and inflammation—results from the Trial of Angiotensin Converting Enzyme Inhibition and Novel Cardiovascular Risk Factors study–. The American journal of clinical nutrition, 2005. 82(2): p. 428-434.
238. Mohamed-Ali, V., S. Goodrick, A. Rawesh, et al., Subcutaneous adipose tissue releases interleukin-6, but not tumor necrosis factor-α, in vivo. The Journal of Clinical Endocrinology & Metabolism, 1997. 82(12): p. 4196-4200.
239. Visser, M., M. Pahor, D.R. Taaffe, et al., Relationship of interleukin-6 and tumor necrosis factor-α with muscle mass and muscle strength in elderly men and women: the Health ABC Study. The Journals of Gerontology Series A: Biological Sciences and Medical Sciences, 2002. 57(5): p. M326-M332.
240. Murton, A.J., K. Marimuthu, J.E. Mallinson, et al., Obesity appears to be associated with altered muscle protein synthetic and breakdown responses to increased nutrient delivery in older men, but not reduced muscle mass or contractile function. Diabetes, 2015. 64(9): p. 3160-3171.
241. Cohen, A.A., E. Milot, J. Yong, et al., A novel statistical approach shows evidence for multi-system physiological dysregulation during aging. Mechanisms of ageing and development, 2013. 134(3-4): p. 110-117.
242. Weinert, B.T. and P.S. Timiras, Invited review: Theories of aging. J Appl Physiol, 2003. 95(4): p. 1706-1716.
243. López-Otín, C., M.A. Blasco, L. Partridge, et al., The hallmarks of aging. Cell, 2013. 153(6): p. 1194-1217.
244. Samper-Ternent, R., C. Reyes-Ortiz, K.J. Ottenbacher, et al., Frailty and sarcopenia in Bogotá: results from the SABE Bogotá Study. Aging clinical and experimental research, 2017. 29(2): p. 265-272.
245. Fried, L.P., Q.-L. Xue, A.R. Cappola, et al., Nonlinear multisystem physiological dysregulation associated with frailty in older women: implications for etiology and treatment. Journals of Gerontology Series A: Biomedical Sciences and Medical Sciences, 2009. 64(10): p. 1049-1057.

246. Amaral, L.A., A. Díaz-Guilera, A.A. Moreira, et al., Emergence of complex dynamics in a simple model of signaling networks. Proceedings of the National Academy of Sciences, 2004. 101(44): p. 15551-15555.
247. Yates, F.E., Complexity of a human being: changes with age. Neurobiology of aging, 2002. 23(1): p. 17.
248. Li, Q., S. Wang, E. Milot, et al., Homeostatic dysregulation proceeds in parallel in multiple physiological systems. Aging cell, 2015. 14(6): p. 1103-1112.
249. Ghachem, A., L.P. Fried, V. Legault, et al., Evidence from two cohorts for the frailty syndrome as an emergent state of parallel dysregulation in multiple physiological systems. Biogerontology, 2020. 22(1): p. 63-79.
250. Theou, O., L. Cann, J. Blodgett, et al., Modifications to the frailty phenotype criteria: Systematic review of the current literature and investigation of 262 frailty phenotypes in the Survey of Health, Ageing, and Retirement in Europe. Ageing research reviews, 2015. 21: p. 78-94.
251. Gordon, E., N. Peel, M. Samanta, et al., Sex differences in frailty: a systematic review and meta-analysis. Experimental gerontology, 2017. 89: p. 30-40.
252. Varadhan, R., C. Seplaki, Q.L. Xue, et al., Stimulus-response paradigm for characterizing the loss of resilience in homeostatic regulation associated with frailty. Mechanisms of ageing and development, 2008. 129(11): p. 666-670.
253. Fried, L.P., E.C. Hadley, J.D. Walston, et al., From bedside to bench: research agenda for frailty. Science of aging knowledge environment: SAGE KE, 2005. 2005(31): p. pe24-pe24.
254. Fried, L.P., A.A. Cohen, Q.-L. Xue, et al., The physical frailty syndrome as a transition from homeostatic symphony to cacophony. Nature Aging, 2021. 1(1): p. 36-46.
255. Heinonen, I., K.K. Kalliokoski, J.C. Hannukainen, et al., Organ-specific physiological responses to acute physical exercise and long-term training in humans. Physiology, 2014.
256. Greenhaff, P., E. Hultman, and R. Harris, *Carbohydrate metabolism*, in *Principles of exercise biochemistry*. 1993, Karger Publishers. p. 89-136.
257. Das, A.M., U. Steuerwald, and S. Illsinger, Inborn errors of energy metabolism associated with myopathies. Journal of Biomedicine and Biotechnology, 2010. 2010: p. 340849.
258. Radda, G.K., The use of NMR spectroscopy for the understanding of disease. Science, 1986. 233(4764): p. 640-645.
259. Steiner, M.C., R. Evans, S.J. Deacon, et al., Adenine nucleotide loss in the skeletal muscles during exercise in chronic obstructive pulmonary disease. Thorax, 2005. 60(11): p. 932-936.
260. Greenhaff, P., K. Bodin, K. Soderlund, et al., Effect of oral creatine supplementation on skeletal muscle phosphocreatine resynthesis. American Journal of Physiology-Endocrinology And Metabolism, 1994. 266(5): p. E725-E730.
261. Hesselink, M.K., P.L. Greenhaff, D. Constantin-Teodosiu, et al., Increased uncoupling protein 3 content does not affect mitochondrial function in human skeletal muscle in vivo. J Clin Invest, 2003. 111(4): p. 479-86.
262. Andreux, P.A., M.P. van Diemen, M.R. Heezen, et al., Mitochondrial function is impaired in the skeletal muscle of pre-frail elderly. Scientific reports, 2018. 8(1): p. 1-12.

263. Picard, M., R. Godin, M. Sinnreich, et al., The mitochondrial phenotype of peripheral muscle in chronic obstructive pulmonary disease: disuse or dysfunction? Am J Respir Crit Care Med, 2008. 178(10): p. 1040-1047.
264. Boushel, R., E. Gnaiger, P. Schjerling, et al., Patients with type 2 diabetes have normal mitochondrial function in skeletal muscle. Diabetologia, 2007. 50(4): p. 790-796.
265. St-Jean-Pelletier, F., C.H. Pion, J.P. Leduc-Gaudet, et al., The impact of ageing, physical activity, and pre-frailty on skeletal muscle phenotype, mitochondrial content, and intramyocellular lipids in men. Journal of cachexia, sarcopenia and muscle, 2017. 8(2): p. 213-228.
266. Sonjak, V., K.J. Jacob, S. Spendiff, et al., Reduced mitochondrial content, elevated reactive oxygen species, and modulation by denervation in skeletal muscle of prefrail or frail elderly women. The Journals of Gerontology: Series A, 2019. 74(12): p. 1887-1895.
267. Ashar, F.N., A. Moes, A.Z. Moore, et al., Association of mitochondrial DNA levels with frailty and all-cause mortality. Journal of molecular medicine, 2015. 93(2): p. 177-186.
268. Moore, A.Z., M.L. Biggs, A. Matteini, et al., Polymorphisms in the mitochondrial DNA control region and frailty in older adults. PLoS One, 2010. 5(6): p. e11069.
269. Drummond, M.J., O. Addison, L. Brunker, et al., Downregulation of E3 ubiquitin ligases and mitophagy-related genes in skeletal muscle of physically inactive, frail older women: a cross-sectional comparison. J Gerontol A Biol Sci Med Sci, 2014. 69(8): p. 1040-8.
270. Davidson, M.B., The effect of aging on carbohydrate metabolism: a review of the English literature and a practical approach to the diagnosis of diabetes mellitus in the elderly. Metabolism, 1979. 28(6): p. 688-705.
271. Metter, E.J., B.G. Windham, M. Maggio, et al., Glucose and insulin measurements from the oral glucose tolerance test and mortality prediction. Diabetes care, 2008. 31(5): p. 1026-1030.
272. Kalyani, R.R., R. Varadhan, C.O. Weiss, et al., Frailty status and altered glucose-insulin dynamics. Journals of Gerontology: Series A: Biomedical Sciences and Medical Sciences, 2012. 67(12): p. 1300-1306.
273. Goulet, E.D., Z. Khursigara, R. Gougeon, et al., Postprandial insulin sensitivity and thermogenesis in frail elderly women. Applied Physiology, Nutrition, and Metabolism, 2010. 35(4): p. 526-533.
274. Rothman, M.D., L. Leo-Summers, and T.M. Gill, Prognostic significance of potential frailty criteria. Journal of the American Geriatrics Society, 2008. 56(12): p. 2211-2216.
275. Woudstra, T. and A.B. Thomson, Nutrient absorption and intestinal adaptation with ageing. Best practice & research Clinical gastroenterology, 2002. 16(1): p. 1-15.
276. Fink, R.I., O.G. Kolterman, J. Griffin, et al., Mechanisms of insulin resistance in aging. J Clin Invest, 1983. 71(6): p. 1523-35.
277. Barzilay, J.I., C. Blaum, T. Moore, et al., Insulin resistance and inflammation as precursors of frailty: the Cardiovascular Health Study. Archives of internal medicine, 2007. 167(7): p. 635-641.
278. Goulet, E.D., A. Hassaine, I.J. Dionne, et al., Frailty in the elderly is associated with insulin resistance of glucose metabolism in the postabsorptive

state only in the presence of increased abdominal fat. Experimental gerontology, 2009. 44(11): p. 740-744.
279. Peng, P.-S., T.-W. Kao, P.-K. Chang, et al., Association between HOMA-IR and frailty among US middle-aged and elderly population. Scientific reports, 2019. 9(1): p. 1-8.
280. Sorkin, J.D., D.C. Muller, J.L. Fleg, et al., The relation of fasting and 2-h postchallenge plasma glucose concentrations to mortality: data from the Baltimore Longitudinal Study of Aging with a critical review of the literature. Diabetes care, 2005. 28(11): p. 2626-2632.
281. Smith, N.L., J.I. Barzilay, D. Shaffer, et al., Fasting and 2-hour postchallenge serum glucose measures and risk of incident cardiovascular events in the elderly: the Cardiovascular Health Study. Archives of internal medicine, 2002. 162(2): p. 209-216.
282. Casas-Herrero, A., E.L. Cadore, F. Zambom-Ferraresi, et al., Functional capacity, muscle fat infiltration, power output, and cognitive impairment in institutionalized frail oldest old. Rejuvenation research, 2013. 16(5): p. 396-403.
283. Taylor, H.L., D.R. Jacobs Jr, B. Schucker, et al., A questionnaire for the assessment of leisure time physical activities. Journal of chronic diseases, 1978. 31(12): p. 741-755.
284. Eckel, S.P., K. Bandeen-Roche, P.H. Chaves, et al., Surrogate screening models for the low physical activity criterion of frailty. Aging clinical and experimental research, 2011. 23(3): p. 209-216.
285. Oomen, N.M. and J.H. van Dieën, Effects of age on force steadiness: a literature review and meta-analysis. Ageing research reviews, 2017. 35: p. 312-321.
286. Mani, D., A.M. Almuklass, L.D. Hamilton, et al., Motor unit activity, force steadiness, and perceived fatigability are correlated with mobility in older adults. Journal of neurophysiology, 2018. 120(4): p. 1988-1997.
287. Lexell, J., C.C. Taylor, and M. Sjöström, What is the cause of the ageing atrophy?: Total number, size and proportion of different fiber types studied in whole vastus lateralis muscle from 15-to 83-year-old men. Journal of the neurological sciences, 1988. 84(2-3): p. 275-294.
288. Aniansson, A., M. Hedberg, G.B. Henning, et al., Muscle morphology, enzymatic activity, and muscle strength in elderly men: a follow-up study. Muscle & Nerve: Official Journal of the American Association of Electrodiagnostic Medicine, 1986. 9(7): p. 585-591.
289. Dixon, W.T., Simple proton spectroscopic imaging. Radiology, 1984. 153(1): p. 189-194.
290. Glover, G.H., Multipoint Dixon technique for water and fat proton and susceptibility imaging. Journal of Magnetic Resonance Imaging, 1991. 1(5): p. 521-530.
291. Kondo, C., G. Caputo, R. Semelka, et al., Right and left ventricular stroke volume measurements with velocity-encoded cine MR imaging: in vitro and in vivo validation. AJR. American journal of roentgenology, 1991. 157(1): p. 9-16.
292. Messroghli, D.R., A. Radjenovic, S. Kozerke, et al., Modified Look-Locker inversion recovery (MOLLI) for high-resolution T1 mapping of the heart. Magnetic Resonance in Medicine: An Official Journal of the International Society for Magnetic Resonance in Medicine, 2004. 52(1): p. 141-146.

293. Nöth, U., E. Hattingen, O. Bähr, et al., Improved visibility of brain tumors in synthetic MP-RAGE anatomies with pure T1 weighting. NMR in Biomedicine, 2015. 28(7): p. 818-830.
294. Nelson, F., A. Poonawalla, P. Hou, et al. *MPRAGE improves classification of cortical lesions in multiple sclerosis*. in *MULTIPLE SCLEROSIS*. 2007. SAGE PUBLICATIONS LTD 1 OLIVERS YARD, 55 CITY ROAD, LONDON EC1Y 1SP, ENGLAND.
295. Peng, S.L., P. Su, F.N. Wang, et al., Optimization of phase-contrast MRI for the quantification of whole-brain cerebral blood flow. Journal of Magnetic Resonance Imaging, 2015. 42(4): p. 1126-1133.
296. Lu, H. and Y. Ge, Quantitative evaluation of oxygenation in venous vessels using T2-relaxation-under-spin-tagging MRI. Magnetic Resonance in Medicine: An Official Journal of the International Society for Magnetic Resonance in Medicine, 2008. 60(2): p. 357-363.
297. Lu, H., F. Xu, K. Grgac, et al., Calibration and validation of TRUST MRI for the estimation of cerebral blood oxygenation. Magnetic resonance in medicine, 2012. 67(1): p. 42-49.
298. Wright, G.A., B.S. Hu, and A. Macovski, Estimating oxygen saturation of blood in vivo with MR imaging at 1.5 T. Journal of Magnetic Resonance Imaging, 1991. 1(3): p. 275-283.
299. Beale, A.L., P. Meyer, T.H. Marwick, et al., Sex differences in cardiovascular pathophysiology: why women are overrepresented in heart failure with preserved ejection fraction. Circulation, 2018. 138(2): p. 198-205.
300. Garg, P., L.C. Saunders, A.J. Swift, et al., Role of cardiac T1 mapping and extracellular volume in the assessment of myocardial infarction. Anatol J Cardiol, 2018. 19(6): p. 404-411.
301. Schelbert, E.B. and D.R. Messroghli, State of the art: clinical applications of cardiac T1 mapping. Radiology, 2016. 278(3): p. 658-676.
302. Marques, M.D., R. Weinberg, S. Kapoor, et al., Myocardial fibrosis by T1 mapping magnetic resonance imaging predicts incident cardiovascular events and all-cause mortality: the Multi-Ethnic Study of Atherosclerosis. European Heart Journal-Cardiovascular Imaging, 2022. 23(10): p. 1407-1416.
303. Ambale-Venkatesh, B., J. Sesso, J. Walston, et al., WHOLE-BODY MRI TO ASSESS SUBCLINICAL CARDIOVASCULAR DISEASE AND FRAILTY DEVELOPMENT. Innovation in Aging, 2019. 3(Suppl 1): p. S87.
304. Diaz-Navarro, R.A. and P.L.M. Kerkhof, Left Ventricular Global Function Index and the Impact of its Companion Metric. Front Cardiovasc Med, 2021. 8: p. 695883.
305. Mewton, N., A. Opdahl, E.-Y. Choi, et al., Left ventricular global function index by magnetic resonance imaging—a novel marker for assessment of cardiac performance for the prediction of cardiovascular events: the multi-ethnic study of atherosclerosis. Hypertension, 2013. 61(4): p. 770-778.
306. Schulz-Menger, J., D.A. Bluemke, J. Bremerich, et al., Standardized image interpretation and post-processing in cardiovascular magnetic resonance-2020 update. Journal of Cardiovascular Magnetic Resonance, 2020. 22(1): p. 1-22.
307. Gottbrecht, M., C.M. Kramer, and M. Salerno, Native T1 and extracellular volume measurements by cardiac MRI in healthy adults: a meta-analysis. Radiology, 2019. 290(2): p. 317-326.

308. Liu, C.-Y., Y.-C. Liu, C. Wu, et al., Evaluation of age-related interstitial myocardial fibrosis with cardiac magnetic resonance contrast-enhanced T1 mapping: MESA (Multi-Ethnic Study of Atherosclerosis). Journal of the American College of Cardiology, 2013. 62(14): p. 1280-1287.
309. Kawel-Boehm, N., S.J. Hetzel, B. Ambale-Venkatesh, et al., Reference ranges ("normal values") for cardiovascular magnetic resonance (CMR) in adults and children: 2020 update. Journal of cardiovascular magnetic resonance, 2020. 22(1): p. 1-63.
310. Bhuva, A.N., W. Bai, C. Lau, et al., A multicenter, scan-rescan, human and machine learning CMR study to test generalizability and precision in imaging biomarker analysis. Circulation: Cardiovascular Imaging, 2019. 12(10): p. e009214.
311. Tan, A.X., S.J. Shah, J.L. Sanders, et al., Association Between Myocardial Strain and Frailty in CHS. Circ Cardiovasc Imaging, 2021. 14(5): p. e012116.
312. Obokata, M., Y. Nagata, V.C.-C. Wu, et al., Direct comparison of cardiac magnetic resonance feature tracking and 2D/3D echocardiography speckle tracking for evaluation of global left ventricular strain. European Heart Journal-Cardiovascular Imaging, 2016. 17(5): p. 525-532.
313. Cote, A.T., S.S. Bredin, A.A. Phillips, et al., Left ventricular mechanics and arterial-ventricular coupling following high-intensity interval exercise. Journal of applied physiology, 2013. 115(11): p. 1705-1713.
314. Martinez-Naharro, A., T. Kotecha, K. Norrington, et al., Native T1 and extracellular volume in transthyretin amyloidosis. JACC: Cardiovascular Imaging, 2019. 12(5): p. 810-819.
315. Romero-Ortuno, R., L. Cogan, D. O'Shea, et al., Orthostatic haemodynamics may be impaired in frailty. Age and ageing, 2011. 40(5): p. 576-583.
316. Moghtadaei, M., H.J. Jansen, M. Mackasey, et al., The impacts of age and frailty on heart rate and sinoatrial node function. J Physiol, 2016. 594(23): p. 7105-7126.
317. Monfredi, O., H. Dobrzynski, T. Mondal, et al., The anatomy and physiology of the sinoatrial node—a contemporary review. Pacing and clinical electrophysiology, 2010. 33(11): p. 1392-1406.
318. Toosizadeh, N., H. Ehsani, S. Parthasarathy, et al., Frailty and heart response to physical activity. Archives of gerontology and geriatrics, 2021. 93: p. 104323.
319. Eriksen, M., B.A. Waaler, L. Walløe, et al., Dynamics and dimensions of cardiac output changes in humans at the onset and at the end of moderate rhythmic exercise. The Journal of physiology, 1990. 426(1): p. 423-437.
320. Maden-Wilkinson, T.M., H. Degens, D.A. Jones, et al., Comparison of MRI and DXA to measure muscle size and age-related atrophy in thigh muscles. J Musculoskelet Neuronal Interact, 2013. 13(3): p. 320-8.
321. Marcus, R.L., O. Addison, L.E. Dibble, et al., Intramuscular adipose tissue, sarcopenia, and mobility function in older individuals. Journal of aging research, 2012. 2012.
322. Martinikorena, I., A. Martínez-Ramírez, M. Gómez, et al., Gait variability related to muscle quality and muscle power output in frail nonagenarian older adults. Journal of the American Medical Directors Association, 2016. 17(2): p. 162-167.

323. Millor, N., E.L. Cadore, M. Gómez, et al., High density muscle size and muscle power are associated with both gait and sit-to-stand kinematic parameters in frail nonagenarians. Journal of Biomechanics, 2020. 105: p. 109766.
324. Saad, R.K., M. Ghezzawi, R. Horanieh, et al., Abdominal visceral adipose tissue and all-cause mortality: a systematic review. Frontiers in endocrinology, 2022. 13: p. 922931.
325. Li, B., Y. Li, Y. Zhang, et al., Visceral fat obesity correlates with frailty in middle-aged and older adults. Diabetes, Metabolic Syndrome and Obesity: Targets and Therapy, 2022: p. 2877-2884.
326. Su, Y., M. Yuki, and N. Ogawa, Association of visceral fat area with pre-frailty in Japanese community-dwelling older adults: a cross-sectional study. BMC geriatrics, 2022. 22(1): p. 1-8.
327. Hawkins, K.L., L. Zhang, K.N. ALTHOFF, et al., Abdominal obesity, sarcopenia, and osteoporosis are strongly associated with frailty in the MACS. AIDS (London, England), 2018. 32(10): p. 1257.
328. Uchai, S., L. Andersen, J. Johansson, et al., Dual-Energy X-Ray Absorptiometry Derived Adiposity Measures and Pre-Frailty/Frailty among Norwegian Adults: The Tromsø Study 2007–2015. The journal of nutrition, health & aging, 2023: p. 1-8.
329. Bamman, M.M., B.R. Newcomer, D.E. Larson-Meyer, et al., Evaluation of the strength-size relationship in vivo using various muscle size indices. Med Sci Sports Exerc, 2000. 32(7): p. 1307-13.
330. Hughes, V.A., W.R. Frontera, M. Wood, et al., Longitudinal muscle strength changes in older adults: influence of muscle mass, physical activity, and health. The Journals of Gerontology Series A: Biological Sciences and Medical Sciences, 2001. 56(5): p. B209-B217.
331. Li, R., Y. Wu, N. Maffulli, et al., Eccentric and concentric isokinetic knee flexion and extension: a reliability study using the Cybex 6000 dynamometer. British journal of sports medicine, 1996. 30(2): p. 156-160.
332. Piasecki, M., A. Ireland, J. Coulson, et al., Motor unit number estimates and neuromuscular transmission in the tibialis anterior of master athletes: evidence that athletic older people are not spared from age-related motor unit remodeling. Physiological reports, 2016. 4(19): p. e12987.
333. Piasecki, M., A. Ireland, J. Piasecki, et al., The reliability of methods to estimate the number and size of human motor units and their use with large limb muscles. European journal of applied physiology, 2018. 118(4): p. 767-775.
334. Calder, K.M., M.J. Agnew, D.W. Stashuk, et al., Reliability of quantitative EMG analysis of the extensor carpi radialis muscle. Journal of Neuroscience Methods, 2008. 168(2): p. 483-493.
335. Boe, S.G., N.M. Antonowicz, V.W. Leung, et al., High inter-rater reliability in analyzing results of decomposition-based quantitative electromyography in subjects with or without neuromuscular disorder. Journal of neuroscience methods, 2010. 192(1): p. 138-145.
336. Narici, M., Human skeletal muscle architecture studied in vivo by non-invasive imaging techniques: functional significance and applications. Journal of electromyography and kinesiology, 1999. 9(2): p. 97-103.

337. Raj, I.S., S.R. Bird, and A.J. Shield, Ultrasound measurements of skeletal muscle architecture are associated with strength and functional capacity in older adults. Ultrasound in Medicine & Biology, 2017. 43(3): p. 586-594.
338. Yurumez, B., Y. Metin, V. Atmis, et al., A new possible marker: can pennation angle defined by ultrasound predict the frailty? Aging Clinical and Experimental Research, 2024. 36(1): p. 53.
339. Carnavale, B.F., E. Fiogbé, A.C.S. Farche, et al., Complexity of knee extensor torque in patients with frailty syndrome: a cross-sectional study. Brazilian Journal of Physical Therapy, 2020. 24(1): p. 30-38.
340. Clegg, A., J. Young, S. Iliffe, et al., Frailty in elderly people. The lancet, 2013. 381(9868): p. 752-762.
341. Overend, T., D. Cunningham, D. Paterson, et al., Thigh composition in young and elderly men determined by computed tomography. Clinical Physiology, 1992. 12(6): p. 629-640.
342. Frontera, W.R., V.A. Hughes, R.A. Fielding, et al., Aging of skeletal muscle: a 12-yr longitudinal study. Journal of applied physiology, 2000. 88(4): p. 1321-1326.
343. Morse, C.I., J.M. Thom, N.D. Reeves, et al., In vivo physiological cross-sectional area and specific force are reduced in the gastrocnemius of elderly men. Journal of applied physiology, 2005. 99(3): p. 1050-1055.
344. Maganaris, C.N., Force-length characteristics of in vivo human skeletal muscle. Acta Physiol Scand, 2001. 172(4): p. 279-85.
345. Watanabe, K. and H. Akima, Effect of knee joint angle on neuromuscular activation of the vastus intermedius muscle during isometric contraction. Scand J Med Sci Sports, 2011. 21(6): p. e412-20.
346. Larsson, L., X. Li, and W. Frontera, Effects of aging on shortening velocity and myosin isoform composition in single human skeletal muscle cells. American Journal of Physiology-Cell Physiology, 1997. 272(2): p. C638-C649.
347. Reid, K.F., G. Doros, D.J. Clark, et al., Muscle power failure in mobility-limited older adults: preserved single fiber function despite lower whole muscle size, quality and rate of neuromuscular activation. European journal of applied physiology, 2012. 112: p. 2289-2301.
348. Aas, S.N., M. Breit, S. Karsrud, et al., Musculoskeletal adaptations to strength training in frail elderly: a matter of quantity or quality? Journal of Cachexia, Sarcopenia and Muscle, 2020. 11(3): p. 663-677.
349. Pereira, A., M. Izquierdo, A.J. Silva, et al., Effects of high-speed power training on functional capacity and muscle performance in older women. Experimental gerontology, 2012. 47(3): p. 250-255.
350. Reid, K.F. and R.A. Fielding, Skeletal muscle power: a critical determinant of physical functioning in older adults. Exercise and sport sciences reviews, 2012. 40(1): p. 4.
351. Prior, S.J., A.S. Ryan, J.B. Blumenthal, et al., Sarcopenia is associated with lower skeletal muscle capillarization and exercise capacity in older adults. Journals of Gerontology Series A: Biomedical Sciences and Medical Sciences, 2016. 71(8): p. 1096-1101.
352. Kramer, P., P. Coen, P. Cawthon, et al., Skeletal muscle energetics explain the sex disparity in mobility impairment in the Study of Muscle, Mobility and Aging (SOMMA). medRxiv, 2023: p. 2023.11. 08.23298271.

353. Carville, S.F., M.C. Perry, O.M. Rutherford, et al., Steadiness of quadriceps contractions in young and older adults with and without a history of falling. European journal of applied physiology, 2007. 100: p. 527-533.
354. Taylor, A.M., E.A. Christou, and R.M. Enoka, Multiple features of motor-unit activity influence force fluctuations during isometric contractions. J Neurophysiol, 2003. 90(2): p. 1350-61.
355. Yao, W., R.J. Fuglevand, and R.M. Enoka, Motor-unit synchronization increases EMG amplitude and decreases force steadiness of simulated contractions. J Neurophysiol, 2000. 83(1): p. 441-52.
356. Enoka, R.M., E.A. Christou, S.K. Hunter, et al., Mechanisms that contribute to differences in motor performance between young and old adults. J Electromyogr Kinesiol, 2003. 13(1): p. 1-12.
357. Babault, N., M. Pousson, A. Michaut, et al., EMG activity and voluntary activation during knee-extensor concentric torque generation. European Journal of Applied Physiology, 2002. 86: p. 541-547.
358. Roos, M.R., C.L. Rice, D.M. Connelly, et al., Quadriceps muscle strength, contractile properties, and motor unit firing rates in young and old men. Muscle & Nerve: Official Journal of the American Association of Electrodiagnostic Medicine, 1999. 22(8): p. 1094-1103.
359. Hvid, L.G., E.S. Strotmeyer, M. Skjødt, et al., Voluntary muscle activation improves with power training and is associated with changes in gait speed in mobility-limited older adults—a randomized controlled trial. Experimental gerontology, 2016. 80: p. 51-56.
360. Bays, H. and C. Ballantyne, Adiposopathy: why do adiposity and obesity cause metabolic disease? Future Lipidology, 2006. 1(4): p. 389-420.
361. Fujimoto, W.Y., R.W. Bergstrom, E.J. Boyko, et al., Visceral adiposity and incident coronary heart disease in Japanese-American men. The 10-year follow-up results of the Seattle Japanese-American Community Diabetes Study. Diabetes care, 1999. 22(11): p. 1808-1812.
362. Vetrano, D.L., K. Palmer, A. Marengoni, et al., Frailty and Multimorbidity: A Systematic Review and Meta-analysis. J Gerontol A Biol Sci Med Sci, 2019. 74(5): p. 659-666.
363. Marcos-Pérez, D., M. Sánchez-Flores, S. Proietti, et al., Association of inflammatory mediators with frailty status in older adults: results from a systematic review and meta-analysis. GeroScience, 2020. 42(6): p. 1-23.
364. Roubicek, T., M. Bartlova, J. Krajickova, et al., Increased production of proinflammatory cytokines in adipose tissue of patients with end-stage renal disease. Nutrition, 2009. 25(7-8): p. 762-768.
365. Fain, J.N., Release of interleukins and other inflammatory cytokines by human adipose tissue is enhanced in obesity and primarily due to the nonfat cells. Vitamins & Hormones, 2006. 74: p. 443-477.
366. Maltais, M., P. de Souto Barreto, L. Perus, et al., Prospective associations between diffusion tensor imaging parameters and frailty in older adults. Journal of the American Geriatrics Society, 2020. 68(5): p. 1050-1055.
367. Hugenschmidt, C.E., A.M. Peiffer, R.A. Kraft, et al., Relating imaging indices of white matter integrity and volume in healthy older adults. Cerebral cortex, 2008. 18(2): p. 433-442.
368. Ashburner, J. and K.J. Friston, Voxel-based morphometry—the methods. Neuroimage, 2000. 11(6): p. 805-821.

369. Mechelli, A., C.J. Price, K.J. Friston, et al., Voxel-based morphometry of the human brain: methods and applications. Current Medical Imaging, 2005. 1(2): p. 105-113.
370. Palumbo, L., P. Bosco, M. Fantacci, et al., Evaluation of the intra-and inter-method agreement of brain MRI segmentation software packages: A comparison between SPM12 and FreeSurfer v6. 0. Physica Medica, 2019. 64: p. 261-272.
371. Guo, C., D. Ferreira, K. Fink, et al., Repeatability and reproducibility of FreeSurfer, FSL-SIENAX and SPM brain volumetric measurements and the effect of lesion filling in multiple sclerosis. European radiology, 2019. 29: p. 1355-1364.
372. Dahnke, R., R.A. Yotter, and C. Gaser, Cortical thickness and central surface estimation. Neuroimage, 2013. 65: p. 336-348.
373. Yotter, R.A., R. Dahnke, P.M. Thompson, et al., Topological correction of brain surface meshes using spherical harmonics. Human brain mapping, 2011. 32(7): p. 1109-1124.
374. Ashburner, J., A fast diffeomorphic image registration algorithm. Neuroimage, 2007. 38(1): p. 95-113.
375. Velázquez, J., J. Mateos, E.H. Pasaye, et al., Cortical thickness estimation: A comparison of FreeSurfer and three voxel-based methods in a test–retest analysis and a clinical application. Brain Topography, 2021. 34(4): p. 430-441.
376. Dias, M.d.F.M., P. Carvalho, M. Castelo-Branco, et al., Cortical thickness in brain imaging studies using freesurfer and cat12: A matter of reproducibility. Neuroimage: Reports, 2022. 2(4): p. 100137.
377. Griffanti, L., G. Zamboni, A. Khan, et al., BIANCA (Brain Intensity AbNormality Classification Algorithm): A new tool for automated segmentation of white matter hyperintensities. Neuroimage, 2016. 141: p. 191-205.
378. Zhao, J.M., C.S. Clingman, M.J. Närväinen, et al., Oxygenation and hematocrit dependence of transverse relaxation rates of blood at 3T. Magnetic Resonance in Medicine: An Official Journal of the International Society for Magnetic Resonance in Medicine, 2007. 58(3): p. 592-597.
379. Liu, P., F. Xu, and H. Lu, Test–retest reproducibility of a rapid method to measure brain oxygen metabolism. Magnetic resonance in medicine, 2013. 69(3): p. 675-681.
380. Aanerud, J., P. Borghammer, M.M. Chakravarty, et al., Brain energy metabolism and blood flow differences in healthy aging. Journal of Cerebral Blood Flow & Metabolism, 2012. 32(7): p. 1177-1187.
381. O'Brien, C., T.W. Okell, M. Chiew, et al., Volume-localized measurement of oxygen extraction fraction in the brain using MRI. Magnetic Resonance in Medicine, 2019. 82(4): p. 1412-1423.
382. PATRICK, Y., What stimulation of the supplementary motor area in humans tells about its functional organization. Advances in neurology, 1996. 70: p. 199-209.
383. Martino, J., A. Gabarrós, J. Deus, et al., Intrasurgical mapping of complex motor function in the superior frontal gyrus. Neuroscience, 2011. 179: p. 131-142.
384. Seghier, M.L., The angular gyrus: multiple functions and multiple subdivisions. The Neuroscientist, 2013. 19(1): p. 43-61.

385. Sergent, J., S. Ohta, and B. Macdonald, Functional neuroanatomy of face and object processing: a positron emission tomography study. Brain, 1992. 115(1): p. 15-36.
386. Grill-Spector, K., Z. Kourtzi, and N. Kanwisher, The lateral occipital complex and its role in object recognition. Vision research, 2001. 41(10-11): p. 1409-1422.
387. Kovach, C.K., N.D. Daw, D. Rudrauf, et al., Anterior prefrontal cortex contributes to action selection through tracking of recent reward trends. Journal of Neuroscience, 2012. 32(25): p. 8434-8442.
388. Urbanski, M., M.-L. Bréchemier, B. Garcin, et al., Reasoning by analogy requires the left frontal pole: lesion-deficit mapping and clinical implications. Brain, 2016. 139(6): p. 1783-1799.
389. Swick, D., V. Ashley, and Turken, Left inferior frontal gyrus is critical for response inhibition. BMC neuroscience, 2008. 9: p. 1-11.
390. Kurz, M.J., T.W. Wilson, and D.J. Arpin, Stride-time variability and sensorimotor cortical activation during walking. Neuroimage, 2012. 59(2): p. 1602-1607.
391. Luft, A.R., G.V. Smith, L. Forrester, et al., Comparing brain activation associated with isolated upper and lower limb movement across corresponding joints. Human brain mapping, 2002. 17(2): p. 131-140.
392. Post, M., A. Steens, R. Renken, et al., Voluntary activation and cortical activity during a sustained maximal contraction: an fMRI study. Human brain mapping, 2009. 30(3): p. 1014-1027.
393. Buckley, M., D. Gaffan, and E. Murray, Functional double dissociation between two inferior temporal cortical areas: perirhinal cortex versus middle temporal gyrus. Journal of neurophysiology, 1997. 77(2): p. 587-598.
394. Cabeza, R. and L. Nyberg, Imaging cognition II: An empirical review of 275 PET and fMRI studies. Journal of cognitive neuroscience, 2000. 12(1): p. 1-47.
395. Chao, L.L., J.V. Haxby, and A. Martin, Attribute-based neural substrates in temporal cortex for perceiving and knowing about objects. Nature neuroscience, 1999. 2(10): p. 913-919.
396. Kropf, E., S.K. Syan, L. Minuzzi, et al., From anatomy to function: the role of the somatosensory cortex in emotional regulation. Braz J Psychiatry, 2019. 41(3): p. 261-269.
397. Liu, D., M. Ji, K. Zhuang, et al., Regional grey matter volume in the posterior cingulate cortex predicts positive risk-taking: A moderation model. International Journal of Psychology, 2023. 58(1): p. 69-77.
398. Carter, C.S., M. Mintun, T. Nichols, et al., Anterior cingulate gyrus dysfunction and selective attention deficits in schizophrenia:[15O] H2O PET study during single-trial Stroop task performance. American Journal of Psychiatry, 1997. 154(12): p. 1670-1675.
399. Ledberg, A., B.T. O'Sullivan, S. Kinomura, et al., Somatosensory activations of the parietal operculum of man. A PET study. European Journal of Neuroscience, 1995. 7(9): p. 1934-1941.
400. Del Vecchio, M., C. Fossataro, F.M. Zauli, et al., Tonic somatosensory responses and deficits of tactile awareness converge in the parietal operculum. Brain, 2021. 144(12): p. 3779-3787.

401. Oberhuber, M., T. Hope, M.L. Seghier, et al., Four functionally distinct regions in the left supramarginal gyrus support word processing. Cerebral Cortex, 2016. 26(11): p. 4212-4226.
402. Jobson, D.D., Y. Hase, A.N. Clarkson, et al., The role of the medial prefrontal cortex in cognition, ageing and dementia. Brain communications, 2021. 3(3): p. fcab125.
403. Malach, R., J. Reppas, R. Benson, et al., Object-related activity revealed by functional magnetic resonance imaging in human occipital cortex. Proceedings of the National Academy of Sciences, 1995. 92(18): p. 8135-8139.
404. Tisserand, D.J., M.P. van Boxtel, J.C. Pruessner, et al., A voxel-based morphometric study to determine individual differences in gray matter density associated with age and cognitive change over time. Cerebral cortex, 2004. 14(9): p. 966-973.
405. Chen, Y.-S., H.-L. Chen, C.-H. Lu, et al., Reduced lateral occipital gray matter volume is associated with physical frailty and cognitive impairment in Parkinson's disease. European Radiology, 2019. 29: p. 2659-2668.
406. Kaas, J.H., R.J. Nelson, M. Sur, et al., Multiple representations of the body within the primary somatosensory cortex of primates. Science, 1979. 204(4392): p. 521-523.
407. DiSalvio, N.L., C. Rosano, H.J. Aizenstein, et al., Gray matter regions associated with functional mobility in community-dwelling older adults. Journal of the American Geriatrics Society, 2020. 68(5): p. 1023-1028.
408. Chittrakul, J., P. Siviroj, S. Sungkarat, et al., Physical frailty and fall risk in community-dwelling older adults: a cross-sectional study. Journal of aging research, 2020. 2020: p. 1-8.
409. Seaman, K.L., C.T. Smith, E.J. Juarez, et al., Differential regional decline in dopamine receptor availability across adulthood: Linear and nonlinear effects of age. Human brain mapping, 2019. 40(10): p. 3125-3138.
410. Cham, R., S. Perera, S.A. Studenski, et al., Striatal dopamine denervation and sensory integration for balance in middle-aged and older adults. Gait & posture, 2007. 26(4): p. 516-525.
411. Dow, C., M. Seidenberg, and B. Hermann, Relationship between information processing speed in temporal lobe epilepsy and white matter volume. Epilepsy & Behavior, 2004. 5(6): p. 919-925.
412. Martin, A.J., K.J. Friston, J.G. Colebatch, et al., Decreases in regional cerebral blood flow with normal aging. Journal of Cerebral Blood Flow & Metabolism, 1991. 11(4): p. 684-689.
413. Wakita, H., H. Tomimoto, I. Akiguchi, et al., Axonal damage and demyelination in the white matter after chronic cerebral hypoperfusion in the rat. Brain research, 2002. 924(1): p. 63-70.
414. Chiarelli, A.M., M.A. Fletcher, C.H. Tan, et al., Individual differences in regional cortical volumes across the life span are associated with regional optical measures of arterial elasticity. NeuroImage, 2017. 162: p. 199-213.
415. Holroyd, C.B. and S.M. McClure, Hierarchical control over effortful behavior by rodent medial frontal cortex: A computational model. Psychological review, 2015. 122(1): p. 54.

416. Rushworth, M.F., N. Kolling, J. Sallet, et al., Valuation and decision-making in frontal cortex: one or many serial or parallel systems? Current opinion in neurobiology, 2012. 22(6): p. 946-955.
417. Wei, X., Y. Yin, M. Rong, et al., Paracingulate sulcus asymmetry in the human brain: effects of sex, handedness, and race. Scientific Reports, 2017. 7(1): p. 42033.
418. Yücel, M., G.W. Stuart, P. Maruff, et al., Hemispheric and gender-related differences in the gross morphology of the anterior cingulate/paracingulate cortex in normal volunteers: an MRI morphometric study. Cerebral cortex, 2001. 11(1): p. 17-25.
419. Lamballais, S., E.J. Vinke, M.W. Vernooij, et al., Cortical gyrification in relation to age and cognition in older adults. NeuroImage, 2020. 212: p. 116637.
420. Vinke, E.J., M. de Groot, V. Venkatraghavan, et al., Trajectories of imaging markers in brain aging: the Rotterdam Study. Neurobiology of aging, 2018. 71: p. 32-40.
421. Jin, K., T. Zhang, M. Shaw, et al., Relationship between sulcal characteristics and brain aging. Frontiers in aging neuroscience, 2018. 10: p. 339.
422. Lemon, R.N., Descending pathways in motor control. Annu Rev Neurosci, 2008. 31: p. 195-218.
423. Beier, F., M. Löffler, F. Nees, et al., Sensory and motor correlates of frailty: dissociation between frailty phenotype and frailty index. BMC geriatrics, 2022. 22(1): p. 755.
424. Van Essen, D.C., A 2020 view of tension-based cortical morphogenesis. Proceedings of the National Academy of Sciences, 2020. 117(52): p. 32868-32879.
425. Rajagopalan, J., A. Tofangchi, and A.S. MT, Drosophila neurons actively regulate axonal tension in vivo. Biophys J, 2010. 99(10): p. 3208-15.
426. Franze, K., J. Gerdelmann, M. Weick, et al., Neurite branch retraction is caused by a threshold-dependent mechanical impact. Biophysical journal, 2009. 97(7): p. 1883-1890.
427. Inano, S., H. Takao, N. Hayashi, et al., Effects of age and gender on white matter integrity. American Journal of Neuroradiology, 2011. 32(11): p. 2103-2109.
428. Kochunov, P., P.M. Thompson, T.R. Coyle, et al., Relationship among neuroimaging indices of cerebral health during normal aging. Human brain mapping, 2008. 29(1): p. 36-45.
429. Osawa, Y., Q. Tian, Y. An, et al., Longitudinal associations between brain volume and knee extension peak torque. The Journals of Gerontology: Series A, 2021. 76(2): p. 286-290.
430. Seidler, R., B. Erdeniz, V. Koppelmans, et al., Associations between age, motor function, and resting state sensorimotor network connectivity in healthy older adults. Neuroimage, 2015. 108: p. 47-59.
431. Ali, P., M. Labriffe, P. Paisant, et al., Associations between gait speed and brain structure in amnestic mild cognitive impairment: a quantitative neuroimaging study. Brain Imaging and Behavior, 2022: p. 1-11.
432. Alexander, N.B. and J.M. Hausdorff, Guest editorial: linking thinking, walking, and falling. The Journals of Gerontology Series A: Biological sciences and medical sciences, 2008. 63(12): p. 1325-1328.

433. Sheridan, P.L. and J.M. Hausdorff, The role of higher-level cognitive function in gait: executive dysfunction contributes to fall risk in Alzheimer's disease. Dementia and geriatric cognitive disorders, 2007. 24(2): p. 125-137.
434. Yogev-Seligmann, G., J.M. Hausdorff, and N. Giladi, The role of executive function and attention in gait. Movement disorders: official journal of the Movement Disorder Society, 2008. 23(3): p. 329-342.
435. Tian, Q., S.M. Resnick, C. Davatzikos, et al., A prospective study of focal brain atrophy, mobility and fitness. Journal of internal medicine, 2019. 286(1): p. 88-100.
436. van Lieshout, J.J., F. Pott, P.L. Madsen, et al., Muscle tensing during standing: effects on cerebral tissue oxygenation and cerebral artery blood velocity. Stroke, 2001. 32(7): p. 1546-1551.
437. Ogoh, S., R.M. Brothers, Q. Barnes, et al., The effect of changes in cardiac output on middle cerebral artery mean blood velocity at rest and during exercise. The Journal of physiology, 2005. 569(2): p. 697-704.
438. Meng, L., W. Hou, J. Chui, et al., Cardiac output and cerebral blood flow: the integrated regulation of brain perfusion in adult humans. Anesthesiology, 2015. 123(5): p. 1198-1208.
439. Zhang, H., Y. Wang, D. Lyu, et al., Cerebral blood flow in mild cognitive impairment and Alzheimer's disease: A systematic review and meta-analysis. Ageing Research Reviews, 2021. 71: p. 101450.
440. Samper-Ternent, R., S. Al Snih, M.A. Raji, et al., Relationship between frailty and cognitive decline in older Mexican Americans. Journal of the American Geriatrics Society, 2008. 56(10): p. 1845-1852.
441. Zlatar, Z.Z., C.C. Hays, Z. Mestre, et al., Dose-dependent association of accelerometer-measured physical activity and sedentary time with brain perfusion in aging. Experimental Gerontology, 2019. 125: p. 110679.
442. Hock, C., K. Villringer, F. Müller-Spahn, et al., Decrease in parietal cerebral hemoglobin oxygenation during performance of a verbal fluency task in patients with Alzheimer's disease monitored by means of near-infrared spectroscopy (NIRS)—correlation with simultaneous rCBF-PET measurements. Brain research, 1997. 755(2): p. 293-303.
443. Fukuyama, H., M. Ogawa, H. Yamauchi, et al., Altered cerebral energy metabolism in Alzheimer's disease: a PET study. Journal of nuclear medicine: official publication, Society of Nuclear Medicine, 1994. 35(1): p. 1-6.
444. Murrell, C.J., J.D. Cotter, K.N. Thomas, et al., Cerebral blood flow and cerebrovascular reactivity at rest and during sub-maximal exercise: effect of age and 12-week exercise training. Age, 2013. 35(3): p. 905-920.
445. Kilgour, A.H., O.M. Todd, and J.M. Starr, A systematic review of the evidence that brain structure is related to muscle structure and their relationship to brain and muscle function in humans over the lifecourse. BMC Geriatr, 2014. 14: p. 85.
446. Harris, R. and E. Dyson, Recruitment of frail older people to research: lessons learnt through experience. Journal of advanced nursing, 2001. 36(5): p. 643-651.
447. Chatfield, M.D., C.E. Brayne, and F.E. Matthews, A systematic literature review of attrition between waves in longitudinal studies in the elderly shows a consistent pattern of dropout between differing studies. Journal of clinical epidemiology, 2005. 58(1): p. 13-19.

448. Walsh, B., C. Fogg, S. Harris, et al., Frailty transitions and prevalence in an ageing population: longitudinal analysis of primary care data from an open cohort of adults aged 50 and over in England, 2006–2017. Age and Ageing, 2023. 52(5): p. afad058.
449. Provencher, V., W.B. Mortenson, L. Tanguay-Garneau, et al., Challenges and strategies pertaining to recruitment and retention of frail elderly in research studies: a systematic review. Archives of gerontology and geriatrics, 2014. 59(1): p. 18-24.
450. Peters, S.A., S.H. Bots, and M. Woodward, Sex differences in the association between measures of general and central adiposity and the risk of myocardial infarction: results from the UK Biobank. Journal of the American Heart Association, 2018. 7(5): p. e008507.
451. Bycroft, C., C. Freeman, D. Petkova, et al., The UK Biobank resource with deep phenotyping and genomic data. Nature, 2018. 562(7726): p. 203-209.
452. Cesari, M., G. Gambassi, G. Abellan van Kan, et al., The frailty phenotype and the frailty index: different instruments for different purposes. Age and ageing, 2014. 43(1): p. 10-12.
453. Blodgett, J., O. Theou, S. Kirkland, et al., Frailty in NHANES: comparing the frailty index and phenotype. Archives of gerontology and geriatrics, 2015. 60(3): p. 464-470.